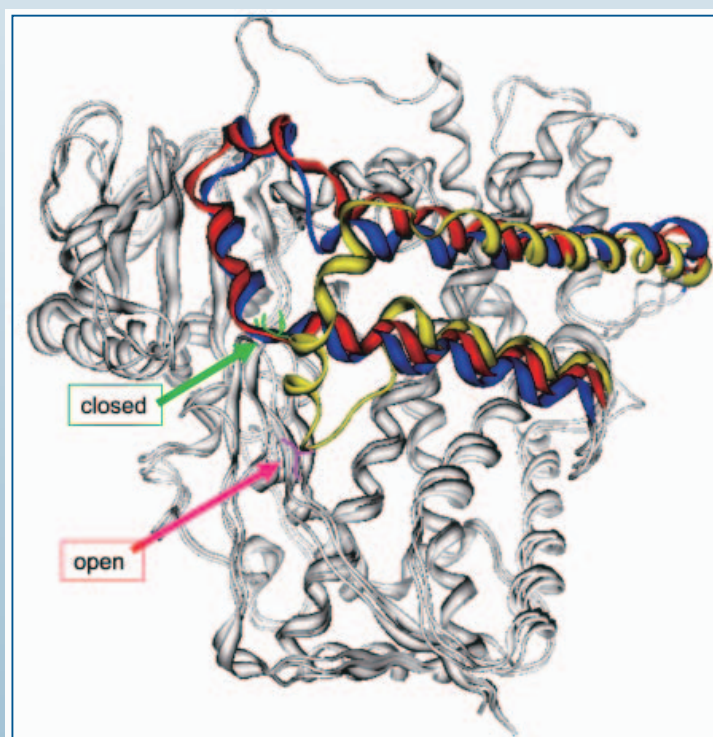


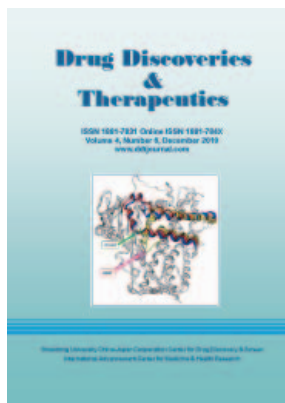
Drug Discoveries & Therapeutics

ISSN 1881-7831 Online ISSN 1881-784X
Volume 4, Number 6, December 2010
www.ddtjournal.com



Shandong University China-Japan Cooperation Center for Drug Discovery & Screen
International Advancement Center for Medicine & Health Research

Drug Discoveries & Therapeutics



Editor-in-Chief:

Kazuhisa SEKIMIZU
(The University of Tokyo, Tokyo, Japan)

Associate Editor:

Norihiro KOKUDO
(The University of Tokyo, Tokyo, Japan)

Drug Discoveries & Therapeutics is a peer-reviewed international journal published bimonthly by *Shandong University China-Japan Cooperation Center for Drug Discovery & Screen (SDU-DDSC)* and *International Advancement Center for Medicine & Health Research Co., Ltd. (IACMHR Co., Ltd.)*.

Drug Discoveries & Therapeutics mainly publishes articles related to basic and clinical pharmaceutical research such as pharmaceutical and therapeutical chemistry, pharmacology, pharmacy, pharmacokinetics, industrial pharmacy, pharmaceutical manufacturing, pharmaceutical technology, drug delivery, toxicology, and traditional herb medicine. Studies on drug-related fields such as biology, biochemistry, physiology, microbiology, and immunology are also within the scope of this journal.

Subject Coverage: Basic and clinical pharmaceutical research including Pharmaceutical and therapeutical chemistry, Pharmacology, Pharmacy, Pharmacokinetics, Industrial pharmacy, Pharmaceutical manufacturing, Pharmaceutical technology, Drug delivery, Toxicology, and Traditional herb medicine.

Language: English

Issues/Year: 6

Published by: IACMHR and SDU-DDSC

ISSN: 1881-7831 (Online ISSN 1881-784X)

CODEN: DDTRBX

Editorial and Head Office

Wei TANG, MD PhD
Executive Editor
Drug Discoveries & Therapeutics
Pearl City Koishikawa 603,
2-4-5 Kasuga, Bunkyo-ku,
Tokyo 112-0003, Japan
Tel: 03-5840-9697
Fax: 03-5840-9698
E-mail: office@ddtjournal.com
URL: www.ddtjournal.com



Drug Discoveries & Therapeutics

Editorial Board

Editor-in-Chief:

Kazuhisa SEKIMIZU (*The University of Tokyo, Tokyo, Japan*)

Associate Editor:

Norihiro KOKUDO (*The University of Tokyo, Tokyo, Japan*)

Executive Editor:

Wei TANG (*The University of Tokyo, Tokyo, Japan*)

Managing Editor:

Munehiro NAKATA (*Tokai University, Kanagawa, Japan*)

Web Editor:

Yu CHEN (*The University of Tokyo, Tokyo, Japan*)

English Editors:

Curtis BENTLEY (*Roswell, GA, USA*)

Thomas R. LEBON (*Los Angeles Trade Technical College, Los Angeles, CA, USA*)

China Office:

Wenfang XU (*Shandong University, Shandong, China*)

Editorial Board Members:

| | |
|--|--|
| Yoshihiro ARAKAWA (<i>Tokyo, Japan</i>) | Yuxiu LIU (<i>Nanjing, China</i>) |
| Santad CHANPRAPAPH (<i>Bangkok, Thailand</i>) | Hongxiang LOU (<i>Jinan, China</i>) |
| Fen-Er CHEN (<i>Shanghai, China</i>) | Ken-ichi MAFUNE (<i>Tokyo, Japan</i>) |
| Zhe-Sheng CHEN (<i>Queens, NY, USA</i>) | Norio MATSUKI (<i>Tokyo, Japan</i>) |
| Zilin CHEN (<i>Wuhan, China</i>) | Tohru MIZUSHIMA (<i>Kumamoto, Japan</i>) |
| Guanhua DU (<i>Beijing, China</i>) | Abdulla M. MOLOKHIA (<i>Alexandria, Egypt</i>) |
| Chandradhar DWIVEDI (<i>Brookings, SD, USA</i>) | Masahiro MURAKAMI (<i>Osaka, Japan</i>) |
| Mohamed F. EL-MILIGI (<i>Cairo, Egypt</i>) | Yoshinobu NAKANISHI (<i>Ishikawa, Japan</i>) |
| Harald HAMACHER (<i>Tuebingen, Germany</i>) | Yutaka ORIHARA (<i>Tokyo, Japan</i>) |
| Hiroshi HAMAMOTO (<i>Tokyo, Japan</i>) | Xiao-Ming OU (<i>Jackson, MS, USA</i>) |
| Xiaojiang HAO (<i>Kunming, China</i>) | Weisan PAN (<i>Shenyang, China</i>) |
| Waseem HASSAN (<i>Santa Maria, RS, Brazil</i>) | Rakesh P. PATEL (<i>Gujarat, India</i>) |
| Langchong HE (<i>Xi'an, China</i>) | Shafiqur RAHMAN (<i>Brookings, SD, USA</i>) |
| David A. HORNE (<i>Duarte, CA, USA</i>) | Shivanand P. PUTHLI (<i>Mumbai, India</i>) |
| Yongzhou HU (<i>Hangzhou, China</i>) | Adel SAKR (<i>Cincinnati, OH, USA</i>) |
| Wei HUANG (<i>Shanghai, China</i>) | Abdel Aziz M. SALEH (<i>Cairo, Egypt</i>) |
| Yu HUANG (<i>Hong Kong, China</i>) | Tomofumi SANTA (<i>Tokyo, Japan</i>) |
| Hans E. JUNGINGER (<i>Phitsanulok, Thailand</i>) | Yasufumi SAWADA (<i>Tokyo, Japan</i>) |
| Amrit B. KARMARKAR (<i>Mumbai, India</i>) | Brahma N. SINGH (<i>Commack, NY, USA</i>) |
| Toshiaki KATADA (<i>Tokyo, Japan</i>) | Hongbin SUN (<i>Nanjing, China</i>) |
| Gagan KAUSHAL (<i>Charleston, WV, USA</i>) | Benny K. H. TAN (<i>Singapore, Singapore</i>) |
| Ibrahim S. KHATTAB (<i>Safat, Kuwait</i>) | Renxiang TAN (<i>Nanjing, China</i>) |
| Hiromichi KIMURA (<i>Tokyo, Japan</i>) | Chandan M. THOMAS (<i>Bradenton, FL, USA</i>) |
| Shiroh KISHIOKA (<i>Wakayama, Japan</i>) | Murat TURKOGLU (<i>Istanbul, Turkey</i>) |
| Kam Ming KO (<i>Hong Kong, China</i>) | Zhengtao WANG (<i>Shanghai, China</i>) |
| Nobuyuki KOBAYASHI (<i>Nagasaki, Japan</i>) | Stephen G. WARD (<i>Bath, UK</i>) |
| Toshiro KONISHI (<i>Tokyo, Japan</i>) | Takako YOKOZAWA (<i>Toyama, Japan</i>) |
| Masahiro KUROYANAGI (<i>Hiroshima, Japan</i>) | Liangren ZHANG (<i>Beijing, China</i>) |
| Chun Guang LI (<i>Victoria, Australia</i>) | Jianping ZUO (<i>Shanghai, China</i>) |
| Hongmin LIU (<i>Zhengzhou, China</i>) | |
| Jikai LIU (<i>Kunming, China</i>) | |

(as of December 25, 2010)

Review

- 388 - 391 **Clinical development of histone deacetylase inhibitor romidepsin.**
Peng Guan, Hao Fang

Brief Report

- 392 - 398 **Synthesis, characterization, and anthelmintic activity of novel 6,7,8,9-tetrahydro-5H-5-phenyl-2-benzylidene-3-substituted hydrazino thiazolo (2,3-b) quinazoline derivatives and analogues.**
Theivendren P. Selvam, Palanirajan V. Kumar

Original Articles

- 399 - 404 **A new furoquinoline alkaloid with antifungal activity from the leaves of *Ruta chalepensis* L.**
Ahmed Emam, Mohamed Eweis, Medhat Elbadry
- 405 - 411 **Taxonomic identification of a novel strain of *Streptomyces cavourensis* subsp. *washingtonensis*, ACMA006, exhibiting antitumor and antibacteria activity.**
Xianwen Yuan, Ruili Yang, Xue Cao, Jianjun Gao
- 412 - 417 **Novel CYP2C19 629c>a mutant gene detection in Japanese subjects and estimation of its effect on conformation.**
Sayaka Kimura, Setsuo Hasegawa, Ai Kobayashi, Hiroki Yamaguchi, Masafumi Yohda, Takahiro Kubota
- 418 - 422 **Quantification of nebivolol hydrochloride in human plasma by liquid chromatography using fluorescence detection: Use in pharmacokinetic study.**
Laila Abdel-Fattah, Lobna Abdel-Aziz, Amira El-Kosasy, Mariam Gaied
- 423 - 434 **Use of factorial design in formulation and evaluation of ophthalmic gels of gatifloxacin: Comparison of different mucoadhesive polymers.**
Indrajeet D. Gonjari, Amrit B. Karmarkar, Trushali S. Khade, Avinash H. Hosmani, Rajesh B. Navale
- 435 - 441 **Improvement in the dissolution profile of diacerein using a surfactant-based solid dispersion technique.**
Snehal B. Patil, Dhanashri K. Shete, Sarika B. Narade, Sharda S. Surve, Ziya K. Khan, Satish B. Bhise, Yogesh V. Pore
- 442 - 452 **Solid-state characterization and *in vitro* dissolution behavior of lorazepam: Hydroxypropyl- β -cyclodextrin inclusion complex.**
Rakesh Patel, Manisha Patel
- 453 - 458 **Formulation, development, and optimization of immediate release nateglinide tablets by factorial design.**
Nihar R. Pani, Lila K. Nath, Biswanath Bhunia

CONTENTS

(Continued)

- 459 - 471 **Formulation of microemulsion gel systems for transdermal delivery of celecoxib: *In vitro* permeation, anti-inflammatory activity and skin irritation tests.**
Sara M. Soliman, Nevine S. Abdel Malak, Omaima N. El-Gazayerly, Abdel Aziz Abdel Rehim
- 472 - 483 **Preparation and characterization of oxybenzone-loaded solid lipid nanoparticles (SLNs) with enhanced safety and sunscreens efficacy: SPF and UVA-PF.**
Rania A. Sanad, Nevine S. Abdel Malak, Tahany S. El-Bayoomy, Alia A. Badawi
- 484 - 492 **Comparative study on the different techniques for the preparation of sustained-release hydrophobic matrices of a highly water-soluble drug.**
Shady M. Abd El-Halim, Maha M. Amin, Omaima N. El-Gazayerly, Nabaweya A. Abd El-Gawad
- 493 - 498 **Effect of Ceolus KG-802 on the dissolution rate of fenofibrate liquisolid tablets: Preformulation and formulation development studies.**
Amrit B. Karmarkar

Case Report

- 499 - 503 **The treatment effect of the atopic dermatitis by electrolytic-reduction ion water lotion.**
Tetsuo Shu, Masahiro Okajima, Yuko Wada, Ken-ichi Shimokawa, Fumiyoshi Ishii

Index

- 504 - 506 **Author Index**
- 507 - 512 **Subject Index**

Acknowledgements

Guide for Authors

Copyright

Review

Clinical development of histone deacetylase inhibitor romidepsin

Peng Guan, Hao Fang*

Department of Medicinal Chemistry, School of Pharmacy, Shandong University, Ji'nan, Shandong, China.

ABSTRACT: Histone deacetylase inhibitors have emerged as a promising epigenetic therapy for neoplastic indications. The US Food and Drug Administration granted approval to romidepsin for treatment of cutaneous T cell lymphoma (CTCL) in 2009. Phase I/II trials of romidepsin as monotherapy or hybrid therapy have demonstrated substantial efficacy profoundly in CTCL and peripheral T-cell lymphoma and marginally in other hematological malignancies and solid tumors, with a tolerable safety and toxicity profile. The current status of the clinical evaluation of romidepsin is detailed in the present contribution.

Keywords: Histone deacetylase inhibitors, romidepsin, clinical activity and toxicities

1. Histone deacetylases (HDACs)

A high level of interest has been focused on epigenetic regulation for cancer therapy over the past few years due to facilitated reverse of biochemical modifications in DNA or its chromatin protein complexes by chemotherapeutic intervention relative to genetic lesions in primary DNA sequence (1). Acetylation is probably among the best dissected epigenetic alterations and thus HDACs are recognized as an important enzyme of tumor epigenome for the corroborant competence to deacetylate histone as well as non-histone proteins (2). Indeed, extensive studies have recently revealed that HDACs can be tethered mechanistically to the oncogenesis, maintenance, and progression of cancer (2).

Eighteen HDACs have been identified in the mammalian genome and grouped to four classes based on their homology to the respective yeast transcriptional control factor sequence. Class III HDACs (Sirtuin-1 to -7) share domains with yeast silencing protein Sir2

and their dependence on NAD⁺ for deacetylase activity attenuates concerns here. Classical HDACs comprising Classes I, II, and IV HDAC family members are Zn²⁺-dependent: Class I HDACs (HDAC-1, -2, -3, and -8) are closely related to yeast reduced potassium dependency-3 (Rpd3); Class II HDACs, including Class IIa (HDAC-4, -5, -7, and -9) and Class IIb (HDAC-6 and -10), possess sequence similarity to yeast histone deacetylase-1 (Hda1); HDAC11 is homologues of both Rpd3 and Hda1, consequently defining Class IV HDAC. Classes I and IV HDACs are pervasively expressed in diverse tissues and generally localized to the nucleus (3). Nevertheless, Class II HDACs, which are restricted to certain cell types, display an uncertain cellular localization owing to their ability to shuttle between nucleus and cytoplasm (3).

2. Histone deacetylase inhibitors (HDACi) that have entered clinical studies

Recent research has shown that aberrant phenotypes of certain HDAC isoforms make them function nonredundantly to modulate hallmarks in several tumors (4). HDACi induce, to a variable extent, cell cycle and growth arrest, differentiation or apoptosis of malignant cells in *in vitro* models and *in vivo* xenografts (2). Strikingly, their antitumor efficacy has been clinically substantiated in broad spectrum neoplasms from both hematological and solid origins (5). Increasing amounts of HDACi have entered clinical evaluation for various cancers since vorinostat was first approved by FDA for the treatment of cutaneous T cell lymphoma (CTCL) (6). These candidates, with few exceptions, can be placed into major HDACi chemical classes including hydroxamates (vorinostat, CUDC-101, SB939, panobinostat, belinostat, resminostat, PCI-24781, givinostat, AR-42, CHR-2845, CHR-3996, JNJ-26481585, and R306465), cyclic peptides (romidepsin), benzamides (entinostat, mocetinostat, chidamide, and tacedinaline), and carboxylates (valproic acid, butyrate, AN-9, and phenylbutyrate). Their structures and clinical phases are shown in Figure 1.

Romidepsin has displayed good activity in hematological and solid malignancies with a tolerable safety profile as monotherapy or hybrid therapy in the clinic (7-19). On November 5, 2009, FDA granted

*Address correspondence to:

Dr. Hao Fang, Department of Medicinal Chemistry, School of Pharmacy, Shandong University, 44 West Wenhua Road, Ji'nan 250012, Shandong, China.
e-mail: haofangcn@sdu.edu.cn

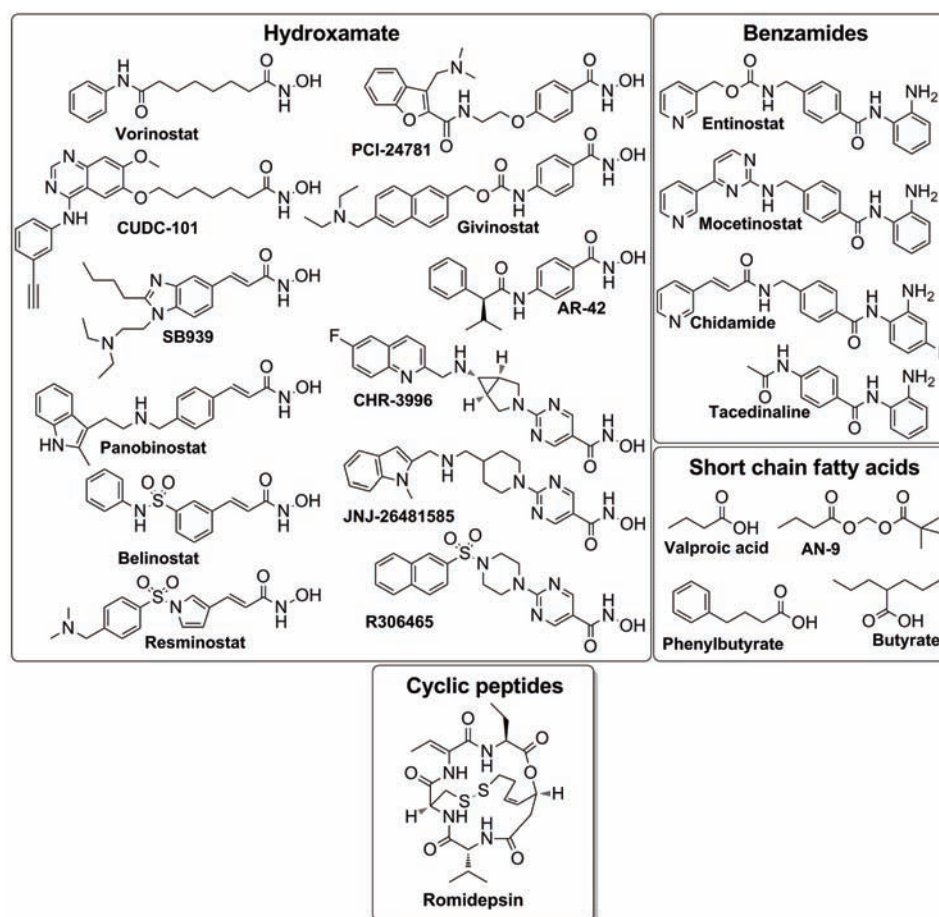


Figure 1. HDAC inhibitors under clinical development. Clinical trials for each candidate have been performed as follows: vorinostat, phase I/II/III; CUDC-101, phase I; SB939, phase I/II; panobinostat, phase I/II/III; belinostat, phase I/II; resminostat, phase II; PCI-24781, phase I/II; givinostat, phase II; AR-42, A phase I trial is not yet open for participant recruitment; CHR-3996, phase I; JNJ-26481585, phase I; R306465, A phase I trial has been completed; romidepsin, phase I/II; entinostat, phase I/II; mocetinostat, phase II; chidamide, phase II; tacedinaline, phase II/III; valproic acid, phase I/II/III; phenylbutyrate, phase I/II; AN-9, phase II; butyrate, phase II.

approval to use romidepsin for injection for treatment of CTCL in patients who have received at least one prior systemic therapy (20), which will hopefully accelerate the investigation of vorinostat for a broader range of cancers. We concentrate next on describing development of clinical application for romidepsin.

3. Clinical evaluation of romidepsin

In a pharmacokinetic report in T-cell lymphoma, romidepsin at doses of 14 or 18 mg/m² as a 4-hour intravenous (IV) infusion resulted in moderate interindividual variability in pharmacokinetics as exemplified by the population clearance of 15.9 L/h with between-patient variability of 37% (21).

Romidepsin demonstrated significant and durable single-agent clinical efficacy in CTCL, making it a valuable therapeutic option for treatment. It was reported that there were two phase II, open-label, multicenter trials in patients with CTCL of romidepsin at a dose of 14 mg/m² 4-hour IV infusion on days 1, 8, and 15 every 28 days (7-10). One clinical trial GPI-04-0001 enrolled 96 patients with stage IB-IVA CTCL who had

received one or more prior systemic therapies (7,8). The objective response rate (ORR) was 34% (6 patients with complete response (CR) and 27 patients with partial response (PR)) with median duration of response (DOR) of up to 15 months. Thirty-eight percent of 68 patients with advanced-stage (stages \geq IIB) disease had a response including 5 CRs. Response was determined by a composite endpoint comprised of cutaneous disease, lymph node involvement, and abnormal circulating T-cells (7). Additionally, 6 patients with a \geq 50% skin response, 5 patients with \geq 30% of the longest diameter node, and 27 patients with \geq 50% reduction in circulating Sézary cells did not achieve a composite response (8). The other clinical trial NCI 1312 involved 71 patients with CTCL at stage IA-IVB (9,10). There were 6 CRs and 21 PRs contributing to an ORR of 36% at all stages of disease. Responses were noted in 32% of patients at stage \geq IIB and 20% of patients at stage IV. An additional 27% of the enrolled patients had stable disease (SD) for at least 90 days. Median DOR was 11 months and the maximum progression-free survival was more than 5.5 years (9). Data from these two studies were pooled for an ORR of 35% in all stages (Table 1). It is noted that there was an

ORR of 42% in stage \geq IIB (10). The ORR, CR, DOR, improvement in all disease compartments, and responses at all stages make romidepsin an important therapeutic option for treatment of CTCL. Romidepsin is a robust and preferential therapy on the basis of the ORR, DOR, and improvement in total tumor burden at all stages.

A profound and sustained clinical benefit for romidepsin was observed in peripheral T-cell lymphoma (PTCL) besides CTCL as reported by Piekarz *et al.* (11). The ORR was 39% as shown in Table 2. The median DOR for all patients was 8.3 months (range from 1.6 months to more than 4.8 years) and that for CRs was 8.5 months (range from 4.6 months to more than 4.8 years) (11).

With increasing proof of limited clinical activity in other forms of hematologic and solid neoplasms (Table 2) (12-18), romidepsin was advanced into assessment as a combination therapy. Harrison *et al.* reported

that romidepsin in combination with bortezomib and dexamethasone attained a high response rate of 95% (ORR 67% + minimal response 28%) in impressive depth (44% CR + very good partial responses) in multiple myeloma (MM) (19).

Romidepsin showed a tolerable toxicity profile in CTCL. The most frequent drug-related adverse events (AEs) were generally mild and included nausea (67%), fatigue (49%), anorexia (37%), electrocardiography T-wave changes (29%), anemia (26%), dysgeusia (23%), neutropenia (22%), and leucopenia (20%). Serious AEs of supraventricular arrhythmia, ventricular arrhythmia, infection, neutropenia, white blood cell decrease, hyperuricemia, and hypotension were seen in 2% of patients (10). As for PTCL the most common AEs attributable to the study drug were nausea (86%), fatigue (79%), decreased platelets (70%) and decreased absolute granulocyte count (63%) (11). Cabell *et al.* evaluated the potential cardiac effects of romidepsin and found it mild on the QT interval which is below the threshold of regulatory and clinical concerns (22).

Romidepsin is being clinically evaluated in multiple phase I/II investigations as monotherapy and combination therapy for cancers of the urothelium, esophageal, pleural, and neuroendocrine areas, as well as acute myeloid leukemia, chronic lymphocytic leukemia, and small lymphocytic lymphoma in addition to the indications mentioned above (Table 3) (23).

Table 1. Data from clinical trial GPI-04-0001 and NCI 1312 and their pooled analyses

| | Clinical trials | | Pooled |
|------------|-----------------|-------------|--------------|
| | GPI-04-0001 | NCI 1312 | |
| CR, n (%) | 6/96 (6%) | 4/71 (6%) | 10/167 (6%) |
| PR, n (%) | 27/96 (28%) | 21/71 (30%) | 48/167 (29%) |
| ORR, n (%) | 33/96 (34%) | 25/71 (36%) | 58/167 (35%) |
| DOR | 15 months | 11 months | 13.8 months |

Table 2. Data from clinical trials of romidepsin

| Indication | CR, n (%) | PR, n (%) | SD, n (%) | Reference |
|--|------------|-------------|-------------|-----------|
| Peripheral T-cell lymphoma (PTCL) | 7/43 (16%) | 10/43 (23%) | NA | (11) |
| Acute myelogenous leukemia (AML) | 1/11 (9%) | 0 | 6/11 (55%) | (12) |
| Metastatic renal cell cancer | 1/29 (3%) | 1/29 (3%) | NA | (13) |
| Hormone refractory prostate cancer | 0 | 1/21 (5%) | 2/21 (10%) | (14) |
| Nonmedullary thyroid carcinoma | 0 | 0 | 10/20 (50%) | (15) |
| Lung cancer | 0 | 0 | 9/18 (50%) | (16) |
| Squamous cell carcinoma of the head and neck | 0 | 0 | 2/10 (20%) | (17) |
| Colorectal cancer | 0 | 0 | 4/25 (16%) | (18) |

Table 3. Ongoing clinical trials of romidepsin (23)

| Clinical trial | Indication | Clinical phase | Therapy |
|----------------|---|----------------|----------------|
| NCT00383565 | Relapsed/refractory non-Hodgkin's lymphoma | II | Monotherapy |
| NCT00007345 | Cutaneous T-cell lymphoma and relapsed peripheral T-cell lymphoma | II | Monotherapy |
| NCT00477698 | Early stage cutaneous T-cell lymphoma | I | Monotherapy |
| NCT00426764 | Progressive/relapsed peripheral T-cell lymphoma | II | Monotherapy |
| NCT00299351 | Peripheral T-cell lymphoma | II | Monotherapy |
| NCT00062075 | Relapsed/refractory acute myeloid leukemia | II | Monotherapy |
| NCT00963274 | Chronic lymphocytic leukemia/small lymphocytic lymphoma | I | + Bortezomib |
| NCT00431990 | Relapsed myeloma | I/II | + Bortezomib |
| NCT00066638 | Relapsed/refractory multiple myeloma | II | Monotherapy |
| NCT00098813 | Radioiodine-refractory metastatic thyroid carcinoma | II | Monotherapy |
| NCT00084461 | Metastatic neuroendocrine tumors | II | Monotherapy |
| NCT00112463 | Metastatic/unresectable soft tissue sarcomas | II | Monotherapy |
| NCT00084682 | Unresectable recurrent or metastatic squamous cell carcinoma of the head and neck | II | Monotherapy |
| NCT00104884 | Advanced malignant melanoma | II | Monotherapy |
| NCT00087295 | Advanced cancer of the urothelium | II | Monotherapy |
| NCT00098644 | Advanced lung, esophageal, or pleural cancer | I | + Flavopiridol |

4. Conclusions and future perspectives

HDACi create a robust avenue in epigenetic therapy for malignant diseases. Romidepsin has shown robust activity in hematological malignancies and solid tumors as well as tolerability in the clinic according to monotherapeutic and combined therapeutic regimens. Work is underway to continue clinical evaluation of current synergies and preclinical exploration of novel indications for optional treatment of cancers.

Acknowledgments

This work was supported by Shandong Provincial Natural Science Foundation, China (Grant No. ZR2010HM028).

References

- Egger G, Liang G, Aparicio A, Jones PA. Epigenetics in human disease and prospects for epigenetic therapy. *Nature*. 2004; 429:457-463.
- Bolden JE, Peart MJ, Johnstone RW. Anticancer activities of histone deacetylase inhibitors. *Nat Rev Drug Discov*. 2006; 5:769-784.
- Minucci S, Pelicci PG. Histone deacetylase inhibitors and the promise of epigenetic (and more) treatments for cancer. *Nat Rev Cancer*. 2006; 6:38-51.
- Johnstone RW. Histone-deacetylase inhibitors: Novel drugs for the treatment of cancer. *Nat Rev Drug Discov*. 2002; 1:287-299.
- Glaser KB. HDAC inhibitors: Clinical update and mechanism-based potential. *Biochem Pharmacol*. 2007; 74:659-671.
- FDA Approval for Vorinostat. <http://www.cancer.gov/cancertopics/druginfo/fda-vorinostat>
- Whittaker SJ, Demierre MF, Kim EJ, Rook AH, Lerner A, Duvic M, Scarisbrick J, Reddy S, Robak T, Becker JC, Samtsov A, McCulloch W, Kim YH. Final results from a multicenter, international, pivotal study of romidepsin in refractory cutaneous T-cell lymphoma. *J Clin Oncol*. 2010; 28:4485-4491.
- Kim E, Rook A, Kim Y, Demierre M, Lerner A, Duvic M, Robak T, Becker J, McCulloch W, Whittaker S. Romidepsin activity in all three disease compartments (skin, blood, lymph nodes) in patients with cutaneous T-cell lymphoma (CTCL). *ASCO Meeting Abstracts*. 2010; 28:8047.
- Bates S, Piekarz R, Wright J, *et al*. Final clinical results of a phase 2 NCI multicenter study of romidepsin in recurrent cutaneous T-cell lymphoma (molecular analyses included). *ASH Annual Meeting Abstracts*. 2008; 112:1568.
- Demierre M, Whittaker S, Kim Y, Kim E, Piekarz R, Prince M, Nichols J, Balsler J, Prentice A, Bates S, on behalf of all investigators. Pooled analyses of two international, multicenter clinical studies of romidepsin in 167 patients with cutaneous T-cell lymphoma (CTCL). *ASCO Meeting Abstracts*. 2009; 27:8546.
- Piekarz R, Wright J, Frye R, Allen SL, Craig M, Geskin L, Hutchins L, Joske D, Kirschbaum M, Leonard JP, Prince M, Reeder CB, Jaffe E, Bates S. Results of a phase 2 NCI multicenter study of romidepsin in patients with relapsed peripheral T-cell lymphoma (PTCL). *ASH Annual Meeting Abstracts*. 2008; 112:1567.
- Klimek VM, Fircanis S, Maslak P, Guernah I, Baum M, Wu N, Panageas K, Wright JJ, Pandolfi PP, Nimer SD. Tolerability, pharmacodynamics, and pharmacokinetics studies of depsipeptide (romidepsin) in patients with acute myelogenous leukemia or advanced myelodysplastic syndromes. *Clin Cancer Res*. 2008; 14:826-832.
- Stadler WM, Margolin K, Ferber S, McCulloch W, Thompson JA. A phase II study of depsipeptide in refractory metastatic renal cell cancer. *Clin Genitourin Cancer*. 2006; 5:57-60.
- Parker C, Molife R, Karavasilis V, Reid A, Patterson SG, Riggs C, Higano C, Stadler WM, McCulloch W, de Bono J. Romidepsin (FK228), a histone deacetylase inhibitor: Final results of a phase II study in metastatic hormone refractory prostate cancer (HRPC). *J Clin Oncol (Meeting Abstracts)*. 2007; 25:15507.
- Sherman EJ, Fury MG, Tuttle RM, Ghossein R, Stambuk H, Baum M, Lisa D, Su YB, Shaha A, Pfister DG. Phase II study of depsipeptide (DEP) in radioiodine (RAI)-refractory metastatic nonmedullary thyroid carcinoma. *J Clin Oncol (Meeting Abstracts)*. 2009; 27:6059.
- Schrump DS, Fischette MR, Nguyen DM, Zhao M, Li X, Kunst TF, Hancox A, Hong JA, Chen GA, Kruchin E, Wright JJ, Rosing DR, Sparreboom A, Figg WD, Steinberg SM. Clinical and molecular responses in lung cancer patients receiving Romidepsin. *Clin Cancer Res*. 2008; 14:188-198.
- Haigentz M Jr, Kim M, Sarta C, Keresztes RS, Smith RV, Belbin TJ, Mariadason JM, Grealley JM, Shapiro GI, Haddad RI. Clinical and translational studies of depsipeptide (romidepsin), a histone deacetylase (HDAC) inhibitor, in patients with squamous cell carcinoma of the head and neck (SCCHN): New York Cancer Consortium Trial P6335. *J Clin Oncol (Meeting Abstracts)*. 2007; 25:6065.
- Whitehead RP, Rankin C, Hoff PM, Gold PJ, Billingsley KG, Chapman RA, Wong L, Ward JH, Abbruzzese JL, Blanke CD. Phase II trial of romidepsin (NSC-630176) in previously treated colorectal cancer patients with advanced disease: A Southwest Oncology Group study (S0336). *Invest New Drugs*. 2009; 27:469-475.
- Harrison SJ, Quach H, Yuen K, *et al*. High response rates with the combination of bortezomib, dexamethasone and the pan-histone deacetylase inhibitor romidepsin in patients with relapsed or refractory multiple myeloma in a phase I/II clinical trial. *ASH Annual Meeting Abstracts*. 2008; 112:3698.
- FDA Approval for Romidepsin. <http://www.cancer.gov/cancertopics/druginfo/fda-romidepsin>
- Woo S, Gardner ER, Chen X, Ockers SB, Baum CE, Sissung TM, Price DK, Frye R, Piekarz RL, Bates SE, Figg WD. Population pharmacokinetics of romidepsin in patients with cutaneous T-cell lymphoma and relapsed peripheral T-cell lymphoma. *Clin Cancer Res*. 2009; 15:1496-1503.
- Cabell C, Bates S, Piekarz R, Whittaker S, Kim Y, Godfrey C, Schoonmaker C, McCulloch W, Nichols J, Burris HA. Systematic assessment of potential cardiac effects of the novel histone deacetylase (HDAC) inhibitor romidepsin. *ASCO Meeting Abstracts*. 2009; 27:19533.
- US National Institutes of Health. <http://clinicaltrials.gov/>

(Received November 21, 2010; Revised November 30, 2010; Accepted December 6, 2010)

Brief Report**Synthesis, characterization, and anthelmintic activity of novel 6,7,8,9-tetrahydro-5H-5-phenyl-2-benzylidene-3-substituted hydrazino thiazolo (2,3-b) quinazoline derivatives and analogues**Theivendren P. Selvam^{1,*}, Palanirajan V. Kumar²¹ Department of Biotechnology, Acharya Nagarjuna University, Guntur, Andhrapradesh, India;² School of Pharmacy, UCSI (University College Sadaya International) University, Cheras, Kuala Lumpur, Malaysia.

ABSTRACT: Several novel 6,7,8,9-tetrahydro-5H-5-phenyl-2-benzylidene-3-substituted hydrazino thiazolo (2,3-b) quinazoline derivatives were synthesized and evaluated for their anthelmintic activity in a passive avoidance test. Chemical structures of all of the newly synthesized compounds were confirmed by infrared spectroscopy, ¹H-nuclear magnetic resonance, mass spectroscopy, and elemental analyses. Out of 15 compounds, only 6e and 6o had good anthelmintic activity. Experimental data led to the conclusion that the synthesized compounds have anthelmintic activity.

Keywords: Thiazolo quinazoline, thiazolo quinazoline phenyl hydrazone, aromatic aldehyde substitution, benzylidene thiazolo quinazoline phenyl hydrazone, anthelmintic activity

1. Introduction

Parasitic nematodes are one of the most frequent sources of many infections in plants, animals, and humans particularly in tropical countries. Only three classes of broad-spectrum anthelmintics, benzimidazoles, imidazothiazoles, and macrocyclic lactones, are widely in use at the present. The search for novel anthelmintic drugs occupies an important role in veterinary medicine (1). In the course of a search for new anthelmintics, quinazoline was selected because quinazoline and substituted quinazoline rings are important building blocks of medicinal chemistry and have led to the discovery of a number of derivatives endowed with anthelmintic (2), antimicrobial (3-5), anti-inflammatory (6,7), diuretic (8), anticonvulsant

(9), antiallergic (10), antihypertensive (11,12), and antiparkinsonian activities (13). These findings led to the evaluation of a novel series of 6,7,8,9-tetrahydro-5H-5-phenyl-2-benzylidene-3-substituted hydrazino thiazolo (2,3-b) quinazoline compounds (6a-o) for their potential use as anthelmintics.

2. Materials and Methods**2.1. Instruments**

Melting points were determined in an open capillary tube and are uncorrected. Infrared spectroscopy (IR) spectra were recorded with KBr pellets (ABB Bomem FT-IR spectrometer MB 104; ABB Limited India, Bangaluru, India). ¹H-nuclear magnetic resonance (NMR) spectra (Bruker 400 NMR spectrometer; Bruker India, Mumbai, India) were recorded with tetramethylsilane as an internal reference. Mass spectral data were recorded with a Quadrupole mass spectrometer (Shimadzu GCMS QP5000; Shimadzu India, Chennai, India), and microanalyses were performed using a vario EL V300 elemental analyzer (Elementar Analysensysteme India, Chennai, India). The purity of the compounds was checked by thin-layer chromatography on pre-coated SiO₂ gel (HF₂₅₄, 200 mesh) aluminium plates (E. Merck, Mumbai, India) using ethyl acetate:benzene (1:3, v/v) and visualized in an ultraviolet chamber. IR, ¹H-NMR, mass spectral data, and elemental analyses were consistent with the assigned structures of all compounds.

2.2. Chemistry

The synthesis strategy leading to key intermediate and target compounds is illustrated in Figure 1. 6,7,8,9-tetrahydro-5H-5-(2'-hydroxy phenyl) thiazolo (2,3-b) quinazolin-3(2H)-one **3** prepared with equimolar quantities (0.039 mol) of cyclohexanone and benzaldehyde (0.039 mol) was collected in a beaker. A sodium hydroxide solution was added to make the solution alkaline, and the resulting solution was shaken

*Address correspondence to:

Dr. Theivendren Panneer Selvam, Department of Biotechnology, Acharya Nagarjuna University, Guntur-522510, Andhrapradesh, India.
e-mail: tpsphc@gmail.com

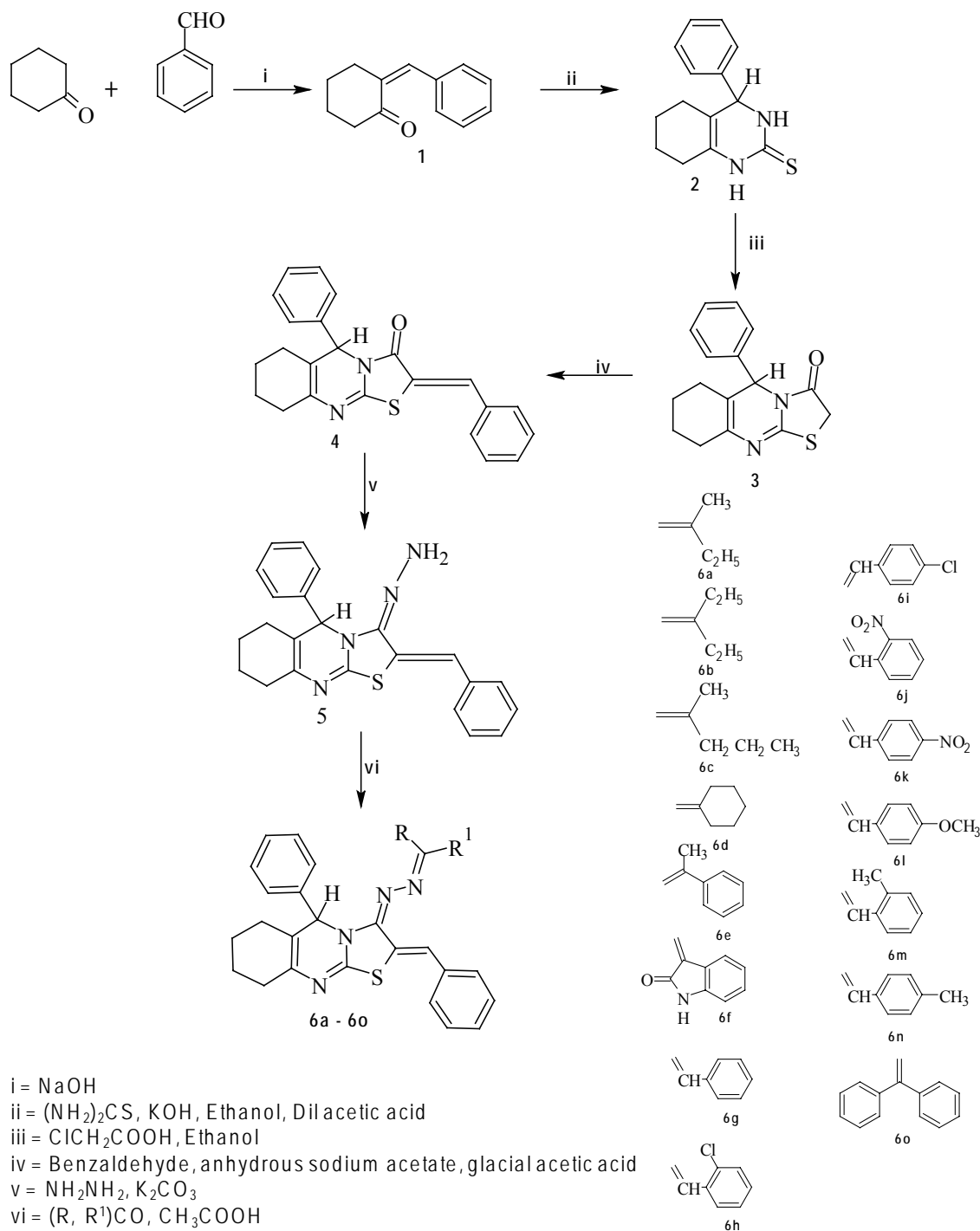


Figure 1. Synthetic scheme leading to key intermediate and target compounds.

and stored indoors. The solid thus obtained was filtered, washed with water, and recrystallized from absolute ethanol. A mixture of 2-benzylidene cyclohexanone ring **1** (0.039 mol), thiourea (0.03 mol), and potassium hydroxide (2.5 g) in ethanol (100 mL) was heated under reflux for 3 h. The reaction mixture was concentrated to half of its volume, diluted with water, and then acidified with dilute acetic acid and stored overnight. The solid thus obtained was filtered, washed with water, and recrystallized from ethanol to yield 3,4,5,6,7,8-hexahydro-4-phenyl quinazolin-2-thione **2**.

Chloroacetic acid (0.096 mol) was melted in a water bath and thione (0.009 mol) was added portion-wise to maintain homogeneity. The homogeneous mixture was further heated in a water bath for 30 min and stored overnight. The solid thus obtained was washed with water until neutralized and crystallized from ethanol to yield 6,7,8,9-tetrahydro-5H-5-phenyl thiazolo (2,3-b) quinazolin-3(2H)-one **3** (*14*), a cream-colored solid, (yield: 83%) mp. 142-144°C. IR cm^{-1} : 3,079 (Ar-CH), 3,012 (cycloalkane C-H), 1,727 (C=O), 1,615 (C=C); $^1\text{H-NMR}$ (CDCl_3): δ 6.74-7.76 (m, 5H, Ar-H), 5.75 (s,

1H, H-5), 3.40 (s, 2H, CH₂ thiazole ring), 1.64-2.35 (m, 8H, 4 × CH₂); EI-MS (m/z): 284 (M⁺); (Calcd for C₁₆H₁₆N₂OS; 284.38). Anal. Calcd for C₁₆H₁₆N₂OS; C, 67.58; H, 5.67; N, 9.85; Found: C, 67.60; H, 5.74; N, 9.90.

A mixture of **3** (0.002 mol), benzaldehyde (0.002 mol), and anhydrous sodium acetate (0.002 mol) in glacial acetic acid (10 mL) was heated under reflux for 4 h. The reaction mixture was stored overnight and the solid thus separated was filtered, washed with water, and recrystallized from ethanol to furnish 6,7,8,9-tetrahydro-5H-5-phenyl-2-benzylidene thiazolo (2,3-*b*) quinazolin-3(2H)-one **4**, a pale yellow solid, (yield: 75%), mp. 146-148°C, IR cm⁻¹: 3,100 (cycloalkane C-H), 3,059 (Ar-CH), 1,742 (C=O), 1,613 (C=C); ¹H-NMR (CDCl₃): δ 6.82-7.46 (m, 10H, Ar-H), 5.86 (s, 1H, H-5), 6.57 (s, 1H, =CH), 1.82-2.24 (m, 8H, 4 × CH₂); EI-MS (m/z): 372 (M⁺); (Calcd for C₂₃H₂₀N₂OS; 372.48). Anal. Calcd for C₂₃H₂₀N₂OS; C, 74.16; H, 5.41; N, 7.52; Found: C, 74.26; H, 5.31; N, 7.44.

Equimolar quantities of compound **4** (0.004 mol) and hydrazine hydrate (99%) (0.004 mol) were dissolved in 10 mL of warm ethanol and refluxed for 30 min. After standing for approximately 24 h at room temperature, the two compounds were separated by filtration, vacuum-dried, and recrystallized from warm ethanol to yield 6,7,8,9-tetrahydro-5H-5-phenyl-2-benzylidene-3-hydrazino thiazolo (2,3-*b*) quinazoline **5**, a dark brown solid, (yield: 69%), mp. 169-171°C, IR cm⁻¹: 3,144 (Ar-CH), 3,076 (cycloalkane C-H), 1,618 (C=C), 3,378 (N-H), 1,341 (N-H), 1,654 (C=N); ¹H-NMR (CDCl₃): δ 6.74-7.86 (m, 10H, Ar-H), 7.26 (s, 2H, NH₂), 5.56 (s, 1H, H-5), 6.38 (s, 1H, =CH), 1.90-2.42 (m, 8H, 4 × CH₂); EI-MS (m/z): 386 (M⁺); (Calcd for C₂₃H₂₂N₄S; 386.51). Anal. Calcd for C₂₃H₂₂N₄S; C, 71.47; H, 5.74; N, 14.50; Found: C, 71.42; H, 5.68; N, 14.66. A mixture of **5** (0.004 mol) and appropriate ketones/aldehydes (0.004 mol) in glacial acetic acid was refluxed for 38 h. The reaction mixture was poured into ice water. The solid obtained was recrystallized from ethanol to yield 6,7,8,9-tetrahydro-5H-5-phenyl-2-benzylidene-3-substituted hydrazino thiazolo (2,3-*b*) quinazoline compounds **6a-o**. Chemical data for derivatives **6a-o** are presented in the Appendix.

2.3. Animals

Indian adult earthworms (*Pheretima posthuma*) were used to study anthelmintic activity. The earthworms were collected from moist soil and washed to remove all fecal material. Earthworms 3-5 cm in length and 0.1-0.2 cm in width were used for all experimental protocols. Earthworms resemble intestinal roundworm parasites of human beings both anatomically and physiologically and hence can be used to study anthelmintic activity (15).

2.4. Anthelmintic activity

The newly synthesized compounds were tested for anthelmintic activity (16). *P. posthuma* (earthworms obtained from Lalbagh Botanical Garden, Bangalore, India) of nearly equal size (6 ± 1 cm) were selected randomly for the present study (17-19). The worms were acclimatized to laboratory conditions before experimentation. The earthworms were divided into four groups of six earthworms each. Albendazole, diluted with normal saline solution to obtain 0.1, 0.2, 0.5, and 1% (w/v), served as a reference and was poured into Petri dishes. The synthesized compounds were dissolved in a minimal quantity of dimethyl sulfoxide and diluted to prepare four concentrations, *i.e.* 0.1, 0.2, 0.5, and 1% (w/v), for each compound. Normal saline served as the control. Six earthworms of nearly equal size (6 ± 1 cm) were selected for use with each concentration and were placed in Petri dishes at room temperature (20). The time taken for complete paralysis and death were recorded. The mean time until paralysis and mean time until death were calculated for each sample (each reading was done in triplicate). The time taken for worms to become motionless was denoted as time until paralysis. To ascertain the time until death, each worm was frequently subjected to external stimuli to stimulate and induce movement in the earthworm if alive (21).

3. Results and Discussion

3.1. Chemistry

The series of heterocycles **6a-o** were synthesized by the reaction of **3** with appropriate hydrazine hydrate and ketones/aldehydes in the presence of anhydrous sodium acetate and glacial acetic acid, as indicated in Figure 1. Results of IR, ¹H-NMR, mass spectroscopy, and elemental analyses of the new compounds were in accordance with the assigned structures. The IR spectra of compounds **3** and **4** had stretching bands of the keto group at 1,715-1,740 cm⁻¹. In **5**, stretching and bending NH bands of thiazolo quinazoline moiety appeared at 3,300-3,400 cm⁻¹ and 1,300-1,350 cm⁻¹, respectively. The absence of keto group absorption at 1,715-1,740 cm⁻¹ and appearance of a strong intensity band in the IR spectra of compound **5** in the range of 1,610-1,655 cm⁻¹, attributable to C=N, provides strong evidence for condensation and also confirms the formation of azomethine **5**. The proton NMR spectra of thiazolo quinazoline and their corresponding derivatives have been recorded in CDCl₃. For **5**, the NH signal of 6,7,8,9-tetrahydro-5H-5-phenyl-2-benzylidene-3-hydrazino thiazolo (2,3-*b*) quinazoline moiety appeared at 7.26 (s) ppm. The position and presence of an NH signal in the ¹H-NMR spectra of final compounds confirmed the secondary NH proton in the thiazolo

quinazoline moiety. This clearly indicates that the thiazole-3-one moiety is involved in 6,7,8,9-tetrahydro-5H-5-phenyl-2-benzylidene-3-hydrazino thiazolo (2,3-*b*) quinazoline formation. All of these findings clearly demonstrate that the 3rd position of the keto group in the thiazole ring is converted into a secondary amino group, as indicated in Figure 1, and confirms the proposed structure of **5**.

3.2. Anthelmintic activity

Anthelmintic screening of 6,7,8,9-tetrahydro-5H-5-phenyl-2-benzylidene-3-substituted hydrazino thiazolo (2,3-*b*) quinazoline compounds **6a-o** indicated that they had better activity than albendazole, a standard anthelmintic. Of the compounds, 6,7,8,9-tetrahydro-5H-5-phenyl-2-benzylidene-3-(*N'*-3-pentylidene-hydrazino) thiazolo (2,3-*b*) quinazoline **6b** had maximum anthelmintic activity that was close to that of albendazole, a standard anthelmintic. Compound **6a** with the *N'*-sec-butylidene substituent had good activity; increased lipophilicity (1-ethylpropylidene group, compound **6b**; Figure 2) resulted in increased activity. Replacement of the 1-ethyl-propylidene group with its isomer 1-methyl-butylidene group (compound **6c**) retained this activity. Replacement of the alkyl chain with a cycloalkyl group and aryl alkyl groups (compounds **6d-6i**, respectively) resulted in decreased anthelmintic activity and replacement with an aryl group (compounds **6j-6o**) resulted in poor activity. The anthelmintic activity of test compounds decreased in the order of **6b** > **6c** > **6a** > **6d** > **6e** > **6f** > **6g** > **6h** > **6i**, as summarized in Table 1.

In conclusion, this paper describes the synthesis of novel substituted 6,7,8,9-tetrahydro-5H-5-phenyl-2-benzylidene-3-substituted hydrazino thiazolo (2,3-*b*)

quinazolines **6a-o** with strong anthelmintic activity compared to albendazole, a standard anthelmintic. The results demonstrate that substituents of the pentylidene and butylidene side chains had exceptional anthelmintic activity. Groups such as cycloalkyl, aryl alkyl, and aryl side chains in the 3-hydrazino position of the thiazolo quinazoline ring resulted in decreased or poor anthelmintic activity. Therefore, a similar range of lipophilicity could prove important to anthelmintic activity.

Acknowledgements

The authors wish to thank the Administration of D.C.R.M. Pharmacy College for the use of their facilities and Prof. D. Baggiya Selvi, Department of Pharmacognosy, Karnataka College of Pharmacy, Bangalore, India for her valued support.

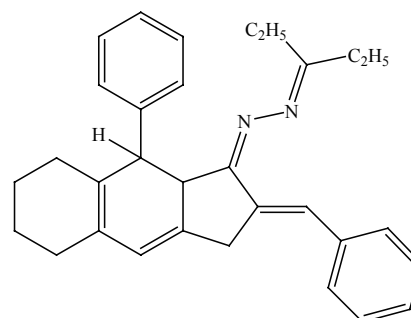


Figure 2. Structure of 6,7,8,9-tetrahydro-5H-5-phenyl-2-benzylidene-3-(*N'*-3-pentylidene-hydrazino) thiazolo (2,3-*b*) quinazoline.

Table 1. Anthelmintic activity of 6,7,8,9-tetrahydro-5H-5-phenyl-2-benzylidene-3-substituted hydrazino thiazolo (2,3-*b*) quinazoline

| Compound | Time until paralysis (min) | | | | Time until death (min) | | | |
|-------------|----------------------------|-------------|-------------|-------------|------------------------|-------------|-------------|-------------|
| | Concentration (%) | | | | Concentration (%) | | | |
| | 0.1 | 0.2 | 0.5 | 1 | 0.1 | 0.2 | 0.5 | 1 |
| 6a | 2.12 ± 0.11 | 2.53 ± 0.13 | 2.13 ± 0.02 | 1.22 ± 0.12 | 4.42 ± 0.01 | 3.12 ± 0.24 | 3.12 ± 0.01 | 1.43 ± 0.21 |
| 6b | 2.12 ± 0.11 | 2.02 ± 0.12 | 1.51 ± 0.02 | 0.63 ± 0.11 | 3.11 ± 0.04 | 2.53 ± 0.01 | 1.41 ± 0.13 | 1.12 ± 0.01 |
| 6c | 2.12 ± 0.12 | 2.13 ± 0.15 | 1.51 ± 0.05 | 1.01 ± 0.10 | 3.22 ± 0.05 | 2.61 ± 0.19 | 1.81 ± 0.24 | 1.13 ± 0.15 |
| 6d | 4.22 ± 0.12 | 4.15 ± 0.17 | 3.80 ± 0.17 | 2.31 ± 0.10 | 5.15 ± 0.12 | 4.10 ± 0.32 | 4.16 ± 0.31 | 2.11 ± 0.13 |
| 6e | 5.31 ± 0.02 | 4.21 ± 0.13 | 3.22 ± 0.04 | 3.52 ± 0.02 | 6.51 ± 0.13 | 6.11 ± 0.02 | 4.71 ± 0.13 | 3.22 ± 0.12 |
| 6f | 5.12 ± 0.01 | 4.13 ± 0.12 | 3.11 ± 0.15 | 2.32 ± 0.14 | 5.25 ± 0.13 | 4.13 ± 0.32 | 4.12 ± 0.31 | 2.13 ± 0.13 |
| 6g | 5.33 ± 0.01 | 4.22 ± 0.13 | 3.22 ± 0.07 | 2.11 ± 0.03 | 6.11 ± 0.43 | 6.42 ± 0.05 | 4.43 ± 0.14 | 3.22 ± 0.14 |
| 6h | 5.15 ± 0.52 | 4.55 ± 0.17 | 3.51 ± 0.16 | 2.52 ± 0.50 | 5.55 ± 0.52 | 4.15 ± 0.36 | 4.53 ± 0.35 | 2.15 ± 0.16 |
| 6i | 5.62 ± 0.07 | 4.23 ± 0.14 | 3.61 ± 0.14 | 2.16 ± 0.16 | 6.61 ± 0.13 | 6.16 ± 0.62 | 4.63 ± 0.13 | 3.27 ± 0.16 |
| 6j | 6.37 ± 0.02 | 5.23 ± 0.12 | 4.21 ± 0.03 | 4.51 ± 0.40 | 7.94 ± 0.18 | 8.13 ± 0.01 | 6.13 ± 0.14 | 5.29 ± 0.13 |
| 6k | 6.12 ± 0.12 | 5.15 ± 0.17 | 4.81 ± 0.18 | 4.32 ± 0.10 | 7.15 ± 0.12 | 7.14 ± 0.33 | 6.13 ± 0.32 | 5.12 ± 0.14 |
| 6l | 6.32 ± 0.02 | 5.22 ± 0.14 | 4.21 ± 0.04 | 4.51 ± 0.01 | 7.91 ± 0.13 | 7.12 ± 0.01 | 6.73 ± 0.12 | 5.29 ± 0.12 |
| 6m | 6.22 ± 0.10 | 5.12 ± 0.11 | 4.42 ± 0.15 | 4.22 ± 0.24 | 7.75 ± 0.23 | 7.44 ± 0.13 | 6.18 ± 0.13 | 5.22 ± 0.14 |
| 6n | 6.20 ± 0.02 | 5.21 ± 0.11 | 4.22 ± 0.25 | 4.72 ± 0.42 | 7.14 ± 0.27 | 8.22 ± 0.22 | 6.23 ± 0.13 | 5.14 ± 0.13 |
| 6o | 6.11 ± 0.15 | 5.17 ± 0.13 | 4.12 ± 0.15 | 4.22 ± 0.14 | 7.26 ± 0.18 | 7.27 ± 0.22 | 6.11 ± 0.31 | 5.23 ± 0.15 |
| Albendazole | 2.13 ± 0.17 | 2.03 ± 0.19 | 1.52 ± 0.03 | 0.83 ± 0.14 | 3.11 ± 0.05 | 2.52 ± 0.09 | 1.81 ± 0.14 | 1.13 ± 0.05 |

Values are expressed as mean ± S.E.M.

References

- Besier B. New anthelmintics for livestock: The time is right. *Trends Parasitol.* 2007; 23:21-24.
- Srivastava B, Shukla JS, Prabhakar YS, Saxena AK. Synthesis and QSAR in 2,3,6,8-substituted 1,3,4H-quinazolin-4-ones as potential anthelmintics. *Indian J Chem.* 1991; 30B:332.
- Pandeya SN, Sriram D, Nath G, De Clercq E. Synthesis, antibacterial, antifungal and anti-HIV valuation of Schiff and Mannich bases of isatin derivatives with 3-amino-2-methyl-mercapto quinazolin-4(3H)-one. *Pharma Acta Helv.* 1999; 74:11-17.
- Ishihara T, Kohno K, Ushio S, Iwaki K, Ikeda M, Kurimoto M. Tryptanthrin inhibits nitric oxide and prostaglandin E(2) synthesis by murine macrophages. *Eur J Pharmacol.* 2000; 407:197-204.
- Bekhit AA, Habib NS, el-Din A, Bekhit A. Synthesis and antimicrobial evaluation of chalcone and syndrome derivatives of 4(3H)-quinazolinone. *Boll Chim Farm.* 2001; 140:297-301.
- Chao Q, Deng L, Shih H, Leoni LM, Genini D, Carson DA, Cottam HB. Substituted isoquinolines and quinazolines as potential antiinflammatory agents. Synthesis and biological evaluation of inhibitors of tumor necrosis factor alpha. *J Med Chem.* 1999; 42:3860-3873.
- Maggio B, Daidone G, Raffa D, Plescia S, Mantione L, Catena Cutuli VM, Mangano NG, Caruso A. Synthesis and pharmacological study of ethyl 1-methyl-5-(substituted 3,4-dihydro4-oxoquinazolin-3-yl)-1H-pyrazole-4-acetates. *Eur J Med Chem.* 2001; 36:737-742.
- Eisa HM, el-Ashmawy MB, Tayel MM, el-Magd SA, el-Kashef HA. Fused pyrimidines. Synthesis of new derivatives of potential diuretic activity. *Boll Chim Farm.* 1996; 135:585-590.
- Laszóczi B, Kovács R, Nyikos L, Kardos J. A glutamate receptor subtype antagonist inhibits seizures in rat hippocampal slices. *Neuroreport.* 2002; 13:351-356.
- Singh SK, Paliwal JK, Grover PK, Gupta RC. Quantification of 2,3-dihydro-7-methoxy-pyrrolo-[2,1-b]-quinazolin-9(1H)-one, a new antiallergic agent, by high-performance liquid chromatography in serum. *J Chromatogr B Biomed Sci Appl.* 1994; 658:198-201.
- López-Farré A, Rodríguez-Feo JA, García-Colis E, Gomez J, López-Blaya A, Fortes J, de Andrés R, Rico L, Casado S. Reduction of the soluble cyclic GMP vasorelaxing system in the vascular wall of stroke-prone spontaneously hypertensive rats: Effect of the alpha1-receptor blocker doxazosin. *J Hypertens.* 2002; 20:463-470.
- Benning CM, Kyprianou N. Quinazoline-derived alpha1-adrenoceptor antagonists induce prostrate cancer cell apoptosis via an alpha1-adenoceptor-independent action. *Cancer Res.* 1992; 62:597-602.
- Srivastava VK, Palit G, Agarwal AK, Shanker K. Antiparkinsonian activity and behavioural effects of newer quinazolinones. *Pharmacol Res Commun.* 1987; 19:617-628.
- Sharma R, Kumar S, Pujari HK. Reaction of 3,4,5,6,7,8-hexahydro-4-phenyl quinazoline-2-thione with chloro acetic acid. *Indian J Chem.* 1991; 30B:425-426.
- Patil UK, Saraf S, Dixit VK. Hypolipidemic activity of seeds of *Cassia tora* Linn. *J Ethnopharmacol.* 2009; 90:249-252.
- Kuppast IJ, Nayak V. Anthelmintic activity of fruits of *Cordia dichotoma*. *Indian J Nat Prod.* 2003; 19:27-29.
- Dash GK, Suresh P, Kar DM, Ganpaty S, Panda SB. Evaluation of *Evolvulus alsinoids* Linn. for anthelmintic and antimicrobial activities. *J Nat Rem.* 2002; 2:182-185.
- Szewezuk VD, Mongelli ER, Pomilio AB. Antiparasitic activity of *Melia azadirach* growing in Argentina. *Molecular Med Chem.* 2003; 1:54-57.
- Shivkar YM, Kumar VL. Anthelmintic activity of latex of *Calotropis procera*. *Pharma Biol.* 2003; 41:263-265.
- Kaushik RK, Katiyar JC, Sen AB. Studies on the mode of the action of anthelmintics with *Ascaridia galli* as a test parasite. *Indian J Med Res.* 1974; 62:1367-1375.
- Lal J, Chandra S, Raviprakash V, Sabir M. *In vitro* anthelmintic action of some indigenous medicinal plants on *Ascaridia galli* worms. *Indian Physiol Pharmacol.* 1976; 20:64-68.

(Received October 10, 2010; Revised October 19, 2010; Re-revised November 1, 2010; Accepted November 6, 2010)

Appendix

6a. 6,7,8,9-Tetrahydro-5H-5-phenyl-2-benzylidene-3-(N'-2-butylidene-hydrazino) thiazolo (2,3-b) quinazoline

Yellow solid; yield: 78%; mp. 176-178°C; IR cm^{-1} : 3,078 (Ar-CH), 2,912 (cycloalkane C-H), 1,534 (C=C), 2,868 (C-H in CH_3), 1,656 (C=N); $^1\text{H-NMR}$ (CDCl_3): δ 6.82-7.46 (m, 10H, Ar-H), 6.18 (s, 1H, =CH), 5.18 (s, 1H, H-5), 2.64 (s, 3H, CH_3), 1.80-2.32 (m, 8H, $4 \times \text{CH}_2$), 1.4 (q, 2H, CH_2CH_3), 1.82 (t, $J = 7.0$ Hz, 3H, CH_2CH_3); EI-MS (m/z): 440 (M^+); (Calcd for $\text{C}_{27}\text{H}_{28}\text{N}_4\text{S}$; 440.60). Ana. Calcd for $\text{C}_{27}\text{H}_{28}\text{N}_4\text{S}$: C, 73.60; H, 6.41; N, 12.72; Found: C, 73.56; H, 6.49; N, 12.78.

6b. 6,7,8,9-Tetrahydro-5H-5-phenyl-2-benzylidene-3-(N'-3-pentylidene-hydrazino) thiazolo (2,3-b) quinazoline

Pale yellow crystals; yield: 72%; mp. 164-166°C; IR cm^{-1} : 3,065 (Ar-CH), 2,987 (cycloalkane, C-H), 1,541 (C=C), 2,833 (C-H in CH_3), 1,649 (C=N); $^1\text{H-NMR}$ (CDCl_3): δ 6.44-7.88 (m, 10H, Ar-H), 6.20 (s, 1H, =CH), 5.08 (s, 1H, H-5), 1.76-2.46 (m, 8H, $4 \times \text{CH}_2$), 1.92 (t, $J = 7.0$ Hz, 6H, CH_2CH_3), 1.52 (q, 4H, CH_2CH_3); EI-MS (m/z): 454 (M^+); (Calcd for $\text{C}_{28}\text{H}_{30}\text{N}_4\text{S}$; 454.63). Ana. Calcd for $\text{C}_{28}\text{H}_{30}\text{N}_4\text{S}$: C, 73.97; H, 6.65; N, 12.32; Found: C, 73.85; H, 6.68; N, 12.34.

6c. 6,7,8,9-Tetrahydro-5H-5-phenyl-2-benzylidene-3-(N'-2-pentylidene-hydrazino) thiazolo (2,3-b) quinazoline

Cream-colored crystals; yield: 68%; mp. 178-180°C; IR cm^{-1} : 3,068 (Ar-CH), 2,952 (cycloalkane C-H), 2,870 (C-H in CH_3), 1,544 (C=C), 1,660 (C=N); $^1\text{H-NMR}$ (CDCl_3): δ 6.72-7.36 (m, 10H, Ar-H), 6.24 (s, 1H, =CH), 5.22 (s, 1H, H-5), 2.84 (t, 3H, CH_2CH_3), 2.68 (s,

3H, CH₃), 1.82-2.36 (m, 8H, 4 × CH₂), 1.33 (sext, 2H, CH₂ CH₂CH₃), 0.91 (t, 2H, CH₂ CH₂CH₃); EI-MS (m/z): 454 (M⁺); (Calcd for C₂₈H₃₀N₄S; 454.63). Ana. Calcd for C₂₈H₃₀N₄S: C, 73.97; H, 6.65; N, 12.32; Found: C, 73.99; H, 6.63; N, 12.28.

6d. 6,7,8,9-Tetrahydro-5H-5-phenyl-2-benzylidene-3-(N'-cyclohexylidene-hydrazino) thiazolo (2,3-b) quinazoline

Yellow crystals; yield: 82%; mp. 182-184°C; IR cm⁻¹: 3,028 (Ar-CH), 2,924 (cycloalkane C-H), 1,666 (C=N), 1,544 (C=C); ¹H-NMR (CDCl₃): δ 6.92-7.86 (m, 10H, Ar-H), 6.24 (s, 1H, =CH), 5.26 (s, 1H, H-5), 1.60-2.04 (m, 18H, 9 × CH₂); EI-MS (m/z): 466 (M⁺); (Calcd for C₂₉H₃₀N₄S; 466.64). Ana. Calcd for C₂₉H₃₀N₄S: C, 74.64; H, 6.48; N, 12.01; Found: C, 74.68; H, 6.52; N, 12.11.

6e. 6,7,8,9-Tetrahydro-5H-5-phenyl-2-benzylidene-3-(N'-1-phenylethylidene-hydrazino) thiazolo (2,3-b) quinazoline

Yellow solid; yield: 84%; mp. 146-148°C; IR cm⁻¹: 3,098 (Ar-CH), 2,928 (cycloalkane C-H), 2,918 (C-H in CH₃), 1,606 (C=N), 1,542 (C=C); ¹H-NMR (CDCl₃): δ 6.62-7.16 (m, 15H, Ar-H), 6.06 (s, 1H, =CH), 2.74 (s, 3H, CH₃), 5.06 (s, 1H, H-5), 1.74-2.38 (m, 8H, 4 × CH₂); EI-MS (m/z): 488 (M⁺); (Calcd for C₃₁H₂₈N₄S; 488.65). Ana. Calcd for C₃₁H₂₈N₄S: C, 76.20; H, 5.78; N, 11.47; Found: C, 76.30; H, 5.82; N, 11.49.

6f. 6,7,8,9-Tetrahydro-5H-5-phenyl-2-benzylidene-3-(N'-1-oxo-indolin-2-one-3-ylidene-hydrazino) thiazolo (2,3-b) quinazoline

Pale yellow solid; yield: 70%; mp. 156-158°C; IR cm⁻¹: 3,086 (Ar-CH), 2,934 (cycloalkane C-H), 1,726 (C=O), 1,616 (C=N), 1,538 (C=C), 1,338 (C-N); ¹H-NMR (CDCl₃): δ 8.06 (s, 1H, NH), 6.60-7.18 (m, 14H, Ar-H), 6.12 (s, 1H, =CH), 5.16 (s, 1H, H-5), 1.78-2.32 (m, 8H, 4 × CH₂); EI-MS (m/z): 515 (M⁺); (Calcd for C₃₁H₂₅N₅OS; 515.63). Ana. Calcd for C₃₁H₂₅N₅OS: C, 72.21; H, 4.89; N, 13.58; Found: C, 72.18; H, 4.92; N, 13.48.

6g. 6,7,8,9-Tetrahydro-5H-5-phenyl-2-benzylidene-3-(N'-benzylidene-hydrazino) thiazolo (2,3-b) quinazoline

Cream-colored crystals; yield: 72%; mp. 159-160°C; IR cm⁻¹: 3,048 (Ar-CH), 2,934 (cycloalkane C-H), 1,608 (C=N), 1,568 (C=C); ¹H-NMR (CDCl₃): δ 8.1 (s, 1H, CH), 6.90-7.68 (m, 15H, Ar-H), 6.34 (s, 1H, =CH), 5.22 (s, 1H, H-5), 1.61-2.10 (m, 8H, 4 × CH₂); EI-MS (m/z): 474 (M⁺); (Calcd for C₃₀H₂₆N₄S; 474.62). Ana. Calcd for C₃₀H₂₆N₄S: C, 75.92; H, 5.52; N, 11.80; Found: C, 75.96; H, 5.58; N, 11.90.

6h. 6,7,8,9-Tetrahydro-5H-5-phenyl-2-benzylidene-3-

(N'-(2-chloro-benzylidene-hydrazino) thiazolo (2,3-b) quinazoline

Brown crystals; yield: 77%; mp. 162-164°C; IR cm⁻¹: 3,056 (Ar-CH), 2,926 (cycloalkane C-H), 1,598 (C=N), 1,562 (C=C), 816 (C-Cl); ¹H-NMR (CDCl₃): δ 8.12 (s, 1H, CH), 6.80-7.58 (m, 14H, Ar-H), 6.38 (s, 1H, =CH), 5.32 (s, 1H, H-5), 1.66-2.20 (m, 8H, 4 × CH₂); EI-MS (m/z): 511 (M⁺); (Calcd for C₃₀H₂₅ClN₄S; 509.60). Ana. Calcd for C₃₀H₂₅ClN₄S: C, 70.78; H, 4.95; N, 11.01; Found: C, 70.80; H, 4.99; N, 11.11.

6i. 6,7,8,9-Tetrahydro-5H-5-phenyl-2-benzylidene-3-(N'-(4-chloro-benzylidene-hydrazino) thiazolo (2,3-b) quinazoline

Yellow solid; yield: 79%; mp. 144-146°C; IR cm⁻¹: 3,058 (Ar-CH), 2,928 (cycloalkane C-H), 1,590 (C=N), 1,566 (C=C), 826 (C-Cl); ¹H-NMR (CDCl₃): δ 8.22 (s, 1H, CH), 6.76-7.52 (m, 14H, Ar-H), 6.36 (s, 1H, =CH), 5.34 (s, 1H, H-5), 1.68-2.28 (m, 8H, 4 × CH₂); EI-MS (m/z): 511 (M⁺); (Calcd for C₃₀H₂₅ClN₄S; 509.60). Ana. Calcd for C₃₀H₂₅ClN₄S: C, 70.78; H, 4.95; N, 11.01; Found: C, 70.82; H, 4.98; N, 11.08.

6j. 6,7,8,9-Tetrahydro-5H-5-phenyl-2-benzylidene-3-(N'-(2-nitro-benzylidene-hydrazino) thiazolo (2,3-b) quinazoline

Cream-colored crystals; yield: 77%; mp. 166-168°C; IR cm⁻¹: 3,048 (Ar-CH), 2,930 (cycloalkane C-H), 1,584 (C=N), 1,542 (C=C); ¹H-NMR (CDCl₃): δ 8.44 (s, 1H, CH), 6.72-7.58 (m, 14H, Ar-H), 6.22 (s, 1H, =CH), 5.24 (s, 1H, H-5), 1.52-2.18 (m, 8H, 4 × CH₂); EI-MS (m/z): 519 (M⁺); (Calcd for C₃₀H₂₅N₅O₂S; 519.62). Ana. Calcd for C₃₀H₂₅N₅O₂S: C, 69.34; H, 4.85; N, 13.48; Found: C, 69.38; H, 4.89; N, 13.54.

6k. 6,7,8,9-Tetrahydro-5H-5-phenyl-2-benzylidene-3-(N'-(4-nitro-benzylidene-hydrazino) thiazolo (2,3-b) quinazoline

Pale yellow crystals; yield: 71%; mp. 142-144°C; IR cm⁻¹: 3,066 (Ar-CH), 2,922 (cycloalkane C-H), 1,562 (C=N), 1,538 (C=C); ¹H-NMR (CDCl₃): δ 8.32 (s, 1H, CH), 6.68-7.52 (m, 14H, Ar-H), 6.12 (s, 1H, =CH), 5.32 (s, 1H, H-5), 1.40-2.20 (m, 8H, 4 × CH₂); EI-MS (m/z): 519 (M⁺); (Calcd for C₃₀H₂₅N₅O₂S; 519.62). Ana. Calcd for C₃₀H₂₅N₅O₂S: C, 69.34; H, 4.85; N, 13.48; Found: C, 69.40; H, 4.82; N, 13.46.

6l. 6,7,8,9-Tetrahydro-5H-5-phenyl-2-benzylidene-3-(N'-(4-methoxy-benzylidene-hydrazino) thiazolo (2,3-b) quinazoline

Brown solid; yield: 75%; mp. 150-152°C; IR cm⁻¹: 3,050 (Ar-CH), 2,968 (cycloalkane C-H), 1,560 (C=N), 1,550

(C=C); $^1\text{H-NMR}$ (CDCl_3): δ 8.44 (s, 1H, CH), 6.75-7.56 (m, 14H, Ar-H), 6.35 (s, 1H, =CH), 5.22 (s, 1H, H-5), 3.73 (s, 3H, OCH_3), 1.80-2.60 (m, 8H, $4 \times \text{CH}_2$); EI-MS (m/z): 504 (M^+); (Calcd for $\text{C}_{31}\text{H}_{28}\text{N}_4\text{OS}$; 504.65). Ana. Calcd for $\text{C}_{31}\text{H}_{28}\text{N}_4\text{OS}$: C, 73.78; H, 5.59; N, 11.10; Found: C, 73.82; H, 5.63; N, 11.14.

6m. 6,7,8,9-Tetrahydro-5H-5-phenyl-2-benzylidene-3-(N'-(2-methyl-benzylidene-hydrazino) thiazolo (2,3-b) quinazoline

Cream-colored crystals; yield: 80%; mp. 136-138°C; IR cm^{-1} : 3,054 (Ar-CH), 2,972 (cycloalkane C-H), 1,568 (C=N), 1,548 (C=C); $^1\text{H-NMR}$ (CDCl_3): δ 8.64 (s, 1H, CH), 6.70-7.52 (m, 14H, Ar-H), 6.36 (s, 1H, =CH), 5.33 (s, 1H, H-5), 3.73 (s, 3H, CH_3), 1.88-2.66 (m, 8H, $4 \times \text{CH}_2$); EI-MS (m/z): 488 (M^+); (Calcd for $\text{C}_{31}\text{H}_{28}\text{N}_4\text{S}$; 488.65). Ana. Calcd for $\text{C}_{31}\text{H}_{28}\text{N}_4\text{S}$: C, 76.20; H, 5.78; N, 11.47; Found: C, 76.24; H, 5.82; N, 11.49.

6n. 6,7,8,9-Tetrahydro-5H-5-phenyl-2-benzylidene-3-(N'-(4-methyl-benzylidene-hydrazino) thiazolo (2,3-b)

quinazoline

Cream-colored crystals; yield: 82%; mp. 148-150°C; IR cm^{-1} : 3,060 (Ar-CH), 2,976 (cycloalkane C-H), 1,574 (C=N), 1,554 (C=C); $^1\text{H-NMR}$ (CDCl_3): δ 8.60 (s, 1H, CH), 6.77-7.57 (m, 14H, Ar-H), 6.40 (s, 1H, =CH), 5.38 (s, 1H, H-5), 3.75 (s, 3H, CH_3), 1.90-2.70 (m, 8H, $4 \times \text{CH}_2$); EI-MS (m/z): 488 (M^+); (Calcd for $\text{C}_{31}\text{H}_{28}\text{N}_4\text{S}$; 488.65). Ana. Calcd for $\text{C}_{31}\text{H}_{28}\text{N}_4\text{S}$: C, 76.20; H, 5.78; N, 11.47; Found: C, 76.26; H, 5.88; N, 11.52.

6o. 6,7,8,9-Tetrahydro-5H-5-phenyl-2-benzylidene-3-(N'-(2-phenyl-benzylidene-hydrazino) thiazolo (2,3-b) quinazoline

Pale brown solid; yield: 78%; mp. 152-154°C; IR cm^{-1} : 3,088 (Ar-CH), 2,988 (cycloalkane C-H), 1,584 (C=N), 1,572 (C=C); $^1\text{H-NMR}$ (CDCl_3): δ 6.90-7.70 (m, 20H, Ar-H), 6.32 (s, 1H, =CH), 5.36 (s, 1H, H-5), 1.84-2.52 (m, 8H, $4 \times \text{CH}_2$); EI-MS (m/z): 550 (M^+); (Calcd for $\text{C}_{36}\text{H}_{30}\text{N}_4\text{S}$; 550.72). Ana. Calcd for $\text{C}_{36}\text{H}_{30}\text{N}_4\text{S}$: C, 78.51; H, 5.49; N, 10.17; Found: C, 78.55; H, 5.54; N, 10.22.

Original Article

A new furoquinoline alkaloid with antifungal activity from the leaves of *Ruta chalepensis* L.

Ahmed Emam^{1,*}, Mohamed Eweis², Medhat Elbadry³

¹ Department of Biochemistry, Faculty of Agriculture, Fayoum University, Fayoum, Egypt;

² Department of Botany, Faculty of Science, Cairo University, Cairo, Egypt;

³ Department of Agricultural Microbiology, Faculty of Agriculture, Fayoum University, Fayoum, Egypt.

ABSTRACT: Bioassay-guided separation with an eye toward antifungal activity led to the isolation of the new alkaloid 5-(1,1-dimethylallyl)-8-hydroxy-furo[2-3-b] quinoline (1) and the known bis-coumarin daphnoretin (2) as the active constituents of the chloroform extract obtained from the leaves of *Ruta chalepensis*. The structures of the metabolites were elucidated on the basis of their spectral characteristics (NMR, UV, and MS) and were compared with the literature. The antifungal activity of the isolated compounds was evaluated against the phytopathogenic fungi *Rhizoctonia solani*, *Sclerotium rolfsii*, and *Fusarium solani*, which cause root-rot and wilt diseases in several economically important food crops such as potato, sugar beet, and tomato.

Keywords: Furoquinoline alkaloid, bis-coumarin, *Ruta chalepensis*, Rutaceae, phytopathogenic fungi

1. Introduction

The increasing demand for food by the world's rapidly expanding population is exacerbated by the inevitable and substantial loss of crops due to plant diseases. Phytopathogenic fungi are among the most serious agriculture pests, and synthetic fungicides continue to be the least expensive and thus the most common approach for crop protection (1). Despite the effectiveness of these fungicides, the widespread use of chemicals has triggered public concern and scrutiny, mainly due to their persistence in the environment, toxicity to mammals and humans, harmful effects on non-target organisms, and induction of resistance and development of resistant strains of pathogens (2). Additionally, the number of new pesticides in the last

years has decreased mainly due to rising development and registration costs (2). As these facts demonstrate, there is an urgent need for new, safer, and ecologically compatible antifungal agents.

Over the past few years, significant efforts have been made to evaluate the effectiveness and safety of plant extracts and/or their metabolites for use in controlling plant diseases. Screening of plant extracts allows fast detection of potential sources of new bioactive molecules that can have applications in medicine or the control of agricultural pests (3).

Ruta chalepensis L. (syn. *Ruta bracteosa* DC., *Ruta angustifolia* Pers.), an evergreen shrub with the common name "Egyptian rue" indigenous to the Mediterranean region, is now cultivated in many parts of the world (4). The biological activities of *R. chalepensis* are frequently utilized in herbal therapy and the plant is used as a promoter of menstruation, treatment for hypertension, a topical treatment for ear aches and headaches, and an external treatment in the form of a skin antiseptic and insect repellent (5,6). Rue's active ingredients have antifungal and insecticidal properties that could prove beneficial to agriculture as well (7,8). Previous phytochemical investigation of this plant resulted in the isolation of a number of alkaloids and coumarins (9-11). Using an aqueous extract of the plant's leaves, a recent study isolated two flavonoids, which are thought to be responsible for its antioxidant activity (12), and two furoquinoline alkaloids, which are thought to be responsible for its antibacterial activity (13).

The objective of the present study was to detect and isolate new metabolites with antifungal activity from a chloroform extract of *R. chalepensis* leaves and then evaluate their inhibition of *Rhizoctonia solani*, *Sclerotium rolfsii*, and *Fusarium solani* since these phytopathogenic fungi cause root-rot and wilt diseases in several economically important crops.

2. Materials and Methods

2.1. General experimental procedures

Analytical and preparative thin-layer chromatography

*Address correspondence to:

Dr. Ahmed M. Emam, Department of Biochemistry, Faculty of Agriculture, Fayoum University, Fayoum 63514, Egypt.
e-mail: maoudimam@yahoo.com

(TLC) was carried out on Merck precoated silica gel plates (F₂₅₄ thickness: 0.25 mm and 2.0 mm, respectively). Spots were visualized under ultraviolet (UV) light (254 and 365 nm) and by spraying with 30% H₂SO₄ in methanol followed by heating at 105°C for 5 min and by spraying with modified Dragendorff's reagent to detect alkaloids. The preliminary phytochemical screening of the purified compounds for saponins, flavonoids, alkaloids, tannins, and glycosides was performed on TLC plates according to the methods described (14). ¹H, ¹³C, and heteronuclear multiple bond correlation (HMBC) nuclear magnetic resonance (NMR) spectra were recorded in dimethyl sulfoxide (DMSO)-d₆ on a Varian Mercury VXR 300 spectrometer (300 MHz for ¹H and 75 MHz for ¹³C; Varian, Inc., Palo Alto, CA, USA). NMR experiments were performed at the Central Laboratory of the Faculty of Science, Cairo University, Giza, Egypt. UV spectra were recorded on a Cecil 3000 Series spectrophotometer (Cecil Instruments Ltd., Cambridge, UK). Mass spectra (MS) were recorded on a GC/MS QP 100 EX Shimadzu Mass spectrometer (Shimadzu, Kyoto, Japan) at 70 eV. The MS experiments were carried out at the Macro-Analytical Center, Faculty of Science, Cairo University.

2.2. Plant material

Leaves of *R. chalepensis* (Rutaceae) were collected in the flowering stage in June 2004 from plants growing on the experimental farm of the Faculty of Agriculture, Cairo University, Giza, Egypt. Plant taxonomists in the Botany Department, Faculty of Science, Cairo University confirmed the taxonomic identification of the plant species. A vouchered specimen (R.C. 30) was deposited in the herbarium of the Department of Biochemistry, Faculty of Agriculture, Fayoum University, Fayoum, Egypt.

2.3. Extraction and isolation

Powdered air-dried leaves (350 g) were extracted three times overnight with 80% ethanol (700 mL each time) at room temperature (25 ± 2°C). After filtration, the combined extracts were evaporated under reduced pressure to yield 55.2 g of residue. A portion of the ethanol extract (40 g) was dispersed in water (150 mL) and partitioned with chloroform (3 × 50 mL) to remove the chloroform-soluble components (Fr A, 6.5 g). The aqueous layer was freeze-dried (33.5 g) and then extracted with chloroform:methanol:water (70:30:5, v/v; 150 mL). After centrifugation, both the supernatant and the precipitate were dried under reduced pressure to yield 4.6 g (Fr B) and 28.8 g (Fr C), respectively. Fractions A, B, and C were subsequently tested for their antifungal activity.

Bioactive fraction A (6.5 g) was subjected

to chromatography in order to isolate antifungal components as follows: 6.0 g of Fr A were loaded on a chromatographic column (2 cm × 60 cm) packed with silica gel (230-400 mesh, 150 g, Merck & Co., Inc., Whitehouse Station, NJ, USA) and eluted with a gradient of chloroform:methanol:water (100:0:0, 90:10:0, 85:15:0, 70:30:5, 60:40:5, and 0:100:0, v/v; 200 mL for each eluent). Ten fractions of each eluent were collected. Because of their similarities in TLC, the collected fractions were combined with 17 fractions that were further tested for antifungal activity. Two fractions (1 and 2) exhibited strong antifungal activity. Fraction 1 eluted with 100% chloroform (441 mg) was further purified on silica gel with chloroform:benzene (50:50, v/v) as the mobile phase to provide six fractions (A'-F'). Fraction A' (341.8 mg) containing the major metabolite was further purified on a Sephadex LH 20 column (GE Healthcare Bio-Sciences, Piscataway, NJ, USA) with methanol followed by preparative TLC with chloroform:benzene (60:40, v/v) to yield 275 mg of pure active compound **1**. Fraction 2 also eluted with 100% chloroform (870 mg) was further purified on silica gel using chloroform:benzene (80:20, v/v; 400 mL). On the basis of their similarities in TLC, 40 fractions were combined with 10 fractions (G'-P'). Fraction I' (410.2 mg) was further purified several times on Sephadex LH 20 with methanol as the eluent followed by preparative TLC with chloroform:benzene (70:30, v/v) to give 226 mg of pure active compound **2**.

2.4. Test organisms

Fungicidal activity tests were performed with *R. solani*, *S. rolfisii*, and *F. solani*. These fungi had been isolated from diseased sugar beet roots and identified and their pathogenicity had been confirmed (15). The cultures were maintained on malt extract agar (MEA) medium (malt extract 20 g, peptone 5 g, and agar 15 g per liter of culture) and covered with phosphate buffer (pH 6.5) at 4 ± 1°C (16).

2.5. Preliminary fungicidal activity tests

The disk diffusion technique was used to test the fungicidal activity of the aqueous ethanol extract of *R. chalepensis* leaves and its fractions against each of the three phytopathogenic fungi on MEA medium at 25 ± 1°C (17).

2.6. Evaluation of the antifungal activity of the isolated compounds

2.6.1. Percent germination of sclerotia

Sclerotia of *R. solani* and *S. rolfisii*, produced on potato dextrose agar (PDA), were surface-disinfected by soaking them for 5 min in bromine/water (1:400, w/v)

to kill hyphal extensions, washed thoroughly with distilled water, and dried. Ten sclerotia per Petri dish of each pathogen were plated on an agar surface (1.5%, w/v) supplemented with relevant amounts of each purified compound to produce concentrations in the range of 10-40 µg/mL in the medium (15). The dishes were incubated at 27°C for 16 h for *R. solani* and 30 h for *S. rolfisii*, and the percentage of germinated sclerotia was determined and the average length of hyphal elongation was measured at 45× magnification using a calibrated micrometer in the microscope eyepiece. Five plates were prepared for each treatment and the means were compared.

2.6.2. Percent germination of conidial spores

Glass slides were supported on a glass rod in Petri dishes lined with moist filter paper. One mL of spore suspension (1×10^5 conidia/mL) of *F. solani* in an aqueous solution with the desired compound concentration or with distilled sterile water (DSW) as a control (check) was placed on each slide. Slides were then incubated at 27°C for 16 h in complete darkness. The percent germination was assessed and the average length of the germ tubes was measured at 45× magnification using a calibrated micrometer in the microscope eyepiece (18). Five slides were used per each treatment and the means were compared.

2.6.3. Production of sclerotia and conidiospores

Each purified compound was mixed aseptically with MEA medium in amounts calculated to produce the required concentration and then poured into Petri dishes. The fungi *R. solani* and *S. rolfisii* that produced sclerotia and *F. solani* that produced conidiospores were grown in the dark on PDA at 27°C for 4 days. Four-mm diameter agar plugs were removed from the leading edges of colonies with a sterile cork borer, and one such plug was placed in the center of a 90-mm Petri dish (plate) containing MEA medium of the required concentration. Plates were wrapped with parafilm and incubated at 27°C for 9 days (15). For *R. solani* and *S. rolfisii*, the number of sclerotia produced per plate was visually counted for each treatment. For *F. solani*, the number of spores produced was calculated with a hemacytometer (15). Five plates were prepared for each treatment and the means were compared.

2.6.4. Dry mass of mycelia

Each purified compound was mixed aseptically with the malt extract broth MEB medium in amounts calculated to produce concentrations of 10-40 µg/mL and dispensed in 50 mL aliquots into 250-mL Erlenmeyer flasks. The fungi *R. solani*, *S. rolfisii*, and *F. solani* were grown in the dark on PDA at 27°C for 4 days. A four-

mm diameter agar plug was removed and incubated at 27°C for 9 days as described above. The mycelia were harvested, dried to constant weight at 80°C, and then the dry mass yield and final pH value were recorded. Five flasks were prepared for each treatment and the means were compared. The natural antifungal agent chitosan (9012-76-4; Sigma-Aldrich, St Louis, MO, USA) at a concentration of 20 µg/mL was used as a positive control.

2.7. Statistical analysis

Experiments were conducted 5 times, and the results obtained were submitted to analysis of variance. Significance was expressed as the least significant difference (LSD) at levels of 5 and 1%.

3. Results and Discussion

The ethanol extract (80%) of the *R. chalepensis* leaves exhibited antifungal activity against the three phytopathogenic fungi *R. solani*, *S. rolfisii*, and *F. solani* when tested with the disk diffusion technique. The inhibition zone diameter was 10, 18, and 12 mm, respectively. The active ethanol extract (80%) of *R. chalepensis* leaves was fractionated into three fractions with chloroform (Fr A, 6.5 g), and then extracted with chloroform:methanol:water to yield 4.6 g (Fr B) and 28.8 g (Fr C), respectively. Fractions A, B, and C were tested for antifungal activity with the disk diffusion technique. Among the tested fractions, only the chloroform-soluble component (fraction A') possessed antifungal activity against the three pathogenic fungi. Bioactivity-guided purification of this fraction with chromatography led to the isolation of two compounds, I (275 mg, 4.58%) and II (226 mg, 3.77%), in pure form.

Metabolite I was obtained as a colorless amorphous powder and had a positive color reaction with modified Dragendorff's reagent on TLC, suggesting an alkaloid. Electron ionization MS revealed a molecular ion peak (M^+) at m/z 253 (100%), indicating a molecular formula of $C_{16}H_{15}NO_2$, which agreed with the results of elemental analysis. The UV spectrum of this compound indicated a conjugated aromatic system (287 and 234 nm), and this was confirmed by the NMR spectra.

The furoquinoline skeleton of this compound was established because of the presence of 6 aromatic, 2 quaternary (δ 138.7 and 158.8 ppm), and 3 olefinic carbons (δ 98.2, 106.5 and 150.6 ppm) as well as the presence of 3 olefinic proton signals at δ 7.03 (1H, d, $J = 2.1$ Hz), 8.04 (1H, d, $J = 2.01$ Hz), characteristic of furan ring protons (H-3 and H-2), and at δ 7.59 (1H, s; H-4) along with two adjacent aromatic protons coupled with each other at δ 7.93 ppm (2H, d, $J = 6.3$ Hz; H-6 and 7). The presence of only two aromatic protons

indicated that all other carbons were substituted. These data matched the furoquinoline skeleton of many alkaloids isolated from the Rutaceae family (19-21).

The presence of a dimethyl allyl group was indicated by resonances in the ^1H -NMR spectrum corresponding to a pair of geminal methyls at δ 1.14 (6H, s) and a vinylic group at δ 5.05 (2H, ddd, $J = 1.2, 10.5, 17.4$ Hz) and 6.14 (1H, dd, $J = 11.1, 17.4$ Hz) as well as by comparison with published metabolites having the same functionality (22).

The presence of a hydroxyl group was established by elemental analysis as well as by the presence of a bathochromic shift in the UV spectrum upon addition of sodium acetate. The position of this hydroxyl group was established by comparison to chemical shifts reported in the literature (19-21).

The ^1H and ^{13}C -NMR data for this compound were similar to those for a furoquinoline alkaloid (robustine) isolated from *Philothea deserti* belonging to the family Rutaceae (21) but differed due to the absence of the methoxy group at C-4 and the presence of the 1,1-dimethylallyl group at C-5. On the basis of these findings, the furoquinoline alkaloid (**I**) was deduced to be 5-(1,1-dimethylallyl)-8-hydroxy-furo [2-3-b] quinoline (**1**). This structure was confirmed by heteronuclear correlations obtained from HMBC data (Table 1).

Metabolite **2** was obtained as a colorless amorphous powder. The mass spectrum had a molecular ion peak at m/z 352 in accordance with the molecular

formula $\text{C}_{19}\text{H}_{12}\text{O}_7$. This compound was identified as the bis-coumarin daphnoretin by comparing its ^1H and ^{13}C -NMR data with those previously reported for daphnoretin isolated from the Rutaceae family (23,24). This is the first report of daphnoretin from *R. chalepensis*.

The antifungal efficacy of the isolated compounds 5-(1,1-dimethylallyl)-8-hydroxy-furo [2-3-b] quinoline (compound **1**) and daphnoretin (compound **2**) against the three phytopathogenic fungi was studied *in vitro* and the results are shown in Table 2. The data obtained indicated that the percent germination (G %) of *R. solani* and *S. rolfsii* sclerotia decreased with an increasing concentration of the two compounds. Metabolite **2** was responsible for strong inhibition of sclerotia or spore germination (79.83%, 83.7%, and 88%) whereas lower inhibition in the range of 70.03%, 76.7%, and 70.7% was achieved with compound **1** for *R. solani*, *S. rolfsii*, and *F. solani*, respectively, at a concentration of 20 $\mu\text{g/mL}$. However, *S. rolfsii* was found to be more sensitive to compounds **1** and **2** than the fungus *R. solani* was.

The average length of hyphal extensions (L_h , μm) and dry mass yield (D_m , mg) were also affected. Inhibition increased proportionally with the concentration of compounds **1** and **2**. Compound **2** was found to be more effective than compound **1** in this respect.

The number of *R. solani* and *S. rolfsii* sclerotia produced per plate at different concentrations was

Table 1. NMR data for compound 1 (in DMSO- d_6)

| Atom No. | ^{13}C | ^1H | HMBC |
|----------|-----------------|-----------------------------|----------------------------|
| 1 | — | — | |
| 2 | 150.6 | 8.04 (d, 2.1) | C3, C3a |
| 3 | 106.5 | 7.03 (dd, 0.9, 2.1) | C2, C9a, C4 |
| 3a | 138.7 | — | |
| 4 | 98.2 | 7.59 (s) | C3a, C4a, C9a, C8a, C5, C3 |
| 4a | 131.7 | — | |
| 5 | 124.2 | — | |
| 6 | 120.3 | 7.93 (d, 6.3) | C5, C7, C1', C8, C4a |
| 7 | 115.5 | 7.93 (d, 6.3) | C6, C8, C5, C8a |
| 8 | 155.1 | — | |
| 8a | 145.3 | — | |
| 9 | — | — | |
| 9a | 158.8 | — | |
| 1' | 43.3 | — | |
| 2' | 111.9 | 6.14 (dd, 11.1, 17.4) | C'1, C'3, C5, C'4, C'5 |
| 3' | 147.5 | 5.05 (ddd, 1.2, 10.5, 17.4) | C2', C1' |
| 4' | 25.9 | 1.41 (s) | C1', C5, C2' |
| 5' | 25.9 | 1.41 (s) | C1', C5, C2' |

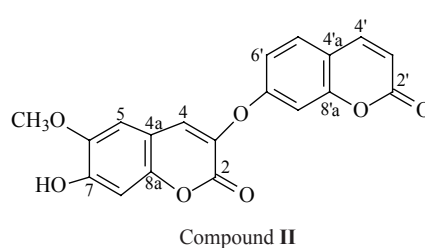
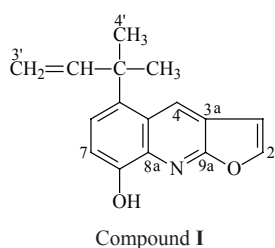


Table 2. Effect of metabolites 1 and 2 on the germination (G%), average length of hyphal extensions (L_h), dry mass yield (D_m), and production of sclerotia of *R. solani* and *S. rolfsii* and macroconidia of *F. solani*

| Treatment | Metabolite 1 ($\mu\text{g/mL}$) | | | | Metabolite 2 ($\mu\text{g/mL}$) | | | |
|-------------------|-----------------------------------|-------------------------|------------|--------------------------------------|-----------------------------------|-------------------------|------------|--------------------------------------|
| | G% | L_h (μm) | D_m (mg) | Number of sclerotia or macroconidia* | G% | L_h (μm) | D_m (mg) | Number of sclerotia or macroconidia* |
| <i>R. solani</i> | | | | | | | | |
| Positive control | 47.2 | 707.5 | 869.1 | 48 | | | | |
| Negative control | 71.4 | 877.1 | 1108.1 | 63 | 71.4 | 877.1 | 1108.1 | 68 |
| 10 | 38.1 | 574.1 | 791.2 | 44 | 22.6 | 385.2 | 587.3 | 23 |
| 20 | 21.4 | 380.2 | 583.4 | 22 | 14.4 | 130.2 | 241.2 | 13 |
| 30 | 13.2 | 128.7 | 234.1 | 14 | 4.5 | 98.2 | 160.2 | 7 |
| 40 | 4.8 | 101.2 | 171.3 | 7 | – | – | – | – |
| LSD at 1% | 3.8 | 12.8 | 16.5 | 6.1 | 3.9 | 11.8 | 15.3 | 6.0 |
| LSD at 5% | 1.4 | 7.6 | 8.7 | 2.8 | 1.5 | 7.5 | 7.8 | 3.1 |
| <i>S. rolfsii</i> | | | | | | | | |
| Positive control | 42.4 | 502.7 | 470.4 | 500 | | | | |
| Negative control | 58.6 | 682.4 | 676.1 | 591 | 58.6 | 682.4 | 676.1 | 591 |
| 10 | 26.4 | 383.1 | 352.1 | 339 | 14.2 | 190.2 | 182.1 | 140 |
| 20 | 13.6 | 198.4 | 181.2 | 145 | 9.5 | 140.2 | 131.2 | 110 |
| 30 | 10.5 | 147.3 | 135.6 | 115 | 3.8 | 62.2 | 84.1 | 80 |
| 40 | 3.4 | 61.2 | 82.1 | 85 | – | – | – | – |
| LSD at 1% | 4.3 | 14.1 | 16.7 | 6.2 | 4.4 | 11.2 | 10.7 | 6.2 |
| LSD at 5% | 1.5 | 8.6 | 8.7 | 2.6 | 1.6 | 7.3 | 6.2 | 2.6 |
| <i>F. solani</i> | | | | | | | | |
| Positive control | 44.8 | 9.1 | 301.8 | 260.7 | | | | |
| Negative control | 60.1 | 13.6 | 399.2 | 332.7 | 60.1 | 13.6 | 399.2 | 332.7 |
| 10 | 21.3 | 8.9 | 229.7 | 196.1 | 14.5 | 7.8 | 181.2 | 158.2 |
| 20 | 17.6 | 7.6 | 190.2 | 159.6 | 7.6 | 5.3 | 142.1 | 130.2 |
| 30 | 10.9 | 5.9 | 160.1 | 131.1 | 5.4 | 3.9 | 110.1 | 93.2 |
| 40 | 8.9 | 4.0 | 122.1 | 100.2 | – | – | – | – |
| LSD at 1% | 4.1 | 2.4 | 9.6 | 12.5 | 4.0 | 2.5 | 8.3 | 12.1 |
| LSD at 5% | 2.2 | 1.3 | 5.5 | 7.2 | 2.1 | 1.2 | 4.6 | 7.6 |

* Data represent the number of sclerotia per plate of *R. solani* and *S. rolfsii* or macroconidia ($\times 10^4/\text{mL}$) of *F. solani*.

reduced proportionally with increased concentrations of compound 1 or compound 2. Compound 2 was responsible for a respective reduction in sclerotia of 80.8% and 81.4%, whereas compound 1 was responsible for a respective reduction in *R. solani* and *S. rolfsii* of 65.07% and 75.4% at a concentration of 20 $\mu\text{g/mL}$.

The number of conidial spores of *F. solani* per plate decreased with increasing concentrations of compound 1 or compound 2. Maximum reduction was observed with a concentration of 30 $\mu\text{g/mL}$ of metabolite 2. Compound 2 reduced the conidial spores by 60.8% while 1 was responsible for a 52% reduction in *F. solani* at a concentration of 20 $\mu\text{g/mL}$.

Furoquinolines and coumarins are widely distributed in the plant kingdom and are present in notable amounts in the Rutaceae family. These classes have been reported to exhibit a wide array of interesting biological activities (antiplatelet aggregation, cytotoxic activity, inhibition of various enzymes, and antiviral, antibacterial, and antifungal activity) (25,26).

Daphnoretin has been found to have antineoplastic activity against Ehrlich ascites carcinoma (23), but no prior reports have noted its fungicidal activity against the phytopathogenic fungi *R. solani*, *S. rolfsii*, and *F. solani*.

The current data suggest that alkaloids and coumarins might play an important role in the rue

plant's chemical defense against plant pathogens. In the future, the two isolated metabolites can be used as a starting point to provide natural product-based fungicides that control pathogens affecting economically significant plants.

References

1. Agrios GN. Plant Pathology. 5th ed., Elsevier Academic Press, Boston, MA, USA, 2005; pp. 1-5.
2. Zaki K, Misaghi IJ, Heydari A, Shatla MN. Control of cotton seedling damping-off in the field by *Burkholderia (Pseudomonas) cepacia*. Plant Dis. 1998; 82:291-293.
3. Sufferdini IB, Sader HS, Goncalves AG. Screening of antibacterial extracts from plant native to the Brazilian Amazon Rain Forest and Atlantic Forest. Braz J Med Biol Res. 2004; 37:379-384.
4. Polunin O, Huxley A. Flowers of the Mediterranean. Hogarth Press, London, UK, 1987.
5. Steenkamp V. Traditional herbal remedies used by South African women for gynaecological complaints. J Ethnopharmacol. 2003; 86:97-108.
6. Guarrera PM. Traditional antihelminthic, antiparasitic and repellent uses of plants in Central Italy. J Ethnopharmacol. 1999; 68:183-192.
7. Ojala T, Remes S, Haansuu P, Vuorela H, Hiltunen R, Haahtela K, Vuorela P. Antimicrobial activity of some coumarin containing herbal plants growing in Finland. J Ethnopharmacol. 2000; 73:299-305.

8. Mancebo F, Hilje L, Mora GA, Castro VH, Salazar R. Biological activity of *Ruta chalepensis* (Rutaceae) and *Sechium pittieri* (Cucurbitaceae) extracts on *Hypsipyla grandella* (Lepidoptera: Pyralidae) larvae. *Rev Biol Trop*. 2001; 49:501-508.
9. Ulubelen A, Terem B, Tuzbeci E, Cheng KF, Kong YC. Alkaloids and coumarins from *Ruta chalepensis*. *Phytochemistry*. 1986; 25:2692-2693.
10. Ulubelen A, Ertugrul L, Birman H, Yigit R, Erseven G, Olgac V. Antifertility effects of some coumarins isolated from *Ruta chalepensis* and *R. chalepensis* var. *latifolia* in rodents. *Phytotherapy Res*. 1994; 8:233-236.
11. El-Sayed K, Al-Said MS, El-Ferally FS, Ross SA. New quinoline alkaloids from *Ruta chalepensis*. *J Nat Prod*. 2000; 63:995-997.
12. Farag MM, Emam AM, Mohamed MA. *In vitro* evaluation of the antioxidant effect of some botanical ethanolic extracts and isolation of the antioxidant constituent(s) from *Ruta chalepensis* leaves. *Fayoum J Agric Res Develop*. 2005; 19:178-190.
13. Emam AM, Mahmoud MG. Antibacterial activity of furoquinolone alkaloids against potato soft rot bacterium; *Erwinia carotovora* from *Ruta chalepensis* leaves. *J Union Arab Biol Cairo*. 2005; 14B:1-14.
14. Farnsworth NR. Biological and phytochemical screening of plants. *J Pharmaceutical Sci*. 1966; 55:225-276.
15. Eweis M, Elkholy SS, Elsabee MZ. Antifungal efficacy of chitosan and its thiourea derivatives upon the growth of some sugar-beet pathogens. *Int J Biol Macromol*. 2006; 38:1-8.
16. Knudsen IMB, Hockenhull J, Funck Jensen D, Gerhardson B, Hökeberg M, Thavonen R, Teperi E, Sundheim L, Henriksen B. Selection of biological control agents for controlling soil and seed-borne diseases in the field. *Eur J Plant Pathol*. 1997; 103:775-784.
17. Bauer AW, Kirby WM, Sherris JC, Turck M. Antibiotic susceptibility testing by a standardized single disk method. *Am J Clin Pathol*. 1966; 45:493-496.
18. El-Abyad MS, Saleh YE. Studies with *Fusarium oxysporum* f.sp. *Vasinfestum*, the cause of cotton wilt in Egypt. Germination, sporulation and growth. *Trans Br Mycol Soc*. 1971; 57:427-437.
19. Noshita T, Tando M, Suzuki K, Murata K, Funayama S. New quinoline alkaloids from the leaves and stems of *Orixa japonica*, orijanonone, isopteleflorine and 3'-O-methylloxixine. *Biosci Biotechnol Biochem*. 2001; 65:710-713.
20. Fokialakis N, Magialis P, Chinou I, Mitaku S, Tillequin F. Megistoquinones I and II, two quinoline alkaloids with and bacterial activity from bark of *Sarcomelicope megistophylla*. *Chem Pharm Bull (Tokyo)*. 2002; 50:413-414.
21. Chlouchi A, Girard C, Tillequin F, Bevalot F, Watermann PG, Muiyard F. Coumarins and furoquinoline alkaloids from *Philotheca deserti* var. *deserti* (Rutaceae). *Biochem Sys Ecol*. 2005; 34:71-74.
22. Ulubelen A, Terem B. Alkaloids and coumarins from roots of *Ruta chalepensis*. *Phytochemistry*. 1988; 27:650-651.
23. Cordell GA. Studies in the thymelaeaceae 1. NMR spectral assignments of Dephnoetin. *J Nat Prod*. 1984; 47:84-88.
24. Chakrabati R, Das B, Banerji J. Bis-coumarins from *Edgeworthia gardneri*. *Phytochemistry*. 1986; 25:557-558.
25. Gray AI, Watermann PG. Coumarins in the Rutaceae. *Phytochemistry*. 1978; 17:845-864.
26. Michael JP. Quinoline, quinazoline and acridone alkaloids. *Nat Prod Rep*. 2003; 20:476-493.

(Received May 25, 2010; Revised June 18, 2010; Re-revised August 10, 2010; Accepted August 12, 2010)

Original Article**Taxonomic identification of a novel strain of *Streptomyces cavourensis* subsp. *washingtonensis*, ACMA006, exhibiting antitumor and antibacteria activity**Xianwen Yuan^{1,2}, Ruili Yang^{1,*}, Xue Cao¹, Jianjun Gao³¹ Department of Microbiology and Immunology, School of Medicine, Southeast University, Nanjing, Jiangsu, China;² Department of Hepatobiliary Surgery, the Affiliated Hospital of Nanjing University Medical School, Nanjing, Jiangsu, China;³ China-Japan Cooperation Center for Drug Discovery & Screen, Shandong University, Ji'nan, China.

ABSTRACT: Taxonomically diverse and genetically specialized, marine microorganisms have great potential in generating bioactive substances. A previous study isolated a novel actinomycete strain designated ACMA006 and revealed that the fermentation broth of ACMA006 (FBA6) significantly inhibited the growth of a series of tumor cell lines. The present study examined various characteristics of the ACMA006 strain, including its morphological, physiological, and biochemical nature, and the 16S rDNA gene sequence of ACMA006 and biological activity of FBA6. The ACMA006 strain grew at an optimal temperature of 28°C on nearly all media tested, except for Czapek's agar, producing an exuberant substrate and aerial hyphae. Phylogenetic analysis showed that the 16S rDNA gene sequence of ACMA006 was closely related to that of *Streptomyces cavourensis* subsp. *washingtonensis*, with a sequence similarity of nearly 100%. However, ACMA006 differed somewhat from *Streptomyces cavourensis* subsp. *washingtonensis* in terms of its morphological, physiological, and biochemical characteristics. According to a bioactivity assay, FBA6 strongly inhibited the growth of hepatocellular carcinoma cell line HepG2, while it was weakly cytotoxic to human normal hepatocytes LO2 according to an MTT assay. In addition, the growth of bacterial strains *Bacillus subtilis* and *Staphylococcus aureus* but not *Escherichia coli*, *B. aerogenes*, *Pseudomonas fluorescense*, and *B. proteus* was significantly suppressed by FBA6 as indicated by the filter paper disc method. Results of this study indicated that the strain ACMA006 represents a new strain of the *Streptomyces cavourensis* subsp. *washingtonensis* and that the active metabolites of this strain are candidates for utilization as anticancer or antibacterial agents.

Keywords: Streptomycetes, antitumor activity, antibacterial activity, 16S rDNA gene, phylogenetic analysis

1. Introduction

Compounds from marine sources exhibit a variety of bioactivity against tumors, inflammation, allergies, viral infections, and the like (1). Searching among metabolites of marine microorganisms for new drugs has proven to be an important approach to current drug development. Many agents derived from these metabolites have been used clinically, e.g., vidarabine is active against herpes simplex and varicella zoster viruses (2) and cytarabine is a chemotherapy agent used mainly in the treatment of hematological malignancies (3).

Actinomycetes are widely distributed in terrestrial and aquatic ecosystems and especially in soil, where they play a crucial role in the recycling of refractory biomaterials (4). Actinomycetes, and particularly species in the genus *Streptomyces*, are widely known to be prolific producers of bioactive compounds, including antitumor and antibacterial agents (5). Approximately 45% of the bioactive secondary metabolites produced by microorganisms are reportedly found in the metabolites of actinomycetes (6). Therefore, Actinomycetes have great potential in the areas of drug research and development.

A previous study isolated ACMA006, a marine actinomycete, in the laboratory (7). The fermentation broth of ACMA006 (FBA6) was found to be significantly cytotoxic to several cancer cell lines such as human hepatoma cell line SMMC 7721, colorectal cancer cell line Lovo, cervical cancer cell line Hela, and mouse myeloma cell line SP2/0 (7). However, the taxonomy of ACMA006 was not readily apparent and the wide-ranging biological activity of FBA6, and especially its cytotoxicity to normal cells, needed to

*Address correspondence to:

Dr. Ruili Yang, Department of Microbiology and Immunology, School of Medicine, Southeast University, Nanjing 210009, Jiangsu, China.
e-mail: yrl812@sohu.com

be clarified. The current study examined the cultural, morphological, physiological, and biochemical characteristics and chemotaxonomy of ACMA006. The 16S rDNA gene sequence of ACMA006 was also analyzed and compared with that of *Streptomyces cavourensis* subsp. *washingtonensis*. In addition, this study ascertained the bioactivity of FBA6, including inhibition of growth of both hepatoma cell line HepG2 and normal hepatocytes LO2, and certain bacterial strains.

2. Materials and Methods

2.1. Materials

The actinomycete strain ACMA006 was isolated from the marine mud collected in Lianyungang harbor, Jiangsu, China, in a previous study (7). The method of isolating ACMA006 has been patented under Chinese patent No. ZL200710025156.5. The strain was preserved in liquid paraffin in the lab and China General Microbiological Culture Collection Center (CGMCC) (No. 2027).

Fermentation broth of ACMA006 (FBA6) was prepared as described before (8). Passaged from Gause's agar, the strain was inoculated in Gause's fermentation medium and cultivated for 4 h at 28°C. Then, the strain was inoculated in 2216E fermentation medium and cultivated for 6 days at 28°C. The broth was harvested, disrupted using ultrasound, and centrifuged at 10,000 × g for 10 min at 4°C. The supernatant was removed, filtered with a 0.22-µm filter, and stored at -20°C for further study.

2.2. Cell and/or bacterium culture

Human hepatoma cells HepG2 and normal hepatocytes LO2 were obtained from American Type of Cell Culture (Manassas, Virginia, USA). HepG2 and LO2 cells were maintained in RPMI-1640 media supplemented with 10% (v/v) heat-inactivated fetal bovine serum, penicillin-streptomycin (100 IU/mL-100 µg/mL), 2 mM glutamine, and 10 mM HEPES buffer at 37°C in a humid atmosphere (5% CO₂-95% air) and were harvested by brief incubation in 0.02% (w/v) EDTA in PBS (ICN, Aurora, USA) (25).

Bacterial strains employed in the current study including *Bacillus subtilis*, *Staphylococcus aureus*, *Escherichia coli*, *Enterobacter aerogenes*, *Proteus vulgaris*, and *Pseudomonas fluorescens* were obtained from American Type of Cell Culture (Manassas, Virginia, USA). All strains except *Pseudomonas fluorescens* were cultured in nutrient broth (Becton Dickinson. Cockeysville, MD, USA) at 37°C. *Pseudomonas fluorescens* was cultured in Pseudomonas CFC agar (Becton Dickinson. Cockeysville, MD, USA) and incubated at 28°C.

2.3. Cell growth assay

Cells (5 × 10³ per well) seeded in 96-well plates for 24 h were exposed to adriamycin (positive control) or different doses of FBA6 for 96 h at 37°C in a humidified 5% CO₂ atmosphere. The medium was then removed and the cells were washed with PBS. A 3-(4,5-dimethylthiazol-2-yl)-2,5-diphenyltetrazolium bromide (MTT) assay was performed by adding 20 µL MTT (5 mg/mL, Sigma-Aldrich, St Louis, MO, USA) for 4 h. Light absorbance of the solution was measured at 492 nm on a microplate reader (PerkinElmer, Waltham, MA, USA) (9). Experiments were performed in triplicate with three samples.

2.4. Bacteria growth assay

Antibacterial activity of FBA6 was screened for using the filter paper disc method (10). A previously liquefied medium appropriate for the test was inoculated with the requisite quantity of the suspension of microorganisms. The suspension was added to the medium at a temperature between 40-50°C and the inoculated medium was immediately poured into dried Petri dishes to fill a depth of 3 to 4 mm. Paper discs (Whatmann No.2) were cut into smaller discs (6-mm diameter), sterilized at 180°C for 30 min in a hot air oven, and then impregnated with FBA6. The dried discs were placed on the surface of the medium. For strains *B. subtilis*, *Staphylococcus aureus*, *Escherichia coli*, *Enterobacter aerogenes*, and *Proteus vulgaris*, the incubation temperature was 37°C, while for *Pseudomonas fluorescens* the incubation temperature was 28°C. The incubation time for all of the bacterial strains was 16-18 h. The diameter of the circular inhibition zones was subsequently measured.

2.5. Cultural and physical characteristics

Cultural properties of the strain ACMA006 were evaluated as described by Shirling *et al.* and Locci (11,12). ACMA006 was inoculated onto Gause's synthetic agar, glucose asparagine agar, Czapek's agar, inorganic salts/starch agar, glucose-yeast extract agar, Emerson agar, nutrient agar, and glycerol-extractum carnis-peptone agar and incubated at 28°C for 7-10 days to investigate growth. The colors of substrate mycelium, aerial mycelium, spore mycelium, and soluble pigment produced by ACMA006 were also recorded after 14 days of incubation on different agars.

Physical characteristics of ACMA006, including the carbon source utilization pattern and optimal growth temperature requirements, were determined as follows. Utilization of carbon sources was tested by growth on carbon utilization medium (ISP 9) supplemented with 1% carbon sources at 28°C for 2 weeks (13). Temperature ranges for growth were determined on

2216E medium (Sigma, USA) using a temperature gradient incubator (Toyo Kagaku Sangyo, Tokyo, Japan).

2.6. Morphological characteristics

Substrate mycelium and aerial mycelium morphology of ACMA006 were viewed under a light microscope (Olympus BH-2; Olympus, Tokyo, Japan) after 7 days of incubation on Gause's synthetic agar at 28°C. Morphology of the spore chain and the spore surface ornamentation was examined using scanning electron microscopy (JSM-6390LV; JEOL Ltd., Japan) after 14 days of incubation on Gause's synthetic agar (14). Samples for scanning electron microscopy were prepared by fixing the agar block in osmium tetroxide vapor for 12 h, dehydration by critical-point drying, and then sputter coating with palladium under a vacuum.

2.7. Biochemical properties assay

Biochemical properties of ACMA006 were determined in terms of the following aspects: Gram staining, acid-inhibition staining, decomposition of starch, reduction of nitrate, gelatin hydrolysis, growth on cellulose, coagulation of milk, peptonization of milk, production of hydrogen sulfide, and production of melanoid pigment. Biochemical characteristics were tested using standard techniques from the *Manual for identification of Streptomyces* (15).

2.8. Chemotaxonomic characterization

Isomers of diaminopimelic acid (DAP) in whole-cell hydrolysates were determined using thin-layer chromatography (TLC) according to the methods of Becker *et al.* and Hasegawa *et al.* (16,17). Mycolic acids and whole-cell sugars were analyzed using high-performance liquid chromatography (HPLC) according to the method of Butler *et al.* (18).

2.9. 16S rDNA gene-based phylogenetic analysis

Total DNA was extracted according to the method of

Orsini *et al.* (19). The 16S rDNA gene was amplified by PCR using the following primers: Primer A, 5'-ATCCTGGCTCAGGACGAACG-3'; Primer B, 5'-GAGGTGATCCCGCCGCACCT-3'. Programmable temperature cycling was performed with the following cycle profile: 95°C for 5 min and then 30 cycles, with each cycle consisting of denaturation for 1 min at 95°C, annealing for 1 min at 58°C, and extension for 1.5 min at 72°C. After 30 cycles, the reaction tubes were stored for 10 min at 72°C and then at 4°C. Samples were electrophoresed in gels containing 1% agarose (FMC; Rockland, ME, USA) and sequenced by Invitrogen (Shanghai, China). The 16S rDNA gene sequences of ACMA006 were aligned using Clustal X1.8. Sequences of the other members of the genus *Streptomyces* used for alignment and calculation of similarity levels were obtained from the GenBank and EMBL database using the BLAST program. Phylogenetic analyses were performed with MEGA3.1. Evolutionary trees were constructed according to the neighbor-joining method and Kimura's two-parameter model (20,21).

2.10. Statistical analysis

Data were analyzed using a Student's two-tailed *t*-test and are presented as the mean \pm S.D. The limit of statistical significance was $p < 0.05$. Statistical analysis was done with SPSS/Win11.0 software (SPSS, Inc., Chicago, Illinois, USA).

3. Results

3.1. Cultural and physical characteristics

Table 1 shows the cultural characteristics of ACMA006. It grew vigorously on glucose-asparagine agar, inorganic salts-starch agar, glucose-yeast extract agar, Emerson agar, nutrient agar, and glycerol-extractum carnis-peptone agar. It also grew well on Gause's synthetic agar but poorly on Czapek's agar. Generally, the colors of the substrate mycelium and aerial mycelium were yellowish, yellow, or brown on all of the tested media. The spore mycelium was white, pale yellow, or yellow in color. Yellow or brown soluble

Table 1. Cultural characteristics of the strain ACMA006 on various media

| Culture media | Growth status | Substrate mycelium* | Aerial mycelium* | Spore mycelium* | Soluble pigment* |
|--|---------------|-------------------------|-------------------------|-----------------|------------------|
| Gause's synthetic agar | Well | Y to B | W to pale Y | W to pale Y | Y to B |
| Glucose-asparagine agar | Vigorous | W to pale Y | W to pale Y | Y | Y |
| Czapek's agar | Poor | W to lemon Y | W to pale Y | W to pale Y | Light Y to Y |
| Inorganic salts-starch agar | Vigorous | W to pale Y | W to pale Y | Lemon Y | Light Y |
| Glucose-yeast extract agar | Vigorous | Ivory W to lemon Y to Y | Ivory W to lemon Y to Y | W | W to pale Y |
| Emerson agar | Vigorous | Light Y to Y | W to pale Y | W to pale Y | W to pale Y |
| Nutrient agar | Vigorous | Yellow to golden yellow | W to pale Y | W to pale Y | Y |
| Glycerol-extractum carnis-peptone agar | Vigorous | Y to D | Y to D | W to pale Y | Y |

* Y: yellow; B: brown; W: white; D: dark brown.

pigments were produced on Gause's synthetic agar, glucose-asparagine agar, nutrient agar, and glycerol-extractum carnis-peptone agar. White or yellowish soluble pigments were observed on the other culture media.

Glucose, fructose, arabinose, mannitol, glycerol, and sodium succinate were thought to be the main carbon sources used by ACMA006 (Table 2). Xylose and glycerol were mildly or moderately utilized, while sucrose, rhamnose, inositol, and sorbitol were not employed as carbon sources. The temperature range for growth was 10-40°C, whereas the optimal culture temperature was 28°C (data not shown).

3.2. Morphological characteristics

Both aerial mycelium and substrate mycelium were amply produced in this strain. The diameter of the mycelium was about 0.8 μm . The substrate hyphae appeared earlier than aerial hyphae and had thin and elongated features (Figure 1A). The septum developed in the substrate hyphae at the incubation time of 36 h at 28°C, and fragmentation was apparent after day 4. The strain produced aerial mycelia that consisted of long straight or flexuous chains of spores with smooth surfaces (Figure 1B). The spores were formed when spore chains fragmented at the sites of septa and had an oval or columnar appearance.

3.3. Biochemical characteristics

The biochemical properties of ACMA006 are summarized in Table 3. Among the experiments, strongly or moderately positive results were obtained in the decomposition of starch, reduction of nitrate, Gram staining, coagulation of milk, and peptonization of milk, whereas negative results were obtained in acid-inhibition staining, gelatin hydrolysis, growth on cellulose, production of hydrogen sulfide, and production of melanoid pigment.

3.4. Chemotaxonomy

L,L-DAP and glycine were detected in whole-cell hydrolysates of ACMA006 cells (data not shown), suggesting that ACMA006 has a type I cell wall (22). In addition, glucose and rhamnose in the C glycoform were found in whole-cell hydrolysates but characterized sugars were not (data not shown). Mycolic acid was not detected.

3.5. 16S rDNA gene analysis

The complete 16S rDNA gene sequence was determined for the strain ACMA006. The 16S rDNA gene sequence of the ACMA006 strain was 1,507 bp in length. A neighbor-joining tree was generated according to the

Table 2. Utilization of carbon sources in the strain ACMA006

| Carbon source | Results* |
|------------------|----------|
| Glucose | + |
| Fructose | + |
| Xylose | Moderate |
| Sucrose | - |
| Rhamnose | - |
| Arabinose | + |
| Glycerol | Mild |
| Mannitol | + |
| Inositol | - |
| Sorbitol | - |
| Glycerol | + |
| Sodium succinate | + |

* +, positive; -, negative.

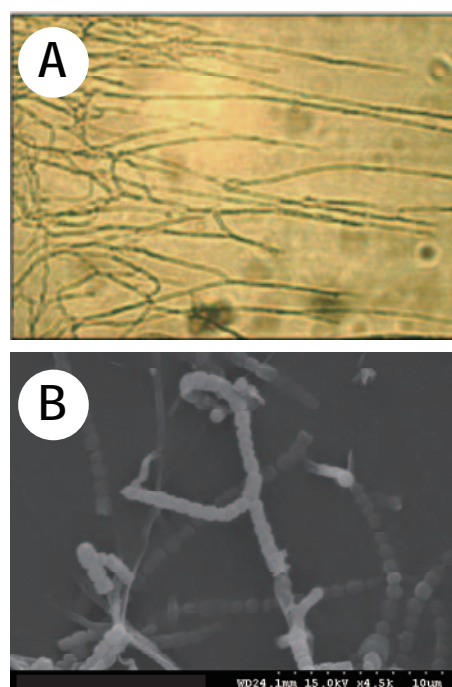


Figure 1. Morphological observation of the strain ACMA006. (A) A typical photograph of the strain ACMA006 under a light microscope (400 \times). **(B)** A typical photograph of spores under a scanning electron microscope (4,500 \times).

Table 3. Biochemical properties of the strain ACMA006

| Tests | Results* |
|--------------------------------|----------|
| Gram staining | + |
| Acid inhibition staining | - |
| Decomposition of starch | ++ |
| Reduction of nitrate | ++ |
| Gelatin hydrolysis | - |
| Growth on cellulose | - |
| Coagulation of milk | + |
| Peptonization of milk | + |
| Production of hydrogen sulfide | - |
| Production of melanoid pigment | - |

* ++, strong positive; +, positive; -, negative.

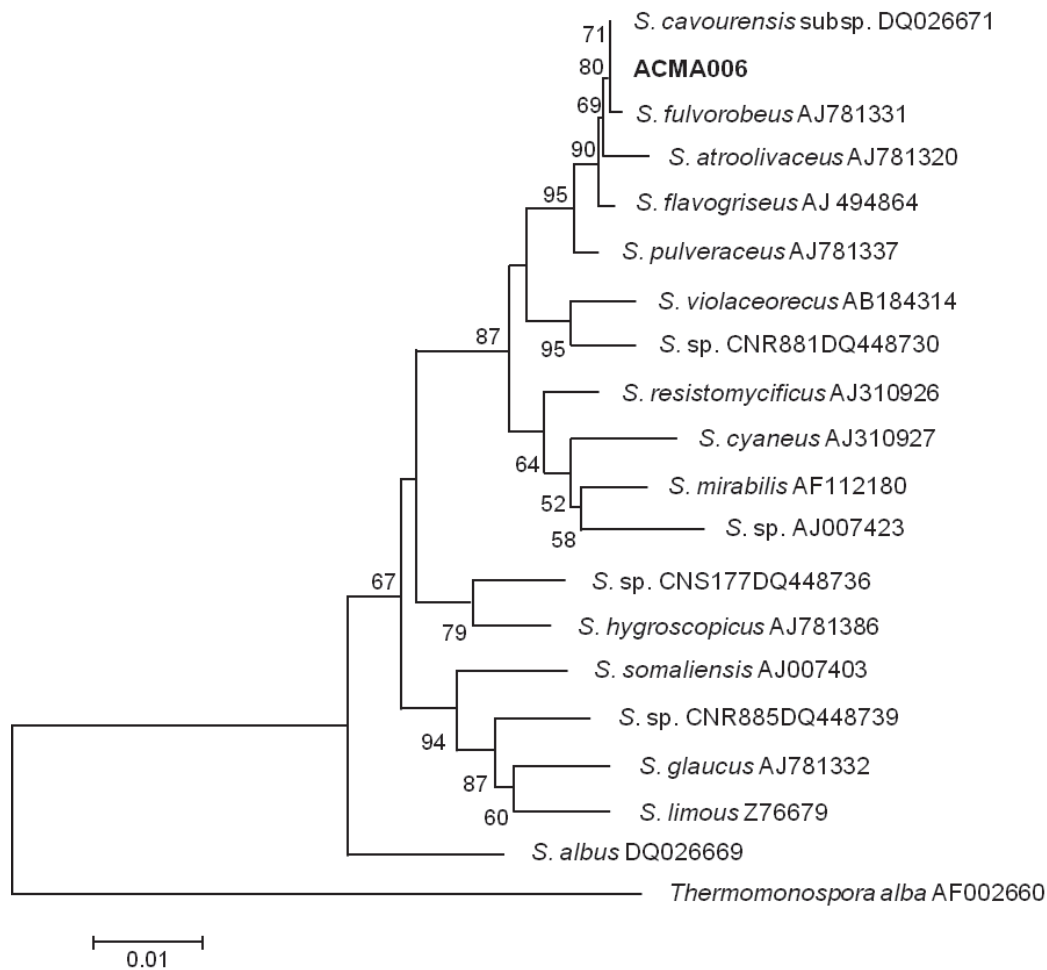


Figure 2. A neighbor-joining dendrogram based on the sequence length of the 16S rDNA gene. The tree was validated by bootstrap analysis (1,000 replications) and values greater than 50% are indicated at the nodes. Bar, 0.01 substitutions per 100 nucleotides.

neighbor-joining method and Kimura's two parameter model (Figure 2). The ACMA006 strain formed a clade with the members of the genus *Streptomyces*. The 16S rDNA gene sequence of the strain was highly similar, with similarity close to 100%, to the 16S rDNA gene sequence (1,490 bp) of the previously described species *Streptomyces cavourensis* subsp. *washingtonensis*.

3.6. Inhibition of cell growth

Cell growth inhibition by FBA6 was examined with human hepatoma cells HepG2 and normal hepatocytes LO2. As shown in Figure 3, FBA6 had an anti-proliferative effect on HepG2 cells in a dose-dependent manner for up to 96 h of exposure ($p < 0.05$ vs. untreated control). Similar proliferation profiles were observed in LO2 cells exposed to FBA6. However, LO2 cells were less sensitive to FBA6 than HepG2 cells. The survival rate for LO2 cells was higher than that for HepG2 cells at the same concentrations.

3.7. Inhibition of bacteria growth

The antibacteria activity of FBA6 was determined

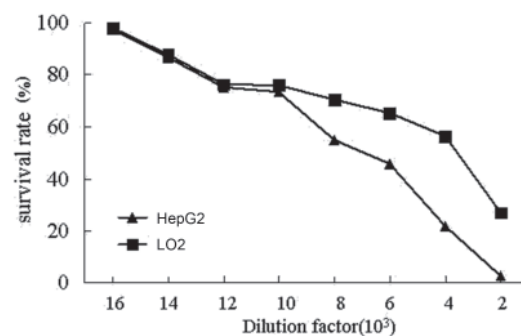


Figure 3. FBA6's inhibition of the growth of hepatoma cells HepG2 and normal hepatocytes LO2. FBA6 was diluted into a series of final concentrations as indicated by the values on the horizontal axis.

with the following bacterial strains: *B. subtilis*, *Staphylococcus aureus*, *Escherichia coli*, *Enterobacter aerogenes*, *Proteus vulgaris*, and *Pseudomonas fluorescens*. As shown in Table 4, the growth of strains *B. subtilis* and *Staphylococcus aureus* was inhibited by FBA6, with inhibition (dia) of 16 and 11 mm, respectively. FBA6 was not found to suppress the growth of other bacterial strains.

Table 4. Antibacterial activity of FBA6 on indicated bacterial strains

| Bacterial strains | Extent of inhibition (diameter in mm)* |
|---------------------------------|--|
| <i>Bacillus subtilis</i> | 16 |
| <i>Staphylococcus aureus</i> | 11 |
| <i>Escherichia coli</i> | – |
| <i>Bacillus aerogenes</i> | – |
| <i>Pseudomonas fluorescense</i> | – |
| <i>Bacillus proteus</i> | – |

* –, negative.

4. Discussion

The present study examined the taxonomic status of the novel strain ACMA006 and evaluated the ability of its fermentation broth to inhibit the growth of human hepatoma HepG2 cells, human normal hepatocytes LO2, and a series of bacterial strains. Complete 16S rDNA gene sequence analysis, cultural, physiological, morphological, and biochemical characteristics, and the results of chemotaxonomic analyses indicated that this strain should be classified as a new strain of the species *Streptomyces cavourensis* subsp. *washingtonensis*. Bioactivity analyses demonstrated that FBA6 was preferentially cytotoxic to hepatoma HepG2 cells. In addition, FBA6 selectively inhibited the growth of the two bacterial strains *B. subtilis* and *Staphylococcus aureus*. These results suggested that metabolites of the strain ACMA006 are candidates for use as antitumor and antibacterial agents in the future.

Members of the genus *Streptomyces* share many phenotypic characteristics and constitute a distinct phyletic line to which over 450 validly described species are assigned (12,23,24). Species in this genus produce extensively branched substrate and aerial mycelia (12). Phylogenetic analyses showed that the gene sequence of 16S rDNA of ACMA006 was almost identical to that of *Streptomyces cavourensis* subsp. *washingtonensis*. However, characteristics such as the production of yellow or pale yellow soluble pigments and H₂S, as were found with the strain ACMA006, have rarely been observed with the strain *Streptomyces cavourensis* subsp. *washingtonensis*. Moreover, the mycelium of the strain ACMA006 had septa in the early stage of culture and subsequently fragmented, features that are rarely found in the genus *Streptomyces* except for in the strain *S. limosus* (15). Given these findings, the strain was determined to be a new strain of the *Streptomyces cavourensis* subsp. *washingtonensis*, according to the *Manual for identification of Streptomyces* (15), *Bergey's Manual of Systematic Bacteriology* (12), and *Systematology of Actinomycetes – Principle, Methods, and Practice* (21). The metabolites in FBA6 that had bioactivity as indicated by the current study have yet to be specifically identified. Purification and identification of these compounds is now underway.

Acknowledgements

This study was supported by a grant from the Health Bureau of Jiangsu Province (No. H200758). The authors wish to thank Professor Zhiheng Liu, Institute of Microbiology, Chinese Academy of Sciences, for his help in identifying the strain ACMA006. The authors also wish to thank Dr. Qinghai Huang, School of Medicine, Southeast University, for his assistance in establishing the strain's phylogenetic tree.

References

- Newman DJ, Cragg GM. Marine natural product and related compounds in clinical and advanced preclinical trials. *J Nat Prod.* 2004; 67:1216-1238.
- Shen W, Kim JS, Kish PE, Zhang J, Mitchell S, Gentry BG, Breitenbach JM, Drach JC, Hilfinger J. Design and synthesis of vidarabine prodrugs as antiviral agents. *Bioorg Med Chem Lett.* 2009; 19:792-796.
- Advani AS, Gundacker HM, Sala-Torra O, Radich JP, Lai R, Slovak ML, Lancet JE, Coutre SE, Stuart RK, Mims MP, Stiff PJ, Appelbaum FR. Southwest Oncology Group Study S0530: A phase 2 trial of clofarabine and cytarabine for relapsed or refractory acute lymphocytic leukaemia. *Br J Haematol.* 2010; 151:430-434.
- Kirby R. Actinomycetes and lignin degradation. *Adv Appl Microbiol.* 2006; 58:125-168.
- Okami Y, Hotta K. Search and discovery of new antibiotics. In: *Actinomycetes in Biotechnology* (Goodfellow M, Williams ST, Mordarski M, eds.). Academic Press, London, UK, 1988; pp. 33-67.
- Nett M, Ikeda H, Moore BS. Genomic basis for natural product biosynthetic diversity in the actinomycetes. *Nat Prod Rep.* 2009; 26:1362-1384.
- Yang RL, Yuan XW, Zheng J, Wang SJ, Li D. Preliminary study on antitumor activity of culture broths from a marine actinomycete. *Journal of Oceanography in Taiwan Strait.* 2007; 26:351-355. (in Chinese)
- Yuan XY, Yang RL, Cao X. Studies on the optimum fermentation conditions of marine actinomycete ACMA006 with antitumor activity. *Chinese Journal of Marine Drugs.* 2008; 27:5-9. (in Chinese)
- Inagaki Y, Tang W, Zhang L, Du G, Xu W, Kokudo N. Novel aminopeptidase N (APN/CD13) inhibitor 24F can suppress invasion of hepatocellular carcinoma cells as well as angiogenesis. *Biosci Trends.* 2010; 4:56-60.
- Qadrie ZL, Jacob B, Anandan R, Raj Kapoor B, Rahamathulla M. Anti-bacterial activity of ethanolic extract of *Indoneesiella echioides* (L) nees. evaluated by the filter paper disc method. *Pak J Pharm Sci.* 2009; 22:123-125.
- Shirling EB, Gottlieb D. Methods for characterization of *Streptomyces* species. *Int J Syst Bacteriol.* 1966; 16:313-340.
- Locci R. *Streptomyces* and related genera. In: *Bergey's manual of systematic bacteriology* (Williams ST, Sharpe ME, Holt JG, eds.). Williams & Wilkins, Baltimore, MD, USA, 1989; pp. 2451-2508.
- Pridham TG, Gottlieb D. The utilization of carbon compounds by some actinomycetales as an aid for species determination. *J Bacteriol.* 1948; 56:107-114.
- O'Donnell AG, Falconer C, Goodfellow M, Ward AC,

- Williams E. Biosystematics and diversity amongst novel carboxydophilic actinomycetes. *Antonie Van Leeuwenhoek*. 1993-1994; 64:325-340.
15. Zhang JZ. Manual for identification of Streptomyces. Fudan University Press, Shanghai, China, 1990; pp. 111-155.
 16. Becker B, Lechevalier MP, Lechevalier HA. Chemical composition of cell-wall preparation from strains of various form-genera of aerobic actinomycetes. *Appl Microbiol*. 1965; 13:236-243.
 17. Hasegawa T, Takizawa M, Tanida S. A rapid analysis for chemical grouping of aerobic actinomycetes. *J Gen Appl Microbiol*. 1983; 29:319-322.
 18. Butler WR, Floyd MM, Silcox V, Cage G, Desmond E, Duffey PS, Guthertz LS, Gross WM, Jost KC, Ramos LS, Thibert L, Warren N. Standardized Method for HPLC Identification of Mycobacteria. U.S. DEPARTMENT OF HEALTH AND HUMAN SERVICES Public Health Service.
 19. Orsini M, Romano-Spica V. A microwave-based method for nucleic acid isolation from environmental samples. *Lett Appl Microbiol*. 2001; 33:17-20.
 20. Saitou N, Nei M. The neighbor-joining method: A new method for reconstructing phylogenetic tree. *Mol Biol Evol*, 1987, 4:406-425.
 21. Xu LH, Li WJ, Liu ZH. Systematology of Actinomycetes – Principle, Methods and Practice. Science Press, Beijing, China, 2007; pp. 150-201.
 22. Lechevalier MP, Lechevalier HA. The chemotaxonomy of actinomycetes. In: Actinomycete Taxonomy (Dietz X, Thayer Y, eds.). Arlington, Texas, USA, 1980; pp. 227-291.
 23. Embley TM, Stackebrandt E. The molecular phylogeny and systematics of actinomycetes. *Annu Rev Microbiol*. 1994; 48:257-289.
 24. Goodfellow M, Manfio GP, Chun J. Towards a practical species concept for cultivable bacteria. In: Species: the Units of Biodiversity (Claridge MF, Dawah HA, Wilson MR, eds.). Chapman & Hall, London, UK, 1997; pp. 25-69.
 25. Yan G, Duan RH, Yin K, Zhu S, Liu Q, Gong M, Wang H, Sun C, Pu D, Tang N, Huang AL. Inhibition of survivin expression to induce the apoptosis of hepatocarcinoma cells by adenovirus-mediated siRNA. *Biosci Trends*. 2008; 2:88-93.
- (Received October 28, 2010; Revised November 3, 2010; Accepted November 29, 2010)

Original Article**Novel CYP2C19 629c>a mutant gene detection in Japanese subjects and estimation of its effect on conformation**Sayaka Kimura¹, Setsuo Hasegawa¹, Ai Kobayashi¹, Hiroki Yamaguchi¹, Masafumi Yohda³, Takahiro Kubota^{1,2,*}¹ Sekino Clinical Pharmacology Clinic, Tokyo, Japan;² Pharmaceutical Department of Scientific Research, Graduate School of Pharmaceutical Sciences, Chiba Institute of Science, Chiba, Japan;³ Department of Biotechnology and Life Science, Graduate School of Technology, Tokyo University of Agriculture and Technology, Tokyo, Japan.

ABSTRACT: Gene polymorphism is considered to be one of the causes of poor metabolism (PM), and approximately 20 mutants have been reported for CYP2C19 thus far. In our analysis of the CYP2C19*3 mutant gene, we detected new CYP2C19 SNPs by cross checking with different procedures. We confirmed a new c>a mutation at the 629 position. Among the 587 healthy Japanese volunteers studied, two subjects carrying a mutant CYP2C19 allele were found to be heterozygotes (0.17%). Accordingly, we predicted the effect of this novel mutation on CYP2C19 conformation. The 629c>a mutation was located on exon 4 and was an amino acid substitution, in which Thr210 was changed to Asn. The modeled structure of CYP2C19 showed that the hydrogen bond between the main chain oxygen of Ile207 and the side chain O γ of Thr210 would be lost when Thr210 was substituted by Asn; however, no steric constraint was observed, although Asn is larger than Thr in size. Although the CYP2C19 629c>a mutation induces an amino acid substitution, it is predicted to scarcely change its conformation. On the basis of these findings, we speculate that the mutant is not a causative gene for PM in CYP2C19 carriers.

Keywords: CYP2C19, poor metabolism, single nucleotide polymorphisms, allele specific-polymerase chain reaction

1. Introduction

Cytochrome P450 enzymes are the most important

enzymes in phase I metabolism. Cytochrome P450 2C19 (CYP2C19) is a member of the cytochrome P450 enzyme superfamily, and plays an important role in the metabolism of drugs (1,2). For individuals possessing the CYP2C19 gene, drug oxidative metabolic capability varies, and those with poor metabolism (PM) are more frequent among Japanese than among Western populations. Genetic polymorphisms in this enzyme, representing approximately 13-23% of Asians and 3-5% of Caucasians, are responsible for the PM of mephenytoin (3,4). Around twenty mutations in the CYP2C19 gene have been reported (5), and five mutant alleles, namely, CYP2C19*2 (g681a), *3 (g636a), *16 (c1324t), *18 (g986a, a991g), and *19 (a151g, a991g) have already been reported in Japan (6-8).

Genotyping for single nucleotide polymorphisms (SNPs) is of great value to biomedical research and the development of personalized medicine, particularly because it can affect how humans respond to pathogens, chemicals, and drugs. A novel automatic SNP-typing system has been developed in collaboration with ARKRAY, Inc., Kyoto, Japan (9). The system performs SNP typing using analysis of the melting temperature (T_m) of the probe DNA hybridized to the target SNP through a fluorescence quenching probe. In this system, contamination during purification can be avoided because genomic DNA is not purified from a blood sample. We also developed a rapid, low cost and high-throughput genotyping method for detecting polymorphisms of drug-metabolizing enzyme genes using allele specific-polymerase chain reaction (AS-PCR), with detection by SYBR Green I (10). When the CYP2C19*3 (g636a) mutation gene was analyzed with AS-PCR (10) and the above automatic SNP-typing system (9), a difference in the analytical results was recognized.

In the present study, by sequencing the surrounding sequences of CYP2C19*3, we found a new 629c>a variation in exon 4 that creates an amino acid substitution, Thr210Asn, on the probe for the system binding regions. Our study was designed to examine the function of

*Address correspondence to:

Dr. Takahiro Kubota, Pharmaceutical Department of Scientific Research, Graduate School of Pharmaceutical Sciences, Chiba Institute of Science, 15-8 Shiomi-cho, Choshi-city, Chiba 288-0025, Japan.
e-mail: tkubota-tky@umin.net

Thr210 with regard to its tertiary structure and effect after mutation to Asn on cytochrome P450 2C19. The conformation was constructed using homology modeling.

2. Materials and Methods

2.1. CYP2C19 genotyping

The novel automatic SNP-typing system performs SNP typing by analysis of the melting temperature (T_m) of the probe DNA hybridized to the target SNP site, using a fluorescence quenching probe (ARKRAY, Inc., Kyoto, Japan). The system enables fully automated SNP genotyping from sample pretreatment to gene amplification and signal detection. We need only to set up two cartridges and apply the samples to the cartridges (9). We performed genotyping of CYP2C19 polymorphisms using blood samples obtained from 587 healthy volunteers.

Five hundred and eighty-five typing sample results were consistent with the results obtained from the SNP typing kit for allele-specific PCR, obtained from Toyobo (Toyobo Co., Ltd., Fukui, Japan). AS-PCR for CYP2C19*2, and *3 has been previously described (10).

All subjects provided written consent for participation in the study, after having been informed both verbally and in writing of the experimental procedures and purpose of the study. The study protocol was approved by the Ethics Committee of Sekino Clinical Pharmacology Clinic (Tokyo, Japan).

2.2. PCR conditions and DNA sequencing

PCR amplification of *2 was performed simultaneously in a buffer containing genomic DNA, 1.25 U Gene Taq FP (Nippon Gene Co., Ltd., Toyama, Japan), 10× Gene Taq Universal Buffer and 0.2 mM dNTPs with 0.5 μM of each primer (5'-GAATTTTCTTCTCAAATCTTGT-3' and 5'-CTCCTTGACCTGTAAACATCC-3'). PCR conditions consisted of an initial denaturation at 95°C for 2 min, followed by 35 cycles of denaturation at 95°C for 30 sec, annealing at 56°C for 30 sec and extension at 72°C for 30 sec, followed by a final extension at 72°C for 7 min. PCR amplification of *3 was performed simultaneously in a buffer containing genomic DNA, 1.25 U TaKaRa Ex Taq (Takara Bio Inc., Shiga, Japan), 10× EX Taq Buffer and 0.2 mM dNTPs with 0.5 μM of each primer (5'-CAT AGGTAAGATATTACTTAAA-3' and 5'-CCAAAGTAC TTTATAGAAAC-3'). PCR conditions consisted of initial denaturation at 95°C for 2 min, followed by 30 cycles of denaturation at 95°C for 30 sec, annealing at 50°C 30 sec and extension at 72°C for 30 sec, followed by a final extension at 72°C for 7 min.

CYP2C19*16, *18 and *19 were amplified by PCR under previously reported reaction conditions (7,8). Sequencing was performed on PCR products using an ABI PRISM 3130 DNA sequencer with a PRISM Dye

Terminator Cycle Sequencing kit, and sequence analysis software (Life Technologies Japan, Inc., Tokyo, Japan).

2.3. Novel SNP evaluation

The 3D structure of CYP2C19 is not yet registered in the Protein Data Bank (PDB). Among the PDB structures of the CYP2 family, human 2C9 (PDB code: 1OG5) was selected as a template structure for homology modeling, which was performed using the Molecular Operating Environment (MOE) (Chemical Computing Group, Inc., Canada). CYP2C19 and 2C9 share 90% amino acid identity, which is sufficiently high to construct a good model. There was also no insertion-deletion region on the sequence alignment, and this also indicated that the model structure would be reliable. AMBER99 was used for energy optimization. Of the 490 amino acids of CYP2C19, the modeled structure covered the region from amino acid No. 30 to No. 490. Thr210 was mutated to Asn using MOE. No structural optimization calculation was made for the mutated structure obtained here.

3. Results

When the CYP2C19*3 (g636a) mutation was analyzed with AS-PCR (10) and a novel automatic SNP-typing system (9), a difference in the analytical results was recognized. Therefore, when we sequenced the surrounding sequences of this mismatched allele in the present study, we found a new variation 629c>a on the probe for the system binding regions. Five mutant alleles, namely, CYP2C19*2 (g681a), *3 (g636a), *16 (c1324t), *18 (g986a, a991g), and *19 (a151g, a991g) have already been reported in the Japanese population (6-8). These five mutant alleles were not found in subjects with the 629c>a variant and thus the 629c>a variation was clearly identified as a novel variant. The new variation was found in two subjects as heterozygotes at a frequency of 0.17% (95% confidence level, 0.0-0.6%). The variation was 629c>a in exon 4 resulting in an amino acid change of Thr210 to Asn (Figure 1).

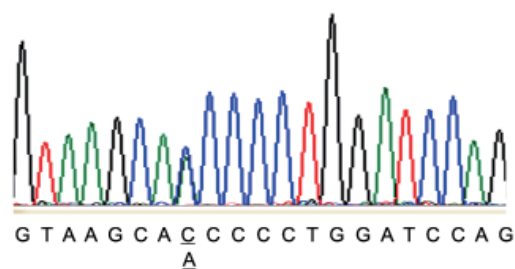


Figure 1. Nucleotide sequences of the CYP2C19 gene in exon 4 containing the 629c>a polymorphism. Both strands were sequenced, although only the sequences for sense strands are shown. The variation at 629c>a in exon 4 resulted in an amino acid change from Thr210 to Asn. Underlining indicates the position of the variant nucleotide.

There were four reasons for selecting the human 2C9 structure (PDB code: 1OG5) as a template for homology modeling. First, the amino acid identity was the highest among the CYP2C family. There were three human 2C9 structures that shared 90% identity with human 2C19. Second, there was no insertion-deletion region near the mutation site, Thr210. Third, there were Pro residues between each helix of HelixF, HelixF', HelixG', and HelixG, which probably acted to bend the helices. The position of Pro matched perfectly with that of 1OG5 (Alignment: Figure 2A, Structure: Figure 2B). Fourth, 1OG5 was a co-crystal structure. In many cases, information regarding ligand interaction is useful. As mentioned above, 1OG5 was selected as a template for homology modeling of human 2C19.

The model structure of CYP2C19 obtained is shown in Figure 3A. Thr210 was located between the F and F' helices. The side chain O γ of Thr210 had a hydrogen bond with the main chain carbonyl oxygen of Ile207 of helix F (Figures 3B and 3C). On the basis of these findings, we could speculate that Thr210 functions to maintain the bent configuration of the F-F' helices. When Thr210 was mutated to Asn, observation of the modeled structure of Thr210Asn revealed that Asn had no specific steric constraints with the other residues (Figure 4). On the basis of this finding, Thr210Asn would not cause any steric hindrance; however, the energy contribution due to hydrogen bonding between Thr210 and Ile207 might be lost.

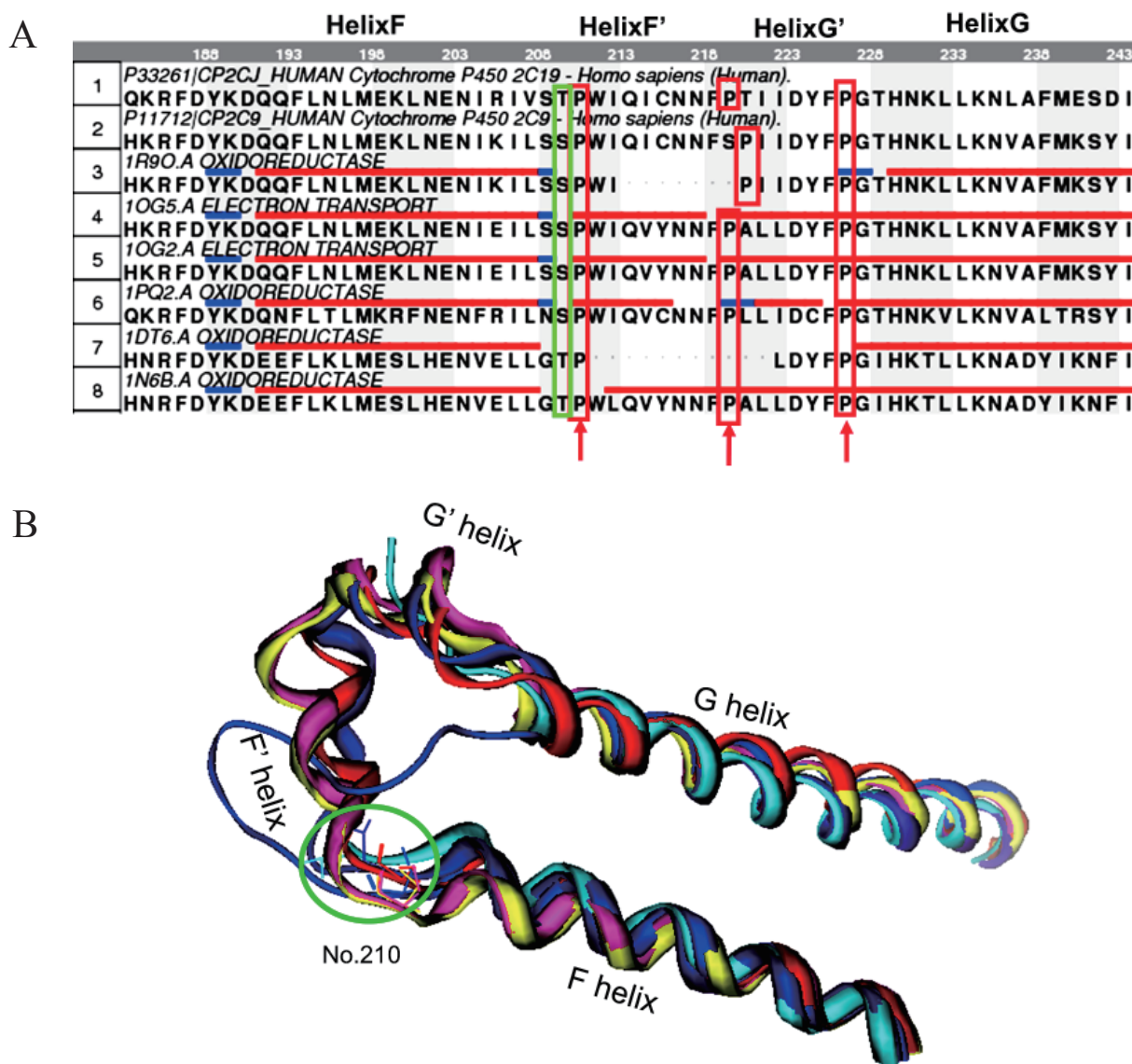


Figure 2. Alignment of CYP2C families and superimposition of F-G helix regions. (A) From top to bottom: 1, human 2C19 sequence; 2, human 2C9 sequence; 3, 1R90 (sequence of human 2C9 in PDB); 4, 1OG5 (sequence of human 2C9 in PDB); 5, 1OG2 (sequence of human 2C9 in PDB); 6, 1PQ2 (sequence of human 2C8 in PDB); 7, 1DT6 (sequence of rabbit 2C5 in PDB); 8, 1N6B (sequence of rabbit 2C5 in PDB). The amino acid corresponding to No. 210 of 2C19 is enclosed in green. The Pro between the F-G helices is colored pink. The horizontal red lines on the sequences indicate α helix regions. Blank spaces indicate an absence of coordinates. (B) Sequence numbers of the alignment shown in Figure 2A: 3, blue; 4, pink; 5, yellow; 6, orange; 7, cyan; 8, purple. The amino acid in Figure 2A is shown as a stick figure and is circled in green.

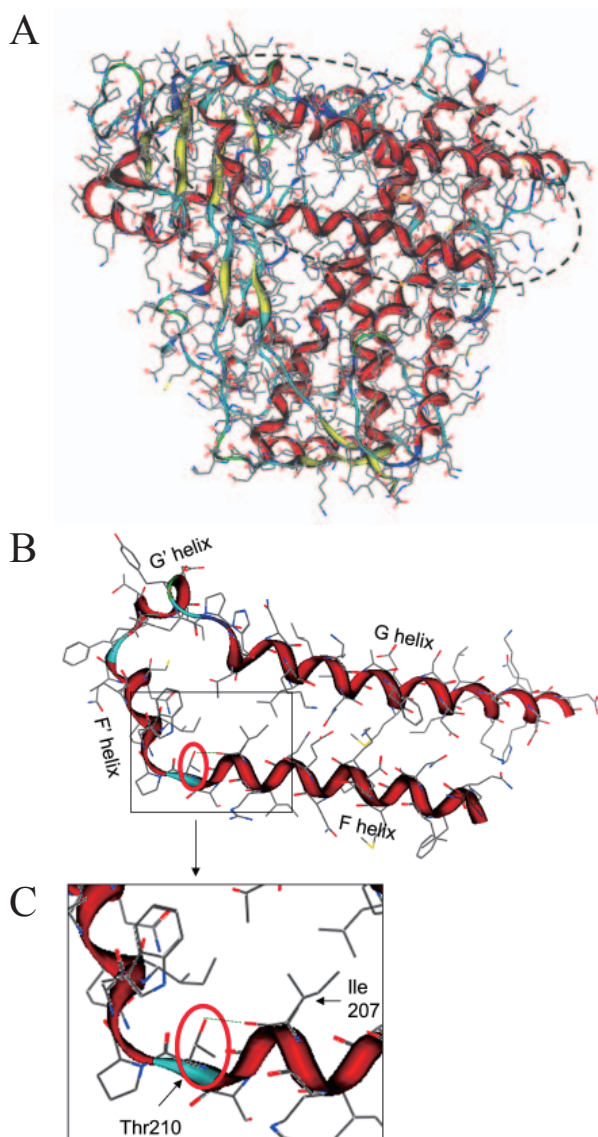


Figure 3. Human CYP2C19 model structure and magnified view of the surrounding area of Thr210 in the CYP2C19 model structure. The entire structure is shown as a stick figure. The main chain is shown as a ribbon shape. The red region in the main chain shows the α helix and the yellow region shows the β strand.

4. Discussion

Operability is improved with the SNP analysis system, which uses various methods. However, there is a limit to each technique, and there is a danger of obtaining inaccurate results. In this study, we were able to detect a novel mutation by comparing the results of two methods (9,10).

It was speculated that Thr210 functions to maintain the bent configuration of the F-F' helices *via* a hydrogen bond with Ile207 (Figure 3C). Observation of the mutated Thr210Asn structure revealed that there were no specific steric constraints with other residues. Thus, it is very likely that metabolic activity is maintained. It is essential to predict the phenotype of a subject on the basis of a genotype that confirms the effect of a

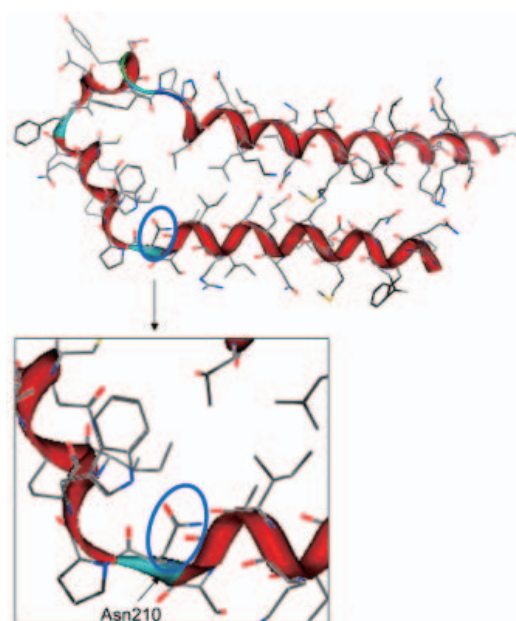


Figure 4. F-G helix region in the Thr210Asn model structure of CYP2C19 and magnified view of the area surrounding Thr210Asn.

novel mutation on function. Accordingly, we examined the function of Thr210 with regard to its tertiary structure and effect after mutation to Asn on the basis of cytochrome P450 2C19, with the conformation constructed using homology modeling. Metabolic activity comparisons are generally performed by protein expression within a different kind of cell. However, we can infer function, as in this report, if the protein crystallization structure is clear.

3D structures in the PDB show that CYP has both open and closed structures. It is considered that the F-G helices have a role of opening and shutting the gate of the pocket for substrates entering and exiting. This was speculated on the basis of a comparison between the open structure of rabbit CYP2B4 (PDB code: 1PO5) and the closed structure of rabbit CYP2B4 (PDB code: 1SUO) (11-13). The human CYP2C9 (PDB code: 1OG5) used as a template in the present study is a closed structure. Accordingly, our SNP evaluation was used to assess the effect on the closed structure, but not on the open structure, or on movement from open to closed or *vice versa*. Information about the structural movement of a CYP family member when it binds to a substrate would be useful for predicting the effect of SNPs more precisely. To predict the position of the amino acid corresponding to Thr210 of 2C19, the structures of rabbit CYP2B4 (open: PDB code: 1PO5, closed: PDB code: 1SUO) and human 2C9 (PDB code: 1OG5) were superimposed (Figure 5). In the closed structure, the amino acid was located in the position colored green in Figure 5, whereas in the open structure, it shifted to the position colored pink. In CYP2B4, the amino acid colored pink was Ser. Even when Ser was mutated to Asn, no effect appeared to be exerted on the structure as

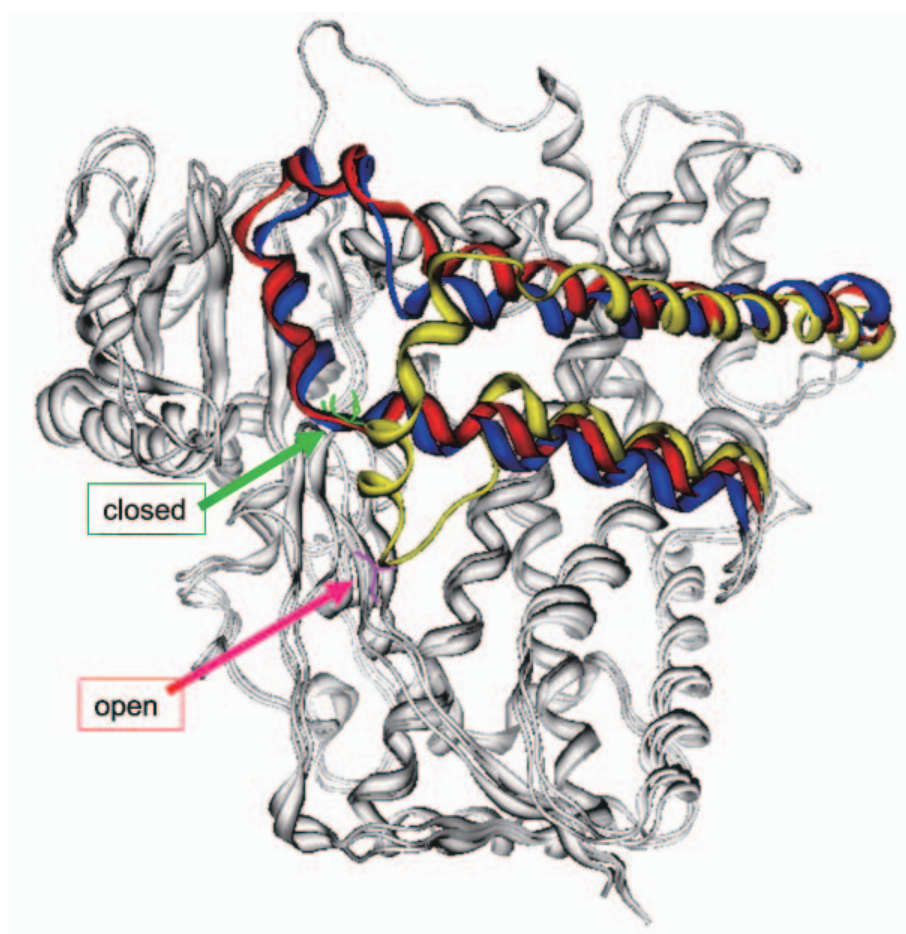


Figure 5. Superimposition of open and closed structures of CYP2B4 and 1OG5. The main chain is shown as a ribbon shape. Only the F-G helices are colored: yellow, CYP2B4 open structure (PDB code: 1PO5); blue, CYP2B4 closed structure (PDB code: 1SU0); red, CYP2C9 closed structure of template (PDB code: 1OG5).

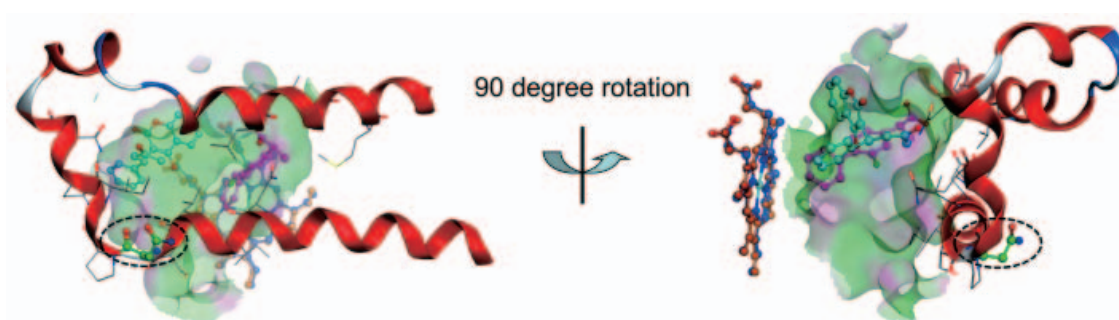


Figure 6. Position of the mutation site and substrate binding pocket. Left: F-G helices are shown in red ribbon. The surfaces of the substrate binding pocket are colored green (hydrophobic regions) and pink (hydrogen bonding regions), with a slightly transparent view. Two ligands from PDB, S-Warfarin (cyan, PDB code: 1OG5) and Flurbiprofen (pink, PDB code: 1R9O), are shown in the substrate binding pocket. Heme is situated at the most rear site, the structure of which was obtained from 1OG5 and 1R9O. The mutated residue is colored green and enclosed by a dotted black circle. Right: The same structure as that on the left, but rotated -90 degrees around the Y axis.

there was space in the surrounding area. Accordingly, assuming 2C19 has a similar open structure as 2B4, it was speculated that Thr210Asn does not exert an effect on the open structure, and this speculation is consistent with that for the closed structure. On the mutated 2C19 structure, the side chain of Asn210 is directed to the external side of the molecule, which is on the opposite side of the substrate binding pocket (Figure 6). From

this observation, it is speculated that T210N does not affect substrate binding.

On the basis of these findings, the Thr210Asn variant of 2C19 likely exerted an effect that reduced the configuration stability of helices F-F', because the hydrogen bonding of Thr210 with Ile207 on helix F was lost. However, no steric constraints were found. Thus, it is speculated that the variant might not exert an

effect sufficient to transform the structure. This novel mutation CYP2C19 629c>a that we identified results in a single amino acid substitution, Thr210>Asn, and occurs with very low frequency. Because metabolic activity is likely maintained, it does not seem reasonable that the mutation generates the gene responsible for CYP2C19 poor metabolizers.

Acknowledgements

This work was supported in part by a Grant-in-Aid for Scientific Research [C:20590156] from the Japan Society for the Promotion of Science (JSPS); and the Takeda Science Foundation.

References

1. Goldstein JA, Faletto MB, Romkes-Sparks M, Sullivan T, Kitareewan S, Raucy JL, Lasker JM, Ghanayem BI. Evidence that CYP2C19 is the major (S)-mephenytoin 4'-hydroxylase in humans. *Biochemistry*. 1994; 33:1743-1752.
2. Goldstein JA, de Morais SM. Biochemistry and molecular biology of the human CYP2C subfamily. *Pharmacogenetics*. 1994; 4:285-299.
3. Goldstein JA, Ishizaki T, Chiba K, de Morais SM, Bell D, Krahn PM, Evans DA. Frequencies of the defective CYP2C19 alleles responsible for the mephenytoin poor metabolizer phenotype in various Oriental, Caucasian, Saudi Arabian and American black populations. *Pharmacogenetics*. 1997; 7:59-64.
4. Goldstein JA. Clinical relevance of genetic polymorphisms in the human CYP2C subfamily. *Br J Clin Pharmacol*. 2001; 52:349-355.
5. Ingelman-Sundberg M, Daly AK, Nebert DW. Human Cytochrome P450 (CYP) Allele Nomenclature Committee. CYP2C19 allele nomenclature. [cited October 19, 2009] Available from: Human Cytochrome P450 (CYP) Allele Nomenclature Committee. <http://www.cypalleles.ki.se/cyp2c19.htm>
6. Kubota T, Chiba K, Ishizaki T. Genotyping of S-mephenytoin 4'-hydroxylation in an extended Japanese population. *Clin Pharmacol Ther*. 1996; 60:661-666.
7. Morita J, Kobayashi K, Wanibuchi A, Kimura M, Irie S, Ishizaki T, Chiba K. A novel single nucleotide polymorphism (SNP) of the CYP2C19 gene in a Japanese subject with lowered capacity of mephobarbital 4'-hydroxylation. *Drug Metab Pharmacokinet*. 2005; 19:236-238.
8. Fukushima-Uesaka H, Saito Y, Maekawa K, Ozawa S, Hasegawa R, Kajio H, Kuzuya N, Yasuda K, Kawamoto M, Kamatani N, Suzuki K, Yanagawa T, Tohkin M, Sawada J. Genetic variations and haplotypes of CYP2C19 in a Japanese population. *Drug Metab Pharmacokinet*. 2005; 20:300-307.
9. Matsumoto N, Kakihara F, Kimura S, Kurebayashi Y, Hirai M, Yohda M, Hasegawa S. Single nucleotide polymorphism genotyping of CYP2C19 using a new automated system. *Anal Biochem*. 2007; 370:121-123.
10. Ishiguro A, Kubota T, Soya Y, Sasaki H, Yagyu O, Takarada Y, Iga T. High-throughput detection of multiple genetic polymorphisms influencing drug metabolism with mismatch primers in allele-specific polymerase chain reaction. *Anal Biochem*. 2005; 337:256-261.
11. Scott EE, He YA, Wester MR, White MA, Chin CC, Halpert JR, Johnson EF, Stout CD. An open conformation of mammalian cytochrome P450 2B4 at 1.6-Å resolution. *Proc Natl Acad Sci U S A*. 2003; 100:13196-13201.
12. Scott EE, White MA, He YA, Johnson EF, Stout CD, Halpert JR. Structure of mammalian cytochrome P450 2B4 complexed with 4-(4-chlorophenyl)imidazole at 1.9-Å resolution: Insight into the range of P450 conformations and the coordination of redox partner binding. *J Biol Chem*. 2004; 279:27294-27301.
13. Poulos TL. Cytochrome P450 flexibility. *Proc Natl Acad Sci U S A*. 2003; 100:13121-13122.

(Received June 14, 2010; Accepted June 23, 2010)

Original Article

Quantification of nebivolol hydrochloride in human plasma by liquid chromatography using fluorescence detection: Use in pharmacokinetic study

Laila Abdel-Fattah¹, Lobna Abdel-Aziz², Amira El-Kosasy², Mariam Gaied^{2,*}

¹ Analytical Chemistry Department, Faculty of Pharmacy, Misr University for Science and Technology, 6 October city, Egypt;

² Pharmaceutical Analytical Chemistry Department, Faculty of Pharmacy, Ain Shams University, Cairo, Egypt.

ABSTRACT: A simple, rapid, and sensitive method of reversed-phase high-performance liquid chromatography with fluorescence detection has been developed and validated for use in determining levels of nebivolol·HCl in human plasma. Sample preparation involves a simple single-step protein precipitation procedure and extraction of nebivolol in acetonitrile. The separation was performed on a Kromasil[®] RP-C18 column (Φ 4.6 mm \times 250 mm, 5 μ m) with a mobile phase consisting of 0.05 M potassium dihydrogen phosphate buffer/acetonitrile (40:60, v/v) adjusted to pH 3 using orthophosphoric acid. Analysis was carried out under isocratic conditions at a flow rate of 1.5 mL/min and at room temperature using a fluorescence detector with excitation at 288 nm and emission at 310 nm. The chromatographic run was 4 min. The calibration curve was linear over the concentration range 0.2-20 ng/mL. The method was validated in terms of its accuracy, precision, and specificity. The assay enabled the measurement of nebivolol with a minimum quantification limit of 0.16 ng/mL. The average recovery of nebivolol from spiked human plasma was $98.4 \pm 3.3\%$. This method was successfully used in a pharmacokinetic study of oral administration of 5-mg tablets to healthy human volunteers.

Keywords: Nebivolol, plasma, high performance liquid chromatography, fluorescence detection, pharmacokinetic study

*Address correspondence to:

Dr. Mariam Gaied, Pharmaceutical Analytical Chemistry Department, Faculty of Pharmacy, Ain Shams University, P.O.B. 11566, Street of "The African Union Organization", Abbaseya, Cairo, Egypt.
e-mail: dr_mariamhany@yahoo.com

1. Introduction

Chemically, nebivolol·HCl is (1RS,1'RS)-1,1'-[(2RS,2'SR)-bis(6-fluoro-3,4-dihydro-2H-1-benzopyran-2-yl)]-2,2'-iminodiethanol hydrochloride (Figure 1). Nebivolol is approximately 3.5 times more β_1 -adrenoceptor-selective than other β_1 -adrenergic blockers in human myocardium and thus might be the most β_1 -adrenoceptor-selective antagonist available for clinical practice at the moment (1). It has a combined vasodilating β_1 -blocker activity with a vasodilating effect mediated by the endothelial L-arginine nitric oxide pathway (2,3). Nebivolol is a racemic mixture of L-nebivolol (RSSS) and D-nebivolol (SRRR) present in equal proportions, as both are necessary for the drug to have maximum effect (4,5). The effect of nebivolol on heart rate is exclusively exerted by D-nebivolol (affinity for β_1 -receptors that is 100-fold higher than that of the L-isomer). Both the D- and L-isomers facilitate nitric oxide release to induce a vasodilator effect (6,7).

Several methods for determining levels of nebivolol in pharmaceutical dosage forms have been described, including UV spectrophotometry (8), capillary electrophoresis (9), high-performance thin-liquid chromatography (HPTLC) (10), and high-performance liquid chromatography (HPLC) (10,11) with UV detection. Two chromatographic methods focused on the separation of enantiomers (12) and the determination of nebivolol metabolites (13). Few methods for determining the level of nebivolol in human plasma or serum have been reported, and all depend on mass detection (14-16). Although they are sensitive and have low quantitation limits, mass detection has its limitations. The equipment is complex and requires extensive technical expertise for its

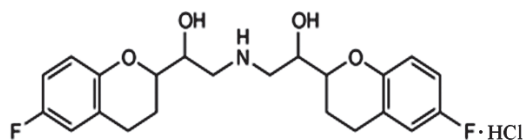


Figure 1. Chemical structure of nebivolol hydrochloride.

maintenance and operation. Moreover, it is not affordable and not easily available to most research laboratories because of the high cost (17,18). Only one of these methods has been used in a study of the pharmacokinetics of fixed oral dosage forms combining nebivolol and valsartan. Although one method of determining the level of nebivolol in plasma based on fluorescence detection was previously developed (19), it suffered from the disadvantage of lengthy and highly complicated sample pretreatment. The extraction method was time-consuming due to multiple-step procedures. With the reported method, nebivolol was extracted from alkalinized human plasma with heptane/isoamyl alcohol (95:5, v/v), back-extracted with dilute sulfuric acid, and re-extracted after alkalization. These multiple steps compromised the accuracy and sensitivity of the method.

This paper describes the development and validation of a simple, rapid, and sensitive method of isocratic reversed-phase HPLC for determining the level of nebivolol in human plasma using fluorescence detection. The method described here is an approach to simplify the sample preparation procedures while maintaining a high level of sensitivity and specificity and minimizing the operating cost. Sample preparation involves simple single-step protein precipitation. In addition, the use of a small sample volume and short analysis time provides advantages for analyzing nebivolol in plasma. The method was successfully used in a pharmacokinetic study of humans.

2. Materials and Methods

2.1. Chemicals

Nebivolol·HCl was generously supplied by Berlin Chemie AG, Berlin, Germany. HPLC-grade water, acetonitrile, and methanol were obtained from Sigma GmbH, Mannheim, Germany. Orthophosphoric acid and potassium dihydrogen phosphate were obtained from Ridel-de Haën, Germany. Nebilet® tablets produced by Berlin Chemie AG, batch No. 74529, labeled to contain 5 mg of nebivolol·HCl, were obtained from a local market.

2.2. Equipment and chromatographic conditions

The chromatographic apparatus consisted of an HPLC system (Young Lin, Anyang, Korea) equipped with a gradient pump (HPLC pump SP 930D), Young Lin Acme 9000 vacuum degasser & mixer, and LC305 fluorescence detector. Data acquisition was performed with Autochrom-3000 software, version 2.0.0. Separation was performed on a Kromasil® RP-C18 column (Φ 4.6 mm \times 250 mm, 5 μ m; Eka Chemicals AB, Bohus, Sweden). The mobile phase used was acetonitrile/50 mM phosphate buffer, pH 3, adjusted using orthophosphoric acid (40:60, v/v). All analyses were carried out under isocratic conditions at a flow rate of 1.5 mL/min and at

room temperature using a fluorescence detector with excitation at 288 nm and emission at 310 nm. The mobile phase was prepared daily and degassed by ultrasonication. All solvents were filtered through a 0.45- μ m disposable membrane filter immediately before use.

2.3. Standard solutions

A stock solution (100 μ g/mL) of nebivolol·HCl was prepared in methanol. Then, 10 μ g/mL and 100 ng/mL working standards were prepared in the mobile phase.

2.4. Sample preparation

One mL acetonitrile was added to 1 mL of spiked human plasma. The mixture was vortexed for 2 min and centrifuged for 10 min at 8,000 rpm. The upper layer was filtered through a 0.45- μ m Millipore syringe filter. Twenty μ L of the supernatant were injected onto the liquid chromatograph for analysis.

2.5. Plasma standard curve

Blank plasma was prepared from heparinized whole-blood samples collected from healthy volunteers and stored at -20°C . After thawing, 1-mL blank (drug-free) plasma samples were spiked with nebivolol working standard solutions to provide concentrations of 0.2, 0.5, 1, 1.5, 2, 3, 4, 10, 15, and 20 ng/mL. The samples were then prepared for analysis as described above.

2.6. Selectivity and specificity

Control human plasma, obtained from 12 healthy volunteers, was assessed by the procedure described above and compared with respective plasma samples to evaluate the selectivity of the method.

2.7. Precision and accuracy

The precision and accuracy of the method were examined by adding known amounts of nebivolol·HCl to pool plasma. For intraday precision and accuracy, three samples at each concentration were assayed on the same day. The interday precision and accuracy were evaluated on three different days.

2.8. Limit of quantification (LOQ) and recovery

The limit of quantification (LOQ) is the analyte concentration producing a signal-to-noise (S/N) ratio ≥ 10 . For spiked plasma samples, the relative analytical recovery at three different concentrations of nebivolol (0.5, 4, and 10 ng/mL) was determined by comparing the peak areas for nebivolol extracted from spiked plasma and a standard solution of nebivolol in acetonitrile with the same initial concentration (three

samples for each concentration level).

2.9. Biological samples

Twelve healthy male volunteers were included in this study. The study was conducted in accordance with the International Ethical Guidelines for clinical studies in humans set out in the Declaration of Helsinki (20) as well as with the latest guidelines on Good Clinical Practice of the International Conference on Harmonization (21). Written informed consent was obtained from the volunteers. Nebivolol·HCl was administered to volunteers in a single dose of a 5-mg tablet after fasting overnight. Fourteen blood samples were collected at 0, 15, 30, and 45 min, 1, 1.5, 2, 2.5, 3, 4, 6, 9, 12, and 24 h after dosing. The collected samples were immediately centrifuged and the plasma was frozen and stored at -20°C until analysis. Plasma samples were labeled by protocol number, the subject's initials, treatment, and sample time, and samples were then forwarded to the laboratory.

3. Results and Discussion

3.1. Method development

A protein precipitation technique was used as an extraction method for sample preparation in this work. A protein precipitation technique can help produce a spectrometrically clean sample and avoid interference with the analyte by endogenous substances in plasma. The mobile phase at different concentrations of acetonitrile was evaluated as a precipitating solvent, but pure acetonitrile was found to be optimal. It produced clean chromatograms for blank plasma samples and yielded the highest recovery for the analyte from human plasma (data not shown).

The chromatographic conditions, including the detector settings, were optimized through several trials to achieve good resolution and symmetric peaks of the analyte as well as a short run time. The effect of the acetonitrile concentration in the mobile phase on the separation of nebivolol was studied. As the concentration of acetonitrile increased, the retention of nebivolol decreased (data not shown). The optimum acetonitrile concentration was found to be 30-45%, as it produced an acceptably short retention time (data not shown). In addition, the effect of buffer pH was investigated. Orthophosphoric acid was found to be necessary in order to lower the pH to protonate the nebivolol and thus deliver a good peak (data not shown). The buffer was adjusted to pH 3. At a higher pH, nebivolol was carried out faster with the mobile phase, but higher un-ionized species led the drug to stick out or partition with the stationary phase (data not shown). This resulted in tailing and hence increased asymmetry of the peak. At a lower pH, the ionized hydrophilic species were not substantially partitioned with the stationary phase and hence produced

a symmetric peak (data not shown). Satisfactory results were obtained at a pH between 3.5 and 2.5. The use of a pH lower than 2.5 was not recommended to avoid deterioration of the column. Thus, the best chromatographic separation was achieved at pH 3. The average retention time \pm S.D., obtained for six replicates, was found to be 1.81 ± 0.04 min (data not shown). The run time was 4 min, which offers the advantage of rapid analysis and reduction of the consumed solvents.

3.2. Method validation

The linearity of the calibration curve was determined by plotting the average peak area versus the nominal concentration of nebivolol·HCl. To evaluate the linearity of the method, plasma calibration curves were determined in triplicate on three different days. Good linearity was observed over the concentration range 0.2-20 ng/mL and the correlation coefficient was 0.9999. No significant changes were observed in the values of the slope, intercept, and correlation coefficient on both interday and intraday calibrations. The lower limit of quantitation of nebivolol using the described method was found to be 0.16 ng/mL (producing a signal-to-noise (S/N) ratio ≥ 10). This was sensitive enough for drug monitoring in pharmacokinetic studies. The instrumental response sensitivity is the slope of the calibration line because a method with a large slope is better able to discriminate between small differences in analyte content (22). The relative standard deviation (R.S.D.) values for the recovery of nebivolol at three different concentrations were 3.04 and 3.87% for intraday and interday precision, respectively. According to the Washington Conference Report (23), the maximum R.S.D. for a method using plasma should be $\leq \pm 15\%$ (and at the limit of quantitation $\leq \pm 20\%$). This indicates that the proposed method is highly precise. The results of assay validation are summarized in Table 1. For each point of calibration standards, the concentrations were recalculated from the equation of the linear regression curves. The average recovery of nebivolol from spiked plasma samples was $98.4 \pm 3.3\%$ ($n = 3$). Table 2 shows the average recovery of nebivolol from spiked plasma samples at different concentrations. Table 3 shows the results of interday and intraday precision.

Several validation documents (23,24) require only six different sources of blank matrices to be analyzed to demonstrate that there is no interference in the chromatographic region of the analyte. The proposed method was tested for specificity by comparing chromatograms of 12 different sources of blank human plasma (from 12 volunteers). The chromatograms were free from any interfering peaks at the retention time of nebivolol·HCl. Thus, the proposed method can be used to determine the level of nebivolol·HCl in plasma without interference by endogenous plasma components. A typical chromatogram of human plasma

Table 1. Results of assay validation of the proposed HPLC method for determination of nebivolol·HCl in human plasma

| Parameters | Values |
|-----------------------------------|-------------|
| Linearity range (ng/mL) | 0.2 to 20 |
| Slope | 1,326 |
| Intercept | 52.78 |
| Accuracy | 98.4 ± 3.3% |
| Correlation coefficient (r^2) | 0.9999 |
| Intraday precision (R.S.D. %)* | 3.04 |
| Interday precision (R.S.D. %)* | 3.87 |

* The intraday and the interday relative standard deviations were determined using samples with a concentration of 0.5, 4, and 10 ng/mL performed in triplicate.

Table 2. Determination of human plasma samples spiked with nebivolol·HCl using the proposed HPLC method

| Sampled (ng/mL) | Found* (ng/mL) | % Recovery (mean ± S.D.) |
|-----------------|----------------|--------------------------|
| 0.2 | 0.186 | 92.9 ± 5.9 |
| 0.5 | 0.477 | 95.4 ± 2.9 |
| 1 | 0.957 | 95.7 ± 1.0 |
| 1.5 | 1.45 | 96.8 ± 1.9 |
| 2 | 1.97 | 98.4 ± 6.0 |
| 3 | 3.05 | 101.5 ± 3.6 |
| 4 | 4.05 | 101.2 ± 4.2 |
| 10 | 10.22 | 102.2 ± 2.8 |
| 15 | 14.70 | 88.0 ± 1.3 |
| 20 | 20.35 | 101.7 ± 4.7 |
| Mean ± R.S.D. | | 98.4 ± 3.3 |

* Mean of three determinations.

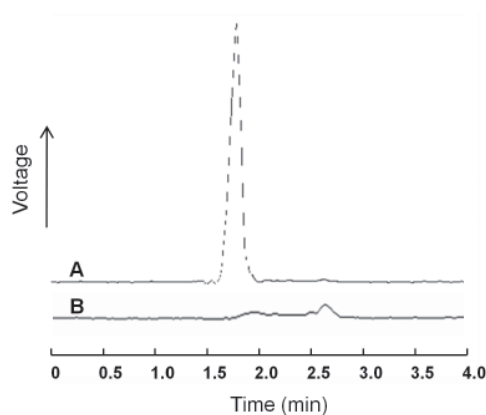
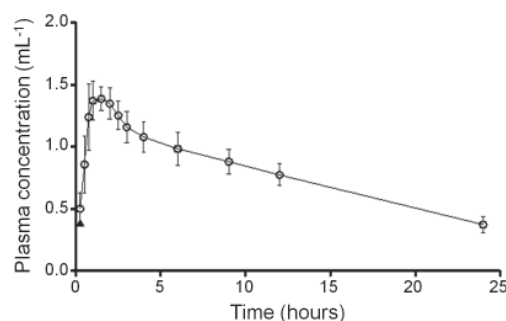
Table 3. Reproducibility of the analysis of nebivolol in human plasma

| Concentration added (ng/mL) | Recovery (mean ± S.D.)* | |
|-----------------------------|-------------------------|--------------|
| | Intraday | Interday |
| 0.5 | 0.48 ± 0.02 | 0.47 ± 0.02 |
| 4 | 4.01 ± 0.13 | 4.10 ± 0.20 |
| 10 | 10.22 ± 0.29 | 10.24 ± 0.34 |

* $n = 3$.

spiked with nebivolol·HCl is shown in Figure 2A, and a chromatogram of blank drug-free human plasma is shown in Figure 2B. The spiked human plasma samples, stored at -20°C and injected over a period of 1 month, did not exhibit any appreciable changes in assay values and were able to meet the criterion mentioned above (data not shown). Nebivolol was also found to be stable in human plasma for more than a month and its stability was maintained at room temperature for more than 12 h. Extraction efficiency was verified by the accuracy of the proposed method and there were no significant differences in the recovery from extracted and non-extracted samples containing the same concentration of nebivolol·HCl (data not shown).

The developed method was successfully used in a pharmacokinetics study of 12 healthy male volunteers

**Figure 2. Typical HPLC chromatograms of human plasma. A, human plasma spiked with nebivolol·HCl; B, blank drug-free human plasma.****Figure 3. Plasma concentration time curve for nebivolol following oral administration of Nebilet® tablets.****Table 4. Summary of pharmacokinetic parameters of nebivolol·HCl following oral administration of Nebilet®**

| Pharmacokinetic parameters | Values (mean ± S.D.) |
|--|----------------------|
| C_{\max} (ng/mL) | 1.52 ± 0.09 |
| T_{\max} (h) | 1.17 ± 0.47 |
| AUC_{0-24} (ng/mL·h) | 18.84 ± 1.92 |
| $AUC_{0-\infty}$ (ng/mL·h) | 25.75 ± 3.42 |
| $K_{\text{elimination}}$ (h^{-1}) | 0.056 ± 0.005 |
| $t_{1/2 \text{ elimination}}$ (h) | 12.63 ± 1.11 |

who took a 5-mg oral tablet of nebivolol after fasting overnight. Figure 3 shows the mean plasma concentration-time curve for nebivolol·HCl. The plasma concentration reached a maximum 1.17 ± 0.47 h after dosing with a level of 1.52 ± 0.09 ng/mL. The derived pharmacokinetic parameters of the 12 healthy volunteers are summarized in Table 4. These pharmacokinetic parameters are in good agreement with those noted previously (16,25,26).

4. Conclusion

A rapid, sensitive, and accurate method of liquid chromatography with fluorescence detection was developed to determine the level of nebivolol·HCl in human plasma. The method has a high sensitivity with a LOQ of 0.16 ng/mL, good linearity in a concentration

range of 0.2-20 ng/mL, and good specificity without interference from endogenous substances in plasma. The method has additional advantages such as a short run time (4 min), low sample volume (20 μ L), and simplicity of sample preparation (single-step protein precipitation). These advantages, combined with the relatively inexpensive and readily available equipment used, led to its successful use in a pharmacokinetic study of nebivolol·HCl in human volunteers.

References

- Bristow MR, Nelson P, Minobe W, Johnson C. Characterization of β 1-adrenergic receptor selectivity of nebivolol and various other beta-blockers in human myocardium. *Am J Hyperten*. 2005; 18:A51-A52.
- Mangrella M, Ross F, Fici F, Rossi F. Pharmacology of nebivolol. *Pharmacol Res*. 1998; 38:419-431.
- Ritter JM, Dawes M, Brett SE, Cockcroft JR, Chowieczyk PJ. Mechanism of vasodilating action of Nebivolol. *Biomed Pharmacother*. 1996; 50:396-399.
- Tuchalski G, Emmerling F, Gröger K, Hänsicke A, Nagel T, Reck G. X-ray investigations of nebivolol and its isomers. *J Mol Struct*. 2006; 800:28-44.
- Ignarro LJ. Different pharmacological properties of two enantiomers in a unique beta-blocker, nebivolol. *Cardiovasc Ther*. 2008; 26:115-134.
- Xhonneux R, Wouters L, Reneman RS, Janssen PA. The l-enantiomer of nebivolol potentiates the blood pressure lowering effect of the d-enantiomer. *Eur J Pharmacol*. 1990; 181:261-265.
- Poirier L, Cleroux J, Lefebvre I, Archambault F, Lacourcière Y. Comparative efficacy of D-nebivolol and dl-nebivolol in confirmed ambulatory hypertensive subjects. *Am J Hypertens*. 1995; 8:129A.
- Kamila MM, Mondal N, Ghosh LK, Gupta BK. A validated UV spectrophotometric method for estimation of nebivolol hydrochloride in bulk and pharmaceutical formulation. *Pharmazie*, 2007; 62:486-487.
- Mangelings D, Discry J, Maftouh M, Massart DL, Vander Heyden Y. Strategy for the chiral separation of non-acidic pharmaceuticals using capillary electrochromatography. *Electrophoresis*. 2005; 26:3930-3941.
- Patel LJ, Suhagia BN, Shah PB. RP-HPLC and HPTLC methods for the estimation of nebivolol hydrochloride in tablet dosage form. *Indian J Pharm Sci*. 2007; 69:594-596.
- Rajeswari KR, Sankar GG, Rao AL, Raju DB, Rao S. RP-HPLC estimation of Nebivolol in bulk and pharmaceutical dosage form. *Asian J Chem*. 2005; 17:1259-1263.
- Aboul-Enien HY, Ali I. HPLC enantiomeric resolution of nebivolol on normal and reversed amylose based chiral phases. *Pharmazie*, 2001; 56:214-216.
- Hendrickx J, Bockx M, Zwijsen C, Borgmans C, Mannens G, Meuldermans W, Heykants J. Location of the hydroxyl functions in hydroxylated metabolites of nebivolol in different animal species and human subjects as determined by on-line high-performance liquid chromatography-diode-array detection. *J Chromatogr A*. 1996; 729:341-354.
- Maurer HH, Tenberken O, Kratzsch C, Weber AA, Peters FT. Screening for library-assisted identification and fully validated quantification of 22 beta-blockers in blood plasma by liquid chromatography – mass spectrometry with atmospheric pressure chemical ionization. *J Chromatogr A*. 2004; 1058:169-181.
- Ramakrishna NV, Vishwottam KN, Koteshwara M, Manoj S, Santosh M, Varma DP. Rapid quantification of nebivolol in human plasma by liquid chromatography coupled with electrospray ionization tandem mass spectrometry. *J Pharm Biomed Anal*. 2005; 39:1006-1013.
- Selvan PS, Gowda KV, Mandal U, Solomon WD, Pal TK. Simultaneous determination of fixed dose combination of nebivolol and valsartan in human plasma by liquid chromatographic-tandem mass spectrometry and its application to pharmacokinetic study. *J Chromatogr B Analyt Technol Biomed Life Sci*. 2007; 858:143-150.
- Murugaiyah V, Chan KL. Analysis of lignans from *Phyllanthus niruri* L. in plasma using a simple HPLC method with fluorescence detection and its application in a pharmacokinetic study. *J Chromatogr B Analyt Technol Biomed Life Sci*. 2007; 852:138-144.
- Thieme D, Sachs H. Improved screening capabilities in forensic toxicology by application of liquid chromatography – tandem mass spectrometry. *Anal Chim Acta*. 2003; 492:171-186.
- Woestenborghs R, Embrechts L, Heykants J. HPLC-fluorescence method for the determination of the new β 1-adrenoreceptor blocking agent nebivolol in human plasma. *Methodol Surv Biochem Anal*. 1988; 18:215-216.
- World Medical Association's Declaration of Helsinki, Ethical principles for medical research involving human subjects. Adopted by the 18th World Medical Assembly (WMA), Helsinki, Finland, June 1964. Amended by the 29th WMA General Assembly, Tokyo, Japan, October 1975; 35th WMA General Assembly, Venice, Italy, October 1983; 41st WMA General Assembly, Hong Kong, September 1989; 48th WMA General Assembly, Somerset West, Republic of South Africa, October 1996, and 52nd WMA General Assembly, Edinburgh, Scotland, October 2000.
- ICH Guidelines (1996) Topic E6: Guideline for Good Clinical Practice – Consolidated Guideline, International Federation of Pharmaceutical Manufacturers, Geneva, Switzerland (<http://www.ich.org/pdf/ICH/e6.pdf>).
- Guidance for the Industry: Bioanalytical Method Validation, Department of Health and Human Services, US Food and Drug Administration, Center for Drug Evaluation and Research (CDER), Rockville, MD, 2001 (<http://www.fda.gov/cder/guidance/4252fnl.pdf>).
- Shah VP, Midha KK, Dighe S, McGilveray IJ, Skelly JP, Yacobi A, Layloff T, Viswanathan CT, Cook CE, McDowall RD, Pittman KA, Spector S. Analytical methods validation: Bioavailability, bioequivalence and pharmacokinetic studies. *Pharm Res*. 1992; 9:588-592.
- International Organization for Standardization, Accuracy (Trueness and Precision) of Measurement Methods and Results, Geneva, Switzerland, 1994.
- Cheyamol G, Woestenborghs R, Snoeck E, Ianucci R, Le Moing JP, Naditch L, Levron JC, Poirier JM. Pharmacokinetic study and cardiovascular monitoring of nebivolol in normal and obese subjects. *Eur J Clin Pharmacol*. 1997; 51:493-498.
- Anthony C, Moffat AC, Osselton DM, Widdop B, eds. *Clarke's Analysis of Drugs and Poisons*, 3rd ed., Vol. 2. Pharmaceutical Press, Chicago, IL, USA, 2004; p. 1322.

(Received September 14, 2010; Revised October 10, 2010; Accepted October 30, 2010)

Original Article**Use of factorial design in formulation and evaluation of ophthalmic gels of gatifloxacin: Comparison of different mucoadhesive polymers****Indrajeet D. Gonjari^{1,*}, Amrit B. Karmarkar^{1,*}, Trushali S. Khade¹, Avinash H. Hosmani¹, Rajesh B. Navale²**¹ *Pharmaceutics Dept., Govt. College of Pharmacy, Karad, Maharashtra, India;*² *Govt. College of Pharmacy, Aurangabad, Maharashtra, India.*

ABSTRACT: The aim of this research was to develop different ophthalmic gels of gatifloxacin using mucoadhesive polymers. To improve intraocular delivery of topically applied drugs such as gatifloxacin, gel formulations were prepared since solutions have a shorter ocular residence time because of tear turnover. A 3² factorial design was used to investigate the combined effect of two independent formulation variables in the preparation of the gels. Nine batches were prepared as per experimental design and evaluated for gelation temperature, gel strength, bioadhesion, viscosity, permeation, and antimicrobial efficacy. A surface plot was also created to graphically represent the effect of the independent variables on the evaluation parameters. Drug polymer compatibility was evaluated by differential scanning calorimetry and Fourier transform infrared spectroscopy. The prepared gels were observed to have a satisfactory gelation temperature, gel strength, and bioadhesion. Rheological study of the formulations indicated that gels exhibited pseudoplastic rheology. A modified device was used to evaluate drug permeation through a sheep's corneal membrane. *In vitro* permeation studies showed that a Peppas model was the best-fit model. Antimicrobial studies also indicated efficacy comparable to that of a marketed formulation. This systematic approach to formulation design should help in investigating the effect of variables in formulation processing.

Keywords: Factorial design, ophthalmic gels, gatifloxacin, poloxamer.

1. Introduction

Ophthalmic delivery is one of the most interesting and challenging areas of pharmaceutical research (1,2). Topical ocular infections and especially fungal infections can be effectively treated with ocular delivery itself rather than with oral delivery of drugs. Eyedrops and suspensions are often used for topical administration of ophthalmically active drugs to tissues around the ocular cavity. A drawback of these preparations is that the active constituent present is diluted by tear film as the dosage form is introduced into the cul-de-sac and is rapidly drained away from pre-corneal cavity by constant tear flow and lacrimo-nasal drainage. As a result, only a small fraction of the dose is absorbed by ocular tissue. Hence, frequent administration and use of concentrated solutions appears to be a better approach to obtain the desired therapeutic effect (3). Some ocular delivery systems extend the duration of drug action by enhancing corneal absorption (4). These include soluble gels and emulsions (5,6), hydrophilic ocular inserts (7), ion-pair associations (8), and prodrugs and liposomes (9-12). The use of gels for the ocular administration of drugs offers many advantages compared to conventional eyedrops, mainly as a consequence of the more prolonged corneal contact time (13). Many techniques have been utilized to modify the response to drugs that are delivered topically to the eye. The concept of *in situ* forming gels using poloxamers has been reviewed by Karmarkar *et al.* (14) and such systems have been investigated using phase-transition polymers (15-19). Sodium alginate has been used extensively to form polymeric dispersions in buffers that typically show low viscosity up to pH 5 and coacervate in contact with tears and thus form gels (20). *In situ* gels of these polymers can be conveniently applied to the conjunctival sac where they undergo transition from a sol to gel. Prolongation of residence time due to these *in situ* gelling systems will help to deliver a drug continuously in a controlled manner to the anterior chamber of the eye and will eliminate frequent administration of the drug, thus leading to better patient compliance and extended action. This will result in a

*Address correspondence to:

Dr. Indrajeet D. Gonjari and Amrit B. Karmarkar, Pharmaceutics Dept., Govt. College of Pharmacy, Karad, Maharashtra, India.
e-mail: indrajeetgonjari@gmail.com (Gonjari ID), abkarmarkar@gmail.com (Karmarkar AB).

dose reduction and help to minimize local and systemic side effects (21). The present work emphasizes the preparation and evaluation of various *in situ* gels of gatifloxacin prepared through use of sodium alginate and mucoadhesive polymers such as poloxamer 407, Carbopol 974P, and hydroxyethyl cellulose (HEC). A 3² factorial design was used to investigate the combined effect of two independent formulation variables in the preparation of *in situ* gels. A surface plot was also created to graphically represent the effect of independent variables on the evaluation parameters.

2. Materials and Methods

2.1. Materials

Gatifloxacin was donated by Cipla (Mumbai, India). Poloxamer 407 and Carbopol 974P were supplied by BASF (Schwarzeide, Germany) and Noveon (Mumbai, India), respectively. HEC was donated by Okasa Pharma (Maharashtra, India) and sodium alginate was purchased from Loba Chemie (Mumbai, India). All other chemicals were of analytical grade.

2.2. Differential scanning calorimetry (DSC)

Differential scanning calorimetry (DSC; SDT2960, TA Instruments Inc., New Castle, DE, USA) was performed using assess thermotropic properties and thermal behaviors of gatifloxacin, poloxamer 407, HEC, sodium alginate, a physical mixture of gatifloxacin/sodium alginate (1:1), Carbopol 974P, a physical mixture of gatifloxacin/sodium alginate/HEC (1:1:1), a physical mixture of gatifloxacin/poloxamer 407/HEC (1:1:1), a physical mixture of gatifloxacin/Carbopol 974P/HEC (1:1:1), and a physical mixture of gatifloxacin/poloxamer 407/Carbopol 974P/HEC (1:1:1:1). Samples (3-5 mg) were placed in aluminum pans with lids at a constant heating range of 15°C/min in a temperature range up to 300°C. Nitrogen was used as a purge gas through the DSC cell.

2.3. Fourier transform infrared spectroscopy (FTIR)

For Fourier transform infrared spectroscopy (FTIR), infrared spectra were obtained using a Perkin-Elmer

Spectrum-one FTIR spectrometer (Shelton, CT, USA) with KBr disks. The samples (gatifloxacin, poloxamer 407, HEC, sodium alginate, Carbopol 974P, and their physical mixtures) were previously ground and mixed thoroughly with KBr. The KBr disks were prepared by compressing the powder. The scanning range was kept at 4,000-500 cm⁻¹.

2.4. 3² Factorial design and regression analysis

Batches were prepared using a 3² factorial design (22,23). The advantages of a factorial design include greater precision. Using a factorial design allows examination of the effect of one variable when other factors are changed, something which is not possible using traditional methods of investigation. A statistical model incorporating interactive and polynomial terms was utilized to evaluate the responses.

$$Y = \beta_0 + \beta_1 X_1 + \beta_2 X_2 + \beta_{12} X_1 X_2 + \beta_{11} X_1^2 + \beta_{22} X_2^2$$

--- Eq. 1

where Y is the dependent variable, β_0 is the arithmetic mean response of the nine runs, and β_1 is the estimated coefficient for the factor X₁. The main effects (X₁ and X₂) represent the average results of changing one factor at a time from a low to high value. The interaction terms (X₁X₂) show how the response changes when two factors are simultaneously changed. The polynomial terms (X₁² and X₂²) are included to investigate non-linearity. Multiple regression analysis and F statistics were used to identify statistically significant terms.

2.5. Preparation of ophthalmic gels

2.5.1. Composition of poloxamer gel

Formulations were prepared using a 3² factorial design (Tables 1 and 2). Different formulations of poloxamer 407 were prepared by the cold method

Table 1. Experimental design of poloxamer 407 gels

| Variables | Level 1 | Level 2 | Level 3 |
|---|---------|---------|---------|
| Poloxamer 407 (% w/w) (X ₁) | 18 | 20 | 22 |
| HEC (% w/w) (X ₂) | 1 | 2 | 3 |

Table 2. Compositions of ophthalmic gels using poloxamer

| Formulation code | Gatifloxacin (% w/w) | Poloxamer 407 (% w/w) | HEC (% w/w) | Tween 20 (% w/w) | Benzalkonium chloride (% w/w) |
|------------------|----------------------|-----------------------|-------------|------------------|-------------------------------|
| P1 | 0.3 | 18 | 1 | 2 | 0.01 |
| P2 | 0.3 | 18 | 2 | 2 | 0.01 |
| P3 | 0.3 | 18 | 3 | 2 | 0.01 |
| P4 | 0.3 | 20 | 1 | 2 | 0.01 |
| P5 | 0.3 | 20 | 2 | 2 | 0.01 |
| P6 | 0.3 | 20 | 3 | 2 | 0.01 |
| P7 | 0.3 | 22 | 1 | 2 | 0.01 |
| P8 | 0.3 | 22 | 2 | 2 | 0.01 |
| P9 | 0.3 | 22 | 3 | 2 | 0.01 |

(24). A calculated amount of poloxamer 407 was added to cold distilled water with continuous agitation using a magnetic stirring bar and then the required quantity of HEC was added with continuous stirring until it completely dissolved. The resulting dispersion was left at 4°C overnight until a clear solution was obtained. Gatifloxacin was dissolved in 0.1 N HCl and the solution was neutralized with 0.1 N NaOH. Benzalkonium chloride and Tween 20 were added to the above solution. The drug solution was added to the poloxamer solution. Volume was then brought up using phosphate buffer, pH 7.4. The developed formulations were placed in 10-mL amber glass vials closed with gray butyl rubber stoppers and sealed with aluminium caps. The formulations in their final form were subjected to terminal sterilization by autoclaving at 121°C and 15 psi for 20 min.

2.5.2. Composition of Carbopol 974P gels

Formulations were prepared using a 3² factorial design (Tables 3 and 4). The detailed procedure for preparing the *in situ* gel-forming system of gatifloxacin is as follows: buffer salts were dissolved in 75 mL of purified water, and HEC was added and allowed to hydrate. Carbopol 974P was sprinkled over this solution and allowed to hydrate overnight. The solution was stirred with an overhead stirrer and Tween 20 was added with stirring. Gatifloxacin was dissolved in 0.1 N HCl solution and pH was adjusted with 0.1 N NaOH. Benzalkonium chloride was then added as a preservative. Volume was brought up using purified water. The developed formulations were placed in 10-mL amber glass vials closed with gray butyl rubber stoppers and sealed with aluminium caps. The formulations in their final form were subjected to terminal sterilization by autoclaving at 121°C and 15 psi for 20 min.

Table 3. Experimental design of ophthalmic gels using Carbopol 974P

| Variables | Level 1 | Level 2 | Level 3 |
|---|---------|---------|---------|
| Carbopol 974P (% w/w) (X ₁) | 0.25 | 0.5 | 0.75 |
| HEC (% w/w) (X ₂) | 1 | 2 | 3 |

Table 4. Compositions of ophthalmic gels using Carbopol 974P

| Formulation code | Gatifloxacin (% w/w) | Carbopol 974P (% w/w) | HEC (% w/w) | Tween 20 (% w/w) | Benzalkonium chloride (% w/w) |
|------------------|----------------------|-----------------------|-------------|------------------|-------------------------------|
| C1 | 0.3 | 0.25 | 1 | 2 | 0.01 |
| C2 | 0.3 | 0.25 | 2 | 2 | 0.01 |
| C3 | 0.3 | 0.25 | 3 | 2 | 0.01 |
| C4 | 0.3 | 0.5 | 1 | 2 | 0.01 |
| C5 | 0.3 | 0.5 | 2 | 2 | 0.01 |
| C6 | 0.3 | 0.5 | 3 | 2 | 0.01 |
| C7 | 0.3 | 0.75 | 1 | 2 | 0.01 |
| C8 | 0.3 | 0.75 | 2 | 2 | 0.01 |
| C9 | 0.3 | 0.75 | 3 | 2 | 0.01 |

2.5.3. Preparation of gels containing both poloxamer 407 and Carbopol 974P

For preparation of poloxamer and Carbopol solutions (Tables 5 and 6), the already swelled Carbopol solution was cooled down to 4°C and the required amount of poloxamer 407 was added. The solutions were left at 4°C until a clear solution was obtained. Volume was brought up using phosphate buffer, pH 7.4. For preparation of drug-containing polymer solutions, gatifloxacin was dissolved in 0.1 N HCl solution, pH was adjusted with 0.1 N NaOH, and then this solution was added to the polymer solutions prepared as described above. Benzalkonium chloride was then added as a preservative. All of the sample solutions were adjusted to required pH values by 0.5 M NaOH solution and then stored in a refrigerator. The developed formulations were placed in 10-mL amber glass vials closed with gray butyl rubber stoppers and sealed with aluminum caps. The formulations in their final form were subjected to terminal sterilization by autoclaving at 121°C and 15 psi for 20 min.

2.5.4. Preparation of sodium alginate gels

Formulations of gatifloxacin containing different concentrations of sodium alginate and HEC were prepared using a 3² factorial design (Tables 7 and 8). The ion-sensitive polymer, sodium alginate, was dissolved in 75 mL of phosphate buffer, pH 7.4. HEC was added with continuous stirring until it completely dissolved. Gatifloxacin was dissolved in 0.1 N HCl and the solution was neutralized with 0.1 N NaOH. Benzalkonium chloride was then added as a preservative to the above solution. Poloxamer 407 was added at a concentration of about 0.5% (w/w) to enhance the solubility of gatifloxacin. Phosphate buffer, pH 7.4, was then added to bring up the volume. The developed formulations were placed in 10-mL amber glass vials closed with gray butyl rubber stoppers and sealed with aluminium caps. The formulations in their final form were subjected to terminal sterilization by autoclaving at 121°C and 15 psi for 20 min.

Table 5. Experimental design of ophthalmic gels using both poloxamer 407 and Carbopol 974P

| Variables | Level 1 | Level 2 | Level 3 |
|---------------------------------|---------|---------|---------|
| Poloxamer 407 (% w/w) (X_1) | 18 | 20 | 22 |
| Carbopol 974P (% w/w) (X_2) | 0.1 | 0.2 | 0.3 |

Table 6. Compositions of ophthalmic gels using both poloxamer 407 and Carbopol 974P

| Formulation code | Gatifloxacin (% w/w) | Poloxamer 407 (% w/w) | Carbopol 974P (% w/w) | HEC (% w/w) | Tween 20 (% w/w) | Benzalkonium chloride (% w/w) |
|------------------|----------------------|-----------------------|-----------------------|-------------|------------------|-------------------------------|
| PC1 | 0.3 | 18 | 0.1 | 1 | 2 | 0.01 |
| PC2 | 0.3 | 18 | 0.1 | 1 | 2 | 0.01 |
| PC3 | 0.3 | 18 | 0.1 | 1 | 2 | 0.01 |
| PC4 | 0.3 | 20 | 0.2 | 2 | 2 | 0.01 |
| PC5 | 0.3 | 20 | 0.2 | 2 | 2 | 0.01 |
| PC6 | 0.3 | 20 | 0.2 | 2 | 2 | 0.01 |
| PC7 | 0.3 | 22 | 0.3 | 3 | 2 | 0.01 |
| PC8 | 0.3 | 22 | 0.3 | 3 | 2 | 0.01 |
| PC9 | 0.3 | 22 | 0.3 | 3 | 2 | 0.01 |

Table 7. Experimental design of gels using sodium alginate gels

| Variables | Level 1 | Level 2 | Level 3 |
|-----------------------------------|---------|---------|---------|
| Sodium alginate (% w/w) (X_1) | 1 | 2 | 3 |
| HEC (% w/w) (X_2) | 1 | 2 | 3 |

Table 8. Composition of gels using sodium alginate

| Formulation code | Gatifloxacin (% w/w) | Sodium alginate (% w/w) | HEC (% w/w) | Poloxamer 407 (% w/w) | Benzalkonium chloride (% w/w) |
|------------------|----------------------|-------------------------|-------------|-----------------------|-------------------------------|
| S1 | 0.3 | 1 | 1 | 0.5 | 0.01 |
| S2 | 0.3 | 2 | 1 | 0.5 | 0.01 |
| S3 | 0.3 | 3 | 1 | 0.5 | 0.01 |
| S4 | 0.3 | 1 | 2 | 0.5 | 0.01 |
| S5 | 0.3 | 2 | 2 | 0.5 | 0.01 |
| S6 | 0.3 | 3 | 2 | 0.5 | 0.01 |
| S7 | 0.3 | 1 | 3 | 0.5 | 0.01 |
| S8 | 0.3 | 2 | 3 | 0.5 | 0.01 |
| S9 | 0.3 | 3 | 3 | 0.5 | 0.01 |

2.6. Determination of gelation temperature

Gelation temperatures of the gels were measured according to method described by Gilbert *et al.* (25). Two-mL aliquots of the gel were transferred to test tubes sealed with parafilm and immersed in a water bath at 4°C. The temperature of the bath was increased in increments of 1°C and left to equilibrate for 15 min at each new setting. The samples were examined for gelation, which was deemed to have occurred when the meniscus would no longer move upon tilting through 90°C. All measurements were performed in triplicate ($n = 3$).

2.7. In vitro bioadhesion evaluations

The bioadhesive force of all batches was determined

by the method described by Choi *et al.* (26). A sheep's corneal membrane was cut from the eye of a sheep and instantly fixed with the mucosal side outwards onto a glass vial using a rubber band. Vials with the corneal membrane were stored at 37°C for 5 min. Then, the next vial with a section of membrane was connected to the balance in an inverted position while first vial was placed on a height-adjustable pan. The gel was placed onto the corneal membrane from the first vial. Then, the height of the second vial was adjusted so that the membrane surfaces of both vials would come in close contact. A contact time of 10 minutes was allotted. Then, the weight was allowed to increase in the pan until the vials detached. The bioadhesive force was the minimum weight required to detach two vials. The corneal membrane was changed for each measurement ($n = 3$).

2.8. Determination of gel strength

A sample of 50 g of gel was placed in a 100-mL graduated cylinder and gelled in a thermostat at 37°C. The apparatus for measuring gel strength as given by Choi *et al.* (26) was allowed to penetrate the gel. Gel strength, *i.e.*, the viscosity of the gels at physiological temperature, was determined by the time (in seconds) taken by the apparatus to sink down 5 cm through the prepared gel. All measurements were performed in triplicate ($n = 3$).

2.9. Rheological studies

Rheological studies were carried out using Brookfield's RVDV-II+ model viscometer (Brookfield Engineering Laboratories; Middleboro, MA, USA). The gel under study was placed in a small sample holder. Spindle LV 2 was used to measure viscosity. The viscosities were measured at room temperature and the speed of rotation of the spindle was increased from 10 to 200 rpm. Evaluations were conducted in triplicate ($n = 3$).

2.10. Permeation studies across a sheep's corneal membrane

A device designed by Gonjari *et al.* (27) was used to evaluate drug permeation through a sheep's corneal membrane. This membrane was tied to a specially designed glass cylinder (open at both ends). Simulated tear fluid (NaHCO₃ 0.218 g, NaCl 0.678 g, CaCl₂·2H₂O 0.0084 g, KCl 0.138 g in 100 mL of water) was used as a diffusion medium. The formulation to be tested was added to the donor chamber with the help of a micropipette. The donor surface of the membrane was constantly in contact with simulated tear fluid. A temperature of 37 ± 0.5°C was maintained throughout the study. A magnetic stirrer in the cell provided continuous agitation. At regular time intervals, 1 mL of sample was withdrawn and replaced with fresh simulated tear fluid in order to maintain sink conditions. The samples were appropriately diluted and the absorbance was measured at 285.5 nm using a Shimadzu 1700UV-VIS spectrophotometer (Shimadzu, Kyoto, Japan).

2.11. Antimicrobial efficacy studies

Antimicrobial efficacy studies were carried out by an agar diffusion test employing Bauer's well method (21). Sterile solutions of gatifloxacin (with a marketed eyedrop solution serving as standard solution) and the developed formulations (test solutions) were poured into wells bored into sterile nutrient agar previously seeded with test organisms (*Pseudomonas aeruginosa* and *Staphylococcus aureus*); after allowing diffusion of the solutions for 2 h, agar plates were incubated at 37°C for 24 h. The zone of inhibition (ZOI) measured

around each well was compared to that of the control. The entire procedure except for incubation was carried out in a laminar airflow unit. Each solution was tested in triplicate. Both positive and negative controls were maintained through the study.

3. Results and Discussion

3.1. Compatibility studies between drug and polymers

DSC studies were carried out to determine interaction between the drug and polymers in the prepared ophthalmic gels. This will also indicate the success of stability studies (28). A gatifloxacin peak was clearly apparent in the DSC thermogram (Figure 1) in the form of a sharp characteristic endothermic peak in a temperature range of 182-185°C corresponding to its melting temperature (T_m). This showed that the gatifloxacin used was in pure form. A mixture of the drug and poloxamer 407 had no peak as poloxamer melted at 50°C, so there was no prominent peak resembling that of the drug. A mixture of the drug and Carbopol 974P and sodium alginate along with HEC showed endothermic peaks resembling the peak of the pure drug.

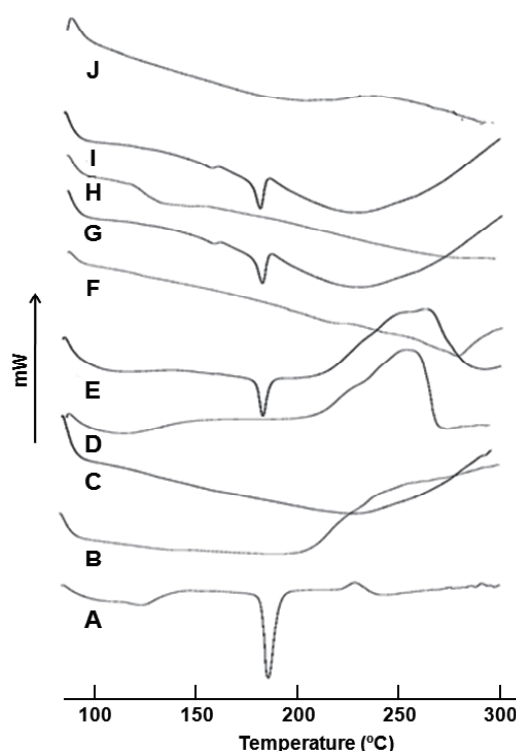


Figure 1. DSC thermograms of gatifloxacin and its mixtures with different polymers. A, gatifloxacin; B, poloxamer 407; C, HEC; D, sodium alginate; E, gatifloxacin/sodium alginate (1:1) physical mixture; F, Carbopol 974P; G, gatifloxacin/sodium alginate/HEC (1:1:1) physical mixture; H, gatifloxacin/poloxamer 407/HEC (1:1:1) physical mixture; I, gatifloxacin/Carbopol 974P/HEC (1:1:1) physical mixture; J, gatifloxacin/poloxamer 407/Carbopol 974P/HEC physical mixture.

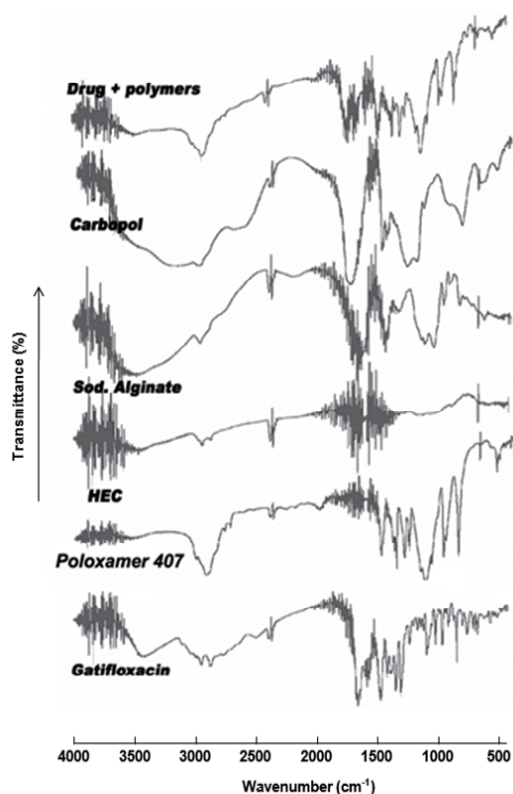


Figure 2. FTIR spectra of gatifloxacin, polymers, and their mixtures.

As shown in Figure 2, gatifloxacin's FTIR spectra showed characteristic peaks at $1,700.86\text{ cm}^{-1}$, $1,507.44\text{ cm}^{-1}$, $3,550.05\text{ cm}^{-1}$, $3,408\text{ cm}^{-1}$, $1,722\text{ cm}^{-1}$, and $1,555\text{ cm}^{-1}$, respectively. These peaks were also mostly seen in the spectra of physical mixtures. There was only a slight shift in some of the groups, characteristic of the drug, poloxamer 407, and Carbopol 974P, that took place with overlapping and broadening of similar peaks. No new bands were detected in the spectra of physical mixtures, indicating no interaction between the drug and polymer mixture.

3.2. Determination of gelation temperature

Poloxamers were previously proven to undergo thermal gelation or sol-gel transition at a temperature of about 25 to 35°C. Below the transition temperature, poloxamer solutions allow a comfortable and precise delivery by the patient to the cul-de-sac, where thermogelation occurs. Immediate gelling increases a drug's residence time and enhances its bioavailability (29). Gels containing poloxamer 407 had good gelation properties in that the gelation temperature of the gel decreased as the concentration of poloxamer increased (Figure 3). This ability of poloxamer 407, a mucoadhesive polymer, to lower the gelation temperature may be due to increased viscosity after polymer dissolution and could be explained by the ability to bind to the polyoxyethylene chains present in the poloxamer 407 molecules. This would promote dehydration, causing

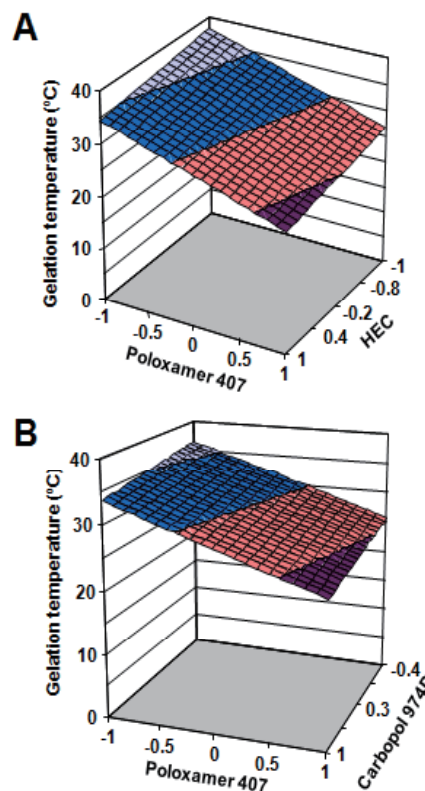


Figure 3. Effect of variables on gelation temperature. **A**, poloxamer 407 gels; **B**, poloxamer 407 and Carbopol 974P gels.

an increase in entanglement of adjacent molecules and extensively increasing intermolecular hydrogen bonding, thus leading to gelation at lower temperature (30). A good degree of gelation was also shown by sodium alginate. Sodium alginate and Carbopol 974P did not have temperature-dependent gelling, so gelation could be determined only by gel strength and viscosity determination. The degree of gelation increased with an increasing concentration of sodium alginate. Out of all of the formulations, batches P1, P2, and PC1 (the composition of each batch is summarized in Tables 2 and 6) had significant *in vitro* gelation temperatures.

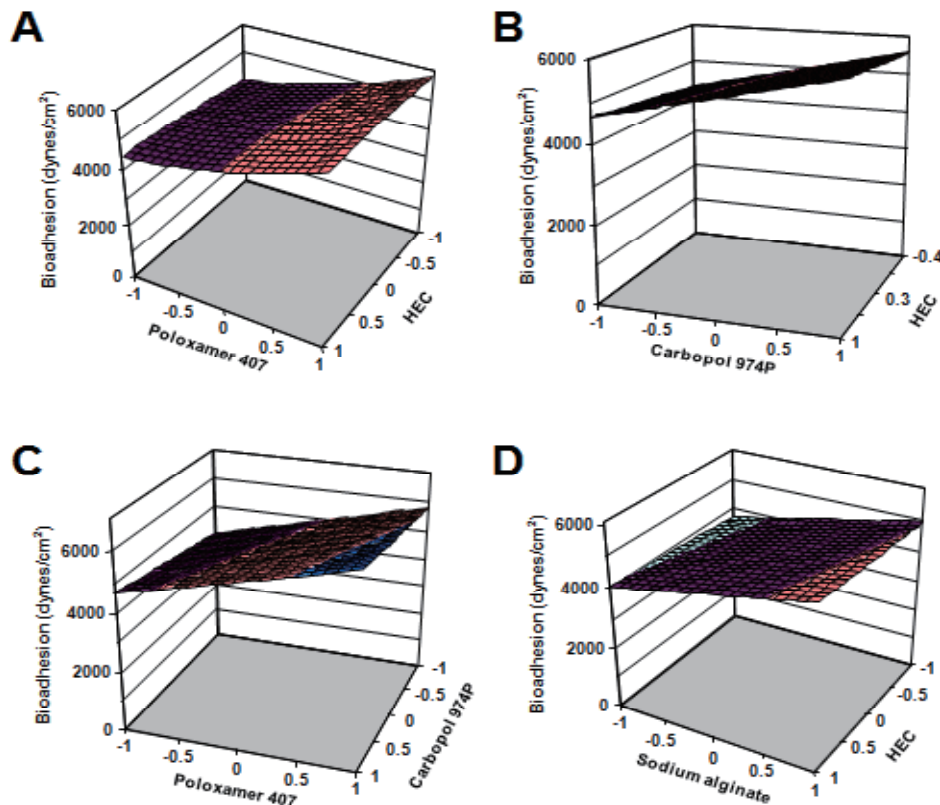
Table 9 summarizes the values of coefficients for the factorial equation. The coefficient of correlation was found to be about 0.98 for P and PC types of formulations. The negative values of β_2 indicate the ability of mucoadhesive polymers to lower the gelation temperature, which may be due to the reasons described previously.

3.3. *In vitro* bioadhesion evaluations

Bioadhesive force means the force with which gels bind to ocular mucosa. Greater bioadhesion is indicative of a prolonged residence time of a gel and thus prevents its drainage from the cul-de-sac. The addition of bioadhesive polymers HEC and Carbopol 974P increased the bioadhesive force (Figure 4). The bioadhesive force increased significantly as the concentration of bioadhesive polymers increased over

Table 9. Regression analysis of different evaluation parameters

| Coefficients | Gelation temperature | <i>In vitro</i> bioadhesion | Gel strength | Permeation studies |
|--|----------------------|-----------------------------|--------------|--------------------|
| Poloxamer gel | | | | |
| β_1 | -5.637* | 836.0* | 6.842* | -1.235* |
| B_2 | -1.733* | 152.9* | 2.422* | -0.2443* |
| β_{11} | 0.4563 | 213.8* | 1.729* | -0.3385* |
| β_{22} | 0.3875 | -94.78* | 0.267 | -0.0760 |
| β_{12} | 0.2025 | 59.87* | 0.406 | -0.1069 |
| R^2 | 0.9882* | 0.9994* | 0.9857* | 0.9936* |
| F | 50.35* | 1073* | 41.31* | 93.22* |
| Carbopol 974 gel | | | | |
| β_1 | - | 630.9* | 16.32* | 0.7033* |
| B_2 | - | 192.1* | 4.873* | 0.3983* |
| β_{11} | - | -56.83* | -5.653* | -0.2934 |
| β_{22} | - | 42.25 | 1.036 | -0.3432* |
| β_{12} | - | 53.10* | -1.624 | -0.4296* |
| R^2 | - | 0.9976* | 0.9825* | 0.9463* |
| F | - | 253.1* | 33.60* | 10.58* |
| Poloxamer 407/Carbopol 974P gel | | | | |
| β_1 | -5.429* | 890.4* | 6.842* | -1.370* |
| B_2 | -1.493* | 335.8* | 2.422* | -0.2348* |
| β_{11} | 0.2109 | 399.9* | 1.729* | -0.1520 |
| β_{22} | 0.4083 | 13.69 | 0.267 | -0.0239 |
| β_{12} | -0.0453 | 88.85 | 0.406 | -0.0834 |
| R^2 | 0.9876* | 0.9767* | 0.9857* | 0.9894* |
| F | 47.83* | 25.05* | 41.31* | 56.21* |
| Sodium alginate gel | | | | |
| β_1 | - | 616.8* | 3.252* | -1.140* |
| B_2 | - | 164.2* | 1.493* | -0.4287* |
| β_{11} | - | 213.8* | 4.599* | 0.2456 |
| β_{22} | - | 73.95 | 1.782 | -0.1731 |
| β_{12} | - | 37.24 | 2.017* | 0.3076 |
| R^2 | - | 0.9836* | 0.9525* | 0.8879* |
| F | - | 35.90* | 12.03* | 4.754* |

**Figure 4. Effect of variables on bioadhesion. A,** poloxamer 407 gels; **B,** Carbopol 974P gels; **C,** poloxamer 407/Carbopol 974P gels; **D,** sodium alginate gels.

the range of 1-3%. Bioadhesive forces of poloxamer solutions enhanced by the polymers used could be explained by the fact that secondary bond-forming groups (*e.g.* hydroxyl, ether oxygen, and amine) are the principal source of bioadhesion. Cellulosic polymers such as HEC have an abundance of hydroxyl and ether groups along their length (31).

Carbopol is known to be an excellent bioadhesive polymer (32). Hence, satisfactory bioadhesion was observed with all ophthalmic Carbopol gel formulations. The detachment stress and gel strength of gels of gatifloxacin were found to increase with the addition of Carbopol 974P (effect seen at high concentrations) (Figure 4). This increase was proportional to the concentration of Carbopol 974P. Efentakis *et al.* (33) reported that bioadhesion is determined by the availability of carboxyl groups. Carbopol 974P has a high percentage of carboxyl groups present. These groups simultaneously bind to the sugar residue in oligosaccharide chains present in the mucus membrane, resulting in a strong bond between the polymer and mucus membrane. The interaction increases with the increased density of hydrogen-bonding groups that interact with the glycoproteins of the mucin. Carbopol may also exhibit conformation, resulting in more favorable macromolecular accessibility of its functional groups for hydrogen bonding. Thus, the increase in the

mucoadhesive force will lead to increased retention time and therefore increased bioavailability (34). In contrast, sodium alginate gels had less bioadhesion than poloxamer and Carbopol gels (Figure 4). However, increased bioadhesion was seen with an increase in the concentration of sodium alginate.

Factorial equation fitting and regression statistics (Table 9) for all types of formulations indicated good correlation coefficients. The interactive term X_1X_2 shows that both factors have a positive effect on bioadhesion.

3.4. Determination of gel strength

Gel strength provides an indication of the viscosity of gel formulations (26). An increase in gel strength was observed with all gel formulations. Specifically, gels containing Carbopol 974P had greater gel strength (Figure 5). This may be due to the reasons described previously. The coefficient of correlation (Table 9) was good. The use of mucoadhesive polymers such as HEC and Carbopol directly affects the gel strength, as indicated by positive β_2 coefficients.

3.5. Rheological studies

Rheological study of the formulations indicated that gels exhibited pseudo-plastic rheology, as evinced

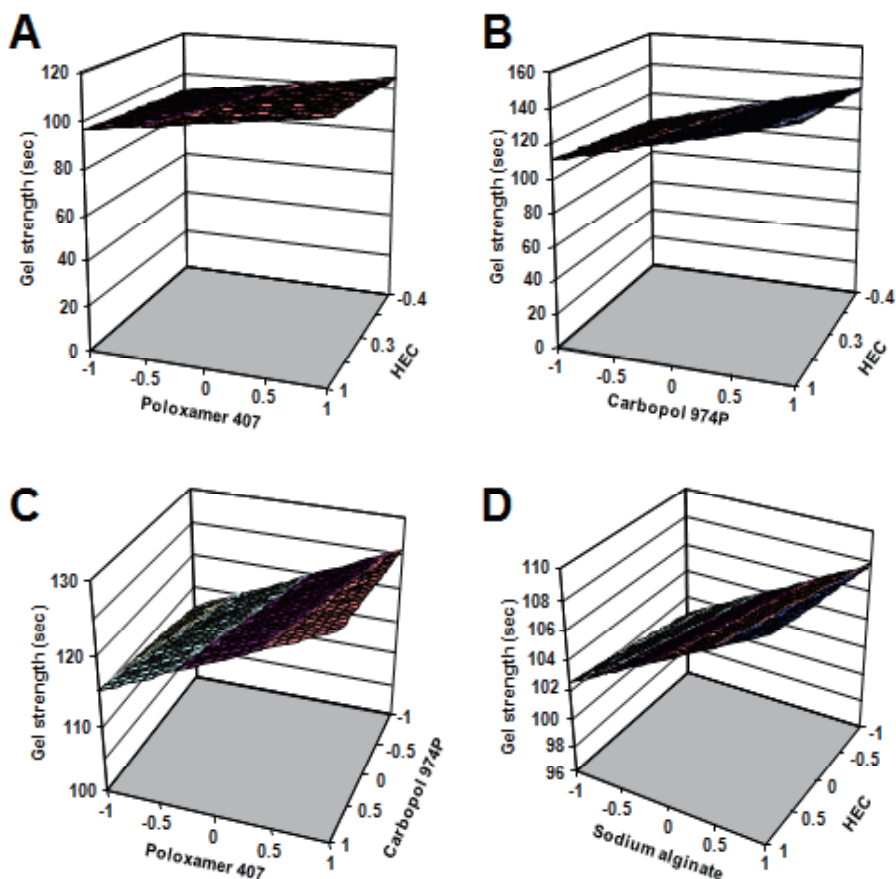


Figure 5. Effect of variables on gel strength. A, poloxamer 407 gels; B, Carbopol 974P gels; C, poloxamer 407/Carbopol 974P gels; D, sodium alginate gels.

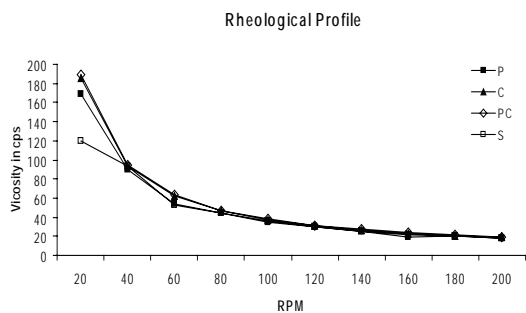


Figure 6. Rheological profile of different ophthalmic gels.

by shear thinning and a decrease in viscosity with increased angular velocity. As shown in Figure 6, viscosity for all formulations decreased in the order PC (poloxamer 407/Carbopol 974P gels) > C (Carbopol 974P gels) > P (poloxamer 407 gels) > S (sodium alginate gels). According to Bothner *et al.* (35), the administration of ophthalmic preparations should have as little effect as possible on the pseudo-plastic character of the precorneal film. The ocular shear rate is very high, ranging from 0.03 sec^{-1} during inter-blinking periods to $4,250\text{-}28,500 \text{ sec}^{-1}$ during blinking (36), so preferred viscoelastic fluids often have a viscosity that is high under low shear rate conditions and one that is low under high shear rate conditions.

3.6. Permeation studies across a sheep's corneal membrane

In vitro permeation across a sheep's corneal membrane was fitted to various release kinetic models. All of the batches indicated that a Peppas model of permeation kinetics was the best-fit model. Initial faster release indicates that initially the drug in the solution quickly diffused in the space outside the gel. Release of the drug within the gel is controlled by the nature and the concentration of the polymer used.

As noted by Gonjari *et al.* (27), drug permeation through the cornea is greater with a thermoreversible gel containing HEC (Figures 7 and 8). The initial fast release of the drug from the formulations of gatifloxacin containing poloxamer 407 may be due to the rapid leaching of extracellular ionized drug. Entrapped in the micelles, the drug may be released rather slowly. These findings correlate those reported by Paavola *et al.* (37), who suggested that drug diffusion from poloxamer 407 gel is through extracellular aqueous channels and microviscosity.

Carbopol 974P gels showed an increase in the release of gatifloxacin, as compared to its release from poloxamer 407 and sodium alginate gels (Figures 7 and 8). HEC seemed to decrease the cumulative release. The retarding effect of the HEC could be attributed to its ability to increase the overall product viscosity (38) as well as its ability to distort or squeeze the extracellular aqueous channels of poloxamer micelles through which the

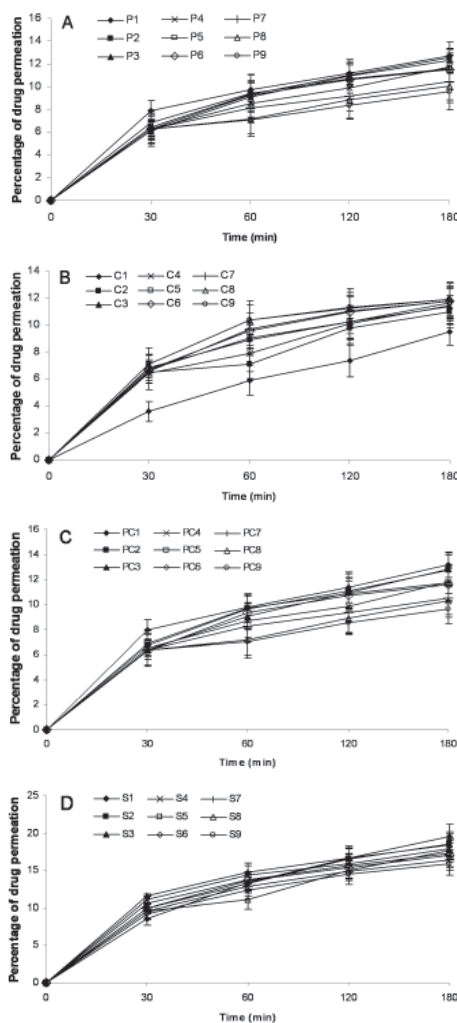


Figure 7. Drug permeation from ophthalmic gels. A, Drug permeation from poloxamer gels; **B,** drug permeation from Carbopol gels; **C,** drug permeation from poloxamer and Carbopol gels; **D,** drug permeation from sodium alginate gels.

drug diffuses, thereby delaying the release process (39). Carbopol 974P might lead to an increase in diffusion. This may be due to rapid swelling and hence faster diffusion of the drug. Electrostatic repulsion of the ionized carboxyl group may also result in decoiling and relaxation of the polymer network, leading to rapid dissolution of the drug and its fast release from the gel. An increased concentration of Carbopol 974P causes increased binding of Ca^{2+} binding sites and increased interaccessibility of Ca^{2+} binding sites causes relaxation of the polymer network (40,41).

A good coefficient of correlation (Table 9) was also noted. The interactive term X_1X_2 had a negative effect for P, C, and PC types of formulations. With the S type of formulations, the term $\beta_2X_2^2$ was found to be negative, indicating non-linearity that suggests that HEC might be responsible for decreasing permeation across the corneal membrane.

3.7. Regression analysis

Factorial equation fitting and regression analysis

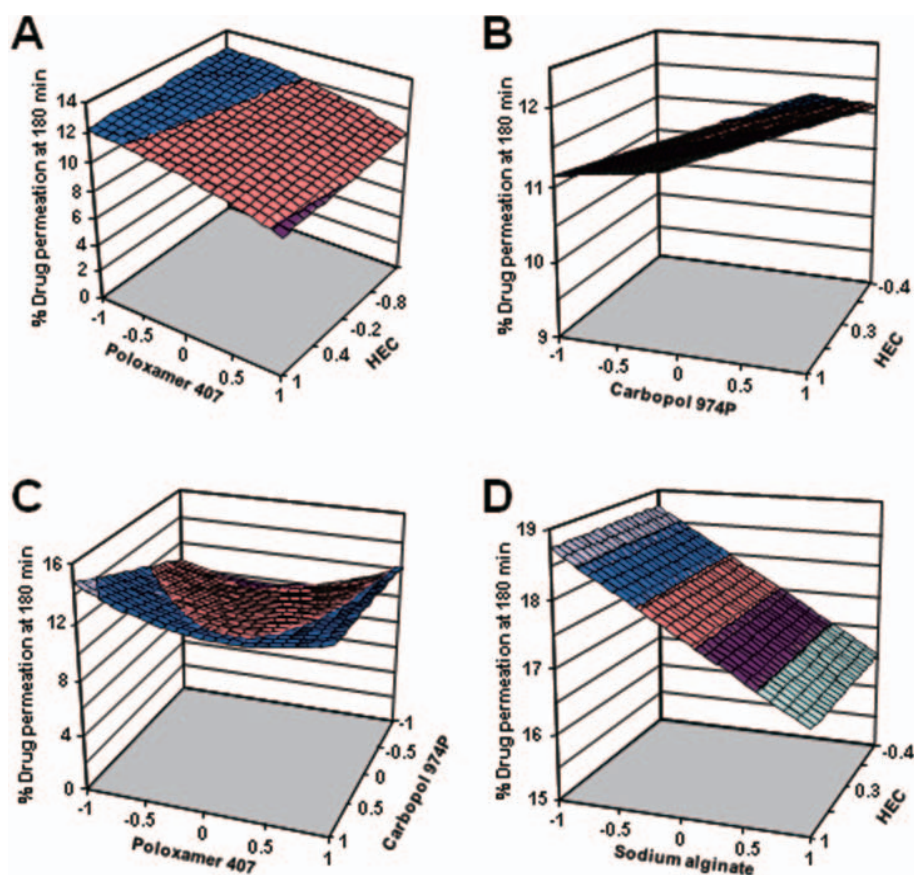


Figure 8. Effect of variables on percent drug permeation at 180 min. A, poloxamer 407 gels; B, Carbopol 974P gels; C, poloxamer 407/Carbopol 974P gels; D, sodium alginate gels.

Table 10. Antimicrobial efficacy studies of gels of Gatifloxacin

| Sr. No | Formulation | Pseudomonas aeruginosa | | Staphylococcus aureus | |
|--------|-------------|------------------------|------------|-----------------------|------------|
| | | ZOI (cm) | % Efficacy | ZOI (cm) | % Efficacy |
| 1 | Standard | 5.2 | 100 | 5.5 | 100 |
| 2 | P | 4.8 | 92.30 | 4.2 | 76.36 |
| 3 | C | 4.8 | 92.30 | 4.3 | 78.18 |
| 4 | S | 5.1 | 98.07 | 5.3 | 96.36 |
| 5 | PC | 5.0 | 96.15 | 5.1 | 98.07 |

of the different evaluation parameters for different formulations are shown in Table 9. The coefficients of the main effects (X_1 and X_2) and interactive terms (X_1X_2) were determined to indicate a change in the values of evaluation parameters when two factors were changed simultaneously. Multiple regression analysis and F statistics were used to identify statistically significant terms. Use of statistical methods has been found to allow greater discrimination among batches (42).

3.8. Antimicrobial efficacy studies

The formulations had satisfactory antimicrobial efficacy according to studies. Out of all four formulations, sodium alginate gels had maximum efficacy. The other three formulations also showed good antimicrobial efficacy, as indicated by zones of inhibition (Table 10, Figure 9).

4. Conclusion

In this study, *in situ* gelling ophthalmic gels of gatifloxacin were developed using mucoadhesive polymers. DSC and FTIR studies indicated compatibility between polymers and the drug. These gels were observed to have a satisfactory gelation temperature, gel strength, and bioadhesion. Rheological study of the formulations indicated that gels exhibited pseudo-plastic rheology, as shown by shear thinning and a decrease in the viscosity with increased angular velocity. *In vitro* permeation studies across corneal mucosa indicated that a Peppas model was the best-fit model. Antimicrobial studies indicated the effectiveness of these formulations. Therefore, these gels appear to be a viable alternative to conventional eyedrops. The results of 3^2 factorial experiments showed that

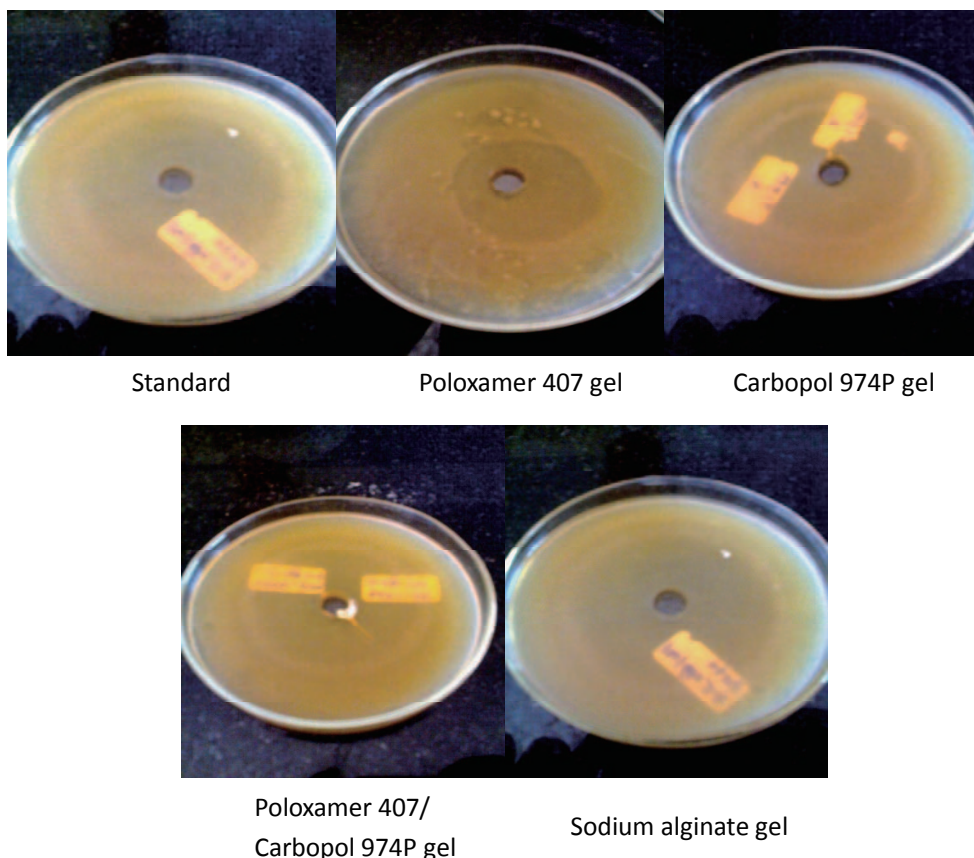


Figure 9. Zones of inhibition obtained during antimicrobial efficacy studies of gatifloxacin gels.

independent variables significantly affected dependent variables. The results obtained indicated that adopting a systematic approach can lead to an optimized formulation with fewer experimental requirements.

Acknowledgements

The authors wish to thank Dr. V. K. Mourya, Principal, Govt. College of Pharmacy, Aurangabad for his kind support and encouragement of the current work.

References

1. Ashim KM. Ophthalmic Drug Delivery System. Vol. 58. Marcel Dekker, New York, NY, USA, 1993; pp. 105-110.
2. Indu P, Kaur AG, Anil KS, Deepika A. Vesicular systems in ocular drug delivery an overview. *Int J Pharm.* 2004; 269:1-14.
3. Chien YW. Ocular drug delivery and delivery systems. In: *Novel Drug Delivery Systems*. Marcel Dekker, New York, NY, USA, 1996; pp. 269-270.
4. Gurny R. Preliminary study of prolonged acting drug delivery system for the treatment of glaucoma. *Pharm Acta Helv.* 1981; 56:130-132.
5. Bamba M, Puisieux F, Marty JP, Carstensen JT. Release mechanism in gel forming sustained release preparations. *Int J Pharm.* 1979; 2:307-315.
6. Goldberg I, Ashburn FS, Kass MA, Becker B. Efficacy and patient acceptance of pilocarpine gel. *Am J Ophthalmol.* 1979; 88:843-846.
7. Coury AJ, Cahalam PT, Jevne AH, Perrault JJ, Kallok MJ. Recent developments in hydrophilic polymers. *Med Device Diagn Ind.* 1984; 6:28-30.
8. Davis SS, Tomlinson E, Wilson CG. The effects of ion association on the transcorneal transport of drugs. *Br J Pharmacol.* 1978; 64:444-445.
9. Knight GG (ed). *Liposomes: From Physical Structure to Therapeutic Applications*, Elsevier Biomedical Press, Amsterdam, the Netherlands, 1981.
10. Shaeffer HE, Krohn DL. Liposomes in topical drug delivery. *Invest Ophthalmol Vis Sci.* 1982; 22:220-227.
11. Smolin G, Okumoto M, Feiler S, Condom D. Idoxuridineliiposome therapy for herpes simple keratitis. *Am J Ophthalmol.* 1981; 91:220-225.
12. Stratford RE, Yang DC, Redell MA, Lee VHL. Effects of topically applied liposomes on disposition of epinephrine and insulin in the albino rabbit eye. *Int J Pharm.* 1983; 13:263-272.
13. Miyazaki S, Suzuki S, Kawasaki N, Endo K, Takahashi A, Attwood D. *In situ* gelling xyloglucan formulations for sustained release ocular delivery of pilocarpine hydrochloride. *Int J Pharm.* 2001; 229:29-36.
14. Karmarkar AB, Gonjari ID, Hosmani AH. Poloxamers and their applications. *Online International Journal Pharmainfo.net.* (<http://www.pharmainfo.net>)
15. Gurny R, Boye T, Ibrahim H. Ocular therapy with nanoparticulate systems for controlled drug delivery. *J Control Release.* 1985; 2:353-361.
16. Miller SC, Donovan MD. Effect of poloxamer 407 gel on the miotic activity of pilocarpine nitrate in rabbits. *Int J Pharm.* 1982; 12:147-152.
17. Stijjenschentz Z, Astin M. *Biopharmaceutics of Ocular*

- Drug Delivery. Boca Raton, CRC Press. 1983: p. 1.
18. Khan M, Barney NP, Brings RM, Bloch KJ, Allensmith MR. Inv. Ophthalmol. Vis Sci. 1990; 31:258.
 19. Pandit JK, Bharathi D, Srinatha A, Ridhurkar DN, Singh S. Long acting ophthalmic formulation of indomethacin: Evaluation of alginate gel systems. Indian J Pharm Sci. 2007; 69:37-40.
 20. Leo WJ, Mc Loughlin AJ. Effects of sterilization treatments on some properties of alginate solutions and gels. Biotechnol Prog. 1990; 6:51-53.
 21. Edsman K, Carlfors J, Peterson R. Rheological evaluation of poloxamer as *in situ* gel for ophthalmic use. Eur J Pharm Sci. 1998; 6:105-112.
 22. Bolton S. Pharmaceutical Statistics. 2nd ed. New York: Marcel Decker, 1990; pp. 234.
 23. Franz RM, Browne JE, Lewis AE. Experiment design, modeling and optimization strategies for product and process development. In: Pharmaceutical Dosage Forms: Disperse Systems (Liebermann HA, Reiger MM, Banker GS, eds). Marcel Dekker, New York, USA, 1988; pp. 427-519.
 24. Schmolka IR. A review of block polymer surfactants. J Am Oil Chem Soc. 1977; 54:110-116.
 25. Gilbert JC, Richardson JL, Davies MC, Palin KJ, Hadgraft J. The effect of solutes and polymers on the gelation properties of Pluronic F127 solutions for controlled drug delivery. J Control Release. 1987; 5:113-118.
 26. Choi HG, Jung JH, Ryu JM. Development of *in situ* gelling and mucoadhesive acetaminophen liquid suppository. Int J Pharm. 1998; 165:33-44.
 27. Gonjari ID, Hosmani AH, Karmarkar AB, Godage AS, Kadam SB, Dhabale PN. Formulation and evaluation of *in situ* gelling thermoreversible mucoadhesive gel of Fluconazole. Drug Discov Ther. 2009; 3:6-9.
 28. Craig, DQM. Pharmaceutical applications of DSC In: Thermal Analysis of Pharmaceuticals (Craig DQM, Reading M, eds). CRC Press Boca Raton. 2007; 53-99.
 29. Koller C, Buri P. Propriétés et intérêt pharmaceutique des gels thermoreversibles à base de Poloxamers et poloxamines. S T P Pharma. 1987; 3:115-124.
 30. Puglia C, Bonina F, Trapani G, Franco M, Ricci M. Evaluation of *in vitro* percutaneous absorption of lorazepam and clonazepam from hydro-alcoholic gel formulations. Int J Pharm. 2001; 228:79-87.
 31. ElHady SSA, Mortada ND, Awad GAS, Zaki NM, Taha RA. Development of *in situ* gelling and mucoadhesive mebeverine hydrochloride solution for rectal administration. Saudi Pharmaceutical Journal. 2003; 11:159-171.
 32. Robinson SS, Robinson JR. Polymer structure features contributing to mucoadhesion. J Control Release. 1990; 12:187-194.
 33. Efentakis M, Koutlis A, Vlachou M. Development and evaluation of oral multiple-unit and single-unit hydrophilic controlled-release systems. AAPS Pharm Sci Tech. 2000; 1:E34.
 34. Kunisawa J, Okudaira A, Tsutusmi Y, Takahashi I, Nakanishi T, Kiyono H, Mayumi T. Characterization of mucoadhesive microspheres for the induction of mucosal and systemic immune responses. Vaccine. 2000; 19:589-594.
 35. Bothner H, Waaler T, Wik O. Rheological characterization of tear substitutes. Drug Dev Ind Pharm. 1990; 16:755-768.
 36. Kumar SR, Himmestein KJ. Modification of *in situ* gelling behavior of Carbopol solutions by hydroxypropyl methylcellulose. J Pharm Sci. 1995; 84:344-348.
 37. Paaavoala A, Yliruusi J, Rosenberg P. Controlled and duramater permeability of lidocain and ibuprofen from injectable poloxamer based gels. J Control Release. 1998; 52:162-178.
 38. Desai SD, Blanchard J. Evaluation of Pluronic F-127 based sustained-release ocular delivery systems for pilocarpine using albino rabbit eye model. J Pharm Sci. 1998; 87:1190-1195.
 39. Pisal SS, Shelke V, Mahadik K, Kadam SS. Effect of organogel components on *in vitro* nasal delivery of propranolol hydrochloride. AAPS Pharm Sci Tech 2004; 5:Article 63.
 40. Lueben HL, Lehr CM, Rentel CO, Noach ABJ, de Boer AG, Verhoef JC, Junginger HE. Bioadhesive polymers for the peroral delivery of peptide drugs. J Control Release. 1994; 29:329-338.
 41. Lueben HL, Rentel CO, Kotzé AF, Lehr CM, de Boer AG, Verhoef JC, Junginger HE. Mucoadhesive polymers in peroral peptide drug delivery. IV. Polycarbophil and chitosan are potent enhancers of peptide transport across intestinal mucosa *in vitro*. J Control Release. 1997; 45:15-23.
 42. Karmarkar AB, Gonjari ID, Hosmani AH, Dhabale PN, Bhise SB. Dissolution rate enhancement of Fenofibrate using liquisolid tablet technique Part II: Evaluation of *in vitro* dissolution profile comparison methods. Lat Am J Pharm (Formerly Acta Farmaceutica Bonaerense). 2009; 28:538-543.

(Received May 16, 2010; Revised September 17, 2010; Accepted October 24, 2010)

Original Article

Improvement in the dissolution profile of diacerein using a surfactant-based solid dispersion technique

Snehal B. Patil, Dhanashri K. Shete, Sarika B. Narade, Sharda S. Surve, Ziya K. Khan, Satish B. Bhise, Yogesh V. Pore*

Department of Pharmaceutical Chemistry, Government College of Pharmacy, Karad, Maharashtra, India.

ABSTRACT: In an attempt to improve the dissolution rate of poorly aqueous soluble diacerein (DCN), solid dispersions (SDs) were prepared with a surfactant Pluronic® F 127 (PXMR) at drug to polymer ratios of 1:0.5, 1:1.5, and 1:2.5 (w/w) by an ordinary melting technique. The interaction of DCN with PXMR in all solid binary systems was evaluated by thin layer chromatography (TLC), Fourier transform infrared spectrometry (FTIR), differential scanning calorimetry (DSC), and scanning electron microscopy (SEM) studies. TLC indicated an absence of chemical interaction of DCN with PXMR whereas FTIR studies demonstrated an existence of strong hydrogen bonding between them. A uniform molecular dispersion of DCN was observed in DSC thermograms, and this finding was further supported by loss of the crystalline and irregular shape of DCN detected in SEM photomicrographs. Dissolution studies were promptly conducted to examine the release rate performance of DCN from all binary systems. The drug dissolution properties of binary systems improved significantly in comparison to crystalline DCN. The rate and extent of DCN release were observed to be strongly dependent on the proportion of PXMR present within the formulations.

Keywords: Diacerein, surfactant, Pluronic®, solid dispersion, dissolution profile

1. Introduction

Despite significant advancements in the science of drug delivery, solubilization of poorly aqueous soluble drugs still remains a challenging task for formulation

experts in the pharmaceutical industry. The solubility of a drug is a prime determinant of its dissolution and consequently its oral bioavailability (1,2). Various formulation techniques have been employed to compensate for the poor aqueous solubility and slow dissolution rate of drugs. These include formulation of an amorphous solid form (3), microparticles (4), use of surfactants (5), inclusion complexation (6), and solid dispersion (7-9). Among these methods, solid molecular dispersions are one of the most widely used techniques to improve drug dissolution and solubility. The mechanisms of drug solubilization from solid dispersions involve reducing the particle size, increasing the surface area, reducing the crystallinity, and increasing the wettability of the drug with surrounding hydrophilic carriers to improve its dissolution rate (10).

In recent years, Pluronic® or poloxamer block copolymers have been used extensively in solid dispersion systems for solubilization of poorly water-soluble drugs (11-13). A high hydrophilic-lipophilic balance (HLB) value and low melting point means that they are best suited to a solid dispersion technique using melt granulation (14). The current article describes enhanced dissolution of poorly-water soluble diacerein (DCN) using a solid dispersion technique with Pluronic® F 127 (PXMR).

DCN, chemically 4,5-diacetoxy-9,10-dioxo-9,10-dihydroanthracene-2-carboxylic acid (Figure 1), is a non-steroidal anti-inflammatory drug and chondroprotective agent used in the treatment of osteoarthritis (15,16). DCN lacks cyclooxygenase inhibitory activity and hence has no effect on prostaglandin synthesis (17-19). It is a selective inhibitor of interleukin-1 with a protective

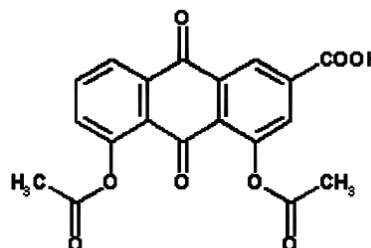


Figure 1. Chemical structure of diacerein.

*Address correspondence to:

Dr. Yogesh Pore, Department of Pharmaceutical Chemistry, Government College of Pharmacy, Karad, Maharashtra 415 124, India.

e-mail: dryogeshpore@rediffmail.com

effect on granuloma-induced cartilage breakdown by its reduction of the concentration of proinflammatory cytokines (20,21). However, the poor aqueous solubility (it is practically insoluble) (22) and hence limited dissolution of DCN mean that only 35-56% (bioavailability) of the drug reaches the systemic circulation (23). Poor bioavailability of a drug often results in a limited therapeutic response. Therefore, the current study sought to improve the dissolution rate of DCN via a solid dispersion technique.

The purpose of this work was to investigate the potential of Pluronic® F 127 (PXMR), a surfactant, for use as a solubilizing agent for DCN in solid dispersions. Solid dispersions (SDs) of DCN were prepared at DCN to PXMR ratios of 1:0.5, 1:1.5, and 1:2.5 (w/w) using a melting technique. Thin layer chromatography (TLC), Fourier transformation infrared spectroscopy (FTIR), differential scanning calorimetry (DSC), and scanning electron microscopy (SEM) were used to characterize the solid-state properties of pure DCN and its SD systems. All formulations including pure DCN were further evaluated for their dissolution performance in a phosphate buffer (pH 6.8).

2. Materials and Methods

2.1. Materials

DCN was donated by Glenmark Pharmaceuticals Ltd., Mumbai, India. Pluronic® F 127 (PXMR) (Lutrol) was donated by Signet Chem Lab, Mumbai, India. All reagents were of analytical grade. Double-distilled water was used throughout the experiment.

2.2. Preparation of SDs

SDs of DCN were prepared by a simple melting method. PXMR was melted at 60°C. DCN was added to the molten polymer, mixed well, and cooled to room temperature to obtain a solid mass. The solidified masses were crushed and passed through a 60- μ mesh sieve. The resulting SDs were stored in desiccators until further analysis.

2.3. TLC

TLC analysis was carried out using silica gel GF 254 (0.2 mm) glass plates with a solvent system of benzene:methanol (90:10, v/v) as a mobile phase to study any interaction between the drug and polymer. Spots were visualized by exposure to iodine vapors. The R_f values of pure drug and binary systems were calculated (24).

2.4. FTIR

FTIR spectra were obtained using a Perkin-Elmer Spectrum-one FTIR spectrometer (Shelton, CT, USA)

spectrometer. The samples were prepared in KBr disks. The scanning range was kept from 4,000 to 450 cm^{-1} .

2.5. DSC

DSC measurements were carried out on a Mettler DSC 30S (Mettler Toledo, Leicester, UK) differential scanning calorimeter. Samples (5 mg) were placed in an aluminum pan and the experiment was carried out in a nitrogen atmosphere (flow rate 40 mL/min) at a scanning rate of 10°C/min in the range of 30-300°C.

2.6. SEM

Photomicrographs of DCN and its all binary systems were obtained by SEM (JSM-6360; JEOL Ltd., Tokyo, Japan). DCN or its formulations were mounted on double-sided adhesive tape and sputtered with gold. Scanning electron photographs were taken at an accelerating voltage of 15 kV and the micrographs obtained were examined at magnifications of $\times 50$, $\times 100$, $\times 200$, $\times 500$, and $\times 1,000$.

2.7. Drug content uniformity

Drug content was determined by dissolving SDs equivalent to 5 mg of DCN in 10 mL of dimethyl formamide (DMF) and then adjusting the volume to 50 mL with distilled water. The solution was filtered through Whatman filter paper No. 41 and suitably diluted. Absorbance was measured at 258 nm using a double beam UV spectrophotometer (Model 1700; Shimadzu, Kyoto, Japan).

2.8. Dissolution studies

Dissolution rate studies of pure DCN and binary systems were conducted in 900 mL of phosphate buffer (pH 6.8) at 75 rpm maintained at $37 \pm 0.5^\circ\text{C}$ in a dissolution apparatus (Model Disso 2000 tablet dissolution test apparatus, LabIndia, Thane, India) using the paddle method. Fifty mg of DCN or an equivalent amount of SDs were added to dissolution medium and the samples were withdrawn at appropriate time intervals. The volume of dissolution medium was adjusted to 900 mL by replacing it with fresh medium. The samples were immediately filtered through a 0.45- μm membrane filter, suitably diluted, and then analyzed spectrophotometrically at 258 nm. The results of dissolution studies were statistically analyzed using ANOVA.

3. Results and Discussion

3.1. Drug content uniformity

Percentage drug content of the formulations was found

Table 1. % Drug content and R_f values of diacerein and solid dispersions

| System | % Drug content* | R_f values |
|----------|-----------------|--------------|
| DCN | --- | 0.49 |
| SD 1:0.5 | 96.45 ± 1.05 | 0.51 |
| SD 1:1.5 | 97.68 ± 0.86 | 0.46 |
| SD 1:1.5 | 98.27 ± 0.65 | 0.47 |

* Data are shown as mean ± S.D. ($n = 3$).
Abbreviations: DCN, diacerein; SD, solid dispersion.

to be in the range of 96.45 ± 1.05 (w/w) to 98.27 ± 0.65 (w/w) for all binary systems (Table 1).

3.2. TLC

The TLC study indicated R_f values from 0.46-0.51 for all binary systems, which were almost identical to the R_f value for pure DCN (Table 1). This indicated that there was no chemical interaction between DCN and PXMR.

3.3. FTIR

FTIR investigations are mainly carried out to examine a molecular change in the drug due to its interaction with excipients (polymers) (25,26).

FTIR spectra of DCN, PXMR, and SDs are shown in Figure 2. The principal absorption peaks of DCN were observed at 3,300 cm^{-1} (O-H, stretch, broad, COOH), 3,069 cm^{-1} (C-H, stretch, aromatic), 2,935 cm^{-1} (C-H, stretch, aliphatic, sym), 1,770 cm^{-1} (C=O, stretch, ester), 1,679 cm^{-1} (C=O, stretch, COOH), 1,693 cm^{-1} (C=O, stretch, ketone), 1,593 cm^{-1} (C=C, stretch, aromatic), 1,450 cm^{-1} (C-O, stretch, COOH), 1,026 cm^{-1} (C-O, stretch, ester), 760 cm^{-1} (m substituted benzene), and 704 cm^{-1} (benzene) (27).

The FTIR spectrum of PXMR is characterized by principal absorption peaks at 3,485 cm^{-1} (O-H, stretch, broad), 2,884 cm^{-1} (C-H, stretch, aliphatic), 1,343 cm^{-1} (in-plane O-H bend) and 1,111 cm^{-1} (C-O stretch) (27), which consistently appeared in all of the binary systems of DCN.

All SD systems displayed frequency shifts and/or the disappearance of characteristic IR bands of either the drug or polymer, indicating alterations in the drug or polymer environment.

The principal absorption peaks of DCN at 3,300, 3,069, 1,693 and 2,935 cm^{-1} disappeared for all SDs. The peak at 1,770 cm^{-1} (C=O, stretch, ester) shifted to a slightly lower frequency at 1,769 cm^{-1} for all SDs whereas the peak at 1,679 cm^{-1} shifted to a slightly higher frequency at 1,680 cm^{-1} in a 1:1.5 SD. No frequency shift was observed for this peak in 1:0.5 and 1:2.5 SDs. The peak of PXMR at 3,485 cm^{-1} shifted to a lower frequency at 3,445, 3,447, and 3,433 cm^{-1} in 1:0.5, 1:1.5, and 1:2.5 SDs, respectively, revealing its involvement in hydrogen bonding with oxygen in

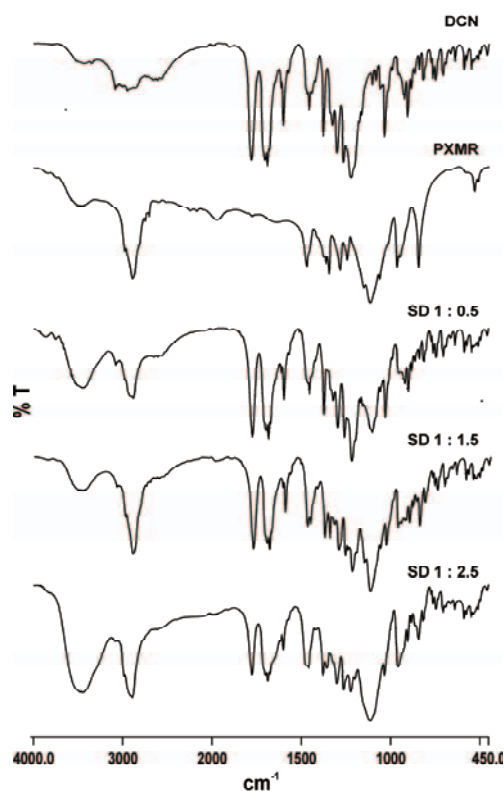


Figure 2. FTIR spectra of diacerein and all its binary systems with Pluronic® F 127. DCN, diacerein; PXMR, Pluronic® F 127; SD, solid dispersion.

the drug (28). The peak of PXMR at 2,884 cm^{-1} also shifted to 2,873, 2,886, and 2,872 cm^{-1} in 1:0.5, 1:1.5, and 1:2.5 SDs, respectively, indicating strong physical interaction between the polymer and drug. None of the binary systems of DCN-PXMR showed any new peaks, indicating the absence of chemical bond formation in those binary systems (29).

3.4. DSC

DSC thermograms of DCN and its corresponding binary systems with PXMR are shown in Figure 3. As shown in the figure, DCN displayed a sharp endothermic T_{max} of 256.14°C, corresponding to the melting point of the crystalline form of DCN. In contrast, PXMR showed a sharp endotherm at 57.40°C, indicating the melting point of the polymer, followed by a broad exotherm at 249.39°C, indicating recrystallization or transfer of heat (energy) to surrounding molecules gained in the melting process.

A very broad endotherm 246.51°C was observed in the DSC thermogram of 1:0.5 SD, indicating the presence of some traces of crystalline DCN. A significant reduction in the intensity of the sharp peak of DCN was noted in 1:1.5 (240.30°C) and 1:2.5 (234.85°C) SDs. With dispersions, peak temperatures shifted to lower temperatures than with the drug alone, indicating a loss of the characteristic features of DCN peaks in these dispersions (30,31). This phenomenon might be attributed to complete molecular dispersion

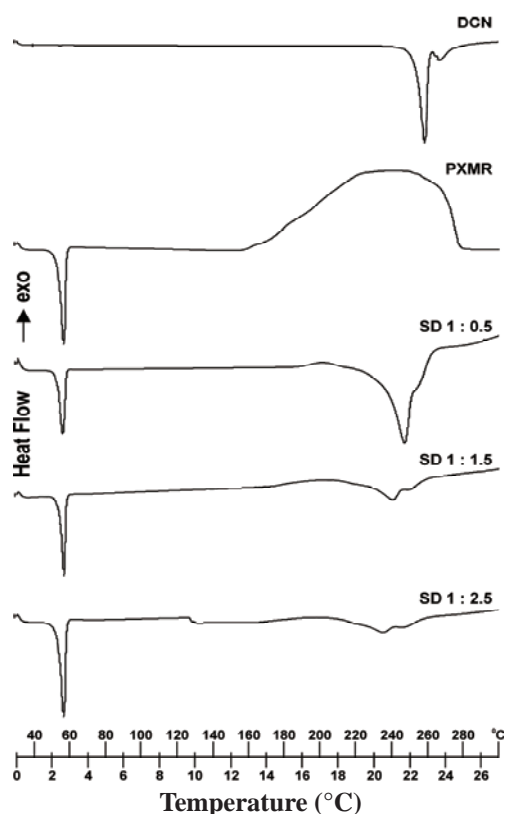


Figure 3. DSC thermograms of diacerein, Pluronic® F 127, and solid dispersions. DCN, diacerein; PXMR, Pluronic® F 127; SD, solid dispersion.

and possibly indicate the presence of an amorphous DCN in these binary systems (32-35). In all of the formulations, a decreased melting point peak for DCN was observed, and this might be attributed to solid-solid phase transition or the transfer of heat energy (from polymer to drug molecules) released after initial melting of the polymer. The peak for the polymer in all of the binary systems consistently appeared in the range of 55.65-56.75°C, which indicated the absence of any chemical interaction between the drug and polymer during the thermal process.

3.5. SEM

SEM microphotographs of pure DCN and its SDs are shown in Figure 4. Pure DCN consisted of some large irregular crystals with fine particles. A marked loss of the crystalline and irregular shape was detected in SEM photomicrographs of SDs as smooth patches of polymer covered the surface of the drug. SDs appeared as irregular particles in which the original morphological features of both the drug and polymer disappeared and tiny aggregates of amorphous pieces of irregular size were present (35). Therefore, the reduced particle size, increased surface area, and the close contact between the hydrophilic carrier and the drug might be responsible for the drug's improved dissolution rate as was observed with SD particles (36,37).

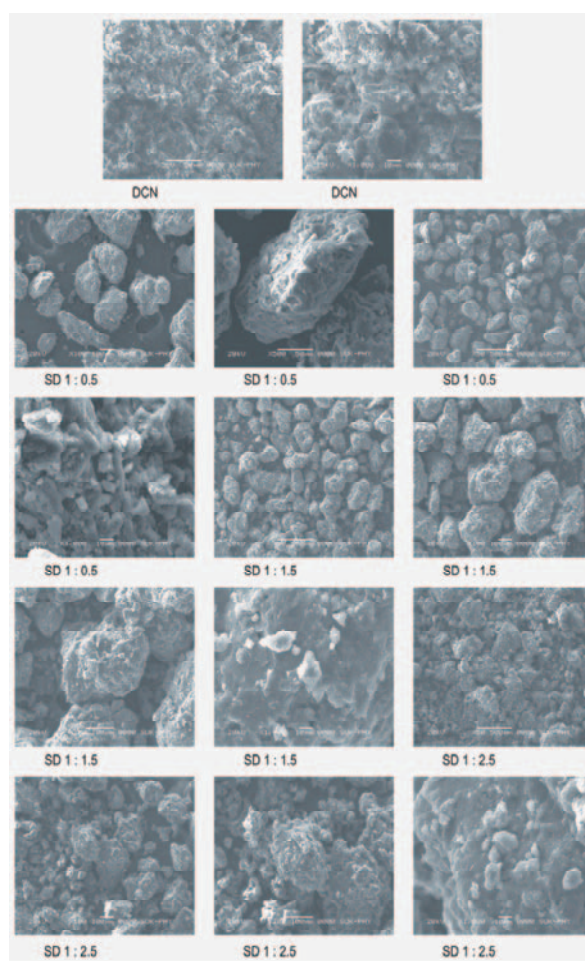


Figure 4. Scanning electron microphotographs of diacerein and solid dispersion particles. DCN, diacerein; SD, solid dispersion.

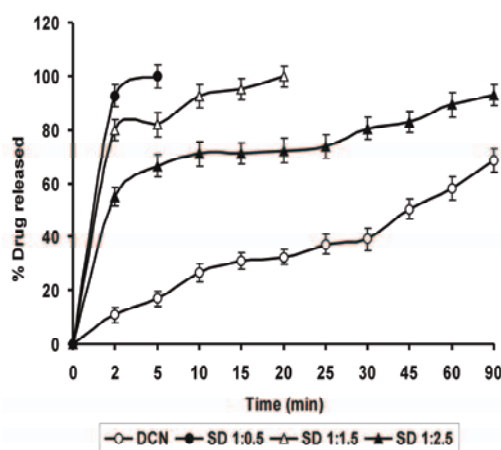


Figure 5. Dissolution curves of diacerein alone and all its solid binary systems. DCN, diacerein; SD, solid dispersion.

3.6. Dissolution rate studies

The dissolution curves of DCN alone and SDs in phosphate buffer (pH 6.8) are shown in Figure 5. The release rate profiles are expressed as the percentage of drug released over (*vs.*) time. All binary systems have an improved rate of DCN dissolution. Table 2 shows

Table 2. Dissolution profile of diacerein and its solid binary systems with Pluronic® F 127 in phosphate buffer (pH 6.8) at 37 ± 0.5°C

| System | DP ₂ * | DP ₅ | DP ₁₅ * | DP ₉₀ * | DE ₅ * |
|----------|-------------------|-----------------|--------------------|--------------------|-------------------|
| DCN | 10.8 ± 2.7 | 16.9 ± 2.9 | 31.1 ± 3.1 | 68.6 ± 4.3 | 10.5 ± 2.2 |
| 1:0.5 SD | 92.7 ± 4.2 | 100.0 ± 4.4 | – | – | 77.4 ± 3.4** |
| 1:1.5 SD | 79.8 ± 3.9 | 81.9 ± 4.6 | 95.1 ± 4.8 | – | 64.5 ± 3.3** |
| 1:2.5 SD | 55.1 ± 3.5 | 66.4 ± 4.1 | 71.2 ± 3.9 | 93.0 ± 4.0 | 47.5 ± 3.0** |

* Data are shown as mean ± S.D. (n = 3). ** Significant difference compared to pure DCN ($p < 0.001$), *i.e.*, significant. Abbreviations: DCN, diacerein; SD, solid dispersion; DP, % drug dissolved; DE, dissolution efficiency.

the % drug dissolved at 2 min (DP₂), 5 min (DP₅), 15 min (DP₁₅), and 90 min (DP₉₀) for all formulations. The dissolution efficiency values (DE₅) at 5 min were statistically analyzed using ANOVA. The results obtained revealed that all binary systems of DCN with PXMR have faster dissolution than DCN alone. The increase in the dissolution rate of DCN was 8.6-, 7.4-, and 5.1-fold greater from 1:0.5, 1:1.5, and 1:2.5 SDs, respectively, within the same period of time.

Statistical analysis (ANOVA) of DE₅ values of DCN and its formulations revealed a significant difference between the dissolution profile of pure DCN and all its binary systems with PXMR ($p < 0.001$). The 1:0.5 ratio of DCN:PXMR SD had the greatest dissolution of DCN among all the binary systems evaluated, indicating almost complete release of the drug from the SD (DP₅: 100.0 ± 4.4). An SD with a 1:1.5 ratio of DCN:PXMR had complete release of the drug within 20 min (DP₂₀: 100.0 ± 3.9). However, the release of the pure drug was incomplete even at 90 min. Of note is the fact that the extent of enhanced dissolution depended on the concentration of the polymer used in the SD, a finding that was evidenced by retardation of drug release from 1:1.5 and 1:2.5 SDs. This might be because of altered rheological characteristics and gelling properties of PXMR at higher concentrations (38). Results indicated that the polymer's surfactant properties, and not the amorphization or reduction in crystallinity of DCN in SDs, played greater role in enhancing the dissolution of DCN. Therefore, a 1:0.5 ratio of SD was found to be optimal for enhancing the dissolution of DCN.

The rapid dissolution of DCN from SDs was attributed to a reduction in the crystallinity of the drug due to its colloidal dispersion in a polymer matrix. As a hydrophilic carrier dissolves, an insoluble drug is exposed to dissolution medium in the form of very fine particles, leading to rapid dissolution (39,40). PXMR copolymers exist in solution as unimers but self-assemble into micelles. At concentrations above the CMC, the hydrophobic propylene oxide (PO) core can incorporate water-insoluble molecules, resulting in increased solubility of the drug molecule. In addition, the greater hydrophilicity and surface properties of PXMR and increased wettability, dispersibility, and reduced particle size of the drug might contribute to

the enhanced dissolution of DCN (29,41). Further, reports have indicated that the solubility of poorly water-soluble indomethacin (11) and insulin (42-44) has been significantly improved with PXMR. The aqueous solubility of piroxicam was enhanced 11-fold by PXMR in an SD (12). The faster and complete dissolution of nifedipine has been achieved from SDs incorporating PXMR (45). Nifedipine is also reportedly converted to an amorphous form in crystalline PXMR, enhancing its dissolution (36). Thus, the results obtained here were in full agreement with those already reported. In conclusion, the greater hydrophilicity and surfactant properties of PXMR result in a reduction in interfacial tension between the hydrophobic drug and dissolution medium, leading to greater wetting of the drug and surface availability for rapid dissolution.

4. Conclusion

The present investigation revealed that PXMR (Pluronic® F 127) is a proper choice as a carrier to enhance the dissolution of DCN from SDs. Among the ratios used, an SD with a 1:0.5 ratio was found to be optimal because of its superior performance in enhancing the dissolution of DCN. In contrast, higher concentrations of PXMR in SDs retarded the release of the drug. This indicated that an increase in the weight fraction of polymer did not offer any advantage in terms of enhancing dissolution. These results led to the conclusion that solid oral dosage forms of DCN with PXMR can be formulated with a high dissolution rate, faster onset of action, and improved bioavailability.

Acknowledgements

The authors wish to thank Glenmark Pharmaceuticals Ltd., Mumbai, India and Signet Chem Lab, Mumbai, India for providing drug and polymer samples, respectively, for research work. The authors also wish to thank Shivaji University, Kolhapur, Maharashtra, India for allowing the use of its FTIR and SEM facilities. The authors also express their sincere thanks to All India Shri Shivaji Memorial Society's College of Pharmacy, Pune, Maharashtra, India for allowing the use of its DSC facilities.

References

- Proudfoot S. Factors affecting bioavailability: Factors influencing drug absorption from gastrointestinal tract. In: *Pharmaceutics: The Science of Dosage Form Design* (Aulton ME, ed.). Churchill Livingstone, Edinburgh, UK, 1991; pp. 135-173.
- Hörter D, Dressman JB. Influence of physicochemical properties on dissolution of drugs in the gastrointestinal tract. *Adv Drug Deliv Rev.* 2001; 46:75-87.
- Hancock BC, Zografi G. Characteristics and significance of the amorphous state in pharmaceutical systems. *J Pharm Sci.* 1997; 86:1-12.
- Motlekar N, Khan MA, Youan BC. Preparation and characterization of genistein containing poly (ethylene glycol) microparticles. *J Appl Polym Sci.* 2006; 101:2070-2078.
- Schott H, Kwan LC, Feldman S. The role of surfactant in the release of very slightly soluble drugs from tablets. *J Pharm Sci.* 1982; 71:1038-1045.
- Rawat S, Jain SK. Solubility enhancement of celecoxib using β -cyclodextrin inclusion complexes. *Eur J Pharm Biopharm.* 2004; 57:263-267.
- Chiou WL, Riegelman S. Pharmaceutical applications of solid dispersion systems. *J Pharm Sci.* 1971; 60:1281-1302.
- Leuner C, Dressman J. Improving drug solubility for oral delivery using solid dispersions. *Eur J Pharm Biopharm.* 2000; 50:47-60.
- Serajuddin AT. Solid dispersion of poorly water-soluble drugs: Early promises, subsequent problems, and recent breakthroughs. *J Pharm Sci.* 1999; 88:1058-1066.
- Craig DQ. The mechanisms of drug release from solid dispersions in water-soluble polymers. *Int J Pharm.* 2002; 231:131-144.
- Dimitrova E, Bogdanova S, Mitcheva M, Tanev I, Minkov E. Development of model aqueous ophthalmic solution of indomethacin. *Drug Dev Ind Pharm.* 2000; 26:1297-1301.
- Shin SC, Cho CW. Physicochemical characterizations of piroxicam-poloxamer solid dispersion. *Pharm Dev Technol.* 1997; 2:403-407.
- Newa M, Bhandari KH, Li DX, Kwon TH, Kim JA, Yoo BK, Woo JS, Lyoo WS, Yong CS, Choi HG. Preparation, characterization and *in vivo* evaluation of ibuprofen binary solid dispersions with poloxamer 188. *Int J Pharm.* 2007; 343:228-237.
- Singhare DS, Khan S, Yeole PG. Poloxamers: Promising block co-polymers in drug delivery. *Indian J Pharm Sci.* 2005; 67:523-531.
- Oneil M, Heckelman PE, Koch CB. In: *The Merck Index. An Encyclopedia of Chemicals: Drugs and Biologicals*, 14th ed., Merck, Whitehouse Station, NJ, USA, 2006; p. 503.
- Toegel S, Huang W, Piana C, Unger FM, Wirth M, Goldring MB, Gabor F, Viernstein H. Selection of reliable reference genes for qPCR studies on chondroprotective action. *BMC Mol Biol.* 2007; 8:13.
- Nicolas P, Tod M, Padoin C, Petitjean O. Clinical pharmacokinetics of diacerein. *Clin Pharmacokinet.* 1998; 35:347-359.
- Pelletier JP, Mineau F, Fernandes JC, Duval N, Martel-Pelletier J. Diacerein and rhein reduce the interleukin 1 β stimulated inducible nitric oxide synthase level and activity while stimulating cyclooxygenase-2 synthesis in human osteoarthritic chondrocytes. *J Rheumatol.* 1998; 25:2417-2424.
- La Villa G, Marra F, Laffi G, Belli B, Meacci E, Fascetti P, Gentilini P. Effects of rhein on renal arachidonic acid metabolism and renal function in patients with congestive heart failure. *Eur J Clin Pharmacol.* 1989; 37:1-5.
- Tamura T, Shirai T, Kosaka N, Ohmori K, Takafumi N. Pharmacological studies of diacerein in animal models of inflammation, arthritis and bone resorption. *Eur J Pharmacol.* 2002; 448:81-87.
- Tamura T, Ohmori K. Rhehin, an active metabolite of diacerein, suppresses the interleukin-1 α -induced proteoglycan degradation in cultured rabbit articular chondrocytes. *Jpn J Pharmacol.* 2001; 85:101-104.
- Diacerein Product Description. Xian Guanyu Bio-Tech Co. Ltd. Available at http://www.bikudo.com/product_search/details/44285/diacerein.html (accessed on August 10, 2009).
- Diacerein Capsules. Ostomod. Available at http://www.cipladoc.com/therapeutic/pdf_cipla/ostomod.pdf (accessed on August 10, 2009).
- Sethi PD. *Identification of Drugs in Pharmaceutical Formulations by TLC*, 1st ed., CBS Publications, New Delhi, India, 1992.
- Pignatello R, Ferro M, Puglisi G. Preparation of solid dispersions of nonsteroidal anti-inflammatory drugs with acrylic polymers and studies on mechanisms of drug-polymer interactions. *AAPS PharmSciTech.* 2002; 3: E10.
- Soliman MS, Khan MA. Preparation and *in vitro* characterization of a semi-solid dispersion of flurbiprofen with Gelucire 44/14 and Labrasol. *Pharmazie.* 2005; 60:288-293.
- Silverstein RM, Bassler GC, Morrill TC. *Spectroscopic Identification of Organic Compounds*. 5th ed., John Wiley & Sons Inc., NY, USA, 1991.
- Kalaiselvan R, Mohanta GP, Manna PK, Manimekalai A. Solid-phase preparation and characterization of albendazole solid dispersion. *ARS Pharm.* 2006; 47:91-107.
- Ford JL. The current status of solid dispersions. *Pharm Acta Helv.* 1986; 61:69-88.
- Suhagia BN, Patel HM, Shah SA, Rathod I, Parmar VK. Preparation and characterization of etoricoxib-polyethylene glycol 4000 plus polyvinylpyrrolidone K30 solid dispersions. *Acta Pharm.* 2006; 56:285-298.
- Wulff M, Aldén M. Solid state studies of drug-cyclodextrin inclusion complexes in PEG 6000 prepared by a new method. *Eur J Pharm Sci.* 1999; 8:269-281.
- Valleri M, Mura P, Maestrelli F, Cirri M, Ballerini R. Development and evaluation of glyburide fast dissolving tablets using solid dispersion technique. *Drug Dev Ind Pharm.* 2004; 30:525-534.
- Shavi GV, Kumar AR, Usha YN, Armugam K, Ranjan O, Ginpallai K, Pandey S, Udupa N. Enhanced dissolution and bioavailability of gliclazide using solid dispersion techniques. *International Journal of Drug Delivery.* 2010; 2:49-57.
- Kim EJ, Chun MK, Jang JS, Lee IH, Lee KR, Choi HK. Preparation of a solid dispersion of felodipine using a solvent wetting method. *Eur J Pharm Biopharm.* 2006; 64:200-205.
- Ruan LP, Yu BY, Fu GM, Zhu DN. Improving the solubility of ampelopsin by solid dispersions and

- inclusion complexes. *J Pharm Biomed Anal.* 2005; 38:457-464.
36. Jung JY, Yoo SD, Lee SH, Kim KH, Yoon DS, Lee KH. Enhanced solubility and dissolution rate of itraconazole by a solid dispersion technique. *Int J Pharm.* 1999; 187:209-218.
37. Ambike AA, Mahadik KR, Paradkar A. Stability study of amorphous valdecoxib. *Int J Pharm.* 2004; 282:151-162.
38. Park YJ, Yong CS, Kim HM, Rhee JD, Oh YK, Kim CK, Choi HG. Effect of sodium chloride on the release, absorption and safety of diclofenac sodium delivered by poloxamer gel. *Int J Pharm.* 2003; 263:105-111.
39. Geneidi AS, Ali AA, Salama RB. Solid dispersions of nitrofurantoin, ethotoin and coumarin with polyethylene glycol 6000 and their coprecipitates with povidone 25,000. *J Pharm Sci.* 1978; 67:114-116.
40. Save T, Venkitachalam P. Studies on solid dispersions of nifedipine. *Drug Dev Ind Pharm.* 1992; 18:1663-1679.
41. Dumortier G, Grossiord JL, Agnely F, Chaumeil JC. A review of poloxamer 407 pharmaceutical and pharmacological characteristics. *Pharm Res.* 2006; 23:2709-2728.
42. Barichello JM, Morishita M, Takayama K, Chiba Y, Tokiwa S, Nagai T. Enhanced rectal absorption of insulin loaded Pluronic® F-127 gels containing unsaturated fatty acids. *Int J Pharm.* 1999; 183:125-132.
43. Barichello JM, Morishita M, Takayama K, Nagai T. Absorption of insulin from Pluronic® F-127 gels following subcutaneous administration in rats. *Int J Pharm.* 1999; 184:189-198.
44. Strickley RG. Solubilizing excipients in oral and injectable formulations. *Pharm Res.* 2004; 21:201-230.
45. Chutimaworapan S, Ritthidej GC, Yonemochi E, Oguchi T, Yamamoto K. Effect of water-soluble carriers on dissolution characteristics of nifedipine solid dispersions. *Drug Dev Ind Pharm.* 2000; 26:1141-1150.

(Received May 18, 2010; Revised September 6, 2010;
Accepted September 20, 2010)

Original Article**Solid-state characterization and *in vitro* dissolution behavior of lorazepam: Hydroxypropyl- β -cyclodextrin inclusion complex**

Rakesh Patel*, Manisha Patel

Department of Pharmaceutics, S. K. Patel College of Pharmaceutical Education and Research, Ganpat University, Kherva, Gujarat, India.

ABSTRACT: The objectives of this research were to prepare and characterize inclusion complexes of lorazepam with hydroxypropyl- β -cyclodextrin and to study the effect of complexation on the dissolution rate of lorazepam, a water-insoluble drug. The phase solubility profile of lorazepam with hydroxypropyl- β -cyclodextrin was an AP-type, indicating the formation of 2:1 stoichiometric inclusion complexes. Gibbs free energy values were all negative, indicating the spontaneous nature of lorazepam solubilization, and they decreased with an increase in the cyclodextrin concentration, demonstrating that the reaction conditions became more favorable as the concentration of cyclodextrins increased. Complexes of lorazepam were prepared with cyclodextrin using various methods such as physical mixing, kneading, spray-drying, and lyophilization. The complexes were characterized by differential scanning calorimetry, Fourier-transform infrared, scanning electron microscopy, and powder X-ray diffraction studies. These studies indicated that a complex prepared by lyophilization had successful inclusion of the lorazepam molecule into the cyclodextrin cavity. Complexation resulted in a marked improvement in the solubility and wettability of lorazepam. Among all the samples, a complex prepared with hydroxypropyl- β -cyclodextrin by lyophilization had the greatest improvement in the *in vitro* rate of lorazepam dissolution. The mean dissolution time for lorazepam decreased significantly after preparing complexes and physical mixtures of lorazepam with cyclodextrin. The similarity factor indicated a significant difference between the release profiles of lorazepam from complexes and physical mixtures and from plain lorazepam. Tablets containing complexes prepared

with cyclodextrins had significant improvement in the release profile of lorazepam as compared to tablets containing lorazepam without cyclodextrin.

Keywords: Lorazepam, hydroxypropyl- β -cyclodextrin, inclusion complexation, *in vitro* dissolution studies

1. Introduction

Lorazepam (LRZ), a potent benzodiazepine, is used for the short-term relief of symptoms of anxiety or anxiety associated with depression (1). This drug is often used for preanesthetic medication; it is useful for managing status epilepticus, chemotherapy-induced nausea, and vomiting (1). LRZ binds to central benzodiazepine receptors that interact allosterically with γ -aminobutyric acid (GABA) receptors (1). This potentiates the effects of the inhibitory neurotransmitter GABA, increasing the inhibition of the ascending reticular activating system and blocking the cortical and limbic arousal that occurs following stimulation of the reticular pathways (1). LRZ is an almost white powder that is nearly insoluble in water (0.08 mg/mL) and oil (2). Because of its poor water solubility and extensive metabolism in the liver into pharmacologically inactive glucuronides, LRZ oral therapy is associated with a slow onset of drug action (3). Generally, compounds with very low aqueous solubility are considered to have dissolution rate-limited absorption and hence poor absorption, distribution, and target organ delivery (4). Improving aqueous solubility in such cases is a worthwhile way of improving therapeutic efficacy. In this respect, a fast-dissolving form of the compound with a high level of aqueous solubility is desirable for rapid absorption of the drug during oral benzodiazepine therapy. Complexation of such drugs with cyclodextrins (CDs) represents one way to achieve that goal.

CDs form a group of structurally related oligosaccharides with cylinder-shaped cavities that have the capacity to form inclusion complexes with many drugs by taking a whole drug molecule, or a

*Address correspondence to:

Dr. Rakesh P. Patel, Department of Pharmaceutics and Pharmaceutical Technology, S. K. Patel College of Pharmaceutical Education and Research, Ganpat University, Kherva, Mehsana-Gozaria Highway, PIN-382711, Gujarat, India.
e-mail: raka_77us@yahoo.com

part of it, into the cavity (5). Because of the large number of hydroxyl groups on CDs, they are water-soluble (5). They are known for their ability to molecularly encapsulate a wide variety of drugs into their hydrophobic cavity without the formation of any covalent bonds (5). The binding forces within these inclusion complexes may involve hydrophobic, van der Waals, hydrogen bonding, or dipole interactions (5). CDs have widespread pharmaceutical applications mainly because of their effect on enhancing the solubility and bioavailability of many drug formulations. Complexation with CDs has been reported to enhance the solubility, dissolution rate, and bioavailability of poorly water-soluble drugs (6-9). CDs first came to the fore in marketed products as drug delivery technologies that enabled the development of various prostaglandins (10).

Complexation of pharmaceuticals with β -CD causes enhancement of their solubility and bioavailability as well as stabilization against oxidation, decomposition, hydrolysis, etc. (11). Hydroxypropyl- β -cyclodextrin (HP- β -CD), a chemical derivative of β -CD, is the most accepted representative of hydroxyalkylated derivatives as a hydrophilic drug carrier because of its amorphousness, high water solubility and solubilizing power, and low cost and toxicity (12). Hydroxyalkylated CD derivatives have proven to be very useful in intravenous and other parenteral preparations because of their low hemolytic activity and irritation compared to β -CD and its alkylated forms (12). An inclusion complex of albendazole/HP- β -CD (1:1, molar ratio) has been prepared using coprecipitation and freeze-drying in order to increasing its aqueous solubility (13). Many other drugs such as artemisinin, etodolac, cilostazol, nimesulide, and piroxicam have been tested for CD inclusion to enhance their solubility (14-18).

In vitro dissolution testing provides an easy and convenient means of evaluating the performance of pharmaceutical preparations (19). The *in vitro* dissolution profile is a reliable index to accurately predict a preparation's *in vivo* performance (19). In the current study, an attempt was made to compare the similarities of the *in vitro* dissolution profiles of LRZ from complexes, physical mixtures, and pure LRZ. Dissolution profiles can be compared by calculating the similarity factor (f_2 values), an index that was first reported by Moore and Flanner in 1996 (20). This index has also been adopted by the Center for Drug Evaluation and Research, Food and Drug Administration (US FDA, 1997) and by the Human Medicines Evaluation Unit of the European Agency for the Evaluation of Medicinal Products (EMEA, 1999) as a criterion for the assessment of the similarity of two dissolution profiles. The similarity equation is given in the US FDA guidelines for industry for dissolution testing of immediate-release products (21,22). A value of 100% for the similarity factor (f_2) suggests that the

test and reference profiles are identical (20). Values between 50 and 100 indicate that the dissolution profiles are similar whilst smaller values imply an increase in dissimilarity between release profiles (20).

Mean dissolution time (MDT) reflects the time for the drug to dissolve and is the first statistical moment for the cumulative dissolution process that provides an accurate drug release rate (23). It is an accurate expression of the drug release rate. A higher MDT value indicates greater drug-retarding ability (24).

The objective of the present study was to prepare inclusion complexes of LRZ with HP- β -CD using various methods such as kneading, coevaporation, and physical mixing to improve its aqueous solubility and dissolution rate. The study further aimed to characterize the prepared inclusion complexes by methods such as differential scanning calorimetry (DSC), Fourier transform infrared (FTIR), scanning electron microscopy (SEM), and powder X-ray diffraction (PXRD) studies.

2. Materials and Methods

2.1. Materials

HP- β -CD was donated by Roquette Frères, France. LRZ was donated by Astron Research Center (Ahmedabad, India). Directly compressible lactose, microcrystalline cellulose, talc, and magnesium stearate were donated by Maan Pharmaceuticals Ltd. (Ahmedabad, India). All chemicals and solvents used in this study were of analytical reagent grade. Freshly distilled water was used throughout the work.

2.2. Phase solubility study

Phase-solubility studies were performed according to the method reported by Higuchi and Connors in 1965 (25). Excess LRZ was transferred to screw-capped vials containing 25 mL of aqueous solution of HP- β -CD (molecular weight = 1,500) in various molar concentrations (10, 25, 50, 100, 150, and 200 mM for HP- β -CD). The contents were stirred at 400 rpm on an electromagnetic stirrer (Remi Instruments Ltd., Mumbai, India) for 48 h at $25 \pm 0.1^\circ\text{C}$ and at $37 \pm 0.1^\circ\text{C}$ (this duration was previously tested to be sufficient to reach equilibrium). After reaching equilibrium, samples were filtered through a 0.22- μm membrane filter, suitably diluted, and analyzed spectrophotometrically for drug content at a wavelength of 230 nm using a spectrophotometer (Shimadzu-11700, UV/Vis spectrophotometer; Shimadzu Corp, Kyoto, Japan). Solubility studies were performed in triplicate ($n = 3$). The apparent stability constant (Ks), in accordance with a theoretical 1:1 stoichiometric ratio of complexes, was calculated from the phase-solubility diagrams using the following equation:

$$K_s = \frac{\text{slope}}{S_o(1 - \text{slope})} \quad \text{----- Eq. 1}$$

where the slope is obtained from the initial straight-line portion of the plot of LRZ concentration with respect to the CD concentration and S_o is the equilibrium solubility of LRZ in water.

2.3. Preparation of inclusion complexes

Complexes of HP- β -CD with LRZ were prepared at a molar ratio of 2:1 (on the basis of the phase solubility study) by different methods like physical mixing, kneading, spray-drying, and lyophilization. For ease of discussion, the samples were designated with different abbreviations as shown in Table 1.

2.3.1. Physical mixing

Physical mixtures (PMs) of CDs and LRZ were prepared by simply mixing powders with a spatula for 15 min.

2.3.2. Kneading

To prepare complexes by kneading, the required quantities of CDs and distilled water were mixed together in a mortar to obtain a homogeneous paste. LRZ was then added slowly; during grinding, a small quantity of methanol was added to assist the dissolution of LRZ. The mixtures were then ground for 1 h. During this process, an appropriate quantity of water was added to the mixture in order to maintain a suitable consistency. The paste was dried in an oven at 45-50°C for 24 h. The dried complexes were pulverized and then sieved through a #100 sieve.

2.3.3. Spray-drying

For spray-drying, LRZ was dissolved in methanol and HP- β -CD was dissolved in distilled water. Mixtures of both solutions were stirred at room temperature for 24 h and then spray-dried using a Labultima LU222 Advanced Laboratory Spray Dryer under the following conditions: inlet temperature of 70°C, outlet temperature of 45-50°C, flow rate of the solution of 400 mL/h, airflow rate of 40-50 m³/h, and atomizing air pressure of 1.0-1.1 bar.

Table 1. Abbreviations used to designate samples of LRZ prepared with HP- β -CD using different methods

| Type of CDs | Method of preparation | Name of sample |
|-----------------|--------------------------------|----------------|
| HP- β -CD | Physical mixing | PM |
| HP- β -CD | Kneading | KN |
| HP- β -CD | Spray-drying | SP |
| HP- β -CD | Lyophilization (freeze-drying) | LP |

2.3.4. Lyophilization

For lyophilization, LRZ was dissolved in methanol and HP- β -CD was dissolved in distilled water. Mixtures of both solutions were stirred at room temperature for 24 h and then freeze-dried in a VirTis BenchTop Freeze Dryer to yield an amorphous powder. The product was sieved through a #100 sieve.

2.4. Drug content

The complexes prepared by physical mixing, kneading, spray-drying, and freeze-drying were assayed for LRZ content by dissolving a specific amount of the complex in methanol and spectrophotometrically analyzing it for LRZ content at 230 nm in a spectrophotometer (U.V. visible spectrophotometer, Shimadzu-1700).

2.5. Characterization of complexes

2.5.1. DSC analysis

DSC scans of the powdered samples of LRZ, HP- β -CD, and LRZ in PMs and complexes with HP- β -CD were recorded using a DSC-Shimadzu 60 with TDA trend line software. The samples (6-7 mg) were accurately weighed in crimped aluminum pans and heated from 50°C to 300°C at a scanning rate of 10°C/min under an air flow of 100 mL/min.

2.5.2. FTIR spectroscopic analysis

FTIR spectra of moisture-free powdered samples of LRZ, HP- β -CD, and LRZ in PMs and complexes with HP- β -CD were obtained by the potassium bromide (KBr) pellet method using a spectrometer (FTIR-8300, Shimadzu Co.).

2.5.3. SEM

The surface morphology of free powdered samples of LRZ, HP- β -CD, and LRZ in PMs and complexes with HP- β -CD were examined using a scanning electron microscope (Philips, LC ESEM). The samples were fixed onto a brass stub using double-sided tape and then rendered electrically conductive by coating them with a thin layer of copper in a vacuum. Photographs were taken with a Pentax (model MZ-10) camera at an excitation voltage of 10 kV and magnification of $\times 200$ and $\times 3,500$.

2.5.4. PXRD analysis

PXRD patterns of LRZ, HP- β -CD, and LRZ in PMs and complexes with HP- β -CD were determined using an Expert Phillips IW 1830 generator with a CuK α anode at 40 kV and 30 mA and a scan rate of 1° min⁻¹ from 2 θ

in a range from 1° to 40°. Analysis was conducted by SICART, Vallabh Vidyanagar, India.

2.5.5. Wettability and dissolution studies

A wettability study was performed using open capillary tubes filled with LRZ, HP- β -CD, and LRZ in PMs and complexes with HP- β -CD in which the lower capillary ends were dipped into colored water (0.01% eosin in water). The upward migration of the colored front was recorded over time (26).

Dissolution studies of LRZ, PM, KN, SP, and LP in powder form were performed to evaluate their *in vitro* drug release profile. Dissolution studies were carried out using a type II USP dissolution apparatus with 100 mL dissolution medium (distilled water) at $37 \pm 0.5^\circ\text{C}$ and 50 rpm for 4 h. At different time intervals, 5 mL aliquots were withdrawn, filtered, suitably diluted with distilled water:methanol (50:50, v/v), and then assayed for LRZ content by measuring the absorbance at 230 nm using a spectrophotometer. Fresh medium (5 mL) was replaced after each sampling to maintain a constant volume of dissolution medium throughout the test.

LRZ, PM, KN, SP, and LP were evaluated *via in vitro* dissolution rate studies. Dissolution studies were performed three times, and calculated mean values of cumulative drug release were used while plotting the release curves. MDT values were calculated to compare the extent of improvement in the dissolution rate of PM, KN, SP, and LP. Preliminary tests determined that there was no change in the λ_{max} of LRZ due to the presence of HP- β -CD dissolved in the dissolution medium.

2.6. Formulation studies

Formulation excipients were selected on the basis of preliminary tests which found no interference by these excipients with the λ_{max} of LRZ. Tablets containing 4 mg of LRZ were made by direct compression using different formulation excipients like directly compressible lactose, microcrystalline cellulose, talc, and magnesium stearate. Tablets equivalent to 4 mg LRZ that contained complexes prepared by kneading, spray-drying, and freeze-drying were similarly produced but the quantity was adjusted with lactose to prepare a tablet of equal weight. The blend was compressed on an eight-station single rotary machine (Cadmach Machinery Co., Ahmedabad, India) using round-shaped flat punches to obtain tablets with a hardness of 4 to 6 kg/cm² and thickness of 3.3 to 3.6 mm. For the assay, three tablets were crushed and a blend equivalent to 4 mg of LRZ was weighed and dissolved in the dissolution medium. The tablets were studied five times ($n = 5$) to determine the release profile of the drug using the same methodology as described in the *in vitro* dissolution studies.

2.7. Statistical analysis

A model-independent mathematical approach as proposed by Moore and Flanner (20) for calculating the similarity factor, f_2 , was used to compare the dissolution profiles of different samples. f_2 is a measure of similarity of two dissolution curves in terms of the percentage dissolution and is defined by following equation (20):

$$f_2 = 50 \times \log \left\{ \left[1 + \left(\frac{1}{n} \right) \sum_{t=1}^n w_t (R_t - T_t)^2 \right]^{-0.5} \times 100 \right\}$$

---- Eq. 2

where n is the number of samples taken, R_t is the percentage of the reference formulation dissolved at time point t , and T_t is the percentage of the test formulation dissolved at time point t .

A value of 100% for f_2 suggests that the test and reference profiles are identical. Values between 50 and 100 indicate that the dissolution profiles are similar whilst smaller values imply an increase in dissimilarity between release profiles (20).

3. Results and Discussion

3.1. Phase solubility study

Phase solubility analysis has been among the preliminary requirements for optimizing the development of inclusion complexes of drugs as it permits the evaluation of the affinity between a CD and drug molecule in water. This process has been used by many researchers to determine the exact molar ratios at which drugs can form complexes with CDs (27-29).

The phase solubility curve of LRZ in the presence of CDs is shown in Figure 1. This curve indicated an increase in the solubility of LRZ with an increase in the concentration of the CD in water. Increasing the amount of the CD increased the amount of LRZ entering the water, improving the aqueous solubility of LRZ. The solubility of LRZ increased by 420-fold at 37°C and 322-fold at 25°C at a 200 mM concentration of HP-

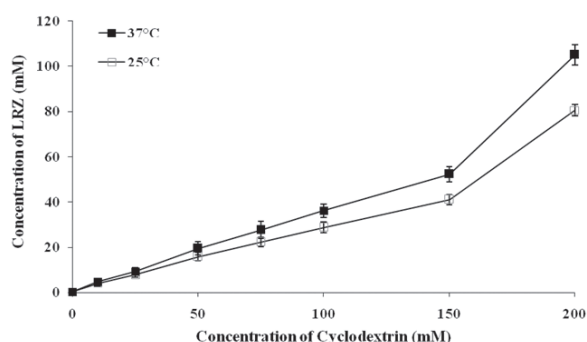


Figure 1. Phase solubility curve of LRZ in aqueous solution of HP- β -CD at 37°C and 25°C . Open circle, 37°C ; Closed circle, 25°C .

β -CD. Increased solubility may be due to improved dissolution of LRZ particles in water due to the presence of CDs.

An indication of the process of transfer of LRZ from pure water to the aqueous solution of CDs was obtained from the values for the Gibbs free energy change. The Gibbs free energy of transfer (ΔG_{tr}°) of LRZ from pure water to aqueous solutions of CDs was calculated using the following equation (30):

$$\Delta G_{tr}^\circ = -2.303RT \log\left(\frac{S_o}{S_s}\right) \quad \text{---Eq. 3}$$

where S_o/S_s is the ratio of molar solubility of LRZ in an aqueous solution of HP- β -CD compared to that in pure water. The obtained values for Gibbs free energy are shown in Table 2. These data provide information regarding the increased solubility of LRZ in the presence of HP- β -CD. In other words, the Gibbs free energy values provide information on whether the reaction conditions favor or disfavor drug solubilization in the aqueous carrier solution. Negative Gibbs free energy values indicate favorable conditions. ΔG_{tr}° values were all negative for HP- β -CD at various concentrations, indicating the spontaneous nature of LRZ solubilization, and the values decreased with an increase in concentration, indicating that the reaction was favored more as the concentration of HP- β -CD increased.

The enthalpy of transfer (ΔH_t°) and entropy (ΔS) can be calculated from a modification of the van't Hoff equation (31):

$$\frac{d \ln(S_c/S_o)}{dT} = \frac{\Delta H_t^\circ}{RT^2} \quad \text{---Eq. 4}$$

Rearranging and solving for ΔH_t° yields

$$\Delta H_t^\circ = -R \frac{d \ln(S_c/S_o)}{d(1/T)} \quad \text{---Eq. 5}$$

Linear regression of $\ln(S_c/S_o)$ versus $1/T$ for HP- β -CD concentrations of 10, 25, 50, 75, 100, 150, and 200 mM gives a slope equal to $-\Delta H_t^\circ/R$. This treatment assumes that ΔH_t° is reasonably constant over the temperature range studied.

$$\Delta S = (\Delta H - \Delta G)/T \quad \text{---Eq. 6}$$

Usually, complex formation with HP- β -CD results in a relatively large negative ΔH and a ΔS that can be either positive or negative (31,32). Negative ΔH values suggest that either dipolar or induced dipolar and Van der Waals interactions between the cavity and the substrate are involved in inclusion complexation. The negative change in ΔS observed with HP- β -CD can be attributed to greater order after complexation. This is mainly due to the loss of rotational and translational freedom for the molecules involved in the complexation process (31-34).

The stoichiometric ratio at which optimum complexation occurs was confirmed by phase solubility analysis. The phase solubility plots revealed an A_p type for HP- β -CD (data not shown), which indicated that a 2:1 (HP- β -CD-LRZ) inclusion complex was formed in solution. The values of apparent stability constants (K_s) for the complexes at 25°C and 37°C, assuming a 2:1 stoichiometry, calculated from the slope of the initial straight portion of the phase solubility diagram were 258 M^{-1} at 25°C and 491 M^{-1} at 37°C for HP- β -CD:LRZ, indicating suitable and stable complex formation (data not shown). CD-drug complexes with values of K_s in the range of 200 to 5,000 M^{-1} are reported to exhibit improved dissolution properties and hence better bioavailability (26).

3.2. Drug content

The drug content of PM, KNB, SP, and LP was found out to be $91.2 \pm 10.3\%$, $95.6 \pm 8.5\%$, $98.5 \pm 6.2\%$, and $99.0 \pm 5.0\%$, respectively (data not shown), which roughly corresponds to the stoichiometric ratio of the complex and indicates chemical stability and content uniformity of LRZ in its complex form.

3.3. Characterization of complexes

3.3.1. DSC analysis

DSC enables the quantitative detection of all processes

Table 2. Gibbs free energy of transfer (ΔG), standard enthalpy change (ΔH), and entropy (ΔS) for the solubilization of LRZ in aqueous solutions of cyclodextrins at 37°C and 25°C

| Concentration of cyclodextrins (mM) | ΔG (KJmol ⁻¹) | | ΔH (KJmol ⁻¹) | ΔS (Jmol ⁻¹ K ⁻¹) |
|-------------------------------------|-----------------------------------|--------------|-----------------------------------|--|
| | 25°C | 37°C | | |
| 10 | -6.9 ± 0.04 | -1.3 ± 0.05 | -10.2 ± 0.20 | -0.00860 ± 0.0004 |
| 25 | -8.5 ± 0.06 | -2.3 ± 0.10 | -10.9 ± 0.25 | -0.00508 ± 0.0005 |
| 50 | -10.3 ± 0.10 | -3.2 ± 0.14 | -12.8 ± 0.31 | -0.00507 ± 0.0004 |
| 75 | -11.1 ± 0.12 | -3.5 ± 0.17 | -13.4 ± 0.38 | -0.00424 ± 0.0003 |
| 100 | -11.7 ± 0.20 | -4.4 ± 0.20 | -14.7 ± 0.42 | -0.00615 ± 0.0005 |
| 150 | -12.7 ± 0.26 | -5.1 ± 0.26 | -15.4 ± 0.45 | -0.00514 ± 0.0006 |
| 200 | -14.4 ± 0.29 | -15.6 ± 0.30 | -17.3 ± 0.47 | -0.00552 ± 0.0005 |

Data are shown mean ± S.D. (n = 3).

in which energy is required or produced (*i.e.*, endothermic or exothermic phase transformations) (35). The thermograms for pure LRZ, HP- β -CD, and LRZ in PMs and complexes with HP- β -CD are presented in Figure 2. The DSC curve of LRZ displayed a sharp endotherm at 184.92°C that was due to drug melting, characteristic of an anhydrous crystalline substance. In the thermogram of HP- β -CD, the peak between 90°C and 120°C was due to loss of water from CD molecules.

In PM systems, the drug endothermic peak was clearly distinguishable (Figure 2). This indicates that in such systems the drug has basically maintained its original crystallinity. In KN systems, there was a substantial size reduction and a broadening and a shift to lower temperatures of the drug melting point (175.61°C) (Figure 2). This shift may be due to the decrease in crystallinity and increase in amorphousness of the KN sample. This shift may be ascribed to some drug-CD interaction not found in PM systems.

Disappearance of the fusion peak of the drug is often interpreted as evidence of an inclusion complex formation (36). The disappearance of the LRZ melting peak from the thermogram of SP and LP might be due to the crystalline LRZ being included within the central cavity of the HP- β -CD, suggesting the formation of a

true inclusion complex. The disappearance of this peak also confirmed that spray-drying and lyophilization were the best methods of preparing inclusion complexes.

3.3.2. FTIR spectroscopic analysis

FTIR spectroscopy has been used to assess the interaction between β -CD and guest molecules in their solid state. Chemical interaction between the drug and the carrier often leads to identifiable changes in the infrared profile of complexes. However, some of the changes are very subtle, requiring careful interpretation of the spectra (37).

The IR spectra of PM, KNB, SP, and LP were compared to the spectra of HP- β -CD and LRZ (Figure 3). The spectrum of pure LRZ had characteristic peaks at 3,100-3,250 cm^{-1} (N-H stretching), 3,076 and 3,056 cm^{-1} (aromatic C-H stretching), 1,696 cm^{-1} (carbonyl stretching), 1,615 and 1,582 cm^{-1} (aromatic ring), 1,540 cm^{-1} (asymmetric NO_2 stretching), 1,339 cm^{-1} (symmetric stretching NO_2 stretching), 750 cm^{-1} (4 adjacent free H's, aromatic C-H out of plane bending), and 844 cm^{-1} (2 adjacent free H's, aromatic C-H out-of-plane bending) (Figure 3). The FTIR spectra of HP-

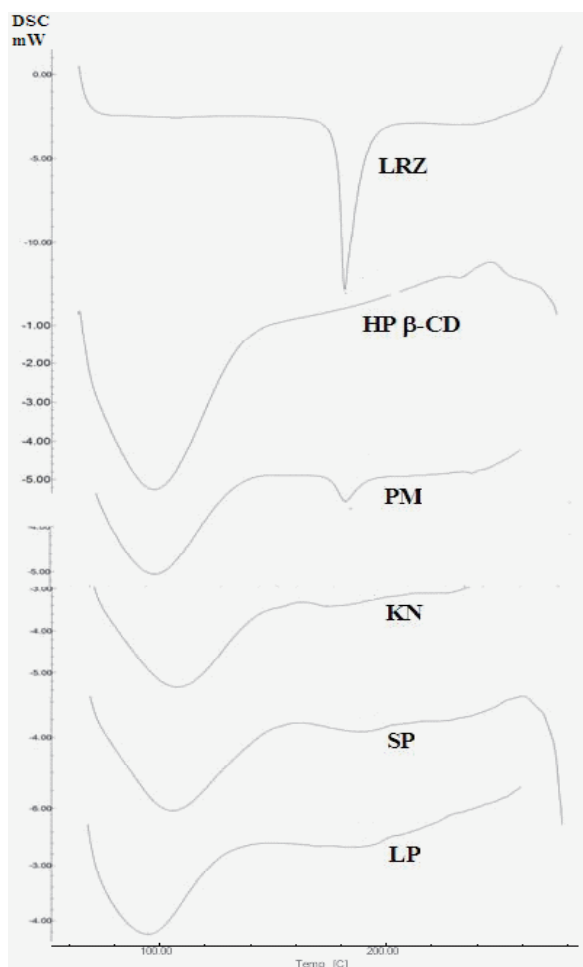


Figure 2. DSC spectra of LRZ, HP- β -CD, PM, KN, SP, and LP.

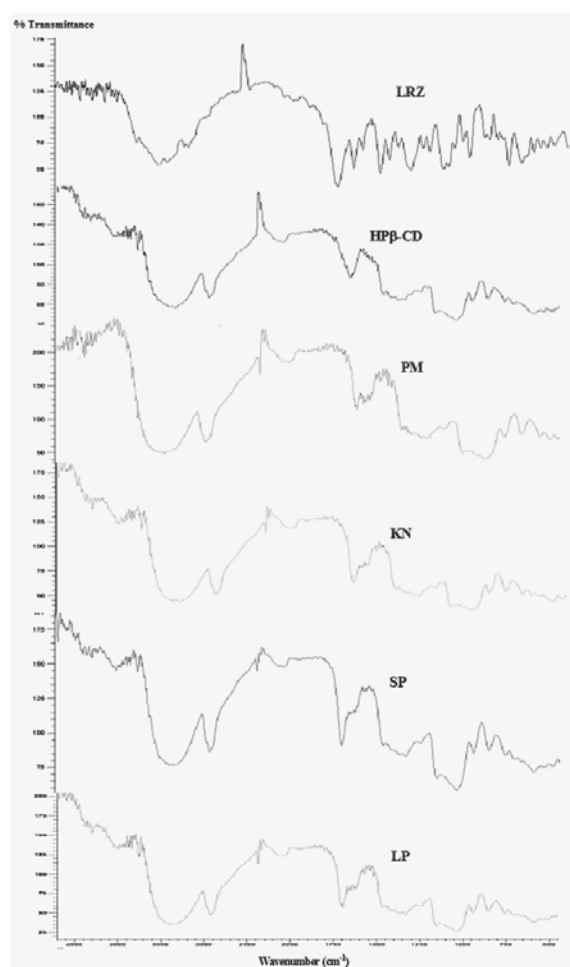


Figure 3. FTIR spectra of LRZ, HP- β -CD, PM, KN, SP, and LP.

β -CD are characterized by intense bands at 3,300-3,500 cm^{-1} due to O-H stretching vibrations (Figure 3). The vibration of the -CH and CH_2 groups appears in the 2,800-3,000 cm^{-1} region. The presence or absence of characteristic peaks associated with specific structural groups of the drug molecule was noted. Any sign of interaction would be reflected by changes in the characteristic peaks of LRZ, depending on the extent of interaction.

The FTIR spectra of PM, KN, SP, and LP showed no peaks other than those of CDs and LRZ. Characteristic peaks of LRZ at 1,696, 1,615, 1,582, 1,540, and 1,339 cm^{-1} remained present, whereas peaks due to the aromatic ring with free H's at 750 and 844 cm^{-1} were absent in the FTIR spectra of PM, KN, SP, and LP (Figure 3). These results indicated that the aromatic ring with free H's was included in the CD cavity while the remaining portion of LRZ oriented toward the upper exterior portion of the CD cavity. Moreover, the FTIR spectra of PM, KN, SP, and LP were equivalent to the addition spectrum of CDs and LRZ, which suggested the absence of well-defined chemical interaction between CDs and LRZ during preparation of complex by lyophilization, spray-drying, and kneading.

3.3.3. SEM

SEM microphotographs of LRZ and HP- β -CD and binary solid systems are shown in Figure 4. LRZ is characterized by regularly shaped crystals and HP- β -CD consists of spherical particles with an amorphous character. In PMs, the characteristic LRZ crystals, which were mixed with or adhered to the surface of excipient particles, were clearly detectable, thus confirming the presence of crystalline drug (Figure 4). With KN, LRZ crystals clustering on the surface of CD particles were apparent although they had lost their original shapes and were smaller in size (Figure 4).

In SP products, the original morphology of the raw materials disappeared, and discerning the two components (drug and CD) was not possible (Figure 4). The SP systems had amorphous and homogeneous aggregates of spherical particles (Figure 4), a particular aspect characteristic of this type of system (38). Finally, LP products appeared to have a less crystalline structure with a soft and fluffy appearance and again, crystals of the single components (drug and CD) were no longer distinguishable.

3.3.4. PXRD analysis

PXRD spectroscopy has been used to assess the degree of crystallinity of a given sample. When complexes of drug and polymer are formed, the overall number of crystalline structures decreases and the number of amorphous structures increases. Therefore, the final product samples have fewer and less intense peaks.

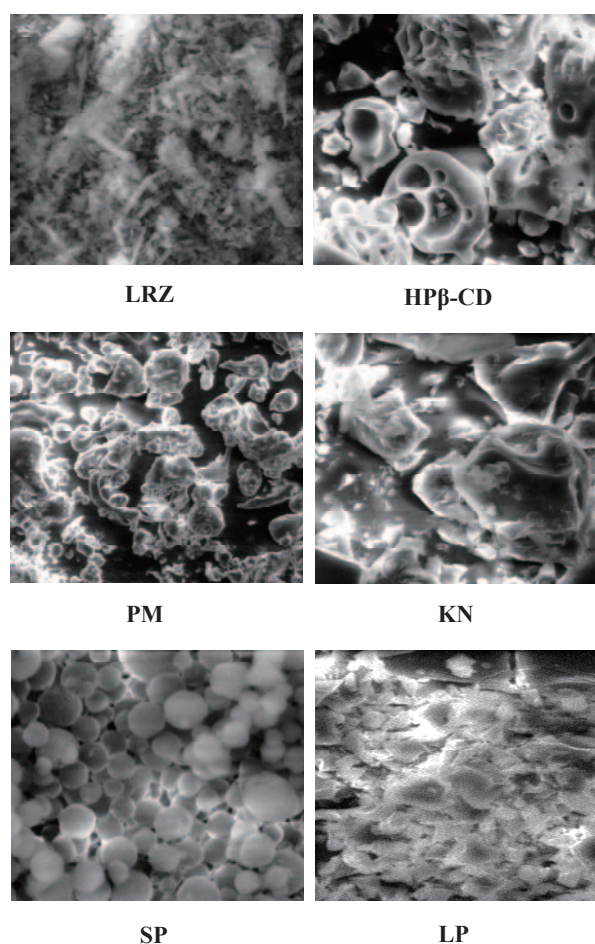


Figure 4. Typical SEM images of LRZ, HP- β -CD, PM, KN, SP, and LP.

This suggests that the crystallinity of complexes has decreased overall and, due to their more amorphous nature, the solubility of those complexes has increased (39,40).

The PXRD spectra of LRZ, HP- β -CD, PM, KN, SP, and LP are shown in Figure 5 and relative degree of crystallinity (RDC) values of these systems are presented in Table 3. In the X-ray diffractogram for LRZ powder, sharp peaks at a diffraction angle (2θ) of 6.77, 12.20, 13.25, 16.12, 17.95, 20.37, 24.52, 25.15, 27.75, 30.13, 37.01, and 38.53 were present (Figure 5), suggesting that the drug is present as a crystalline material. The amorphous structure of HP- β -CD was evident given the absence of any peak in PXRD spectra (Figure 5). The XRD spectra of complexes indicated that the degree of crystallinity decreased with the addition of a polymer, *i.e.*, HP- β -CD. RDC values decreased for all of the prepared inclusion complexes (Table 3). Only one peak related to LRZ was observed for the PM complex and no peaks were observed for KN, SP, and LP (Figure 5). The decrease in RDC values means improvement in the amorphousness of the sample. These results confirm that LRZ is no longer present as a crystalline material and its solid complexes are in an amorphous state.

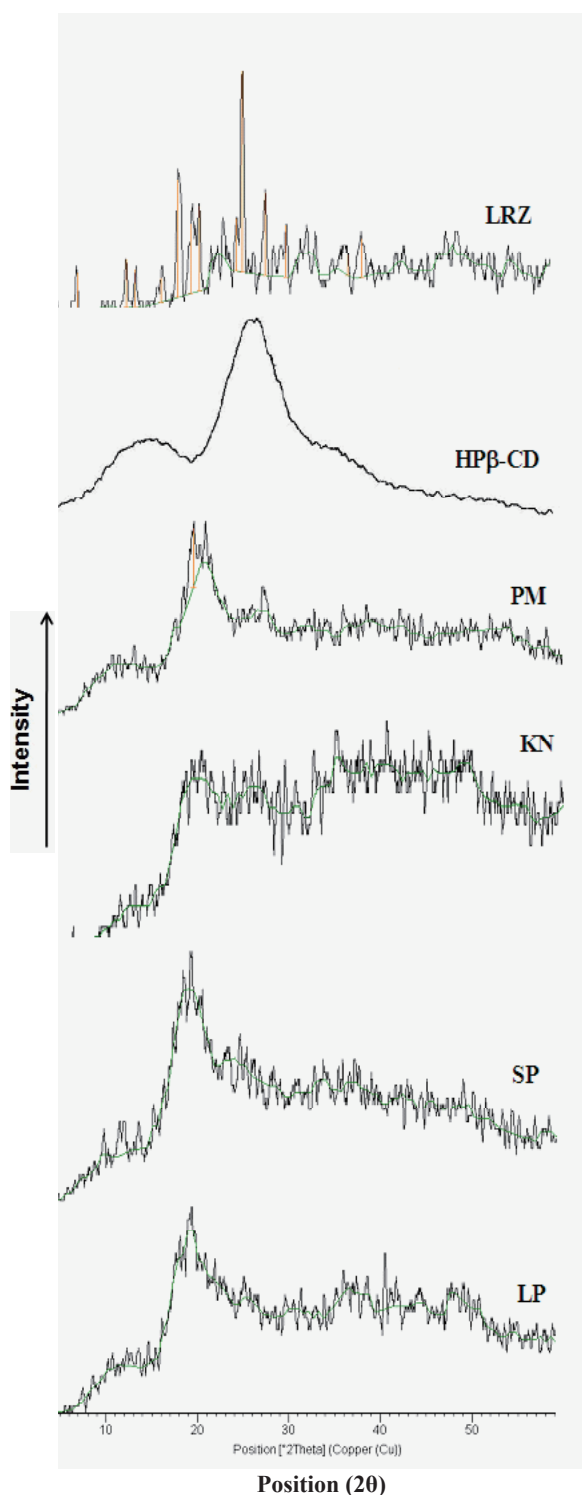


Figure 5. PXRD Spectra of LRZ, HP- β -CD, PM, KN, SP, and LP.

Table 3. RDC values at 25.15° 2 θ for LRZ, its physical mixtures, and complexes with HP- β -CD

| Samples | RDC values |
|---------|------------|
| LRZ | 153 |
| PH | 0.91 |
| KN | 0.52 |
| SP | 0.72 |
| LP | 0.65 |

3.4. Wettability and dissolution studies

The improvement in wettability of LRZ by physical mixing and complexation with HP- β -CD is shown in Figure 6. SP and LP had higher wettability in water (82.4% and 98.6%, respectively) than did plain LRZ (28.0%) at 45 min (Figure 6). Even PMs of LRZ with HP- β -CD had significantly enhanced wettability of LRZ in water compared to plain LRZ. Thus, wettability studies indicated that HP- β -CD improved the wettability of LRZ in water both in complexes as well as in PMs due to its hydrophilicity.

Dissolution of pure LRZ and all other prepared systems (complexes and PMs) was carried out in distilled water. The reported values are arithmetic means of three measurements. DP_{30 min} (percent drug dissolved within 30 min) and T_{50%} (time to dissolve 50% of drug) in water are summarized in Table 4. These data reveal that dissolution of pure LRZ occurred at a very low level in dissolution medium (11.2% within 30 min). KN, SP, and LP considerably enhanced dissolution rates within 30 min compared to pure LRZ and PMs (Table 4). The dissolution profiles of pure LRZ and its PMs and complexes with HP- β -CD in water over a period of 4 h are shown in Figure 7. As is evident, pure LRZ had a very low dissolution rate in water, with about 39.0% of the drug being dissolved in 4 h (Figure 7). KN, SP, and LP significantly enhanced the dissolution rate of LRZ (65-100% in within 4 h) (Figure 7). Possible mechanisms of improved dissolution rates of complexes include reduction of crystallite size, a solubilization effect of the carrier, absence of aggregation of drug crystallites, improved wettability, dispersibility of the drug from dispersion, dissolution of the drug in the hydrophilic carrier, conversion of the drug to an amorphous state, and finally, combinations of the above mechanisms (41).

The dissolution rate of LRZ from PM was higher (50-60% in water) than that of pure LRZ (39.0%)

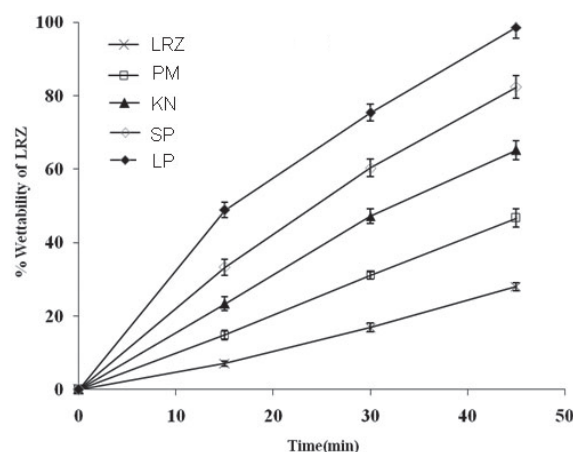


Figure 6. Wettability study of LRZ, HP- β -CD, PM, KN, SP, and LP in distilled water. Open circle, LRZ; Closed circle, HP- β -CD; Open triangle, PM; Closed triangle, KN; Open square, SP; Closed square, LP.

Table 4. Dissolution data for pure LRZ and various prepared systems in water as a dissolution medium

| Samples | % LRZ release | | | | | | | |
|---------|--------------------------|------------|------------------------|------------|------------|------------|--------------------------------|--------|
| | DP _{30 min} (%) | | T _{50%} (min) | | MDT (min) | | f ₂ value (vs. LRZ) | |
| | Complex | Tablet | Complex | Tablet | Complex | Tablet | Complex | Tablet |
| LRZ | 11.2 ± 0.6 | 5.5 ± 0.3 | > 360 | > 360 | 90.4 ± 3.3 | 99.2 ± 8.7 | – | – |
| PM | 23.5 ± 1.1 | 10.3 ± 0.5 | 192.6 ± 9.8 | > 360 | 73.0 ± 3.3 | 87.0 ± 0.2 | 44.8 | 50.2 |
| KN | 36.5 ± 1.2 | 20.8 ± 0.3 | 91.0 ± 8.7 | 73.4 ± 0.2 | 68.1 ± 3.0 | 63.8 ± 0.2 | 27.3 | 29.3 |
| SP | 68.5 ± 1.3 | 50.9 ± 0.6 | 9.0 ± 3.8 | 28.7 ± 7.4 | 31.3 ± 2.9 | 46.0 ± 5.7 | 12.6 | 17.0 |
| LP | 98.2 ± 1.6 | 65.2 ± 1.0 | 5.3 ± 1.0 | 17.2 ± 3.3 | 6.5 ± 2.0 | 33.3 ± 4.2 | 6.2 | 11.0 |

Data are shown as mean ± S.D. (*n* = 3). Abbreviations: DP_{30 min}, % drug dissolved within 30 min; T_{50%}, time to dissolve 50% of drug; MDT, mean dissolution time; f₂, similarity factor.

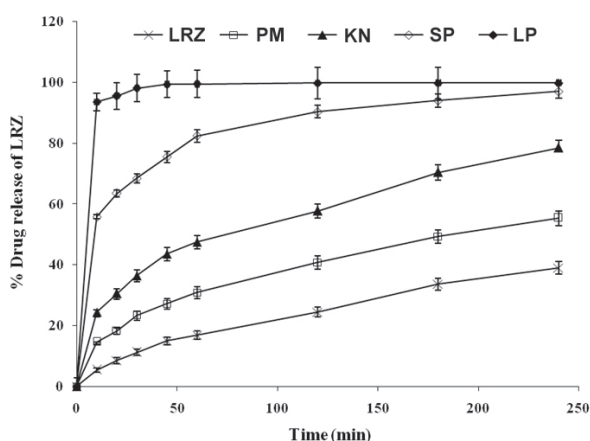


Figure 7. *In vitro* dissolution profiles of LRZ, its physical mixtures, and complexes in distilled water. Open circle, LRZ; Closed circle, HP-β-CD; Open triangle, PM; Closed triangle, KN; Open square, SP; Closed square, LP.

within 4 h (Figure 7). Physical mixing of LRZ with HP-β-CD brings the drug in close contact to the CD. The increased dissolution rate observed with PMs can be attributed to several factors such as the solubilization effect of the CD, improved wettability of the drug, and prevention of particle aggregation.

In order to understand the extent of improvement in the dissolution rate of LRZ from its complexes and PMs, the obtained dissolution data for pure LRZ and its PMs and complexes with CDs were fitted to the following equation (20):

$$MDT_{in\ vivo} = \frac{\sum_{i=1}^n t_{mid} \Delta M}{\sum_{i=1}^n \Delta M} \quad \text{----Eq. 7}$$

Here, *i* is the number of dissolution samples, *n* is number of dissolutions, *t_{mid}* is the time midway between times *t_i* and *t_{i-1}*, and Δ*M* is the amount of LRZ dissolved (μg) between times *t_i* and *t_{i-1}*. MDT reflects the time for the drug to dissolve and is the first statistical moment for the cumulative dissolution process, thus providing an accurate drug release rate (23). It is an accurate expression of the drug release rate. A higher MDT value

indicates greater drug-retarding ability (24). In order to calculate the MDT for pure LRZ and its PMs and complexes with HP-β-CD, the mean (*n* = 3) cumulative drug release (μg) was used. The obtained MDT values for pure LRZ, PM, KN, SP, and LP are presented in Table 4. The MDT for LRZ was 90.4 min in water. The MDT values for LRZ decreased to a greater extent after complexation of LRZ with CDs, *i.e.* 73.0, 68.1, 31.3, and 6.5 min for PM, KN, SP, and LP, respectively, in water (Table 4). Complexes prepared by lyophilization exhibited the best dissolution profile and the lowest MDT value.

A value of 100% for the similarity factor (*f*₂) suggests that the test and reference profiles are identical. Values between 50 and 100 indicate that the dissolution profiles are similar whilst smaller values imply an increase in dissimilarity between release profiles (20). The release profile of LP differed substantially from that for pure LRZ (*f*₂ values 6.23) (Table 4). Release profiles of pure LRZ from PM, KN, SP, and LP also differed significantly from that of pure LRZ in the dissolution medium.

3.5. Formulation studies

Physical properties of the complexes prepared by kneading, spray-drying, and lyophilization (KN, SP, and LP, respectively) were studied to judge their suitability for tableting. In general, compressibility index values up to 15% and an angle of repose between 25° and 30° results in good to excellent flow properties (39). Compressibility, the angle of repose for complexes, and the physical properties of tablets made using these complexes are shown in Table 5. These values indicated good compressibility and flow properties, meaning that these samples are suitable for tableting.

During *in vitro* dissolution studies, tablets prepared by compressing complexes of SP and LP exhibited more than 50% drug release within 15 to 30 min in water, whereas tablets prepared by compressing KN and PM provided the same drug release within 80 to over 360 min (Table 4, Figure 8). The tablets prepared using complexes has faster and reproducible release as compared to the tablets containing pure LRZ (Table 4, Figure 8). Tablets

Table 5 Physical properties of complexes and tablets

| Physical properties | LRZ | KN | SP | LP |
|--------------------------------|------|------|------|------|
| Complex | | | | |
| % Compressibility | 13.7 | 13.5 | 12.4 | 13.3 |
| Angle of repose (°) | 27.6 | 26.1 | 25.3 | 24.3 |
| Tablet | | | | |
| Hardness (kg/cm ²) | 4.3 | 4.7 | 4.6 | 4.8 |
| Friability (%) | 0.50 | 0.60 | 0.90 | 0.70 |
| Diameter (mm) | 7.0 | 6.9 | 6.9 | 7.1 |
| Thickness (mm) | 4.0 | 4.1 | 4.1 | 4.0 |

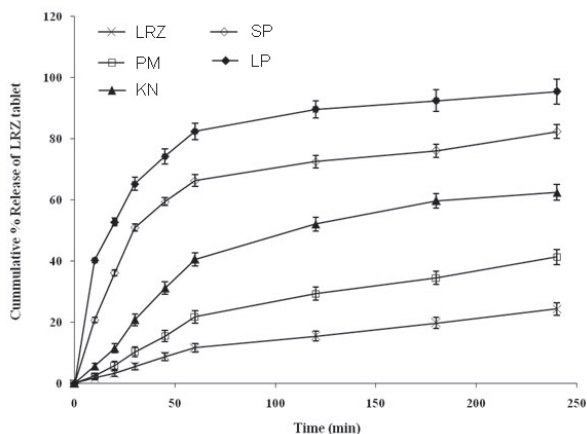


Figure 8. Release profiles of LRZ from conventional tablets containing only LRZ and tablets containing PM, KN, SP, and LP in distilled water. Open circle, LRZ; Closed circle, HP- β -CD; Open triangle, PM; Closed triangle, KN; Open square, SP; Closed square, LP.

prepared using SP and LP had 82.3% and 95.5% release in 4 h, respectively (Figure 8), with a respective $T_{50\%}$ of 28.7 and 17.2 min in water (Table 4). Tablets prepared using KN also showed improvement in the dissolution profiles of LRZ (Table 4, Figure 8). This confirmed the advantage of improving the aqueous solubility of LRZ in complex form since this form can be formulated into tablets with better dissolution characteristics. Release profiles of LRZ from conventional tablets containing LRZ alone differed significantly from those of tablets containing KN, SP, and LP as the f_2 values are 29.3, 17.0, and 11.0, respectively (Table 4). MDT values of LRZ from tablets containing SP and LP (46.0 and 33.3 min, respectively) were significantly lower than those of conventional tablets containing only LRZ (99.2 min) (Table 4).

4. Conclusion

Solubility studies revealed a significant increase in the aqueous solubility of LRZ with an increase in the concentration of HP- β -CD. The maximum concentration of HP- β -CD studied (200 mM at 37°C and 25°C) resulted in 420-fold and 322-fold improvement in the saturation solubility of LRZ. An inclusion complex of LRZ with HP- β -CD at a molar

ratio of 2:1 was successfully prepared by kneading, spray-drying, and lyophilization. This was confirmed by DSC, FTIR, SEM, and XRD studies. The greatest improvement in solubility and *in vitro* drug release was observed with an inclusion complex prepared with HP- β -CD by lyophilization. The solubility and *in vitro* drug release of a physical mixture improved to a lesser degree than did that of complexes prepared by kneading, spray-drying, and lyophilization. These findings are extremely important from a commercial point of view as the prepared complex remedies the drawback of LRZ's poor dissolution profile.

Acknowledgements

The authors wish to thank Roquette Frères, France for donating HP- β -CD and Astron Research Center, Mumbai, India, for donating LRZ. The authors also wish to thank Maan Pharmaceuticals Ltd. for providing formulation excipients. The authors are also grateful to SICART, India for conducting SEM and PXRD studies of the samples.

References

- Skerritt JH, Johnston GA. Enhancement of GABA binding by benzodiazepines and related anxiolytics. *Eur J Pharmacol.* 1983; 89:193-198.
- Rutgers JG, Shearer CM. Lorazepam. In: *Analytical Profiles of Drug Substances, Vol. 9* (Florry K, ed.). Academic Press, New York, NY, 1980; pp. 397-423.
- Rey E, Tréluyer JM, Pons G. Pharmacokinetic optimisation of benzodiazepine therapy for acute seizures. *Focus on delivery routes.* *Clin Pharmacokinet.* 1999; 36:409-424.
- Proudfoot S. Factors affecting bioavailability: Factors influencing drug absorption from the gastrointestinal tract. In: *Pharmaceutics: The Science of Dosage from Design* (Aulton ME, ed.). Churchill Livingstone, Edinburgh, UK, 1991; pp. 135-173.
- Mosher G, Thompson OD. Complexation: Cyclodextrins. In: *Encyclopedia of Pharmaceutical Technology, 3rd ed., Vol. 2*, (Swarbrick J, ed.). Informa Healthcare, London, UK, 2007; pp. 671-1434.
- Kamada M, Hirayama F, Udo K, Yano H, Arima H, Uekama K. Cyclodextrin conjugate-based controlled release system: Repeated- and prolonged-releases of ketoprofen after oral administration in rats. *J Control Release.* 2002; 82:407-416.
- Figueiras A, Carvalho RA, Ribeiro L, Torres-Labandeira JJ, Veiga FJ. Solid-state characterization and dissolution profiles of the inclusion complexes of omeprazole with native and chemically modified beta-cyclodextrin. *Eur J Pharm Biopharm.* 2007; 67:531-539.
- Wang S, Ding Y, Yao Y. Inclusion complexes of fluorofenidone with β -cyclodextrin and hydroxypropyl- β -cyclodextrin. *Drug Dev Ind Pharm.* 2009; 35:808-813.
- Pokharkar V, Khanna A, Venkatpurwar V, Dhar S, Mandpe L. Ternary complexation of carvedilol, β -cyclodextrin and citric acid for mouth-dissolving tablet formulation. *Acta Pharm.* 2009; 59:121-132.

10. Uekama K, Otagiri M. Cyclodextrins in drug carrier systems. *Crit Rev Ther Drug Carrier Syst.* 1987; 3:1-40.
11. Anselmi C, Centini M, Maggiore M, Gaggelli N, Andreassi M, Buonocore A, Beretta G, Facino RM. Non-covalent inclusion of ferulic acid with α -cyclodextrin improves photo-stability and delivery: NMR and modeling studies. *J Pharm Biomed Anal.* 2008; 46:645-652.
12. Szente L, Szejtli J. Highly soluble cyclodextrin derivatives: Chemistry, properties, and trends in development. *Adv Drug Deliv Rev.* 1999; 36:17-28.
13. Castillo JA, Palomo-Canales J, Garcia JJ, Lastres JL, Bolas F, Torrado JJ. Preparation and characterization of albendazole α -cyclodextrin complexes. *Drug Dev Ind Pharm.* 1999; 25:1241-1248.
14. Wong JW, Yuen KH. Inclusion complexation of artemisinin with α -, β -, and γ -cyclodextrins. *Drug Dev Ind Pharm.* 2003; 29:1035-1044.
15. Cappello B, di Maio C, Iervolino M, Miro A, Calignano A. Etodolac/cyclodextrin formulation: Physicochemical characterization and *in vivo* pharmacological studies. *Drug Dev Ind Pharm.* 2009; 35:877-886.
16. Gawali VU, Patil PB, Chede SM, Jagdale SC, Kuchekar BS, Chabukswar AR. Studies on cilostazol and β -cyclodextrin inclusion complexes. *International Journal of PharmTech Research.* 2009; 1:1073-1078.
17. Nalluri BN, Chowdary KP, Murthy KV, Hayman AR, Becket G. Physicochemical characterization and dissolution properties of nimesulide-cyclodextrin binary systems. *AAPS PharmSciTech.* 2003; 4:E2.
18. Zhang X, Wu D, Lai J, Lu Y, Yin Z, Wu W. Piroxicam/2-hydroxypropyl- β -cyclodextrin inclusion complex prepared by a new fluid-bed coating technique. *J Pharm Sci.* 2009; 98:665-675.
19. Mandal U, Ray KK, Gowda V, Ghosh A, Pal TK. *In vitro* and *in vivo* correlation for two gliclazide extended-release tablets. *J Pharm Pharmacol.* 2007; 59:971-976.
20. Moore JW, Flanner H. Mathematical comparison of dissolution profiles. *Pharm Tech.* 1996; 20:64-74.
21. US Food and Drug Administration. Guidance for Industry SUPAC-MR: Modified Release Solid Oral Dosage Forms Scale-Up and Postapproval Changes: Chemistry, Manufacturing, and Controls; *In Vitro* Dissolution Testing and *In Vivo* Bioequivalence Documentation. Rockville, MD, USA, 1997.
22. Human Medicines Evaluation Unit, EMEA. Notes for Guidance on Quality of Modified-Release Products; A Oral Dosage Forms; B Transdermal Dosage Forms, Section 1 (Quality) 1999.
23. Reppas C, Nicolaidis E. Analysis of drug dissolution data, In: Oral Drug Absorption Prediction and Assessment (Dressman JB, Lennernäs H, eds.). Marcel Dekker, New York, NY, USA, 2000; pp. 229-254.
24. Vueba ML, Batista de Carvalho LA, Veiga F, Sousa JJ, Pina ME. Influence of cellulose ether polymers on ketoprofen release from hydrophilic matrix tablets. *Eur J Pharm Biopharm.* 2004; 58:51-59.
25. Higuchi T, Connors KA. Phase solubility techniques. *Adv Anal Chem Instr.* 1965; 4:117-212.
26. Szejtli J. Cyclodextrin inclusion complexes. In: *Cyclodextrin Technology.* Kluwer Academic Publishers, Dordrecht, the Netherlands, 1988; pp. 101-102.
27. Choudhury S, Nelson KF. Improvement of oral bioavailability of carbamazepine by inclusion in 2-hydroxypropyl- β -cyclodextrin. *Int J Pharm.* 1992; 85:175-180.
28. Ventura CA, Giannone I, Musumeci T, Pignatello R, Ragni L, Landolfi C, Milanese C, Paolino D, Puglisi G. Physico-chemical characterization of disoxaril-dimethyl- β -cyclodextrin inclusion complex and *in vitro* permeation studies. *Eur J Med Chem.* 2006; 41:233-240.
29. Wang Z, Deng Y, Sun S, Zhang X. Preparation of hydrophobic drugs cyclodextrin complex by lyophilization monophasic solution. *Drug Dev Ind Pharm.* 2006; 32:73-83.
30. Liu C, Liu C, Desai KG. Enhancement of dissolution rate of valdecoxib using solid dispersions with polyethylene glycol 4000. *Drug Dev Ind Pharm.* 2005; 31:1-10.
31. Bloch DW, Elegakey MA, Speiser PP. Solid dispersion of chlorthalidone in urea phase diagram and dissolution characteristics. *Pharm Acta Helv.* 1982; 57:231-235.
32. Shimpi S, Chauhan B, Shimpi P. Cyclodextrins: Application in different routes of drug administration. *Acta Pharm* 2005; 55:139-156.
33. Moyano JR, Arias-Blanco MJ, Ginés JM, Giordano F. Study of the complexation behaviour of gliclazide with partially methylated β -cyclodextrin in solution and solid state. *Int J Pharm.* 1997; 157:239-243.
34. Loftsson T, Brewster EM. Pharmaceutical application of cyclodextrins. 1. drug solubilization and stabilization. *J Pharm Sci.* 1996; 85:1017-1025.
35. Sreenivasan K. Use of differential scanning calorimetry to study the replacement of a guest molecule from cyclodextrin-guest inclusion complexes. *Anal Lett.* 2001; 34:307-311.
36. Cunha-Filho MS, Dacunha-Marinho B, Torres-Labandeira JJ, Martínez-Pacheco R, Landín M. Characterization of β -lapachone and methylated β -cyclodextrin solid-state systems. *AAPS PharmSciTech.* 2007; 8:E60.
37. Lamcharfi E, Kunesch G, Meyer C, Robert B. Investigation of cyclodextrin inclusion compounds using FT-IR and Raman spectroscopy. *Spectrochimica Acta A Mol Biomol Spectrosc.* 1995; 51:1861-1870.
38. Sinha VR, Anitha R, Ghosh S, Nanda A, Kumria R. Complexation of celecoxib with β -cyclodextrin: Characterization of the interaction in solution and in solid state. *J Pharm Sci.* 2005; 94:676-687.
39. Reddy MN, Rehana T, Ramakrishna S, Chowdary KP, Diwan PV. β -cyclodextrin complexes of celecoxib: Molecular-modeling, characterization, and dissolution studies. *AAPS PharmSci.* 2004; 6:68-76.
40. Zhang X, Zhang Y, Zhong D, Chen Y, Li S. Investigation and physicochemical characterization of clarithromycin-citric acid-cyclodextrins ternary complexes. *Drug Dev Ind Pharm.* 2007; 33:163-171.
41. Tang L, Khan SU, Muhmmad NA. Evaluation and selection of bio-relevant dissolution media for a poorly water soluble new chemical entity. *Pharm Dev Technol.* 2001; 6:531-540.

(Received May 26, 2010; Revised September 8, 2010; Accepted September 20, 2010)

Original Article

Formulation, development, and optimization of immediate release nateglinide tablets by factorial design

Nihar R. Pani^{1,*}, Lila K. Nath², Biswanath Bhunia³

¹ Department of Pharmaceutics, Gayatri College of Pharmacy, Sambalpur, Orissa, India;

² Department of Pharmaceutical Sciences, Dibrugarh University, Dibrugarh, Assam, India;

³ Department of Biotechnology, National Institute of Technology, Durgapur, West Bengal, India.

ABSTRACT: In the present study, selection of superdisintegrants among sodium starch glycolate, cross povidone, Starch-1500 and cross carmellose sodium (CCS) was carried out for development of immediate release nateglinide tablets (NTG). A 3² full factorial design was used to investigate the influence of two independent variables, *i.e.*, amount of selected superdisintegrants and hardness of the tablets, on two dependent variables, *i.e.*, disintegration time and percentage of drug release at 30 min (DR_{0.5h}). The results revealed that CCS was the best superdisintegrant for the development of immediate release tablets of NTG. The sign of the coefficient of the polynomial equation signified that the disintegration time was decreased and DR_{0.5h} was increased by decreasing the hardness of the tablets as well as by increasing the concentration of CCS in the tablets. A checkpoint batch of the tablets was prepared by changing the value of independent variables within the range used in the preparation of factorial batches of tablets to check the validity of the evolved optimized mathematical model. Stability studies of optimized formulations indicated that there was no significant change in the physical parameters, disintegration time, and percentage of drug release of tablets. The systematic formulation approach helped to understand the effect of formulation processing variables.

Keywords: Nateglinide, immediate release tablets, factorial design, superdisintegrants

1. Introduction

Despite increasing interest in controlled release drug delivery systems, more attention has been paid to

formulate poorly soluble drugs as conventional tablets intended to be swallowed to disintegrate and release their medicaments rapidly in the gastro intestinal tract (GIT) for bioavailability. Bioavailability of a poorly soluble drug from a solid oral dosage form depends on the release of the drug substance from the dosage form, *i.e.*, disintegration of the solid oral dosage form which will increase the wettability of the drug by increasing the surface area of the drug particles (1-3). This highlights the importance of proper choice of disintegrant/superdisintegrants, *e.g.* cross carmellose sodium (CCS), sodium starch glycolate, cross povidone, Starch-1500, *etc.* and its consistency of performance which is of critical importance to increase the rate of dissolution and hence its bioavailability (4,5). There are various factors like hardness, concentration of binders, disintegrants, *etc.* which affect the disintegration time and rate of dissolution of the drug. Nateglinide (NTG) is a meglitinide derivative which is mainly used for the treatment of type-2 diabetes mellitus (6,7). The poor aqueous solubility of NTG gives rise to difficulties in the formulation of tablets with a desired dissolution rate. The present study aims to optimize the concentration of superdisintegrants and hardness of immediate release NTG tablets.

2. Materials and Methods

2.1. Materials

NTG was obtained as a gift sample from Glenmark Pharmaceuticals, Nashik, India. Lactose, CCS, sodium starch glycolate, cross povidone, Sarch-1500, polyvinylpyrrolidone, Aerosil[®], talc, and ethanol were procured from SD Fine Chemicals, Mumbai, India. All other chemicals used were of analytical grade.

2.2. Differential scanning calorimetry (DSC)

A differential scanning calorimeter (JADE DSC; PerkinElmer, Waltham, MA, USA) was used for thermal analysis of drug and drug-excipients mixtures (8). Excipients that were used in the development of

*Address correspondence to:

Dr. Nihar Ranjan Pani, Department of Pharmaceutics, Gayatri College of Pharmacy, Sambalpur, Orissa, India. e-mail: niharpani@gmail.com

formulation and their maximum ratio with drug used in a tablet were selected for the present study (Table 1). Individual samples (drug and excipients) as well as physical mixtures of drug and selected excipients (all passed through an 80-mesh sieve) were weighed directly in the DSC aluminum pan and scanned in the temperature range of 50-300°C under a nitrogen atmosphere. A heating rate of 20°C/min was used and thermograms obtained were observed for any interactions.

2.3. Isothermal stress testing

For isothermal stress testing (8,9), drug and different excipients were weighed directly in 4 mL-glass vials ($n = 2$) and mixed on a vortex mixer for 2 min. In each of the vials, 10% (w/w) water was added and the drug-excipients blend was further mixed using a glass capillary (both the ends of which were heat sealed). To prevent any loss of material, the capillary was broken and left inside the vial. Each vial was sealed using a teflon-lined screw cap and stored at 50°C in a hot air oven (Narang Scientific Industries, Haryana, India). These samples were periodically examined for any unusual color change. After 3 weeks storage under the above conditions, samples were quantitatively analyzed using a UV-visible spectrophotometer. Drug-excipients blends without added water, stored in a refrigerator, served as controls.

2.4. Preparation of immediate release tablets

NTG, half quantity of CCS, and lactose were passed through a No. 80 sieve and were mixed in a poly bag for 20 min. An alcoholic solution of povidone (10%, w/v) was added to the mixture in a quantity just sufficient to bind the mass. The wet mass was screened with a No. 20 sieve and dried in a tray dryer at 45°C. The dried granules were mixed with the remaining half of CCS and lubricated with 2% (w/w) talc and 2% (w/w) Aerosil. The granules ready for compression were converted into an 8 mm diameter size tablet using a single-punch tablet punching machine (Hardik, Ahmedabad, India). The composition of the preliminary and factorial design batches is shown in Tables 2 and 3, respectively.

2.5. Evaluation of granules and tablets

The prepared granules were evaluated for angle of repose, bulk density, tapped density, compressibility index, and Hausner ratio (10). The prepared tablets were evaluated for weight variation, friability, hardness, thickness, and disintegration time (11).

The *in vitro* drug release study was carried out in a United States Pharmacopoeia (USP) dissolution apparatus II (TDT-08L; Electrolab, Mumbai, India) using a rotating paddle at 50 rpm in 1,000 mL of 0.1 N HCl + 0.5% sodium lauryl sulphate as dissolution medium while maintaining the temperature at $37 \pm 0.5^\circ\text{C}$ (12). An

Table 1. Results of analysis of isothermal stress testing samples after 3 weeks of storage at stressed conditions

| Samples | Ratios (drug-excipient) | % Drug remaining ^a | |
|----------------|-------------------------|-------------------------------|-------------------------------|
| | | Control samples ^b | Stressed samples ^c |
| NTG | – | 100.8 ± 0.7 | 99.7 ± 2.5 |
| NTG + lactose | 1:2 | 101.4 ± 1.3 | 100.3 ± 1.7 |
| NTG + CCS | 1:1 | 100.7 ± 1.8 | 99.8 ± 1.8 |
| NTG + povidone | 2:1 | 101.8 ± 1.5 | 99.3 ± 1.9 |
| NTG + talc | 3:1 | 100.6 ± 2.7 | 99.3 ± 2.0 |
| NTG + Aerosil | 3:1 | 100.5 ± 1.8 | 99.6 ± 1.2 |

^a Values expressed as average ± standard deviation; ^b Drug excipient blends without added water and stored in refrigerator; ^c Drug excipient blends with 10% (w/w) added water and stored at 50°C for 3 weeks.

Table 2. Results of preliminary batches of immediate release NTG tablets

| Items | Formulation ^a | | | | |
|--|--------------------------|---------|---------|------|-------|
| | T-1 | T-2 | T-3 | T-4 | T-5 |
| Composition | | | | | |
| NTG (% w/w) | 40 | 40 | 40 | 40 | 40 |
| Sodium starch glycolate (% w/w) ^b | – | 6 | – | – | – |
| Starch-1500 (% w/w) ^b | – | – | 6 | – | – |
| Cross povidone (% w/w) ^b | – | – | – | 6 | – |
| CCS (% w/w) ^b | – | – | – | – | 6 |
| Lactose | q.s. ^c | q.s. | q.s. | q.s. | q.s. |
| Disintegration time (sec) | > 3,600 | > 3,600 | > 3,600 | 136 | 20 |
| DR _{0.5h} (% w/w) | 3.2 | 37.7 | 7.2 | 62.6 | 100.6 |

^a All batches contained 10% (w/w) polyvinylpyrrolidone in ethyl alcohol as a binder, 2% (w/w) talc, and 2% (w/w) Aerosil. Hardness of all batches was 5 kg/cm². ^b Intragranular 50% (w/w), extragranular 50% (w/w). ^c quantity sufficient for 100% (w/w). Abbreviations: NTG, nateglinide; CCS, Cross carmellose sodium; DR_{0.5h}, Drug release at 0.5 h.

Table 3. 3² Full factorial design layout

| Batch code ^a | Variable levels in coded form ^b | | Dissolution at 0.5 h ^c (% w/w) | Disintegration time ^c (sec) |
|-------------------------|--|--------------------------------------|---|--|
| | X ₁ (%) | X ₂ (kg/cm ²) | | |
| F-1 | -1 | -1 | 67.8 ± 0.4 | 158.7 ± 3.1 |
| F-2 | -1 | 0 | 61.7 ± 1.0 | 179.3 ± 2.5 |
| F-3 | -1 | +1 | 54.9 ± 0.8 | 193.3 ± 4.5 |
| F-4 | 0 | 0 | 100.3 ± 0.8 | 33.0 ± 2.7 |
| F-5 | 0 | -1 | 94.3 ± 0.6 | 53.7 ± 3.1 |
| F-6 | 0 | +1 | 91.4 ± 1.2 | 39.7 ± 1.5 |
| F-7 | +1 | -1 | 100.0 ± 0.4 | 17.3 ± 1.5 |
| F-8 | +1 | 0 | 100.5 ± 0.7 | 19.7 ± 1.5 |
| F-9 | +1 | +1 | 100.1 ± 0.3 | 30.0 ± 1.0 |
| Check point | -0.5 | +0.5 | 77.8 ± 0.7 | 100.4 ± 3.3 |

^a All batches contained 10% (w/w) polyvinylpyrrolidone in ethyl alcohol as a binder, 2% (w/w) talc, and 2% (w/w) Aerosil. ^b X₁, amount of cross carmellose sodium (% w/w); X₂, hardness of the tablets (kg/cm²). ^c Data are shown as mean ± S.D.

Table 4. Actual value of codes mentioned in Table 3

| Codes values | Actual value | |
|--------------|-----------------------------|-----------------------------|
| | X ₁ [*] | X ₂ [*] |
| -1 | 2 | 3 |
| 0 | 4 | 5 |
| +1 | 6 | 7 |
| -0.5 | 3 | 4 |
| +0.5 | 5 | 6 |

* X₁, amount of cross carmellose sodium (% w/w); X₂, hardness of the tablets (kg/cm²).

aliquot of 5 mL was withdrawn at different time intervals (5, 10, 20, 30, and 45 min) and an equal volume of fresh dissolution medium was added to maintain the sink condition. Samples were suitably diluted and analyzed in a UV-visible spectrophotometer at 210 nm to determine the amount of drug released (13). The fresh dissolution medium replacement was considered in the calculation of the amount of drug released.

2.6. Full factorial design

A 3² randomized full factorial design was used to optimize the variables in the present study. In this design 2 factors were evaluated, each at 3 levels, and experimental trials were performed at all 9 possible combinations (14-16). The percentage (2, 4, and 6%) of CCS (X₁), and hardness (3, 5, and 7 kg/cm²) of tablets (X₂), were selected as independent variables. The disintegration time and percentage of drug released at 0.5 h (DR_{0.5h}) were selected as dependent variables.

2.7. Stability study

The factorial batches were subjected to accelerated stability (40 ± 2°C/75 ± 5% relative humidity) testing. After a specified period of time (1, 2, and 3 months), samples were withdrawn and subjected to assay, disintegration time and *in vitro* dissolution studies. The stability study was conducted as per the International Conference on Harmonization (ICH) guidelines (17).

3. Results and Discussion

A drug-excipient interaction study at an early stage of product development is an important exercise in the development of a stable dosage form. As shown in Figure 1, a sharp endothermic peak was observed at 143°C in the DSC thermogram of NTG. However, the endothermic peak of NTG was well preserved at 143 ± 2°C in the DSC thermogram of NTG-excipients mixtures (Figure 1). This result inferred that there was no interaction between drug and excipients (8).

In isothermal stress testing, it was observed that there was no physical change (color and appearance) as well as drug content after storage of drug-excipient blends under stressed conditions (Table 1), which supported previously reported results of a DSC study on drug-excipient compatibility testing (9).

The flow properties of granules can be judged from the angle of repose, compressibility index and Hausner ratio (10,11). An angle of repose (θ) < 30° indicates free flowing material and > 40° poor flow properties (10). A compressibility index < 10% indicates excellent flow properties and > 38% poor flow properties (11). A Hausner ratio of 1.00-1.11 indicates free flowing and > 1.60 poor flow properties (11). Values for angle of repose (θ), compressibility index (%), and Hausner ratio for all prepared granules were found to be in the range of 22.5 to 25.7°, 7.14 to 7.71%, and 1.07 to 1.08, respectively (Table 5), which showed that the granules were free flowing and can be used for tablet compression. A percentage of weight variation was observed within the limit of ± 7.5% (w/w) for all the prepared tablets (Table 5), which is acceptable for uncoated tablets as per United State Pharmacopoeia, National Formulary (USP-NFXXVI) (18). A friability test of the prepared tablets except batches of formulation-1 to formulation-3 (F-1 to F-3) passed (weight loss < 1%, w/w) (Table 5), which assumed that tablets of formulation-4 to formulation-9 (F-4 to F-9) prepared at higher hardnesses have sufficient mechanical integrity and strength.

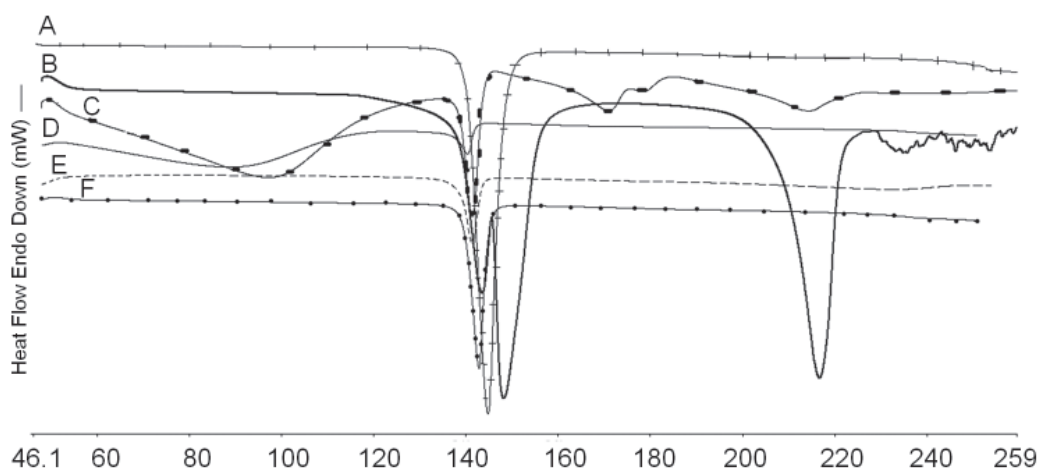


Figure 1. Comparison of DSC thermogram of NTG with drug-exipients mixture. A, NTG; B, Lactose + NTG; C, Cross carmelose sodium + NTG; D, Povidone + NTG; E, Talc + NTG; F, Aerosil + NTG.

Table 5. Evaluation of granules and tablets

| Items | F-1 | F-2 | F-3 | F-4 | F-5 | F-6 | F-7 | F-8 | F-9 |
|--------------------------------|------|------|------|------|------|------|------|------|------|
| Evaluation of granules | | | | | | | | | |
| Angle of repose (θ) | 22.9 | 24.8 | 23.3 | 22.5 | 24.2 | 25.7 | 23.8 | 25.3 | 24.2 |
| Compressibility index (%) | 7.63 | 7.14 | 7.37 | 7.63 | 7.36 | 7.48 | 7.52 | 7.26 | 7.36 |
| Hausner ratio | 1.07 | 1.07 | 1.08 | 1.07 | 1.08 | 1.07 | 1.07 | 1.08 | 1.08 |
| Evaluation of tablets | | | | | | | | | |
| Weight variation (% w/w) | 3.2 | 4.8 | 3.1 | 2.8 | 5.2 | 4.6 | 3.7 | 3.7 | 4.2 |
| Friability weight loss (% w/w) | 2.7 | 1.4 | 1.9 | 0.4 | 0.2 | 0.4 | 0.6 | 0.2 | 0.3 |

Lactose was selected as a soluble diluent for the water insoluble drug NTG by considering its advantages in terms of easy availability, cost-effectiveness, and relative moisture insensitivity. Povidone was used as a binder considering its widespread applicability in industry. The preliminary trial batches were conducted arbitrarily without addition of superdisintegrants (T-1) and in addition with 6% (w/w) of sodium starch glycolate (T-2), Starch-1500 (T-3), cross povidone (T-4), and CCS (T-5) at 5 kg/cm² hardness for the selection of superdisintegrants. As shown in Table 2, while the disintegration time of T-1, T-2 and T-3 were more than 3,600 sec and the disintegration time of T-4 was 136 sec, the batch containing CCS (T-5) showed a lower disintegration time and more DR_{0.5h} than other superdisintegrant containing batches. Hence CCS was considered for further investigation. Hardness of the tablets has an impact on the disintegration time as well as the amount of drug released from tablets (3), therefore it needs to be optimized. In order to investigate the influence of concentration of CCS and hardness of the tablet systematically, a 3² factorial design was employed in this investigation.

The amount of CCS (X_1) in tablets and the hardness of the tablets (X_2) were chosen as independent variables in a 3² full factorial design. A statistical model incorporating interactive and polynomial terms was used to evaluate the responses.

$$Y = b_0 + b_1X_1 + b_2X_2 + b_{12}X_1X_2 + b_{11}X_1^2 + b_{22}X_2^2 \text{ --- Eq. 1}$$

where, Y is the dependent variable, b_0 is the arithmetic mean response of the 9 runs, and b_i is the estimated coefficient for the factor X_i . The main effects (X_1 and X_2) represent the average result of changing one factor at a time from its low to high value. The interaction terms (X_1X_2) showed how the response changes when two factors are simultaneously changed. The polynomial terms (X_1^2 and X_2^2) are included to investigate nonlinearity. As shown in Table 3, the disintegration time and DR_{0.5h} for the 9 batches (F1 to F9) showed a wide variation (*i.e.*, 17.3 to 193.3 sec and 54.9 to 100.5% (w/w), respectively). The data indicates that the dependent variables such as disintegration time and DR_{0.5h} are dependent on the selected independent variables such as concentration of CCS and hardness of the tablets. The fitted equations (full and reduced) relating the disintegration time responses and DR_{0.5h} to the transformed factor are shown in Table 3. The polynomial equations can be used to draw conclusions after considering the magnitude of the coefficient and the mathematical sign it carries (*i.e.*, positive or negative). Table 6 shows the results of the analysis of variance (ANOVA), which was performed to identify insignificant factors (15). High values of the correlation coefficient for disintegration time and DR_{0.5h} indicate a good fit (Table 6). The equations may be used to obtain estimates of the response because a small error of variance was noted in the replicates.

The significance test for regression coefficients was performed by applying the Students' t test. A coefficient

Table 6. Calculations for testing the model in portions

| Items | DF | SS | MS | F | R^2 |
|-------------------------------|----|---------------------|--------------------|--------------------|--------|
| For % of dissolution at 0.5 h | | | | | |
| Regression | | | | | |
| FM | 5 | 8.38×10^3 | 1.68×10^3 | 1.66×10^3 | 0.9969 |
| RM | 4 | 8.38×10^3 | 2.09×10^3 | 2.14×10^3 | 0.9970 |
| Error | | | | | |
| FM | 3 | 11.5 | 3.82 | | |
| RM | 4 | 11.8 | 2.96 | | |
| For disintegration time | | | | | |
| Regression | | | | | |
| FM | 5 | 1.304×10^5 | 2.61×10^4 | 2.76×10^3 | 0.9981 |
| RM | 4 | 1.304×10^5 | 3.26×10^4 | 3.40×10^3 | 0.9980 |
| Error | | | | | |
| FM | 3 | 77.6 | 25.9 | | |
| RM | 4 | 90.1 | 22.5 | | |

Abbreviations: DF, degrees of freedom; SS, sum of squares; MS, mean of squares; F, Fischer's ratio; R^2 , regression coefficient; FM, full model; RM, reduced model. Details of calculations are shown in Mendenhall W and Sincich T (19).

Table 7. Summary of Regression Analysis Results

| Items | b_0 | b_1 | b_2 | b_{11} | b_{22} | b_{12} |
|-------------------------------------|-------|--------|-------|----------|----------|----------|
| For % of dissolution at 0.5 h | | | | | | |
| Respon (% of dissolution at 0.5 h) | | | | | | |
| FM | 95.19 | 19.36 | -3.62 | -14.52 | 0.25 | 3.28 |
| RM | 95.36 | 19.36 | -3.62 | -14.52 | | 3.8 |
| For disintegration time | | | | | | |
| Respon (disintegration time) | | | | | | |
| FM | 41.15 | -77.39 | 11.33 | 57.61 | 1.44 | -5.5 |
| RM | 42.11 | -77.39 | 11.33 | 57.61 | | -5.5 |

Abbreviations: FM, full model; RM, reduced model.

is significant if the calculated t value is greater than the critical value of t . The significance level of coefficient b_{22} was found to be $p = 0.263$ and 0.549 in the full model for disintegration time and $DR_{0.5h}$, respectively (data not shown); therefore it was omitted from the full model for both cases to generate the reduced models. The results of statistical analysis are shown in Table 7. The coefficients b_1 , b_2 , b_{11} , and b_{12} were found to be significant at $p < 0.05$, hence they were both retained in the reduced model. The reduced model was tested in portions to determine whether the coefficient b_{22} contributes significant information for the prediction of disintegration time and $DR_{0.5h}$ or not (16). The results of multiple linear regression analyses (reduced model) reveal that, when increasing the concentration of CCS, a decrease in disintegration time is observed and the b_1 coefficients bear a negative sign. When the b_2 coefficient bears a positive sign it signifies an increase in disintegration time on decreasing the hardness (kg/cm^2) of the tablets. An increase in the value of $DR_{0.5h}$ is observed on increasing the concentration of CCS (b_1 is positive) and on decreasing the hardness (b_2 is negative) of the tablets.

The response surface plot of % of CCS (X_1) and hardness of the tablets (X_2) versus disintegration time and those versus % of $DR_{0.5h}$ are shown in Figures 2A and 2B, respectively. The response plot showed that there is a significant effect of both factors on selected response.

The model predicts the required disintegration

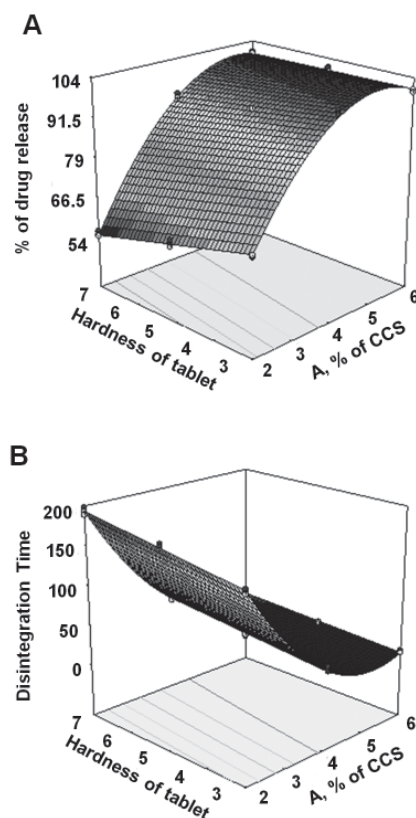


Figure 2. Response surface plot of % of drug release at 0.5 h (A) and disintegration time (B).

time (as per USP limits) and $DR_{0.5h}$ (100%) from point prediction, at 4% CCS and 5 kg/cm² hardness (F-5). Though the model also predicted the required response at a lower concentration of CCS and hardness; the tablets did not have a disintegration time within 3,600 sec at lower CCS concentrations and failed to pass the friability at lower hardness.

A checkpoint batch was prepared at $X_1 = -0.5$ level and $X_2 = +0.5$ (Table 3). From the reduced model, it is expected that the $DR_{0.5h}$ value of the checkpoint batch should be 77.8 and the value of disintegration time should be 100.4 seconds (Table 3). Thus, from the results of statistical optimization techniques it can be concluded that all of the models are mathematically significant.

Stability studies of factorial batches indicate no significant change in appearance of the tablets assay ($p < 0.05$), disintegration time ($p < 0.05$), and percentage drug release ($p < 0.05$).

4. Conclusion

In this study, the dissolution of poorly soluble drug NTG was significantly enhanced by using CCS compared to sodium starch glycolate, cross povidone and Starch-1500 as superdisintegrants in immediate release tablets. The results of a 3² full factorial design revealed that the amount of CCS and hardness of the tablets significantly affect the dependent variables, disintegration time, and percentage of $DR_{0.5h}$ from the tablets. It is concluded that by adopting a systematic formulation approach, an optimum point can be reached in the shortest time with a minimum effort. Tablets containing 4% (w/w) of CCS at 5 kg/cm² met the required disintegration time (as per USP limit) and $DR_{0.5h}$ (100%).

Acknowledgements

The authors thank Glenmark Pharmaceuticals, Nashik, India for providing gift samples of NTG and Sri G.M. Bilakhia College of Pharmacy, Vapi, Gujarat, India for providing the necessary facilities to carry out the research work.

References

1. Sekar V, Chellan VR. Immediate release tablets of telmisartan using superdisintegrant – formulation, evaluation and stability studies. *Chem Pharm Bull (Tokyo)*. 2008; 56:575-577.
2. Mallick S, Pattnaik S, Swain K, De PK. Current perspectives of solubilization: Potential for improved bioavailability. *Drug Dev Ind Pharm*. 2007; 33:865-873.
3. Moneghini M, Carcano A, Persutti B, Rubessa F. Formulation design studies of atenolol tablets. *Pharm Dev Technol*. 2000; 5:297-301.

4. Mahajan HS, Kuchekar BS, Badhan AC. Mouth dissolve tablets of sumatriptan succinate. *Indian J Pharm Sci*. 2004; 66:238-240.
5. Zhao N, Augsburg LL. Functionality comparison of 3 classes of superdisintegrants in promoting aspirin tablet disintegration and dissolution. *AAPS PharmSciTech*. 2005; 6:E634-E640.
6. McLeod JF. Clinical pharmacokinetics of nateglinide: A rapidly-absorbed, short-acting insulinotropic agent. *Clin Pharmacokinet*. 2004; 43:97-120.
7. Ikenoue T, Okazaki K, Fujitani S, Tsuchiya Y, Akiyoshi M, Maki T, Kondo N. Nateglinide suppresses postprandial hypertriglyceridemia in Zucker fatty rats and Goto-Kakizaki rats: Comparison with Voglibose and Glibenclamide. *Biol Pharm Bull*. 1997; 20:354-359.
8. Raghupathi K, Grover V, Chawla HPS, Garg S. Evaluation of compatibility of Ketorolac tromethamine with selected polymers and common tablet excipients by thermal and isothermal stress testing. *STP Pharm Sci*. 2001; 11:449-457.
9. Verma RK, Garg S. Compatibility studies between isosorbide mononitrate and selected excipients used in the development of extended release formulations. *J Pharm Biomed Anal*. 2004; 35:449-458.
10. Lachman L, Liberman HA, Kanig JL. *The Theory and Practice of Industrial Pharmacy*, 3rd ed. Varghese Publishing House, Mumbai, India, 1987; pp. 66-99.
11. Lindberg N, Pålsson M, Pihl A, Freeman R, Freeman T, Zetzener H, Enstad G. Flowability measurements of pharmaceutical powder mixtures with poor flow using five different techniques. *Drug Dev Ind Pharm*. 2004; 30:785-791.
12. US Department of Health and Human Services, Food and Drug Administration, Center for Drug Evaluation and Research (CDER). *Guidance for Dissolution testing*. Rockville, MD, USA, 2007.
13. Basu SK, Rajendran A. Studies in the development of nateglinide loaded calcium alginate and chitosan coated calcium alginate beads. *Chem Pharm Bull (Tokyo)*. 2008; 56:1077-1084.
14. Bolton S. *Pharmaceutical Statistics*, 2nd ed. Marcel Decker Inc., New York, USA, 1990; p. 234.
15. Mendenhall W, Sincich T. *Multiple regression*. 3rd ed., Dellen Publishing Co., San Francisco, CA, USA, 1989; pp. 141-226.
16. Franz RM, Browne JE, Lewis AR. Experiment design, modeling and optimization strategies for product and process development. In: *Pharmaceutical Dosage Forms: Disperse Systems*, Vol 1. 1st ed., Marcel Decker Inc., New York, NY, USA, 1988; pp. 427-519.
17. Stability testing of new drug substances and products. ICH harmonised tripartite guideline. 2003. <http://www.ich.org/LOB/media/MEDIA419.pdf> (accessed Aug 14, 2007).
18. *Weight Variation*, United States Pharmacopoeia-XXVII, NF-22, Asian ed., United States Pharmacopoeial Convention Inc, Rockville, MD, USA, 2004; pp. 2335-2337.

(Received June 6, 2010; Revised August 4, 2010; Re-revised September 14, 2010; Accepted September 20, 2010)

Original Article**Formulation of microemulsion gel systems for transdermal delivery of celecoxib: *In vitro* permeation, anti-inflammatory activity and skin irritation tests**Sara M. Soliman¹, Nevine S. Abdel Malak^{2,*}, Omaila N. El-Gazayerly², Abdel Aziz Abdel Rehim¹¹ Department of Pharmaceutics, Faculty of Pharmacy, 6th of October University, 6th of October City, Egypt;² Department of Pharmaceutics, Faculty of Pharmacy, Cairo University, Egypt.

ABSTRACT: The aim of this study was to develop suitable microemulsion gel systems for transdermal delivery that could assist dissolution enhancement of poorly water soluble celecoxib and thus improve its skin permeability. Long term oral administration of celecoxib causes serious gastrointestinal adverse effects, which makes it a good candidate for transdermal formulations, yet its low water solubility (4 mg/L) makes this challenging. Ternary phase diagrams were constructed using isopropyl myristate and oleic acid as oils, Tween 80 as surfactant, and Cremophor RH40 as cosurfactant. Microemulsion areas were identified and two systems each of 36 formulas were prepared and assessed for visual inspection, spreadability, pH measurements, and droplet size analysis. Drug release and *in vitro* permeation of celecoxib from microemulsion formulas through semi-permeable membranes and excised abdominal rabbit skin, respectively, were carried out and compared to celecoxib cream. In all tested formulas, celecoxib was released and permeation was at a higher rate than that from the corresponding cream. The optimized formula (F12) was found to be superior to all other formulas. This formula increased the permeation rate of celecoxib up to 11 times compared to that of the cream. Its stability was retained after one year of storage under ambient conditions and its anti-inflammatory effect was significantly higher than that of celecoxib cream and the oral commercial formula. Skin irritancy and histopathological investigation of rat skin revealed its safety. The results revealed that the developed microemulsion gel has great potential for transdermal delivery of celecoxib.

Keywords: Microemulsion gel, transdermal, histopathology, celecoxib, anti-inflammatory

*Address correspondence to:

Dr. Nevine Shawky Abdel Malak, Faculty of Pharmacy, Cairo University, Kasr El Ainy Street 11562, Cairo, Egypt. e-mail: pharmnova@yahoo.com

1. Introduction

Celecoxib was the first synthesized non-steroidal anti-inflammatory drug (NSAID) able to selectively inhibit COX-2 activity (1). Celecoxib is used for the treatment of rheumatoid arthritis, osteoarthritis, and acute pain with oral administration (2). Long term oral administration of celecoxib causes serious side effects, such as gastrointestinal toxicity, gastric mucosal ulceration, hemorrhage and recently, cardiotoxic effects, that restrict its oral use and make it a good candidate for transdermal administration (3). Yet, very poor aqueous solubility of celecoxib in water (4 mg/L) and the excellent barrier function of the skin limit its formulation as a transdermal dosage form and make this challenging. Therefore, formulation of celecoxib in a transdermal dosage form with a high degree of skin permeation and safety could be useful.

One of the most important techniques for enhancement of transdermal permeation of drugs is the use of nanoemulsion and microemulsion vehicles (4,5). Microemulsion is defined as an oil-in-water (o/w) or water-in-oil (w/o) emulsion producing a transparent product that has a droplet size < 0.2 μm and does not have a tendency to separate (4,6). It is thermodynamically stable dispersions of oil and water stabilized by an interfacial film of amphiphile blend (surfactants either alone or in combination with co-surfactant) (7-10). Microemulsions have received great attention for various applications including, dermal and transdermal drug delivery due to ease of preparation, thermodynamic stability, permeation enhancement activity of their components, and a high solubilizing capacity for various drugs over conventional topical formulation vehicles (11-16).

Therefore, the aim of this study was to develop suitable microemulsion gel systems (without addition of gelling agent) after screening of oils, surfactants, and cosurfactants for transdermal delivery of celecoxib to enhance its dissolution and to improve its skin permeability with enhanced safety. Microemulsions were prepared using pharmaceutically acceptable

ingredients without using additional chemical enhancers.

The prepared formulas were subjected to extensive physicochemical evaluation, *in vitro* release, and *in vitro* permeation studies. Candidate formula was subjected to assessment of anti-inflammatory activity using the carrageenan-induced rat's paw edema method in addition to skin irritancy test and histopathological investigation of rat skin to investigate the safety of the microemulsion gel formulas for transdermal use.

2. Materials and Methods

2.1. Materials

Celecoxib was obtained as a gift from Amoun Pharmaceutical Co. (Cairo, Egypt). Isopropyl myristate (IPM), oleic acid, Tween 80 (polysorbate 80), and Tween 40 were obtained from Merck-Schuchardt (Hohenbrunn, Germany). Propylene glycol and ethylene glycol were obtained from Fluka AG (Buchs, Switzerland). Chloroform and sodium lauryl sulfate (SLS) were obtained from Adwic, El-Nasr Pharmaceutical Chemical Company (Cairo, Egypt). Cremophor RH40 (polyoxyl 40 hydrogenated castor oil) was from BASF (Schwarzheide, Germany). Synthetic cellulose nitrate membrane (0.45 μm Tuffryn membrane filter) and Celebrex[®] capsules (100 mg celecoxib capsules) were from Sartorius Stedium (Aubagne, France) and Pfizer Egypt (Cairo, Egypt), respectively. Olive oil, white soft paraffin, liquid paraffin, cetostearyl alcohol, and all other chemicals were of analytical grade and used without further purification.

2.2. Screening of oils, surfactants, and cosurfactants for microemulsion preparation

Solubility of celecoxib in various oils such as IPM, oleic acid, and olive oil in surfactants including Tween 80 and Tween 40 and in cosurfactants such as propylene glycol, Cremophor RH40 and ethylene glycol was determined to select the appropriate oil phase, surfactant, and cosurfactant.

An excess amount of celecoxib was added to each oil, surfactant and cosurfactant in stoppered vials and was shaken reciprocally at 30°C for 72 h to reach equilibrium (17). The mixtures were removed from the shaker and centrifuged for 30 min at 2,500 rpm to remove excess undissolved celecoxib. The supernatants were filtered through a 0.45 μm Millipore filter and the drug concentration in the filtrate was determined using a UV spectrophotometer (UV-1601 PC, Shimadzu, Kyoto, Japan) at λ_{max} 258.4 nm after appropriate dilution with chloroform (18).

2.3. Construction of microemulsion phase diagrams

Ternary phase diagrams were constructed to obtain the

concentration range of components for the existing microemulsion zones. Mixtures of oil, surfactant, and cosurfactant at certain weight ratios were weighed into glass vials and were shaken to ensure complete mixing. Phase diagrams were constructed by titrating these mixtures with aliquots of distilled water according to the method mentioned by Aboofazeli and Lawrence (19,20) in 10% increments in a range from 10-50% (w/w). Following each water addition, the mixtures in the vials were mixed using a vortex mixer (VM-300; Gemmy Industrial Corp., Taipei, Taiwan) for 2-3 min and then incubated at 30°C for 24 h before the next addition, for equilibrium. After being equilibrated, the mixtures were assessed visually as microemulsions, crude emulsions, or gels after each addition of distilled water. Thirty-six samples were prepared for each system, and only clear and transparent mixtures with gel consistency visualized after vortexing and equilibrium were considered monophasic, these samples were marked as points on the phase diagrams and were chosen for further addition of the drug. The area covered by these points was considered to be the microemulsion region of existence. The top apex of the diagram represents the high hydrophile-lipophile balance (HLB) surfactant component and the other two apices represent the oil and the cosurfactant.

2.4. Preparation of celecoxib microemulsion gel systems

In order to prepare the drug loaded microemulsions, the appropriate oil, surfactant, and cosurfactant weight ratios were weighed in glass vials. Then, 2% (w/w) of celecoxib was accurately weighed and added to the mixture, vortexed and then water was added drop wise at ambient temperature and vortexing was continued for 5 min. The resultant microemulsions were stored for 24 h at room temperature for equilibrium before further investigation.

2.5. Evaluation of physical properties of the prepared celecoxib microemulsion gel systems

The prepared celecoxib microemulsion gel systems were subjected to the following evaluation tests.

2.5.1. Visual inspection

The prepared celecoxib microemulsion gel systems were examined for optical clarity, fluidity, homogeneity, and phase separation.

2.5.2. pH measurements

pH of 10% (w/w) aqueous solution was measured using a Hanna-213 pH meter (HANNA Instruments, Woonsocket, RI, USA). The solutions were prepared by dissolving 1 g of each prepared formula in 9 g of distilled water using a magnetic stirrer (21).

2.5.3. Test for spreadability

A spreadability test was conducted by pressing 0.5 g of each prepared formula between two glass slides and left for about 5 min until no more spreading was expected. The diameter of the formed circle was measured and used as comparative values for spreadability (22,23).

2.5.4. Droplet size analysis

Droplet size analysis was performed using a laser light scattering particle size analyzer (Master Sizer 2000; Malvern Instruments Ltd., Worcestershire, UK). Microemulsion samples were diluted with distilled water and charged into a wet sample holder.

2.6. Drug release studies using a Franz diffusion cell

For this investigation, static Franz glass diffusion cells (Microette plus; Hanson Research, Chatsworth, CA, USA) were used. These cells consist of donor and receptor chambers between which the cellulose nitrate membrane was positioned. The area for diffusion was 1.7 cm² and the receptor chamber volume was 14 mL. The receptor chamber was maintained at 37 ± 0.5°C in order to ensure a surface skin temperature of 32°C on the surface of the membrane (24). The receptor medium consists of a 1% (w/v) SLS solution. Each cell contains a magnetic stirring bar and was stirred at 100 rpm during the experiment. Weighed amounts of 0.5 g of the microemulsion gel were evenly spread on the surface. Aliquots of 2 mL of the medium were withdrawn at: 0.5, 1, 2, 3, 4, 5, and 6 h and replaced with an equal volume of fresh medium to maintain a constant volume. The concentration of celecoxib was determined spectrophotometrically at the predetermined λ_{max} of 255.2 nm (Shimadzu). The mean percentage of celecoxib released across the membrane was plotted as a function of time. All experiments were run in triplicate and the results were expressed as mean values ± S.D.

2.7. Release kinetics of celecoxib from the prepared microemulsion gel systems

The release data were analyzed using linear regression equations and were fitted to zero order, first order, and simplified Higuchi diffusion models. The following linear regression equations were employed:

$$C_t = C_0 - K_t \text{ (Eq. 1) for zero-order kinetics}$$

$$\text{Log}C_t = \text{log}C_0 - K_t/2.303 \text{ (Eq. 2) for first-order kinetics}$$

$$Q = K_t^{1/2} \text{ (Eq. 3) for Higuchi diffusion model (25)}$$

where, Q is the amount of drug released per unit area at time t. The coefficient of determination (R^2) was

determined and $t_{50\%}$ (time until 50% drug release) was then computed according to the determined order and the release rate of celecoxib was calculated from the slope of the straight line.

For comparison, a 2% o/w celecoxib cream was prepared and subjected to drug release. The cream was composed of 2% (w/w) celecoxib, 30% (w/w) emulsifying ointment, and 68% (w/w) water. The cream was formulated by dispersing celecoxib in melted anionic emulsifying ointment composed of 30% (w/w) emulsifying wax, 20% (w/w) liquid paraffin, and 50% (w/w) white soft paraffin (26). Slightly warmed distilled water was added to this mixture and stirred gently until it became cold, to obtain cream consistency (26). Based on the results of the release study, candidate formulas showing optimum drug release were subjected to further analysis.

2.8. Rheological properties measurements

The selected celecoxib microemulsion gel formulas were tested for rheological behavior at 25°C using a Brookfield digital viscometer (RV-TD; Brookfield Engineering Laboratories, Middleboro, Inc., MA, USA) with a spindle (LV.4).

2.9. In vitro drug permeation studies through excised rabbit skin

2.9.1. Preparation of full excised abdominal rabbit skin barrier membrane

Ethical clearance was obtained from the institutional animal experimentation committee before the study. Rabbits were sacrificed and the full thickness of rabbit skin was excised from the abdominal region and hair was removed with an electric clipper. The subcutaneous tissue was removed surgically and the dermis side was wiped with isopropyl alcohol to remove adhering fat. The cleaned skin was washed with distilled water and stored in the deep freezer until further use. The skin was brought to room temperature and cut into 5 cm diameter circular patches when used.

2.9.2. In vitro permeation

Permeation of celecoxib for the selected microemulsion gel formulas through the skin and drug analysis were carried out according to the procedure adopted for the release study through cellulose nitrate membranes. All experiments were run in triplicate and the results were expressed as mean values ± S.D. The cream containing 2% (w/w) celecoxib was used as a control formula to compare drug permeation through the skin from microemulsion gel formulas with that from the cream.

2.9.3. Permeation data analysis

Average values of three readings of *in vitro* permeation data were calculated and the average cumulative amount of celecoxib permeated through the skin per unit surface area ($\mu\text{g}/\text{cm}^2$) was plotted as a function of time. The drug flux (permeation rate) at steady state (J_{SS}) was calculated from the slope of the straight line. The permeability coefficient (K_p) was calculated using the following equations:

$$K_p = J_{SS}/C_o \text{ (Eq. 4)}$$

where C_o is the initial concentration of the drug. Enhancement ratio (E_r) was calculated by dividing J_{SS} of the respective formulation by J_{SS} of the control formulation (27,28):

$$E_r = J_{SS} \text{ of formulation} / J_{SS} \text{ of control (Eq. 5)}$$

The coefficient of determination (R^2), $t_{50\%}$ (time to 50% drug permeation), and the percentage of drug permeated after 6 h were also determined.

2.10. Thermodynamic stability of celecoxib microemulsion

To assess the thermodynamic stability for the selected microemulsion formulas, the following two tests were carried out for the selected formulas.

2.10.1. Centrifuge stress test (11)

The selected microemulsion gel formulas were centrifuged at 3,000 rpm for 30 min and then examined for liquefaction and phase separation. Formulas that did not show phase separation were considered for a freeze thaw stress test.

2.10.2. Freeze thaw stress test (29)

Selected microemulsion gel formulas were submitted to a total of three complete cycles, each cycle consisting of 24 h at 25°C followed by 24 h at -5°C. These cycles were important for determining the ability of the microemulsion to withstand thermal shock, as well as to evaluate physical stability of the microemulsion.

2.11. Long term stability

The optimized celecoxib loaded microemulsion gel formula showing satisfactory physicochemical properties, highest release, and permeation rate was stored under ambient conditions for one year. The stored microemulsion formula was re-evaluated regarding visual inspection, pH measurement, and spreadability test. In addition, the morphology and the droplet size analysis of the celecoxib microemulsion formula were observed using a transmission electron microscope (TEM). One drop of diluted sample was deposited on a

film-coated 200-mesh copper grid and later stained with one drop of a 2% aqueous solution of phosphotungstic acid (PTA) and allowed to dry and any excess fluid was removed with filter paper before examination using a JEM-100 CX electron microscope (JEOL, Tokyo, Japan).

2.12. Anti-inflammatory studies in rats

The study was conducted in accordance with the principles of Laboratory Animal Care and was approved by the Institutional Ethics Committee. The anti-inflammatory activity of the optimized formula was carried out using the carrageenan-induced paw edema method developed by Winter *et al.* (30,31) in albino rats. Male albino rats weighing 150-180 g were fasted overnight with free access to water and were divided into 4 groups of 6 animals. The dorsal side of the rats was shaved 12 h before starting the experiments except in the control group. The first group (control) received carrageenan only without the drug. The second and third groups received an application of optimized microemulsion, or conventional cream, respectively, at a 11.66 mg/kg dose level (32) on the shaved dorsal region of all animals (except in the control group) half an hour before subplantar injection of carrageenan. The last group received an oral treatment of commercial Celebrex[®] at a dose of 11.66 mg/kg. The animals were injected with 0.1 mL of carrageenan suspension (1%, w/v, in distilled water) in the subplantar region of the right hind paw. Paw edema volume was measured before carrageenan injection as well as after 1, 2, 3, 4, 5, and 6 h following the carrageenan injection using a plethysmometer by the mercury displacement method. The percentage inhibition of edema volume was calculated as follows:

$$\% \text{ Inhibition} = 100 \times [1 - (A - x / B - y)] \text{ (Eq. 6)}$$

where A is paw volume after administration of carrageenan at time t, and x is paw volume before administration of carrageenan. B is the mean paw volume of control rats after administration of carrageenan at time t and y is mean paw volume of control rats before administration of carrageenan.

2.13. Skin irritation test

Although all the materials used for preparation of microemulsions fell under the Generally Regarded as Safe (GRAS) category, concentrations of all materials is a very critical issue for these formulations. For example, a large amount of surfactants is usually an irritant to the skin. Therefore, a skin irritation test was performed to confirm that the concentration of materials used for microemulsion preparation was safe.

The skin irritancy test was carried out to determine any possible localized reaction of the optimized

microemulsion formula on the skin of male albino rats (150-180 g) according to the method described by Draize *et al.* (33). The animals were divided into three groups: the first group served as control (no treatment), the second group received 0.8% (v/v) aqueous formalin solution as a standard irritant, and the third group received the optimized formula. A dose of 0.5 g of optimized formula or 0.5 mL of formalin solution was applied on a 5 cm² area of the shaved dorsal side of the rats daily for three consecutive days (34). The development of erythema and edema were monitored daily for 3 days.

2.14. Histopathological examination of skin specimens

After three days, the rats were sacrificed and skin samples from treated and untreated (control) areas were taken. Each skin sample was stored in 10% (v/v) formalin saline solution. The skin samples were cut vertically in different sections. Each section was dehydrated using ethanol, embedded in paraffin for fixing, and stained with hematoxylin and eosin and then examined through the light electric microscope (Nikon, Tokyo, Japan) fitted with a Canon power shot G3 digital camera (Canon, Tokyo, Japan) and compared with control sample.

3. Results and Discussion

3.1. Screening of oils, surfactants, and cosurfactants for celecoxib

Table 1 summarizes solubility of celecoxib in various solvents such as oils, surfactants, and cosurfactants at 30°C. Celecoxib showed the highest solubility in oleic acid followed by IPM and olive oil. Among surfactants, solubility of the drug in Tween 80 was greater than that in Tween 40. Celecoxib was found to be more soluble in Cremophor RH40 when compared to propylene glycol and ethylene glycol.

3.2. Construction of microemulsion phase diagrams

The aim of the construction of phase diagrams was to

Table 1. Solubility of celecoxib in various oils, surfactants, and cosurfactants at 30°C

| Solvents | Solubility (mg/mL) |
|------------------|--------------------|
| Oleic acid | 22.3 ± 5.0 |
| IPM | 5.6 ± 1.0 |
| Olive oil | 3.4 ± 0.1 |
| Tween 80 | 158.5 ± 10.0 |
| Tween 40 | 137.1 ± 4.0 |
| Cremophor RH40 | 153.3 ± 2.0 |
| Propylene glycol | 22.1 ± 5.0 |
| Ethylene glycol | 4.1 ± 0.3 |

Abbreviation: IPM, isopropyl myristate.

find out the microemulsion existence region. Based on the solubility studies, oleic acid and IPM were chosen to represent the oily phases, Tween 80 was used as surfactant, and Cremophor RH40 was used as cosurfactant for constructing phase diagrams.

Oleic acid, an unsaturated C18 fatty acid, has been widely employed as a pharmaceutical excipient for microemulsion preparation (15,35,36). Similarly IPM, a long chain triglyceride, is often used as an oil phase and as a permeation enhancer in transdermal formulations (37). It is considered to be the most popular and most biocompatible fatty acid ester used for formulation of pharmaceutically accepted microemulsions (38-43). Tween 80 is a non-ionic surfactant with an HLB value of 15 which is widely used in pharmaceutical preparations due to its history of usefulness, safety, and stability (44,45). Cremophor RH40 is a non-irritant, safe, and good emulsifier; it was used as a cosurfactant in preparing ketoprofen microemulsions (46).

Upon increasing the water content from 10-50%, a turbid macroemulsion was formed where the clear microemulsion region was reduced (data not shown). It was found that the microemulsion region obtained using IPM (Figure 1A) was larger when compared to oleic acid (Figure 1B). This may be because oleic acid has a larger molecular size compared to IPM and Tween 80, where a low degree of oil penetration was expected to take place in the interfacial surfactant layer. It was previously reported that the phase behavior is strongly influenced by the size of the molecule of the oil used

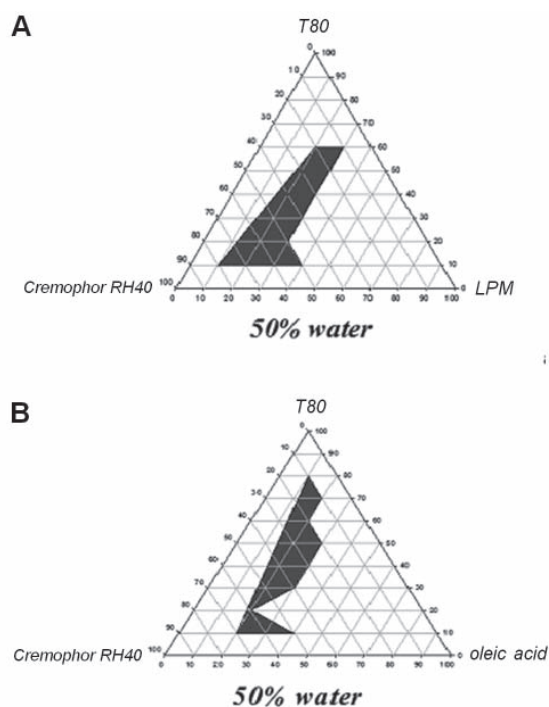


Figure 1. Quaternary phase diagrams of microemulsion containing IPM(A) or oleic acid (B) as oil, Tween80 as surfactant, and Cremophore RH40 as cosurfactant. Water content was 50%.

(20). Similarly, these findings were in agreement with those of Yuan *et al.*, who compared IPM with an oleic acid microemulsion formulation and reported a large microemulsion existence area with IPM and a small area with oleic acid (47).

3.3. Preparation of celecoxib microemulsions

As hundreds of formulations could be prepared from the microemulsion region of each phase diagram, a constant point at 50% water was selected for formulation of celecoxib microemulsions for all phase diagrams. This selection was done for the purpose of formation of a microemulsion gel spontaneously without adding any gelling agent and was based on the fact that the higher the water content in the microemulsion systems, the lower would be the solubility of celecoxib in the microemulsion with an expected higher release. It was previously mentioned that, when increasing the water content, celecoxib solubilization capacity in microemulsions decreased and its release behavior was increased (48). From each phase diagram constructed, different formulas were selected from the microemulsion region for incorporation of drug into the aqueous phase. Sixteen formulas out of seventy-two were adopted from microemulsion systems S1 and S2 (See Table 2 for the composition of these microemulsion systems). The prepared microemulsions were in the form of microemulsion gels and no liquefaction was observed upon increasing the water content up to 50% and upon addition of celecoxib. All other preparations liquefied

upon addition of 2% (w/w) celecoxib, and therefore were excluded. The composition of the selected celecoxib microemulsion formulas for each system is presented in Table 3.

3.4. Evaluation of the physicochemical properties of the prepared celecoxib microemulsion gel systems

3.4.1. Visual inspection

Visual inspection of the prepared microemulsions showed clear homogeneous systems of gel consistency and no phase separation was observed (Table 4).

3.4.2. pH determination

It was previously reported that, for microemulsions to be non-irritant and safe for transdermal application, their pH has to fall in the physiologic accepted range for transdermal preparations, *i.e.*, pH 4-7 units (23). pH measurements of 10% (w/w) aqueous solutions of the microemulsion systems are summarized in Table 4. The pH values were found to be in the range of 3.94-4.44 units for S1 prepared using oleic acid and in the range of 6.20-6.84 units for S2 prepared using IPM. Therefore, the pH of all the prepared formulas was within the required range and was considered to be safe for transdermal application.

3.4.3. Spreadability measurement

The spreadability is an important criterion for uniform and ease of application of transdermal preparations. Spreadability of the microemulsions was measured in terms of average diameter of the spread circle. As shown in Table 4, spreadability values for all prepared microemulsion formulas ranged between 2.35 and 4.80 cm. Needless to say, the larger the diameter, the better the spreadability (49).

Table 2. Composition of the microemulsion systems

| System | Oil | Surfactant | Cosurfactant |
|--------|------------|------------|----------------|
| S1 | Oleic acid | Tween 80 | Cremophor RH40 |
| S2 | IPM | Tween 80 | Cremophor RH40 |

Table 3. Composition (% , w/w) of microemulsion formulas for each system

| System | Formulation code | Oil | Surfactant | Cosurfactant | Celecoxib |
|--------|------------------|-------|------------|--------------|-----------|
| S1 | F1 | 13.07 | 6.53 | 45.73 | 2 |
| | F2 | 13.07 | 13.07 | 39.20 | 2 |
| | F3 | 13.07 | 19.60 | 32.67 | 2 |
| | F4 | 13.07 | 26.13 | 26.13 | 2 |
| | F5 | 13.07 | 32.67 | 19.60 | 2 |
| | F6 | 13.07 | 39.20 | 13.07 | 2 |
| | F7 | 13.07 | 45.73 | 6.53 | 2 |
| S2 | F8 | 19.60 | 6.53 | 39.20 | 2 |
| | F9 | 26.13 | 6.53 | 32.67 | 2 |
| | F10 | 19.60 | 13.07 | 32.67 | 2 |
| | F11 | 6.53 | 19.60 | 39.20 | 2 |
| | F12 | 19.60 | 25.07 | 20.66 | 2 |
| | F13 | 19.60 | 26.13 | 19.60 | 2 |
| | F14 | 13.07 | 32.67 | 19.60 | 2 |
| | F15 | 19.60 | 32.67 | 13.07 | 2 |
| | F16 | 19.60 | 39.20 | 6.53 | 2 |

All formulas contain 32.67% water.

Table 4. Various physicochemical properties of the prepared microemulsion gel formulas

| System | Formulation code | Visual inspection** | pH* | Spreadability (cm)* | Droplet diameter (μm)* | Span |
|--------|------------------|---------------------|-----------------|---------------------|-------------------------------------|------|
| S1 | F1 | Clear | 4.44 \pm 0.01 | 4.50 \pm 0.00 | 0.20 \pm 0.04 | 0.43 |
| | F2 | Clear | 4.37 \pm 0.06 | 4.50 \pm 0.10 | 0.19 \pm 0.03 | 0.47 |
| | F3 | Clear | 4.28 \pm 0.08 | 4.15 \pm 0.05 | 0.25 \pm 0.09 | 0.77 |
| | F4 | Clear | 4.26 \pm 0.01 | 4.25 \pm 0.15 | 0.20 \pm 0.11 | 0.47 |
| | F5 | Clear | 4.21 \pm 0.07 | 4.80 \pm 0.20 | 0.19 \pm 0.08 | 0.80 |
| | F6 | Clear | 4.14 \pm 0.06 | 4.20 \pm 0.10 | 0.22 \pm 0.01 | 0.93 |
| | F7 | Clear | 3.94 \pm 0.02 | 4.30 \pm 0.15 | 0.23 \pm 0.06 | 0.85 |
| S2 | F8 | Clear | 6.38 \pm 0.03 | 2.35 \pm 0.05 | 0.21 \pm 0.12 | 0.85 |
| | F9 | Clear | 6.59 \pm 0.03 | 2.35 \pm 0.05 | 0.24 \pm 0.09 | 0.73 |
| | F10 | Clear | 6.55 \pm 0.04 | 2.95 \pm 0.15 | 0.21 \pm 0.08 | 0.67 |
| | F11 | Clear | 6.53 \pm 0.01 | 3.50 \pm 0.00 | 0.20 \pm 0.07 | 0.60 |
| | F12 | Clear | 6.20 \pm 0.10 | 3.15 \pm 0.05 | 0.20 \pm 0.08 | 0.30 |
| | F13 | Clear | 6.70 \pm 0.05 | 2.95 \pm 0.05 | 0.22 \pm 0.06 | 0.60 |
| | F14 | Clear | 6.70 \pm 0.01 | 4.30 \pm 0.10 | 0.21 \pm 0.40 | 0.86 |
| | F15 | Clear | 6.82 \pm 0.01 | 2.60 \pm 0.10 | 0.24 \pm 0.11 | 0.83 |
| | F16 | Clear | 6.84 \pm 0.01 | 2.85 \pm 0.05 | 0.23 \pm 0.07 | 0.67 |

* Data are shown as mean \pm S.D. ** Clear homogeneous systems of gel consistency with no phase separation was observed.

3.4.4. Droplet size analysis

Droplet size determination may provide information about the influence of the structure of the surfactant system on microemulsions and drug release from the microemulsion (50). A small droplet size makes it an excellent carrier for improving drug percutaneous uptake, thus increasing efficiency in uptake of the drug (51). The mean volume of the droplet sizes and span (polydispersity) are shown in Table 4. All the formulas had droplets ranging from 0.19 ± 0.03 to $0.24 \pm 0.11 \mu\text{m}$ with a low polydispersity index, which would indicate uniformity of droplet size within each formula.

3.5. Release studies

The release of celecoxib from different microemulsion systems and cream was carried out through a cellulose nitrate membrane over a period of 6 h in 1% SLS solution. SLS was added to the dissolution media to maintain the sink conditions during the release study because the release of poorly soluble drugs requires release media that are different from those normally used for water-soluble drugs (49).

Figure 2A shows the release pattern of celecoxib from microemulsion formulas of S1 prepared with oleic acid as oil, Tween 80 as surfactant, and Cremophor RH40 as cosurfactant. The percentage of celecoxib released from S1 could be arranged in a descending order as follows $F1 > F2, F3 > F4 > F5 > F6 > F7$. This might be due to a difference in surfactant concentration. As surfactant concentration was increased from 6.5% (F1) to 45.7% (F7), the percentage of celecoxib released was decreased from 76.11% (F1) to 44.00% (F7). This may be due to an increased thermodynamic activity of the drug in the microemulsion at a lower content of surfactant (51). It was previously found that the increase in surfactant concentration caused a decrease

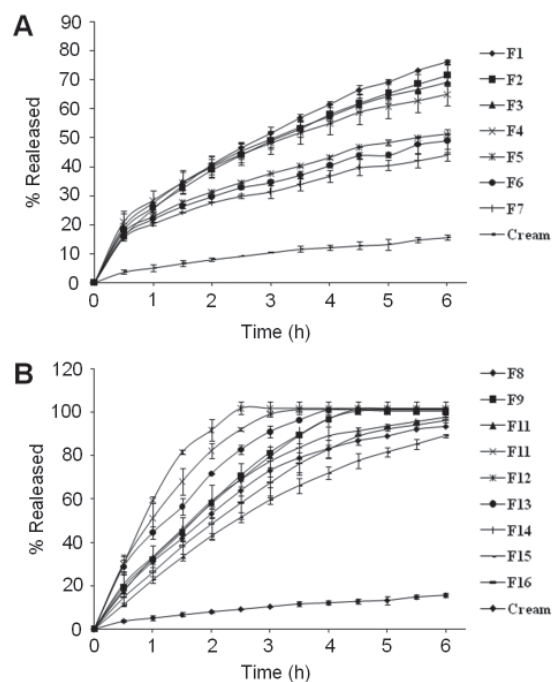


Figure 2. Release pattern of celecoxib from various microemulsion formulas and the corresponding cream. A, S1 prepared with oleic acid as oil, Tween 80 as surfactant, and Cremophor RH40 as cosurfactant; B, S2 prepared with IPM as oil, Tween 80 as surfactant, and Cremophor RH40 as cosurfactant.

in the release of ketoprofen and carbamazepine from microemulsions (46,52).

By applying a one way ANOVA test for the values of $t_{50\%}$ for microemulsion formulas of S1, it was concluded that F1 was superior over all other formulas ($p < 0.05$) except for F2 and F3 where no significant difference was present ($p > 0.05$) (data not shown). There was a high significant difference between all microemulsion formulas of S1 and the corresponding celecoxib cream ($p < 0.05$) (data not shown).

Figure 2B shows the release pattern of celecoxib from microemulsion formulas of S2 containing IPM as oil, Tween 80 as surfactant, and Cremophor RH40 as cosurfactant. Among the microemulsion formulas of S2, F12 showed the highest release where 100% of celecoxib was released within 2.5 h. On the other hand, F15 showed the least drug release. The release of the drug from microemulsion formulas of S2 were 6- to 12-fold greater than drug release from the cream. An ANOVA test revealed that there was a significant difference between the $t_{50\%}$ of celecoxib of different microemulsion formulas of S2 ($p < 0.05$) except F9, F10, and F14 that showed no significant difference between them ($p > 0.05$) (data not shown). The values of $t_{50\%}$ of all microemulsion formulas of S2 were highly significant when compared to the corresponding cream (data not shown).

In spite of the higher solubility of celecoxib in oleic acid, higher drug release was obtained from IPM microemulsions (S2) than that obtained from oleic acid microemulsions (S1). This could be attributed to decreased thermodynamic activity of the drug in microemulsions prepared with oleic acid due to its high affinity for the oil, therefore slowing release of the drug from the vehicle (53). For example, the percent release of celecoxib from F5 of S1 was 51.27% after 6 h (Figure 2A) compared to 97.7% from F14 of S2 (Figure 2B). These results were in agreement with the studies of Ceschel *et al.* who proved that the release of the drug would be favored by selecting the vehicle which had a low affinity for the drug (53).

3.6. Release kinetics of celecoxib from the prepared microemulsions

According to the values of the coefficient of determination (R^2), the mechanism of drug release

was defined. It was found that all the microemulsion formulas and the cream showed a best fit for the Higuchi diffusion model (Table 5). The time required for 50% ($t_{50\%}$) celecoxib to be released from microemulsion formulas of each system and the cream were calculated according to the release model and also the release rate of celecoxib from each formula was determined from the slope of the straight line (Table 5). Based on the results of the release studies, the formulas with the highest release rate namely F1, and F3 of S1 and F11, F12, F13, and F14 of S2 were chosen for further analyses. F5 of S1 was chosen similarly to be compared to F14 of S2 in order to study the effect of changing oil type on the permeation rate because they possessed the same concentration of oil.

3.7. Rheological properties measurements

The results revealed that all the selected microemulsion formulas showed non-Newtonian, pseudoplastic flow with thixotropy as the viscosity decreased with increasing shear rates (Figure 3) (F12 is a representative example). Needless to say, thixotropy is a desirable feature for semisolid drug carriers for dermal application (54). This result was in agreement with the findings of Ambade *et al.*, who found that the rheological behavior of microemulsions containing flurbiprofen showed non-Newtonian, pseudoplastic flow (11).

3.8. In vitro drug permeation studies through excised rabbit skin

In vitro drug permeation was examined through excised rabbit skin over a period of 6 h in 1% SLS solution at $37 \pm 0.5^\circ\text{C}$ for the selected microemulsion formulas and the corresponding cream. Figure 4 shows permeation

Table 5. Release rate and $t_{50\%}$ of celecoxib from various microemulsion gel formulas of S1 and S2 and from the corresponding cream

| System | Formulation code | Mechanism of release | Release rate ($\mu\text{g}/\text{h}^{1/2}$) | $t_{50\%}$ ($\text{h}^{1/2}$) |
|--------|------------------|----------------------|---|---------------------------------|
| S1 | F1 | Higuchi | 35.2 | 1.68 |
| | F2 | Higuchi | 31.3 | 1.76 |
| | F3 | Higuchi | 29.0 | 1.75 |
| | F4 | Higuchi | 25.7 | 1.82 |
| | F5 | Higuchi | 20.1 | 2.34 |
| | F6 | Higuchi | 18.7 | 2.51 |
| | F7 | Higuchi | 16.3 | 2.82 |
| S2 | F8 | Higuchi | 45.8 | 1.35 |
| | F9 | Higuchi | 61.4 | 1.26 |
| | F10 | Higuchi | 62.2 | 1.26 |
| | F11 | Higuchi | 63.7 | 0.97 |
| | F12 | Higuchi | 82.9 | 0.91 |
| | F13 | Higuchi | 58.8 | 1.07 |
| | F14 | Higuchi | 46.6 | 1.26 |
| | F15 | Higuchi | 46.4 | 1.56 |
| | F16 | Higuchi | 50.8 | 1.42 |
| Cream | | Higuchi | 6.88 | 7.50 |

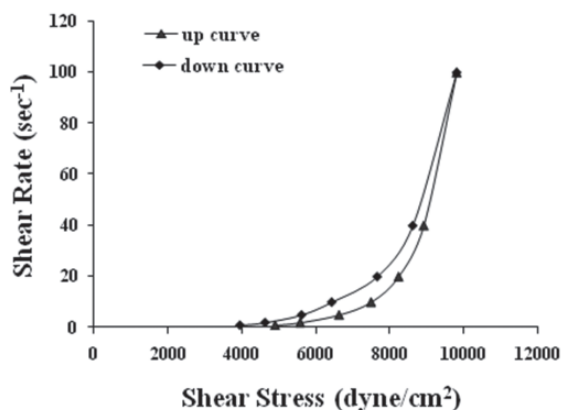


Figure 3. Rheogram of the prepared microemulsion gel system. F12 is a representative example.

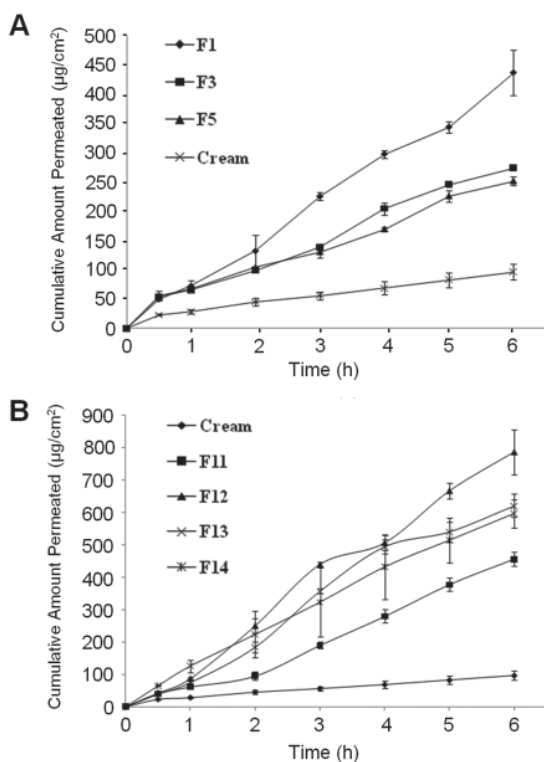


Figure 4. Permeation profiles of celecoxib through rabbit skin from different microemulsion formulas and the corresponding cream. A, S1; B, S2.

Table 6. Permeation data parameters of some selected celecoxib microemulsion gel formulas of S1, S2, and the corresponding cream

| System | Formulation Code | R^2 | Flux (J_{ss}) ($\mu\text{g}/\text{cm}^2/\text{h}$) | K_p (cm/h) | E_r | $t_{50\%}$ (h) | % Permeated after 6 h |
|--------|------------------|-------|--|-----------------|-------|------------------|-----------------------|
| S1 | F1 | 0.994 | 70.5 ± 3.2 | 3.53 ± 0.16 | 5.32 | 5.05 ± 0.21 | 60.3 ± 3.9 |
| | F3 | 0.988 | 42.6 ± 1.2 | 2.13 ± 0.06 | 3.22 | 7.93 ± 0.29 | 37.8 ± 3.0 |
| | F5 | 0.990 | 36.6 ± 2.3 | 1.83 ± 0.12 | 2.77 | 9.02 ± 0.39 | 34.7 ± 1.2 |
| S2 | F11 | 0.981 | 78.5 ± 0.9 | 3.92 ± 0.04 | 5.93 | 4.94 ± 0.02 | 63.2 ± 2.1 |
| | F12 | 0.986 | 137.6 ± 7.7 | 6.88 ± 0.38 | 10.39 | 2.82 ± 0.12 | 102.0 ± 2.8 |
| | F13 | 0.977 | 112.7 ± 5.5 | 5.64 ± 0.27 | 8.51 | 3.35 ± 0.12 | 86.1 ± 3.6 |
| | F14 | 0.997 | 97.3 ± 6.8 | 4.86 ± 0.34 | 7.35 | 3.51 ± 0.51 | 82.7 ± 4.3 |
| Cream | | 0.988 | 13.2 ± 2.1 | 0.66 ± 0.10 | – | 27.66 ± 2.82 | 13.3 ± 1.4 |

profiles of celecoxib through rabbit skin from different microemulsion formulas of S1 and S2. Permeation data analysis of S1 and S2 are represented in Table 6.

For microemulsion formulas of S1 (F1, F3, and F5), *in vitro* skin permeation was the highest from F1 and the lowest from F5 (Figure 4A). This might be due to differences in surfactant concentration. As surfactant concentration increased from 6.5% (F1) to 19.6% (F3) and to 32.67% (F5), the permeation rate of celecoxib decreased. This may be due to decreased thermodynamic activity of the drug in the microemulsion at high surfactant content (51). It is known that the thermodynamic activity of the drug in a formulation is a significant driving force for its release and penetration into skin (55). A similar result was reported by Chen *et al.* who found that the increase in surfactant concentration causes a decrease in the permeation rate of ibuprofen (56).

An ANOVA test revealed that there was a significant difference between the $t_{50\%}$ results of the microemulsion formulas of S1 ($p < 0.05$) and there was a significant difference between all microemulsion formulas of S1 and cream ($p < 0.05$) (Table 6).

Results of the celecoxib permeation study from microemulsion formulas of S2 (F11, F12, F13, and F14) and cream are shown in Figure 4B. Among the microemulsion formulas of S2, F12 showed the highest permeation rate and the least $t_{50\%}$. On the other hand, F11 showed the lowest drug permeation rate and highest $t_{50\%}$. There was a significant difference between the $t_{50\%}$ results of the microemulsion formulas of S2 ($p < 0.05$) and there was a significant difference between microemulsion formulas of S2 and the corresponding cream ($p < 0.05$) (Table 6).

The release and permeation of celecoxib from F14 of S2 containing 13.07% IPM showed a higher rate than F5 of S1 containing 13.07% oleic acid in spite of the higher solubilizing capacity of the latter for celecoxib (Table 6). The possible reason is that drug release and permeation are influenced by the solubility of the drug in the vehicle. If the vehicle can increase the solubility of the drug, then the drug itself would be retained in the vehicle after application on the surface of skin, which results in reduced partition into the skin (54). The same

result was obtained by Zhu *et al.*, who found that the skin permeation of penciclovir in a microemulsion was significantly increased, while the solubility of penciclovir in the microemulsion was decreased (57). Our findings agree with previously reported results regarding the higher permeation ability of IPM than oleic acid for transdermal delivery of some drugs (13,58).

3.9. Thermodynamic stability studies

None of the selected microemulsion formulas showed phase separation using both tests and no changes in physical appearance such as turbidity or creaming was observed (data not shown). These results indicate that all the selected formulas showed good physical stability.

F12 of S2, which showed small droplet size, good spreadability, and the highest release and permeation rates was subjected to long term stability, anti-inflammatory activity, and the skin irritation test.

3.10. Long term stability studies

The optimized microemulsion formula (F12 of S2) was stable when stored under ambient conditions, where there was no change in visual appearance or phase separation, and no significant change in droplet size, pH, and spreadability values (data not shown) which declares the ability of the microemulsion formula to withstand thermal shock (29). The morphology and droplet size analysis of the fresh and stored microemulsion formula were observed using TEM. TEM photographs depicted in Figure 5 reveal that all droplets after storage possessed nearly the same size and spherical shape as freshly prepared ones.

3.11. Anti-inflammatory studies in rats

Figure 6 shows that F12 of S2 produced maximum anti-inflammatory activity where about $83.2 \pm 1.4\%$ inhibition in rat's paw edema volume when compared to conventional cream and oral Celebrex[®] where the percentage of inhibition 6 h after application were $24.8 \pm 2.8\%$ and $43.1 \pm 7.2\%$, respectively. The enhanced anti-inflammatory effects of the microemulsion formula could be due to the enhanced permeation of celecoxib through the skin.

3.12. Skin irritation test

The skin irritancy test was performed to confirm the safety of the optimized microemulsion formula (F12 of S2). The results are shown in Table 7. Draize *et al.* (33) mentioned that a value of the primary irritancy index (PII) < 2 indicates that the applied formulation is a non-irritant to human skin. Therefore, F12 of S2 was considered to be a non-irritant as PII was < 2.

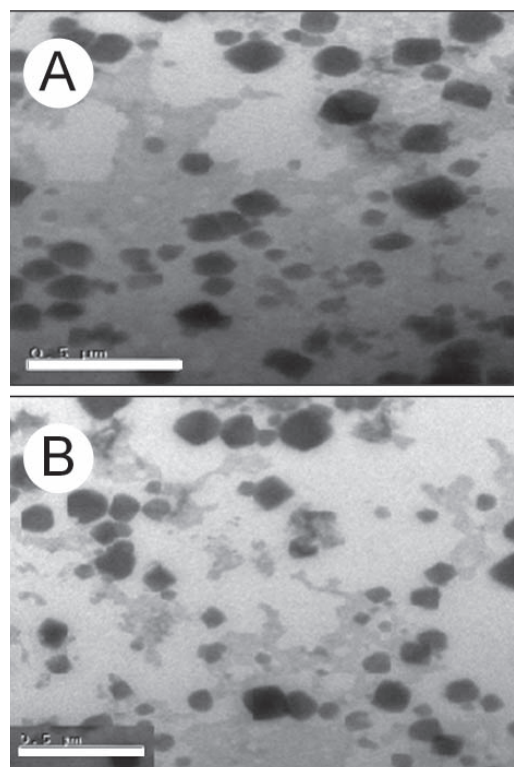


Figure 5. TEM photographs of Celecoxib microemulsion Formula F12 of S2. A, freshly prepared; B, after storage for one year. Bars, 0.5 μ m.

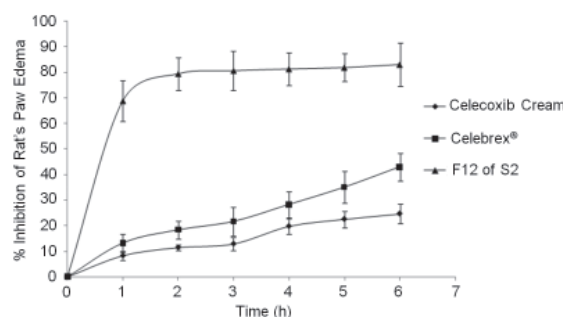


Figure 6. Anti-inflammatory activity of optimized microemulsion formula (F12 of S2), conventional cream, and Celebrex[®] using the carrageenan-induced hind paw edema method.

3.13. Histopathological examination

Histopathological examination of the microemulsion treated and control rat skin was performed using a Nikon light microscope and is illustrated in Figure 7. The photomicrographs of control rat skin (untreated) group I showed normal skin with well defined epidermal and dermal layers as shown in Figure 7A. While the second group (formalin solution as standard irritant), the photomicrograph showed inflammatory cell infiltration and blood capillary dilatation in the dermis (Figures 7B and 7C). When the skin was treated with the optimized microemulsion formula (F12 of S2) for 72 h, the dermis did not show any inflammatory cell infiltration. There was no histopathological alteration or

Table 7. Data of the skin irritation test

| Rats | First group (Control) | | Second group (Formalin solution) | | Third group (F12 of S2 microemulsion) | |
|------|-----------------------|-------|----------------------------------|-------|---------------------------------------|-------|
| | Erythema | Edema | Erythema | Edema | Erythema | Edema |
| 1 | 0.00 | 0.00 | 3 | 1 | 0.00 | 0.00 |
| 2 | 0.00 | 0.00 | 4 | 2 | 0.00 | 0.00 |
| 3 | 0.00 | 0.00 | 4 | 3 | 0.00 | 0.00 |
| 4 | 0.00 | 0.00 | 4 | 3 | 0.5 | 0.00 |
| 5 | 0.00 | 0.00 | 3 | 2 | 1 | 0.00 |
| 6 | 0.00 | 0.00 | 3 | 3 | 1 | 0.00 |
| Mean | 0.00 | 0.00 | 3.5 | 2.33 | 0.42 | 0.00 |
| S.D. | 0.00 | 0.00 | 0.5 | 0.75 | 0.45 | 0.00 |
| PII | 0.00 ± 0.00 | | 5.83 ± 1.17 | | 0.42 ± 0.45 | |

Abbreviation: PII, primary irritancy index.

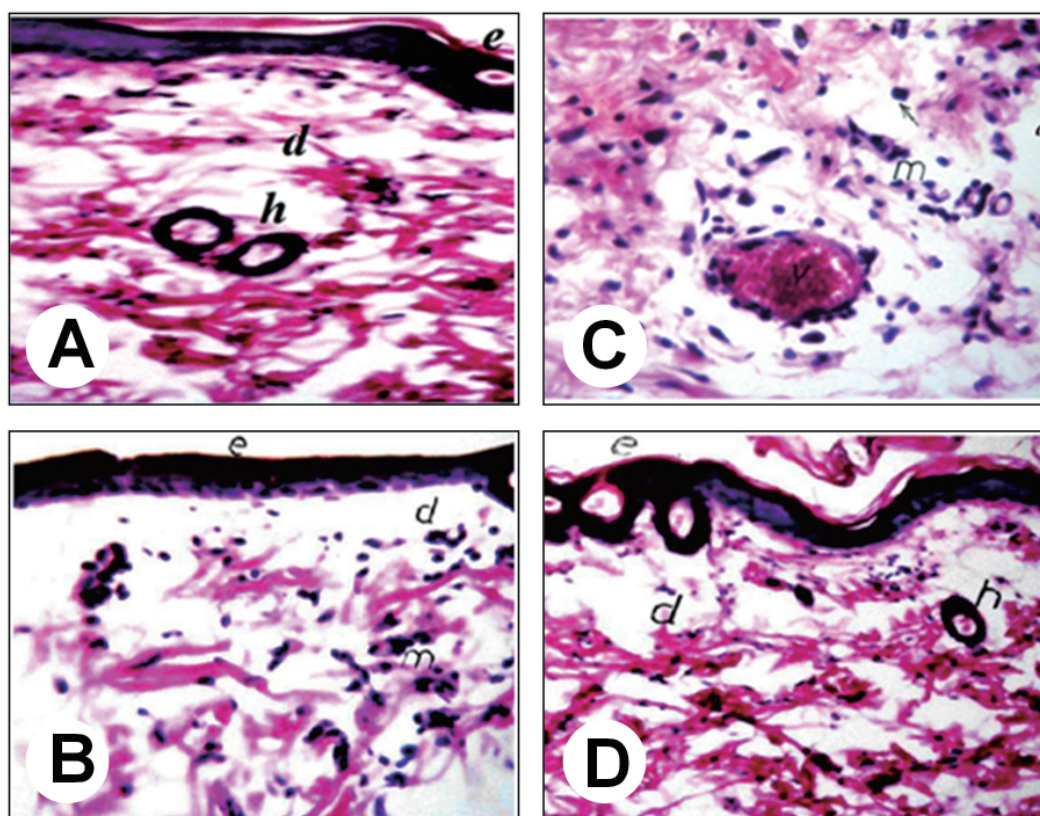


Figure 7. Light micrographs of rat skin untreated (A), treated with standard irritant (B and C) and treated with F12 of S2 microemulsion (D).

apparent signs of skin irritation (erythema and edema) observed on skin specimens indicating the absence of any skin irritation as a consequence of microemulsion treatment (Figure 7D). These results indicated that the developed microemulsion is safe for transdermal delivery of celecoxib.

4. Conclusion

In this study, celecoxib microemulsion systems were prepared and evaluated. All the formulas showed good release profiles and exhibited a rapid rate of permeation when compared to conventional celecoxib cream. The optimized formula (F12 of S2) consisting of 2% (w/w)

of Celecoxib, 19.6% (w/w) of IPM, 25.07% (w/w) of Tween 80, 20.66% (w/w) of Cremophor RH40, and 32.67% of distilled water was found to be superior to all other formulas. It increased the permeation rate of Celecoxib up to 11 times compared to the conventional cream. Its stability was maintained after one year of storage at ambient conditions. The anti-inflammatory studies revealed a significant increase in percent inhibition of F12 as compared to the commercial oral formula ($p < 0.05$) and celecoxib cream. This indicated that the developed microemulsion was efficacious, and the small droplets have enormous interfacial areas, thereby enhancing the solubility of a poorly soluble drug, and influencing its transport properties. Results of

the skin irritation test indicated that F12 could be safe for human use. From these results, it can be concluded that the developed microemulsion gel has great potential for transdermal application of celecoxib.

Acknowledgement

The authors are thankful to Dr. Noha Nagah, Lecturer of Pharmacology, Cairo University, for performing the rat paw edema experiment.

References

- Frampton JE, Keating GM. Celecoxib: A review of its use in the management of arthritis and acute pain. *Drugs*. 2007; 67:2433-2472.
- Clemett D, Goa KL. Celecoxib: A review of its use in osteoarthritis, rheumatoid arthritis and acute pain. *Drugs*. 2000; 59:957-980.
- Gaurel A, Martel AM, Castaner J. Celecoxib, anti-inflammatory, cyclo-oxygenase-2 inhibitor. *Drug Future*. 1997; 22:711-714.
- Cevc G, Vierl U. Nanotechnology and the transdermal route: A state of the art review and critical appraisal. *J Control Release*. 2010; 141:277-299.
- Shakeel F, Ramadan W. Transdermal delivery of anticancer drug caffeine from water-in-oil nanoemulsions. *Colloids Surf B Biointerfaces*. 2010; 75:356-362.
- Lawrence MJ, Rees GD. Microemulsion-based media as novel drug delivery systems. *Adv Drug Del Rev*. 2000; 45:89-121.
- Kreilgaard M. Influence of microemulsions on cutaneous drug delivery. *Adv Drug Del Rev*. 2002; 54:S77-S98.
- Danielsson I, Lindman B. The definition of microemulsion. *Colloids Surf*. 1981; 3:391-392.
- Alany RG, Rades T, Agatonovic-Kustrin S, Davies NM, Tucker IG. Effects of alcohols and diols on the phase behaviour of quaternary systems. *Int J Pharm*. 2000; 196:141-145.
- Rhee YS, Choi JG, Park ES, Chi SC. Transdermal delivery of ketoprofen using microemulsions. *Int J Pharm*. 2001; 228:161-170.
- Marti-Mestres G, Nielloud F. Emulsions in health care applications – an overview. *J Disperse Sci Tech*. 2002; 23:419-439.
- Ambade KW, Jadhav KR, Gambhire MN, Kurmi SD, Kadam VJ, Jadhav KR. Formulation and evaluation of flurbiprofen microemulsion. *Curr Drug Deliv*. 2008; 5:32-41.
- Kamal MA, Limura N, Nabekura T, Kitagawa S. Enhanced skin permeation of diclofenac by ion-pair formation and further enhancement by microemulsion. *Chem Pharm Bull (Tokyo)*. 2007; 55:368-371.
- Chen H, Mou D, Du D, Chang X, Zhu D, Liu J, Xu H, Yang X. Hydrogel-thickened microemulsion for topical administration of drug molecule at an extremely low concentration. *Int J Pharm*. 2007; 341:78-84.
- Zhao X, Liu J, Zhang X, Li Y. Enhancement of transdermal delivery of theophylline using microemulsion vehicle. *Int J Pharm*. 2006; 327:58-64.
- Park ES, Cui Y, Yun BJ, Ko IJ, Chi SC. Transdermal delivery of piroxicam using microemulsions. *Arch Pharm Res*. 2005; 28:243-248.
- Baboota S, Shakeel F, Ahuja A, Ali J, Shafiq S. Design, development and evaluation of novel nanoemulsion formulations for transdermal potential of celecoxib. *Acta Pharm*. 2007; 57:315-332.
- Such H, Jun HW. Physicochemical and release studies of naproxen in poloxamer gels. *Int J Pharm*. 1996; 129:13-20.
- Aboofazeli R, Lawrence MJ. Investigations into the formation and characterization of phospholipid microemulsions: I Pseudo-ternary phase diagrams of systems containing water-lecithin-alcohol-isopropyl myristate. *Int J Pharm*. 1993; 93:161-175.
- Aboofazeli R, Lawrence CB, Wicks SR, Lawrence MJ. Investigations into the formation and characterisation of phospholipid microemulsions. III. Pseudo-ternary phase diagrams of systems containing water-lecithin-isopropyl myristate and either an alkanolic acid, amine, alkanediol, polyethylene glycol alkyl ether or alcohol as cosurfactant. *Int J Pharm*. 1994; 111:63-72.
- Nour SA, Shalaby SH, Afify NN, Abd El-Aal S, Mekhael MK. Formulation and evaluation of econazole nitrate emulgels. *J Drug Res Egypt*. 2002; 24:63-71.
- Demartine ML, Cussler EL. Predicting subjective spreadability, viscosity and stickiness. *J Pharm Sci*. 1975; 64:976-982.
- Lucero MT, Vigo J, Leon MJ. The influence of anti-oxidant on the spreadability of alpha-tocopherol gels. *Drug Develop Ind Pharm*. 1994; 20:2315-2322.
- Wissing SA, Müller RH. Solid lipid nanoparticles as carrier for sunscreens: *In vitro* release and *in vivo* skin penetration. *J Control Release*. 2002; 81:225-233.
- Higuchi T. Physical chemical analysis of percutaneous absorption process from creams and ointments. *J Soc Cosmet Mater*. 1960; 11:85-97.
- Subramanian N, Ghosal SK, Moulik SP. Enhanced *in vitro* percutaneous absorption and *in vivo* anti-inflammatory effect of a selective cyclooxygenase inhibitor using microemulsion. *Drug Dev Ind Pharm*. 2005; 31:405-416.
- Osborne DW, Ward AJ, O'Neill KJ. Microemulsions as topical drug delivery vehicles: *In-vitro* transdermal studies of a model hydrophilic drug. *J Pharm Pharmacol Comm*. 1991; 43:450-454.
- Trotta M, Pattarino F, Gasco MR. Influence of counter ions on the skin permeation of methotrexate from water-oil microemulsions. *Pharm Acta Helv*. 1996; 71:135-140.
- Brime B, Moreno MA, Frutos G, Ballesteros MA, Frutos P. Amphotericin B in oil-water lecithin-based microemulsions: Formulation and toxicity evaluation. *J Pharm Sci*. 2002; 91:1178-1185.
- Winter CA. Anti-inflammatory testing methods: Comparative evaluation of indomethacin and other agents. *Int Symp Nonst Anti-inflamm Drugs*. 1965; 82:190-202.
- Winter CA, Risley EA, Nuss GW. Carrageenan induced oedema in hind paws of the rats as an assay for anti-inflammatory drugs. *Proc Soc Exp Biol Med*. 1962; 111:544-547.
- Dhavan BN. Organization of biological screening program for natural products. *Proceedings of UNESCO-CDRI Workshop on Use of Pharmacological Techniques for the Study of Natural Products*. Central Drug Research Institute Lucknow. 1992; pp. 3-29.
- Draize J, Woodward G, Calvery H. Methods for the study

- of irritation and toxicity of substances applied topically to the skin and mucous membranes. *J Pharmacol Exp Ther.* 1944; 82:377-379.
34. Kaur K, Jain S, Sapra B, Tiwary AK. Niosomal gel for site-specific sustained delivery of anti-arthritic drug: *In vitro-in vivo* evaluation. *Curr Drug Deliv.* 2007; 4:276-282.
 35. Malcolmson C, Satra C, Kantaria S, Sidhu A, Lawrence MJ. Effect of oil on the level of solubilization of testosterone propionate into nonionic oil-in-water microemulsions. *J Pharm Sci.* 1998; 87:109-116.
 36. Hua L, Weisan P, Jiayu L, Ying Z. Preparation, evaluation, and NMR characterization of vinpocetine microemulsion for transdermal delivery. *Drug Dev Ind Pharm.* 2004; 30:657-666.
 37. Kogan A, Garti N. Microemulsions as transdermal drug delivery vehicles. *Adv Colloids Interface Sci.* 2006; 123-126:369-385.
 38. Von Corswant C, Söderman O. Effect of adding isopropyl myristate to microemulsions based on soybean phosphatidylcholine and triglycerides. *Langmuir.* 1998; 14:3506-3511.
 39. Häntzschel D, Enders S, Kahl H, Quitzsch K. Phase behavior of quaternary systems containing carbohydrate surfactants-water-oil-cosurfactant. *Phys Chem Chem Phys.* 1999; 1:5703-5710.
 40. Trotta M, Ugazio E, Peira E, Pulitano C. Influence of ion pairing on topical delivery of retinoic acid from microemulsions. *J Control Release.* 2003; 86:315-321.
 41. Djordjevic L, Primorac M, Stupar M, Krajisnik D. Characterization of caprylocaproyl macrogolglycerides based microemulsion drug delivery vehicles for an amphiphilic drug. *Int J Pharm.* 2004; 271:11-19.
 42. Sintov AC, Botner S. Transdermal drug delivery using microemulsion and aqueous systems: Influence of skin storage conditions on the *in vitro* permeability of diclofenac from aqueous vehicle systems. *Int J Pharm.* 2006; 311:55-62.
 43. Aboofazeli R, Mortazavi SA, Khoshnevis P. *In vitro* release study of sodium salicylate from lecithin based phospholipid microemulsions. *Iranian J Pharm Res.* 2003; 2:95-101.
 44. Yamaguchi M, Yasueda S, Isowaki A, Yamamoto M, Kimura M, Inada K, Ohtori A. Formulation of an ophthalmic lipid emulsion containing an anti-inflammatory steroidal drug, difluprednate. *Int J Pharm.* 2005; 301:121-128.
 45. Shakeel F, Baboota S, Ahuja A, Ali J, Aqil M, Shafiq S. Nanoemulsions as vehicles for transdermal delivery of aceclofenac. *AAPS PharmSciTech.* 2007; 8:E104.
 46. Rhee YS, Choi JG, Park ES, Chi SC. Transdermal delivery of ketoprofen using microemulsions. *Int J Pharm.* 2001; 228:161-170.
 47. Yuan Y, Li SM, Mo FK, Zhong DF. Investigation of microemulsion system for transdermal delivery of meloxicam. *Int J Pharm.* 2006; 321:117-123.
 48. Zvonar A, Rozman B, Rogac BM, Gašperlin M. The influence of microstructure on celecoxib release from a pharmaceutically applicable system: Miglyol 812®/labrasol®/plurol oleique®/water mixtures. *Acta Chim Slov.* 2009; 56:131-138.
 49. Desai KH. Enhanced skin permeation of rofecoxib using topical microemulsion gel. *Drug Dev Res.* 2004; 63:33-40.
 50. Constantinides PP, Yiv SH. Particle size determination of phase-inverted water-in-oil microemulsions under different dilution and storage conditions. *Int J Pharm.* 1995; 115:225-234.
 51. Shah VP. Skin penetration enhancers: Scientific perspectives. In: *Drug Permeation Enhancement; Theory and Applications* (Hsieh DS, ed.). Marcel Dekker, New York, USA, 1994; pp. 19-24.
 52. Kogan A, Kesselman E, Danino D, Aserin A, Garti N. Viability and permeation across Caco-2 cells of CBZ solubilized in fully dilutable microemulsions. *Colloids Surf B Biointerfaces.* 2008; 66:1-12.
 53. Ceschel G, Bergamante V, Maffei P, Lombardi Borgia S, Calabrese V, Biserni S, Ronchi C. Solubility and transdermal permeation properties of a dehydroepiandrosterone cyclodextrin complex from hydrophilic and lipophilic vehicles. *Drug Deliv.* 2005; 12:275-280.
 54. Lippacher A, Muller RH, Mäder K. Liquid and semisolid SLN™ dispersions for topical application: Rheological characterization. *Eur J Pharm Biopharm.* 2004; 58:561-567.
 55. Walters KA, Watkinson AC, Brain KR. *In vitro* skin permeation evaluation: The only realistic option. *Int J Cosmet Sci.* 1998; 20:307-316.
 56. Chen H, Chang X, Du D, Liu J, Xu H, Yang X. Microemulsion-based hydrogel formulation of ibuprofen for topical delivery. *Int J Pharm.* 2006; 315:52-58.
 57. Zhu W, Yu A, Wang W, Dong R, Wu J, Zhai G. Formulation design of microemulsion for dermal delivery of penciclovir. *Int J Pharm.* 2008; 360:184-190.
 58. Paolino D, Ventura CA, Nisticò S, Puglisi G, Fresta M. Lecithin microemulsions for the topical administration of ketoprofen: Percutaneous adsorption through human skin and *in vivo* human skin tolerability. *Int J Pharm.* 2002; 244:21-31.

(Received August 1, 2010; Revised September 1, 2010; Re-revised September 8, 2010; Accepted September 19, 2010)

Original Article**Preparation and characterization of oxybenzone-loaded solid lipid nanoparticles (SLNs) with enhanced safety and sunscreens efficacy: SPF and UVA-PF**Rania A. Sanad¹, Nevine S. Abdel Malak^{2,*}, Tahany S. El-Bayoomy¹, Alia A. Badawi²¹ Department of Pharmaceutics, National Organization of Drug Control and Research (NODCAR), Cairo, Egypt;² Department of Pharmaceutics, Faculty of Pharmacy Cairo University, Cairo, Egypt.

ABSTRACT: The objective of the current study was to formulate solid lipid nanoparticles of oxybenzone to enhance its sunscreens efficacy while reducing its side effects. Solid lipid nanoparticles (SLNs) of oxybenzone were prepared by the solvent diffusion method. A complete 2⁴ factorial design was used to optimize preparations. The study design involves the investigation of four independent variables, namely lipid type (Glyceryl monostearate, GMS; and Witepsol E85, WE85), lipid concentration (5 and 10%), polyvinyl alcohol (PVA) concentration (1 and 2%), and ethanol/acetone ratios (1:1 and 3:1, v/v), in terms of their effect on the particle size and entrapment efficiency. GMS was found to significantly increase the p.s. and EE%. SLNs prepared using 10% lipid had slower drug release compared to those prepared using 5%. The candidate oxybenzone-loaded SLN formula (SLN2) consisting of 0.5% oxybenzone, 10% GMS, 1% PVA, and ethanol/acetone (1:1, v/v) was then formulated into a gel and compared to the corresponding free oxybenzone nanosuspension and placebo SLN. The formulations were evaluated for skin irritation, *in vitro* sun protection factor, and ultraviolet A protection factors. The incorporation of oxybenzone into solid lipid nanoparticles greatly increased the SPF and UVA protection factor of oxybenzone more than five-fold while providing the advantage of overcoming skin irritancy problems.

Keywords: Solid lipid nanoparticle, oxybenzone, skin irritation, Vitro-Skin[®], sun protection factor, UVA protection factor

*Address correspondence to:

Dr. Nevine Shawky Abdel Malak, Faculty of Pharmacy, Cairo University, Kasr El Ainy Street, 11562 Cairo, Egypt.
e-mail: pharmnova@yahoo.com

1. Introduction

Sunlight is composed of a continuous spectrum of electromagnetic radiation that is divided into three main wavelengths: ultraviolet (UV), visible, and infrared (I). UV light is further divided into UVA (320-400 nm), which penetrates the skin and reaches the dermis, causing damage such as immediate and delayed tanning reactions, loss of collagen, diminution in the quantity of blood vessels, and skin photosensitization. UV light is also divided into UVB (290-320 nm), which is the principal cause of sunburn (erythema) and tanning (melanogenesis), and UVC (200-290 nm), which is totally absorbed by the ozone layer (2).

The use of sunscreens to protect against harmful UV radiation has become indispensable to daily life due to the worldwide decrease in the ozone layer and the resulting increase in skin cancer incidents (3). Sunscreens have been divided into chemical absorbers and physical blockers on the basis of their mechanism of action, namely absorbance and reflection (4).

Oxybenzone, a widely used lipophilic, is a broad-spectrum chemical sunscreen agent that effectively absorbs UVB, some UVA, and some UVC light. However, it is the most common cause of photoallergic contact dermatitis (5). Systemic absorption of oxybenzone following topical application to the skin has also been reported (6). While penetration is desired for drugs, it is not for sunscreens because it leads to loss of activity and undesired side effects (7). Therefore, there is an urgent need for the development of safer oxybenzone systems. This can be achieved by formulations that penetrate the skin less or by formulations with a reduced amount of potentially dangerous oxybenzone that maintain the sun protection factor by other means, e.g. carriers with sun-blocking characteristics (3).

Solid lipid nanoparticles have served as carriers for various pharmaceutical and cosmetic actives. These lipid nanoparticles have been found to act as physical sunscreens on their own, i.e. they have the ability to scatter/reflect incoming UV radiation. Incorporation of chemical sunscreens into the solid lipid matrix of the solid

lipid nanoparticle (SLN) prevents penetration of the skin and resulting side-effects (4).

The solvent diffusion method is a technique for preparing SLNs. This technique is characterized by using pharmaceutically acceptable organic solvents, easy handling, and a fast production process (8).

The UV protection properties of the nanoparticles can be described in terms of the sun protection factor (SPF) like in the case of any other sunscreen product. However, the SPF mainly represents the protection against UVB. For this reason, newly developed sunscreens have to provide a description of the protection they provide against not only UVB radiation but also UVA radiation (9).

Vitro-Skin[®], a registered trademark of IMS Inc. (Portland, ME, USA), is an advanced testing substrate used for *in vitro* measurement of SPF. It contains both optimized protein and lipid components and is designed to have topography, pH, critical surface tension, and ionic strength similar to human skin (10). This substrate provides the most consistent correlation with published *in vivo* SPF measurements (11).

The present study attempted to prepare and evaluate oxybenzone-loaded SLNs. A candidate formula with optimum physicochemical characterization was then selected. This formula was then formulated into a gel. A skin irritation test was performed and the *in vitro* SPF and UVA protection factor of free oxybenzone and the selected formula before and after its formulation into a gel were measured using Vitro-Skin[®]. Previously published research has not used Vitro-Skin[®] to determine the SPF and UVAPF of sunscreen in SLNs.

2. Materials and Methods

2.1. Materials

Oxybenzone was obtained from International Specialty Products, USA. Glyceryl monostearate (GMS), which is a mixture of 40-50% mono-, 30-45% di-, and 5-15% triglycerides esters of stearic acid (C₂₁) and palmitic acid (C₁₉) with a melting point of 55-66°C, was obtained from Carl Roth GmbH, Karlsruhe, Germany. Wittepsol E85 (WE85), which is a mixture of 5% mono-, 29% di-, and 66% triglycerides esters of fatty acids (C₈-C₁₈) and with a melting point 42-44°C, was obtained from Dynamit-Nobel Chemicals, Germany. Polyvinyl alcohol (PVA) of average molecular weight 146,000-186,000 was obtained from Celanese, Dallas, TX, USA. Ethanol 95% and acetone were obtained from Honeywell Riedel-de Haen, Seelze, Germany. Carbopol 934 was obtained from Goodrich Chemical Co., Avon Lake, OH, USA. Vitro-Skin[®] was obtained from IMS Inc. (Portland, ME, USA). Transpore[™] Surgical Tape was obtained from 3M Australia Pty Ltd., Pymble, NSW, Australia. A hydrophobic filter assembly, a membrane filter with 0.2- μ m diameter pores, was obtained from Versapor, German Sciences, Germany. All other chemicals and

solvents were of analytical grade.

2.2. Design of the experiments

A complete 2⁴ factorial design was used to optimize preparations of oxybenzone SLNs. The study design involved the investigation of four independent variables, namely lipid type, lipid concentration, PVA concentration, and organic solvent ratio, and their effect on the particle size and entrapment efficiency of oxybenzone SLNs. Table 1 summarizes independent variables along with their levels. The experimental results were analyzed using StatView version 4.57 software (Abacus Concept, Piscataway, NJ, USA).

2.3. Preparation of oxybenzone SLNs

SLNs loaded with 5% oxybenzone were prepared by the solvent diffusion method in an aqueous system (12) with slight modification. The amount of the drug to be added (in grams) was calculated as a percentage of the lipid matrix as follows: 100 g of a 10% SLNs dispersion loaded with 5% drug containing 10 g solid consisting of 9.5 g lipid and 0.5 g drug (13). The lipid-oxybenzone mixture was completely dissolved in a 12-mL mixture of ethanol and acetone (1:1 or 3:1, v/v) in a water bath at 50°C. The resultant lipid solution was poured into 240 mL of an aqueous phase containing PVA (1 or 2%, w/v) under mechanical agitation using a mechanical stirrer (Falc Instruments, Treviglio, Italy) at 400 rpm in a water bath at 70°C for 5 min. The obtained dispersion was allowed to cool to room temperature while stirring with a magnetic stirrer to get rid of the organic solvents, and then oxybenzone-loaded SLNs were finally obtained. The placebo SLN dispersions were prepared exactly in the same manner without adding the drug (14). An overview of the composition of the SLNs is shown in Table 2.

2.4. Characterization of oxybenzone SLNs

2.4.1. Transmission electron microscopy (TEM)

The morphology of the oxybenzone SLNs (selected samples SLN2 and SLN10) was examined with a transmission electron microscope (JEM-100S, Jeol Ltd.,

Table 1. Planned 2⁴ factorial design for the optimization of the prepared oxybenzone SLN dispersions

| Independent variables | Levels | |
|---|--------|------|
| | +1 | -1 |
| Type of lipid | GMS | WE85 |
| Concentration of lipid (% w/w) ^a | 5 | 10 |
| Concentration of PVA (% w/w) ^a | 1 | 2 |
| Organic solvent ratio (ethanol/acetone, v/v) ^b | 1:1 | 3:1 |

^a Percentage of the final SLN dispersion; ^b Ratio with respect to the total organic solvent mixture.

Table 2. Composition of the prepared oxybenzone SLN dispersions

| Formulation code | Lipid Type | | PVA (% w/w) ^a | Ethanol (mL) ^b | Acetone (mL) ^b | Oxybenzone (% w/w) ^a |
|------------------|-------------|--------------|--------------------------|---------------------------|---------------------------|---------------------------------|
| | GMS (% w/w) | WE85 (% w/w) | | | | |
| SLN1 | 5 | 0 | 1 | 6 | 6 | 0.25 |
| SLN2 | 10 | 0 | 1 | 6 | 6 | 0.5 |
| SLN3 | 5 | 0 | 1 | 9 | 3 | 0.25 |
| SLN4 | 10 | 0 | 1 | 9 | 3 | 0.5 |
| SLN5 | 5 | 0 | 2 | 6 | 6 | 0.25 |
| SLN6 | 10 | 0 | 2 | 6 | 6 | 0.5 |
| SLN7 | 5 | 0 | 2 | 9 | 3 | 0.25 |
| SLN8 | 0 | 0 | 2 | 9 | 3 | 0.5 |
| SLN9 | 0 | 5 | 1 | 6 | 6 | 0.25 |
| SLN10 | 0 | 10 | 1 | 6 | 6 | 0.5 |
| SLN11 | 0 | 5 | 1 | 9 | 3 | 0.25 |
| SLN12 | 0 | 10 | 1 | 9 | 3 | 0.5 |
| SLN13 | 0 | 5 | 2 | 6 | 6 | 0.25 |
| SLN14 | 0 | 10 | 2 | 6 | 6 | 0.5 |
| SLN15 | 0 | 5 | 2 | 9 | 3 | 0.25 |
| SLN16 | 0 | 10 | 2 | 9 | 3 | 0.5 |

^a Percentage in the final SLN dispersion; ^b Volume in the final SLN dispersion.

Tokyo, Japan). Samples were prepared by a negative staining technique. The SLNs were dispersed directly into doubly distilled water. Then, a copper grid coated with collodion film was placed in the solution several times. After staining with 2% (w/v) phosphotungstic acid solution and drying at room temperature, the sample was ready for TEM investigation at 70 kV (15).

2.4.2. Particle size analysis

Particle size and polydispersity index (PI) were determined using a laser scattering particle size distribution analyzer (detection limit 0.2-2,000 μm ; LA-920, Horiba, Kyoto, Japan). One day after production, SLN dispersions were diluted with filtered doubly distilled water and subsequently analyzed. Three analyses were performed for each sample and the average values were used. The obtained data were evaluated using the volume distribution (d10%, d50%, d90%). This meant that if the diameter 90% (d90%) was registered as 1 μm then 90% of particles would have a diameter of 1 μm or less (16).

2.4.3. Determination of percent oxybenzone entrapment efficiency (% EE)

The entrapment efficiencies of prepared systems were determined by measuring the concentration of free drug in the dispersion medium. The drug-loaded SLN dispersion was uniformly mixed by gentle shaking; 1.0 mL of this dispersion was diluted with 9.0 mL methanol, centrifuged with a high-speed refrigerated centrifuge (Sigma 3K30, DJB Labcare, Buckinghamshire, UK) for 45 min at 16,000 rpm and then filtered using a Millipore membrane (0.2 μm). The filtrate was collected and appropriately diluted with methanol and measured spectrophotometrically (Model UV-2450, Shimadzu,

Kyoto, Japan) at a λ_{max} of 286 nm. The percent entrapment efficiency % EE was calculated using the following equation (14):

$$\text{Entrapment Efficiency (\% EE)} = \frac{W_a - W_s}{W_a} \times 100 \quad \text{--- Eq. 1}$$

where W_a and W_s were the weight of drug added in system and the analyzed weight of drug in supernatant, respectively.

2.4.4. In vitro release studies of oxybenzone from SLNs: Franz diffusion cells

In vitro release studies of oxybenzone were done using static Franz glass diffusion cells (17). These cells consist of donor and receptor chambers separated by a cellulose membrane (MEMBRA-CEL dialysis tubing with molecular weight cutoff of 3,500-7,000 Da obtained from Serva Electrophoresis GmbH, Heidelberg, Germany); the area of diffusion was 1.7 cm^2 . The dialysis membrane was hydrated in receptor medium, which consisted of a methanolic buffer solution (phosphate-buffered saline, pH7.4/methanol, 3:2, v/v), for 12 h before mounting into a Franz diffusion cell. An oxybenzone SLN dispersion (2 mg/cm^2) was placed in the donor chamber and the receptor chamber was filled with 7.5 mL receptor medium and stirred continuously at 100 rpm at 37°C in order to ensure a surface skin temperature of 32°C on the surface of the membrane (17). After 1, 2, 3, 4, 5, 6, 7, and 8 h, samples were withdrawn from the receptor chamber through a side-arm tube. After each withdrawal of sample, an equal volume of receptor medium was added to the receptor chamber to maintain a constant volume throughout the study. Samples were analyzed for oxybenzone concentration using ultraviolet spectrophotometry at 289.4 nm. Measurements were carried out in triplicate.

Table 3. Composition of the selected dispersions and corresponding gel formulations

| Formulation | Composition |
|-------------|---|
| pSLN2 | 10% GMS, ethanol/acetone (1:1, v/v) in 1% PVA aqueous solution |
| SLN2 | 0.5% oxybenzone (with respect to total formulation), 10% GMS, ethanol/acetone (1:1, v/v) in 1% PVA aqueous solution |
| 0.5% Oxy. | 0.5% oxybenzone (with respect to total formulation), ethanol/acetone (1:1, v/v) in 1% PVA aqueous solution |
| pSLN2G | 1% carbopol 934 incorporated in pSLN2 dispersion |
| SLN2G | 1% carbopol 934 incorporated in SLN2 dispersion |
| 0.5% Oxy.G | 1% carbopol 934 incorporated in 0.5% oxybenzone dispersion |

2.5. Formulation of an SLN-based hydrogel

Based on the previously described characterization, SLN2 with optimal physicochemical properties was selected. The selected SLN dispersion was formulated into a hydrogel by adding 1% (w/w) Carbopol 934 under magnetic stirring at 800 rpm. Stirring was continued till Carbopol was dispersed. The dispersions were neutralized using triethanolamine solution (18). Hydrogel formulations containing 0.5% oxybenzone suspension and placebo SLN2 were prepared for comparison. The composition of gel formulations is shown in Table 3.

2.6. Characterization of the prepared gels

2.6.1. Rheological studies

The viscosity and rheological behavior of the gel formulations were determined using a Cone and Plate viscometer (model HADV-II; Brookfield Engineering Laboratories, Middleboro, MA, USA). All measurements were carried out at a temperature of $25 \pm 1^\circ\text{C}$ using a spindle CP52. The rheological parameters of different gels were studied (19).

2.6.2. Skin irritation test

The study protocol and informed consent form were approved by an institutional review board (IRB00007140), and this study was conducted in accordance with the Declaration of Helsinki (20) and the Guidance for Good Clinical Practice of the International Conference on Harmonization (ICH) of Technical Requirements for Registration of Pharmaceuticals for Human Use (21).

Ten healthy subjects (ages 23-40 years) participated in this study. The participants were briefed on the study procedures, and written informed consent was obtained prior to procedures. Each formulation mentioned in Table 3 was applied once, at a dose of 0.3 g, to a surface area of 5 cm^2 on the forearms. The test specimen was then washed off with tap water after 6 h and skin was observed for any visible changes such as erythema (redness). The mean erythema scores were recorded (ranging from 0 to 4) in accordance with the Draize scale (22) as shown in Table 4.

Table 4. Draize grading scale (erythema formation)

| Skin response | Score |
|---|-------|
| No erythema | 0 |
| Slight erythema (barely perceptible-light pink) | 1 |
| Moderate erythema (dark pink) | 2 |
| Moderate to severe erythema (light red) | 3 |
| Severe erythema (extreme redness) | 4 |

2.6.3. *In vitro* UV-blocking ability

Transpore™ assay (7) is an *in vitro* method of investigating the UV-blocking ability of the investigated dispersions mentioned in Table 3. A concentration of 2 mg/cm^2 of the formulation was spread evenly on top of the Transpore™ tape mounted on a quartz cuvette. After a drying period of 15 min, the samples were scanned spectrophotometrically from 250 to 400 nm and the absorption was measured.

2.6.4. *In vitro* SPF and erythema UVA protection factor (EUVA-PF) measurement

Determination of the SPF of the formulations was done in accordance with the method described by Diffey and Robson (24). Vitro-Skin® was used for sample application. It was hydrated by placing it on the shelf of a closed, controlled-humidity chamber (containing 85% water/15% glycerin in its bottom) for 16-24 h prior to use (23) and then mounted on a quartz cuvette. The intensity of radiation transmitted through the substrate was determined automatically by recording the photocurrent in 5-nm increments from 290 to 400 nm. An appropriate weight (2 mg/cm^2) of each formulation mentioned in Table 3 was applied to the substrate surface by applying spots to several sites throughout the application area (4.5 cm^2). After a drying period of 15 min, transmission measurements were done. These experiments were performed in triplicate.

The *in vitro* SPF was calculated according to the following equation (24):

$$\text{SPF} = \frac{\sum_{290}^{400} E_{\lambda} B_{\lambda}}{\sum_{290}^{400} (E_{\lambda} B_{\lambda} \sqrt{\text{MPF}_{\lambda}})} \quad \text{--- Eq. 2}$$

where E_{λ} was the spectral irradiance of terrestrial sunlight under defined conditions, B_{λ} was erythema effectiveness, and MPF_{λ} was the monochromatic protection factor at each wavelength increment measured as the ratio of

the detector signal intensity without sunscreen applied to the substrate to that with sunscreen applied to the substrate. Given the UVA wavelength range (320-400 nm) and using the terms in the SPF equation, the *in vitro* erythral UVA protection factor was calculated according to the following equation (9):

$$\text{Erythral UV-A protection factor} = \frac{\sum_{320}^{400} E_{\lambda} B_{\lambda}}{\sum_{320}^{400} (E_{\lambda} B_{\lambda} \sqrt{\text{MPF}_{\lambda}})} \quad \text{--- Eq. 3}$$

3. Results and Discussion

3.1. Characterization of oxybenzone solid lipid nanoparticles

3.1.1. TEM

Figure 1 shows transmission electron micrographs of oxybenzone SLNs prepared with GMS and WE85 as lipid bases using the solvent diffusion technique. Both micrographs showed that the particles had nanometer-

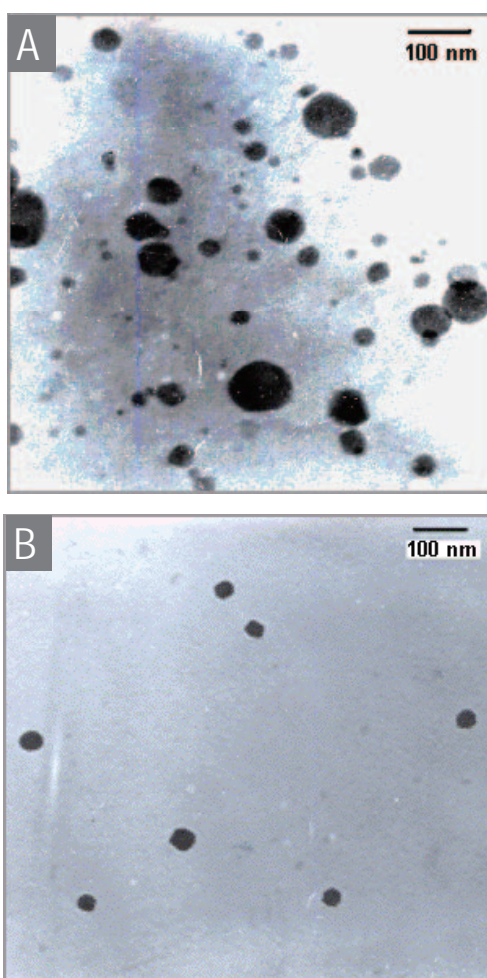


Figure 1. Transmission electron micrographs of oxybenzone-loaded SLNs using GMS (A) and WE85 (B) prepared by the solvent diffusion method in an aqueous system. Scale bar, 100 nm.

sized spherical shapes ranging from 20 to 100 nm for GMS SLNs and from 30 to 50 nm for WE85 SLNs; no rectangular oxybenzone crystals were visible. This could be due to the solvent diffusion procedure during the solvent diffusion to dispersion medium; the lipid matrix might form nanoparticles with a spherical shape to minimize surface energy (25). In addition, the use of GMS and WE85, which are considered to be chemically heterogeneous lipids that are mixtures of mono-, di-, and triglycerides in different portions, favored the formation of ideally spherical lipid nanoparticles (26).

3.1.2. Particle size analysis

In order to obtain more precise information on the size distribution, laser scattering was used (27). The mean particle size, volume size distribution (d10%, d50%, and d90%), and span (which is the measure of polydispersity index) of different SLNs are depicted in Table 5.

The results revealed that all of the prepared SLNs had a considerable small particle size with d90% less than 1 μm . The mean particle size of SLNs ranged from 0.209 ± 0.020 to 0.810 ± 0.032 μm . The sizes of the SLNs determined by laser scattering did not agree with TEM results. This might be because detection of the size of SLNs using laser scattering was carried out in an aqueous state. In such instances, lipid nanoparticles were highly hydrated and the diameters were 'hydrated diameters' that tended to be larger than their genuine diameters. In TEM sample preparation, all of the free water and even some of hydrated water was stained. This implies that the sizes of SLNs determined by TEM might be considerably smaller than their real diameters (28). The span values (Table 5), a characteristic parameter for the extent of particle size distribution, ranged from 0.347 to 0.687 for GMS SLNs and from 0.529 to 0.611 for WE85 SLNs. According to Muller and Schumann (29), these values contributed to a relatively broad size distribution. That said, a polydispersed particle dispersion is suitable for topical application (30).

Statistical analysis was done to evaluate the effect of the lipid type, the lipid concentration, the PVA concentration, and the organic solvent ratio on the particle size. GMS was found to significantly increase the particle size compared to WE85 ($p < 0.0001$). This could be due to GMS possessing a higher melting point ($54\text{--}66^{\circ}\text{C}$) (31) than WE85 ($42\text{--}44^{\circ}\text{C}$) (31) or to the fact that the average particle size of SLNs increases with higher melting lipids, indicating an effect of the higher viscosity of the dispersed phase (32). Additionally, lipids of shorter chain length have been found to yield SLNs of smaller particle size in comparison to those produced by lipids of longer chains (33). Therefore, WE85, which consists of glycerides with shorter hydrocarbon chains ($\text{C}_8\text{--}\text{C}_{18}$) compared to GMS (C_{19} and C_{21}) (31), produced smaller particles.

Table 5. Particle size distribution, mean particle size, polydispersity index, entrapment efficiency, and zeta potential values of different solid lipid nanoparticles dispersions

| Formulation code ^a | Mean volume distribution (μm) | | | Mean particle size (μm, mean ± S.D.) | PI ^b | EE% (mean ± S.D.) | Zeta potential (mean ± S.D.) |
|-------------------------------|-------------------------------|-------|-------|--------------------------------------|-----------------|-------------------|------------------------------|
| | d10% | d50% | d90% | | | | |
| SLN1 | 0.090 | 0.206 | 0.389 | 0.297 ± 0.011 | 0.341 | 44.8 ± 1.9 | -12.3 ± 0.5 |
| SLN2 | 0.200 | 0.389 | 0.704 | 0.590 ± 0.029 | 0.528 | 74.2 ± 2.5 | -47.0 ± 0.8 |
| SLN3 | 0.159 | 0.259 | 0.616 | 0.347 ± 0.02 | 0.531 | 43.2 ± 1.5 | -14.9 ± 0.6 |
| SLN4 | 0.281 | 0.540 | 0.961 | 0.420 ± 0.023 | 0.483 | 72.8 ± 1.1 | -21.5 ± 1.2 |
| SLN5 | 0.215 | 0.389 | 0.751 | 0.443 ± 0.018 | 0.513 | 48.0 ± 2.3 | -12.8 ± 0.7 |
| SLN6 | 0.220 | 0.390 | 0.833 | 0.474 ± 0.03 | 0.510 | 60.6 ± 3.5 | -12.6 ± 0.3 |
| SLN7 | 0.178 | 0.296 | 0.676 | 0.375 ± 0.026 | 0.557 | 38.4 ± 2.1 | -10.6 ± 1.0 |
| SLN8 | 0.564 | 0.800 | 0.968 | 0.810 ± 0.032 | 0.687 | 54.6 ± 1.6 | -17.8 ± 0.5 |
| SLN9 | 0.136 | 0.197 | 0.295 | 0.209 ± 0.02 | 0.581 | 30.0 ± 0.8 | -19.9 ± 0.8 |
| SLN10 | 0.166 | 0.276 | 0.759 | 0.383 ± 0.024 | 0.529 | 41.1 ± 1.3 | -8.8 ± 0.6 |
| SLN11 | 0.171 | 0.238 | 0.361 | 0.258 ± 0.019 | 0.611 | 27.7 ± 1.8 | -20.9 ± 0.9 |
| SLN12 | 0.159 | 0.259 | 0.599 | 0.335 ± 0.01 | 0.543 | 38.4 ± 2.4 | -26.5 ± 2.0 |
| SLN13 | 0.178 | 0.283 | 0.587 | 0.349 ± 0.022 | 0.558 | 24.6 ± 0.9 | -14.7 ± 0.9 |
| SLN14 | 0.182 | 0.265 | 0.481 | 0.322 ± 0.015 | 0.585 | 38.5 ± 3.1 | -47.6 ± 1.3 |
| SLN15 | 0.142 | 0.201 | 0.303 | 0.230 ± 0.017 | 0.606 | 10.9 ± 0.8 | -27.8 ± 2.0 |
| SLN16 | 0.190 | 0.296 | 0.948 | 0.494 ± 0.01 | 0.572 | 32.5 ± 1.4 | -13.1 ± 2.5 |

^a The composition of these formulations is shown in Table 2; ^b Polydispersity index.

Among the lipid concentrations used, 10% resulted in a significantly larger particle size than did 5% ($p < 0.0001$). When the concentration of lipid (GMS or WE85) was increased, the viscosity of the lipid-organic solvent diffusion phase also increased. This reduced the diffusion rates of the solute molecules, which are a critical parameter for the formation of SLNs prepared by the solvent diffusion method. In addition, the collision and aggregation of nanoparticles, which were facilitated by a high lipid concentration, led to the formation of larger particles (8,34).

Among the PVA concentrations used, 1% PVA was found to result in a significantly smaller particle size than did 2% ($p < 0.0001$). This might be due to the fact that the increase in PVA concentration from 1 to 2% increased the viscosity of the external aqueous phase (35). This resulted in a decrease in the net shear stress, reducing the diffusion speed and therefore increasing particle size (36). In addition, higher concentrations of the stabilizer (2% PVA) would not play any further role with regard to particle size once the optimum packing of the stabilizer (PVA) and the minimum droplet size was reached (37). Further addition of PVA caused an increase in nanoparticle size due to the accumulation of excess molecules at the particle surface; loops and tails were formed, eventually leading to bridging between the primary nanoparticles (38).

Concerning the effect of different ratios of organic solvents, ethanol:acetone at a ratio of 1:1 (v/v) was found to significantly decrease the particle size compared to 3:1 (v/v) ($p < 0.0001$), which meant that increasing the ethanol volume led to an increase in the particle size while increasing the acetone volume caused a decrease in the particle size of the prepared SLNs. This may be due to the lower boiling point of acetone (56.53°C) (31) compared to that of ethanol

(78.4°C) (31), so an organic solvent mixture (ethanol/acetone) at a ratio of 1:1 (v/v) would evaporate more rapidly than one at a ratio of 3:1 (v/v) (39). The higher organic solvent evaporation rate led to a higher solvent front kinetic energy, which accordingly increased the rate of diffusion of the solvent from the inner to the outer phase (the critical parameter determining the particle size) and resulted in smaller particles (40).

3.1.3. Zeta potential ζ

The zeta potential ζ values of the prepared SLNs are shown in Table 5. The values ranged from -8.8 mV to -47 mV. Zeta potential values of all formulations in this study were above |8-9| mV, which is a prerequisite for the stability of SLNs prepared using a steric stabilizer (PVA) (41). All SLNs were found to be negatively charged. This negative charge was likely caused by the slightly ionized fatty acids from the glycerides used (GMS and WE85) (42). Zeta potentials above |30 mV| were required for full electrostatic stabilization. However, many experiments demonstrated that electrostatic repulsion had the greatest impact on the stability of nanoparticles; the use of steric stabilizer also favored the formation of a stable nanoparticle dispersion (26).

3.1.4. Entrapment efficiency

The entrapment efficiency of oxybenzone within the different prepared SLNs is shown in Table 5. The entrapment efficiencies were found to range between 20.9 ± 0.8% and 74.3 ± 2.5%.

Concerning the effect of the lipid type, GMS was found to significantly increase the entrapment efficiency compared to WE85 ($p < 0.0001$). This could be due to an increase in the ratio of monoglycerides to more than

30% (GMS consists of 40-50% monoglycerides while WE85 consists of 5% monoglycerides), which might offer more room to accommodate the drug in the lipid matrix (43). In addition, the entrapment efficiency of the prepared SLNs increased as a result of the increased lipophilicity of the lipids used (44). GMS (C_{21}) is more lipophilic than WE85 (C_8-C_{18}) (31) since an increase in the alkyl chain length led to an increase in the lipophilicity of the molecule (45). As a result, GMS had greater accommodation for the lipophilic drug (oxybenzone) than did WE85. In addition, particles of larger sizes have been reported to possess higher entrapment efficiency (46). Therefore, the higher entrapment efficiency of GMS SLNs contributed to their larger particle size compared to WE85 SLNs.

A lipid concentration of 10% significantly increased the entrapment efficiency compared to a concentration of 5% ($p < 0.0001$). This could be due to the increase in the lipid concentration (10%), which led to increased lipophilicity that significantly increased the entrapment efficiency of oxybenzone. This agrees with the findings of Shah *et al.* (18), who observed that the entrapment efficiency of a drug increased in accordance with an increase in the amount of lipids.

Increasing the PVA concentration from 1 to 2% was found to significantly decrease the entrapment efficiency of oxybenzone within the prepared SLNs ($p < 0.0001$). One possible interpretation is that 1% PVA concentration provided sufficient covering of the lipid core so as to minimize possible leaching of the drug (15), while with an increased PVA concentration (2%) more molecules of the drug partitioned out rapidly into

the aqueous phase during the emulsification procedure due to the solubilizing and emulsifying effect of PVA (47). As a result, the entrapment efficiency decreased (38). This agrees with the findings of Paliwal *et al.* (15), who observed that the entrapment efficiency decreased when the amount of the emulsifier was increased.

With regard to ratios of organic solvents, a 1:1 (v/v) ethanol/acetone ratio provided significantly higher entrapment efficiency than did one of 3:1 (v/v). This increase in entrapment efficiency could be due to the increased ratio of ethanol, which might act as a co-emulsifier (48). As the amount of co-emulsifier increased with a constant amount of lipid, the surface of the SLNs formed was too small to adsorb all of the co-surfactant molecules. This might result in the formation of micellar solutions of the drug (oxybenzone). Hence the solubility of the drug in the water phase would increase. Therefore, the drug could partition from the SLNs into the formed micelles in the water phase, thereby reducing the final entrapment efficiency (38).

3.1.5. *In vitro* release study: Franz diffusion cells

The release of oxybenzone from SLNs was investigated for 8 h. The composition of the receptor medium was chosen because of the insufficient solubility of oxybenzone in aqueous media. Oxybenzone was readily soluble in the chosen receptor medium. Since the receptor medium was not intended to mimic skin conditions, it was adequate for the present *in vitro* investigations. Figure 2 shows the release of oxybenzone from the prepared SLNs.

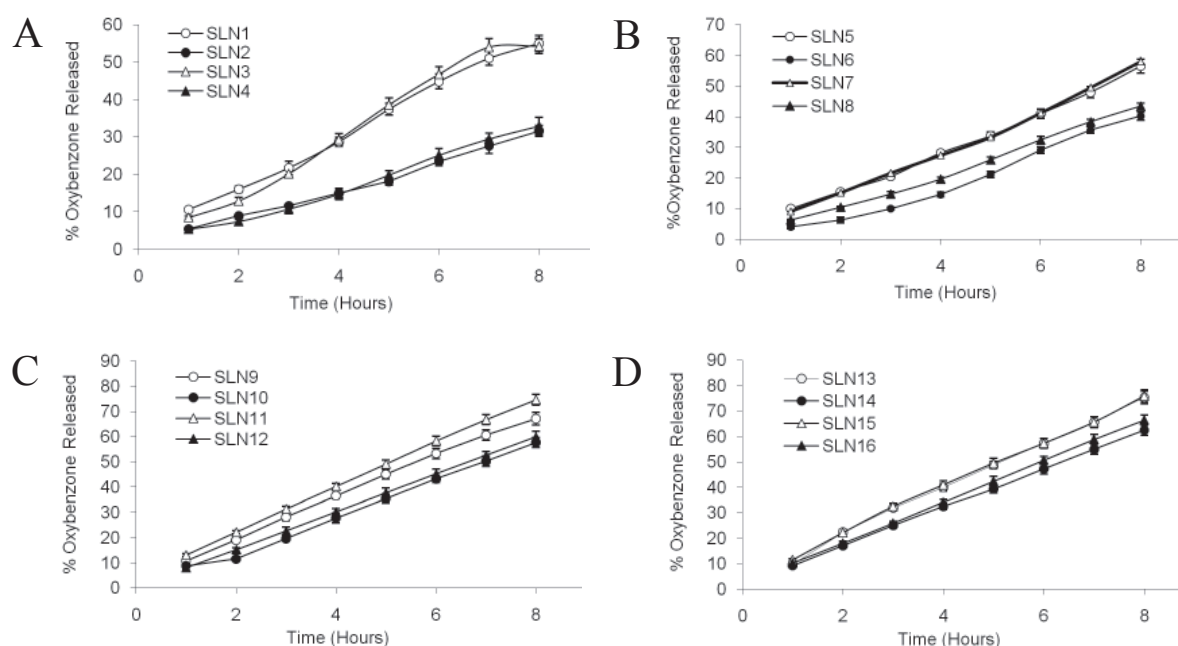


Figure 2. *In vitro* release profile of oxybenzone from different oxybenzone-loaded SLNs in phosphate-buffered saline, pH 7.4/methanol (3:2, v/v). (A) open circle, SLN1; closed circle, SLN2; open triangle, SLN3; closed triangle, SLN4. (B) open circle, SLN5; closed circle, SLN6; open triangle, SLN7; closed triangle, SLN8. (C) open circle, SLN9; closed circle, SLN10; open triangle, SLN11; closed triangle, SLN12. (D) open circle, SLN13; closed circle, SLN14; open triangle, SLN15; closed triangle, SLN16. Data are shown as mean \pm S.D., $n = 3$.

GMS SLNs were found to have slower release than did WE85 SLNs. Slow release of the drug from SLNs suggests homogeneous entrapment of the drug throughout the system (15). Consequently, GMS SLNs with higher entrapment efficiency than WE85 SLNs had slower release profiles. Other factors contributing to a fast release might be the large surface area and the high diffusion coefficient (small molecular size) (49). Therefore, WE85 SLNs with a smaller particle size and consequently higher surface area than GMS SLNs had more rapid release.

Among the lipid concentrations used, oxybenzone was released more easily from SLNs containing a lower lipid content (5%) than a high one (10%). Similar results were obtained by Souto *et al.* (50), who attributed this to the possible formation of a drug-enriched shell as SLNs might develop when using a low lipid concentration. At higher lipid concentration, a drug-enriched core was formed and lower release was observed.

In terms of PVA concentration, 2% PVA was found to result in faster release than 1% (w/w) PVA. This might be due to the diffusion of surfactant (PVA) into the receiver side, altering the barrier properties of the aqueous boundary layer and the permeability of the membrane and subsequently resulted in a high release velocity of drug in the SLN dispersion (51). Moreover, the existence of a large amount of surfactant increased the solubility of the drug in water, resulting in the re-partitioning of drug into the water phase. This allowed spots of the drug domain to be formed on the surface of the SLNs, resulting in faster release (52).

Based on previous characterizations, the SLN2 dispersion prepared using 10% GMS, 1% PVA, and a 1:1 (v/v) ethanol/acetone ratio had the highest EE%, the slowest drug release, the highest zeta potential, and a sufficiently small particle size, so it was chosen for formulation into a gel. The rheological properties, irritancy, UV blocking ability, SPF, and UVA-PF were studied and compared with that of placebo SLN2 and an oxybenzone suspension containing a concentration like that of SLN2 (0.5% with respect to the total formulation).

3.2. Characterization of the prepared gels

3.2.1. Rheological studies

As previously noted, conventional SLN aqueous dispersions contain about 10-20% (w/w) of lipid matrix and 80-90% (w/w) of water. As a result, liquid solid lipid dispersions possess a low viscosity. Therefore, liquid solid lipid dispersions usually have to be incorporated in convenient topical dosage forms like hydrogels to obtain a topical application form with the desired semisolid consistency (53).

Carbopol hydrogels have proven suitable for

nanoparticle incorporation (54). Thus, this study used Carbopol 934 because of its thermal stability, mucoadhesive properties, and optimal rheological properties in order to prepare semi-solid formulations based on SLNs (55).

The rheological properties of a semisolid drug carrier are very important physical parameters for a topical application of that drug (56). Figure 3 shows the rheograms of the prepared gel formulations. The results revealed that gel formulations containing SLN2, either as a placebo or oxybenzone-loaded SLNs, exhibited pseudoplastic flow characteristics with thixotropy. Needless to say, thixotropy is a desirable feature for semisolid drug carriers for use in a topical application (57). As shown in Figures 3A and B, SLN2 gel formulations, either as a placebo or oxybenzone-loaded SLNs, had greater thixotropy (hysteresis area). This could be due to the negatively charged SLNs, which may affect the restoration of hydrogen bonding in the gel. Therefore, restructuring of the three-dimensional network structure took longer and consequently increased the thixotropy of SLN-enriched gels (56).

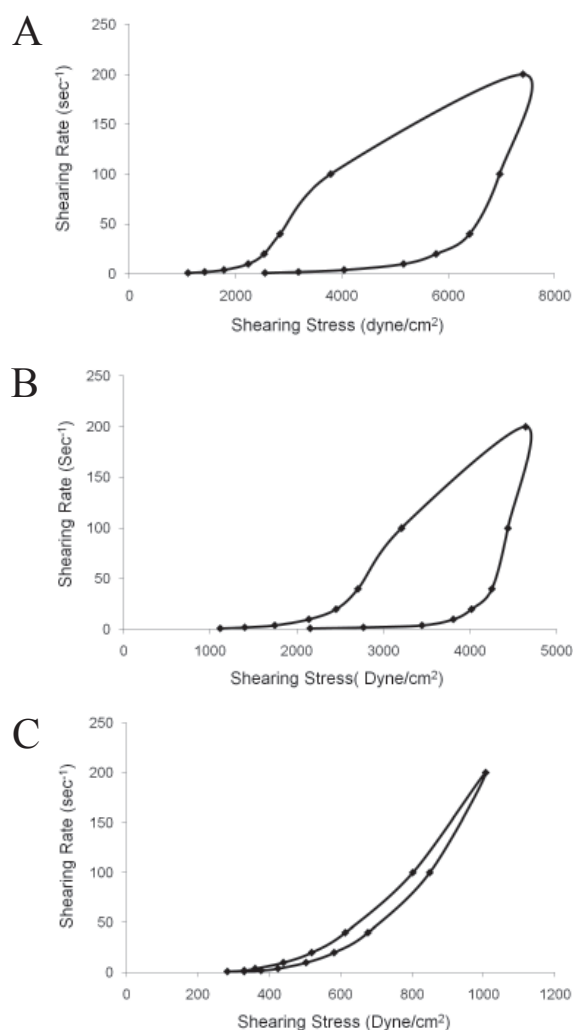


Figure 3. Rheograms of placebo SLNG (A), SLN2G (B), and 0.5% free oxybenzone gels (C).

Table 6. Results from a skin irritation test of the selected dispersions and corresponding gel formulations

| Formulation ^a | Reaction in volunteers ^b | | | | | | | | | |
|--------------------------|-------------------------------------|-----------|-----------|-----------|-----------|-----------|-----------|-----------|-----------|------------|
| | Subject 1 | Subject 2 | Subject 3 | Subject 4 | Subject 5 | Subject 6 | Subject 7 | Subject 8 | Subject 9 | Subject 10 |
| pSLN2 | 0 | 0 | 0 | 0 | 0 | 0 | 0 | 0 | 0 | 0 |
| SLN2 | 0 | 0 | 0 | 1 | 0 | 1 | 0 | 0 | 0 | 0 |
| 0.5% Oxy. | 2 | 2 | 2 | 2 | 2 | 3 | 2 | 1 | 2 | 2 |
| pSLN2G | 0 | 0 | 0 | 0 | 0 | 0 | 0 | 0 | 0 | 0 |
| SLN2G | 0 | 0 | 0 | 1 | 0 | 1 | 0 | 0 | 0 | 0 |
| 0.5% Oxy.G | 2 | 2 | 2 | 3 | 2 | 3 | 2 | 2 | 2 | 2 |

^aThe composition of these formulations is shown in Table 3; ^bThe scoring system is described in Table 4.

3.2.2. Skin irritation test

Results of the skin irritation test are shown in Table 6. No irritation or erythema was observed for placebo SLN2 either in dispersion or gel form, and only very slight erythema (score = 1) was observed in two volunteers with an oxybenzone-loaded SLN2 dispersion or gel. Conversely, a 0.5% oxybenzone suspension and gel resulted in well defined erythema in seven volunteers (score = 2) and moderate to severe erythema (score = 3) in two volunteers. This could be due to the role of oxybenzone-loaded SLN2 in protecting the skin from direct contact with the drug (oxybenzone), which was encapsulated in the lipid matrix. Such encapsulation allows for gradual drug delivery and paves the way to reducing drug-induced skin irritation (58). This agrees with the findings of Kuchlera *et al.* (59), who observed that drug-loaded SLNs were significantly less irritating to the skin compared to the effects of marketed products containing the drug in free form.

3.2.3. In vitro UV-blocking ability

The wavelength scans of the placebo SLN2, oxybenzone-loaded SLN2, and 0.5% oxybenzone dispersions are shown in Figure 4. The absorbance caused by placebo SLN2 was found to be higher than the absorption caused by the 0.5% oxybenzone suspension. This could be due to the particulate character of SLNs since they act as physical sunscreens on their own (60). This agrees with the findings of Wissing and Muller (4), who observed that placebo SLNs were more effective as a sunscreen than reference emulsions containing tocopherol acetate.

Oxybenzone-loaded SLN2 was also found to have a typical absorption pattern of oxybenzone with two peaks at about 340 and 290 nm, indicating that oxybenzone-loaded SLN2 still had absorption in the UVB range (290-320 nm) and the UVA range (320-400 nm). That said, this absorption was about three times higher than the absorbance caused by the 0.5% oxybenzone suspension. This could be due to the fact that the incorporation of chemical sunscreens (oxybenzone) in SLNs led to synergistic UV-blocking behavior (60). Similarly, Song *et al.* (61) observed that 3,4,5-trimethoxybenzoylchitin (sunscreens) had higher UV absorption

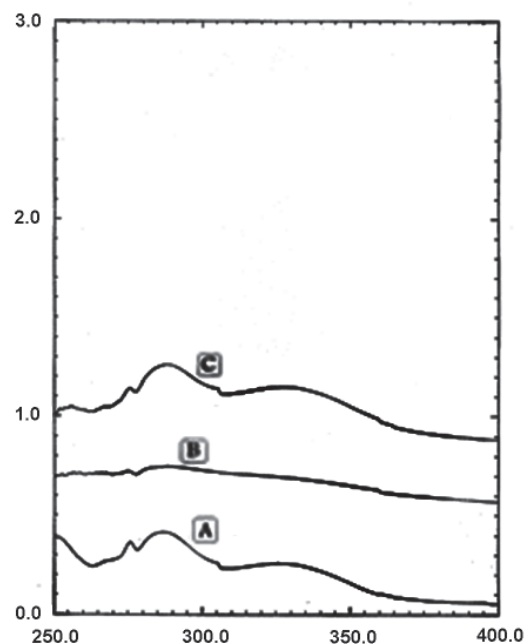


Figure 4. Wavelength scans of 0.5% oxybenzone nanosuspension (0.5% Oxy.) (A), placebo SLN dispersion (PSLN) (B), and oxybenzone-loaded SLN dispersion (SLN2) (C) obtained by the Transpore™ tape assay.

when it was incorporated in SLNs as a vehicle because SLNs provide stronger reflectance of UV radiation.

3.2.4. In vitro SPF and EUVA-PF measurement

The SPF values of the investigated formulations are illustrated graphically in Figure 5. The placebo SLN2 dispersion had a higher SPF value (4.90 ± 0.42) than did the suspension containing 0.5% oxybenzone without lipids (1.80 ± 0.12). When SLN2 was loaded with 0.5% oxybenzone, the resulting SPF values increased by about 6-fold compared to those of the 0.5% oxybenzone suspension (11.13 ± 0.70).

The EUVA-PF is a parameter analog to the SPF and it represents a number derived from the ratio for the duration of exposure to a UV spectrum between 320 nm and 400 nm to produce erythema on human skin in the presence or absence of a sunscreen product. The higher the value, the more UVA protection a sunscreen offers (9). Figure 6 shows that 0.5% oxybenzone alone had

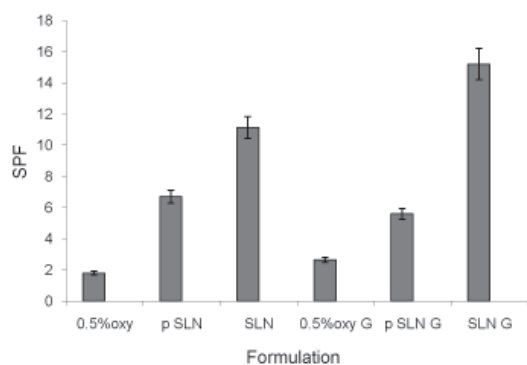


Figure 5. SPF values of different SLNs formulations using Vitro-Skin® as a substrate.

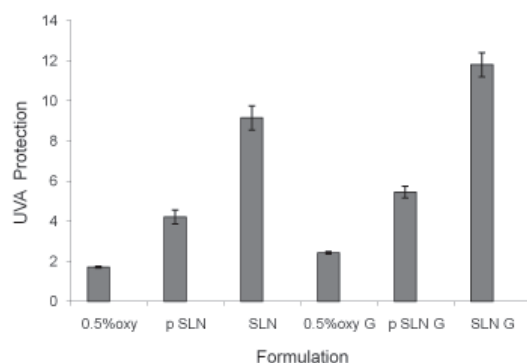


Figure 6. Erythral UVA protection factor for different SLNs formulations using Vitro Skin® as a substrate.

a very low UVA protection factor of about 1.7 ± 0.05 . Conversely, oxybenzone-loaded SLN2 was found to have a high EUVA-PF (9.15 ± 0.6). Since both dispersions contain the same concentration of oxybenzone, the SLN2 formulation was more effective and offered improved photoprotection. This was due to a combination of the reflecting properties of the solid particles and the absorbing characteristics of the oxybenzone (62). Due to this synergistic effect, the concentration of a potentially harmful molecular UV blocker can be decreased while maintaining the desired UV protection without needing an additional physical sunscreen (7). Lipid matrices may have also contributed to a better SPF and EUVA-PF since they provided a fixation medium for oxybenzone when the suspensions were spread over the substrates (29).

The SPF and EUVA-PF results for the prepared gels indicated better protection against UV radiation than that provided by corresponding dispersions. The viscosity values should confirm this observation since increased SPF values always coincide with higher viscosities (29).

Sunscreen formulations with a pseudoplastic flow produce a coherent protective film covering the skin surface with an evenly distributed UV filter, and this activity is important for a higher SPF. Newtonian materials do not behave in this way because they run very quickly when spread on the skin, reducing the

protective film. A pseudoplastic material, however, can break down to allow easy spreading, and the applied film can instantaneously gain viscosity to resist running (19).

4. Conclusion

The present work has shown that SLNs containing the lipophilic sunscreen oxybenzone can be produced by the solvent diffusion method. The advantage of this method is the instantaneous and reproducible formation of SLNs with a high loading capacity. Oxybenzone is insoluble in water and cannot be readily incorporated in a gel base. Once oxybenzone was entrapped in SLNs, it could be easily incorporated into a gel base without the crystallization problems that are common to oxybenzone. Topical application of a gel formulation containing SLNs of oxybenzone was found to be more efficient at protecting against UVA and UVB radiation. This is probably due to the film formation over the skin, which itself acts as a physical barrier to UV radiation. In conclusion, the results of this study emphasize the potential for SLNs to serve as a new topical drug delivery system. As such, they can enhance the sunscreen efficacy of oxybenzone by about 6-fold while using the minimum required concentration of oxybenzone (0.5%). Encapsulation in SLNs also offers the advantage of overcoming solubility and skin irritancy problems.

References

1. Svobodova A, Walterova D, Vostalova J. Ultraviolet light induced alteration to the skin. Biomed Pap Med Fac Univ Palacky Olomouc Czech Repub. 2006; 150:25-38.
2. Srinivas CR. Photoprotection. Indian J Dermatol Venereol Leprol. 2007; 73:73-79.
3. Wissing S, Müller R. The development of an improved carrier system for sunscreen formulations based on crystalline lipid nanoparticles. Int J Pharm. 2002; 242:373-375.
4. Wissing SA, Müller RH. A novel sunscreen system based on tocopherol acetate incorporated into solid lipid nanoparticles. Int J Cosmet Sci. 2001; 23:233-243.
5. Patel M, Jain SK, Yadav AK, Gogna D, Agrawal GP. Preparation and characterization of oxybenzone-loaded gelatin microspheres for enhancement of suncreening efficacy. Drug Deliv. 2006; 13:323-330.
6. Benson HA, Sarveiya V, Risk S, Roberts MS. Influence of anatomical site and topical formulation on skin penetration of sunscreens. Ther Clin Risk Manag. 2005; 1:209-218.
7. Wissing SA, Müller RH. Solid lipid nanoparticles (SLN) – a novel carrier for UV blockers. Pharmazie. 2001; 56:783-786.
8. Zhang J, Fan Y, Smith E. Experimental design for the optimization of lipid nanoparticles. J Pharm Sci. 2009; 98:1813-1819.
9. Villalobos-Hernández JR, Müller-Goymann CC. *In vitro* erythral UV-A protection factors of inorganic

- sunscreens distributed in aqueous media using carnauba wax-decyl oleate nanoparticles. *Eur J Pharm Biopharm.* 2007; 65:122-125.
10. Jermann R, Toumiat M, Imfeld D. Development of an *in vitro* efficacy test for self-tanning formulations. *Int J Cosm Sci.* 2002; 24:35-42.
 11. Springsteen A, Yurek R, Frazier M, Carr KF. *In vitro* measurement of sun protection factor of sunscreens by diffuse transmittance. *Anal Chim Acta.* 1999; 380:155-164.
 12. Hu FQ, Hong Y, Yuan H. Preparation and characterization of solid lipid nanoparticles containing peptide. *Int J Pharm.* 2004; 273:29-35.
 13. zur Mühlen A, Schwarz C, Mehnert W. Solid lipid nanoparticles (SLN) for controlled drug delivery – drug release and release mechanism. *Eur J Pharm Biopharm.* 1998; 45:149-155.
 14. Hu FQ, Jiang SP, Du YZ, Yuan H, Ye YQ, Zeng S. Preparation and characteristics of monostearin nanostructured lipid carriers. *Int J Pharm.* 2006; 314:83-89.
 15. Paliwal R, Rai S, Vaidya B, Khatri K, Goyal AK, Mishra N, Mehta A, Vyas SP. Effect of lipid core material on characteristics of solid lipid nanoparticles designed for oral lymphatic delivery. *Nanomedicine.* 2009; 5:184-191.
 16. Souto EB, Anselmi C, Centini M, Müller RH. Preparation and characterization of *n*-dodecyl-ferulate-loaded solid lipid nanoparticles (SLN®). *Int J Pharm.* 2005; 295:261-268.
 17. Wissing SA, Müller RH. Solid lipid nanoparticles as carrier for sunscreens: *In vitro* release and *in vivo* skin penetration. *J Control Release.* 2002; 81:225-233.
 18. Shah KA, Date AA, Joshi MD, Patravale VB. Solid lipid nanoparticles (SLN) of tretinoin: Potential in topical delivery. *Int J Pharm.* 2007; 345:163-171.
 19. Gaspar LR, Maia Campos PM. Rheological behavior and the SPF of sunscreens. *Int J Pharm.* 2003; 250: 35-44.
 20. Declaration of Helsinki – Current (2008) version. Available at <http://www.wma.net/e/policy/pdf/17c.pdf>
 21. Guidelines for Good Clinical Practice. European Medicines Agency. CPMP/ICH/135/95 July 2002
 22. Cambell RL, Bruce RD. Comparative dermatotoxicology. I. Direct comparison of rabbit and human primary skin irritation responses to isopropylmyristate. *Toxicol Appl Pharmacol.* 1981; 59:555-563.
 23. Vitro Skin®. 2009. <http://www.ims-usa.com>
 24. Diffey BL, Robson J. A new substrate to measure sunscreen protection factors throughout the ultraviolet spectrum. *J Soc Cosmet Chem.* 1989; 40:127-133.
 25. Séhédic D, Hardy-Boismartel A, Couteau C, Coiffard LJ. Are cosmetic products which include an SPF appropriate for daily use? *Arch Dermatol Res.* 2009; 301:603-608.
 26. Mehnert W, Mäder K. Solid lipid nanoparticles: Production, characterization and applications. *Adv Drug Deliv Rev.* 2001; 47:165-196.
 27. Hou D, Xie C, Huang K, Zhu C. The production and characteristics of solid lipid nanoparticles (SLNs). *Biomaterials.* 2003; 24:1781-1785.
 28. Liu J, Gong T, Wang C, Zhong Z, Zhang Z. Solid lipid nanoparticles loaded with insulin by sodium cholate-phosphatidylcholine-based mixed micelles: Preparation and characterization. *Int J Pharm.* 2007; 340:153-162.
 29. Villalobos-Hernández JR, Müller-Goymann CC. Novel nanoparticulate carrier system based on carnauba wax and decyl oleate for the dispersion of inorganic sunscreens in aqueous media. *Eur J Pharm Biopharm.* 2005; 60:113-122.
 30. Souto EB, Müller RH, Gohla S. A novel approach based on lipid nanoparticles (SLN) for topical delivery of α -lipoic acid. *J Microencapsul.* 2005; 22:581-589.
 31. Rowe RC, Sheskey PJ, Owen SC. Handbook of Pharmaceutical Excipients. 5th ed., Butler & Tanner, Somerset, UK, 2006; pp. 308-310.
 32. Siekmann B, Westesen K. Submicron sized parenteral carrier systems based on solid lipids. *Pharm Pharmacol Lett.* 1992; 1:123 -126.
 33. Varshosaz J, Minayian M, Moazen E. Enhancement of oral bioavailability of pentoxifylline by Solid lipid nanoparticles. *J Liposome Res.* 2010; 20:115-123.
 34. Schubert MA, Müller-Goymann CC. Solvent injection as a new approach for manufacturing lipid nanoparticles – evaluation of the method and process parameters. *Eur J Pharm Biopharm.* 2003; 55:125-131.
 35. Abdelwahed W, Degobert G, Fessi H. A pilot study of freeze drying of poly(epsilon-caprolactone) nanocapsules stabilized by poly(vinyl alcohol): Formulation and process optimization. *Int J Pharm.* 2006; 309:178-188.
 36. Song X, Zhao Y, Hou S, Xu F, Zhao R, He J, Cai Z, Li Y, Chen Q. Dual agents loaded PLGA nanoparticles: Systematic study of particle size and drug entrapment efficiency. *Eur J Pharm Biopharm.* 2008; 69:445-453.
 37. Guerrero DQ, Fessi H, Allmann E, Doelker E. Influence of stabilizing agents and preparative variables on the formation of poly(D,L-lactic acid) nanoparticles by an emulsification-diffusion technique. *Int J Pharm.* 1996; 143:133-141.
 38. Tiyaboonchai W, Tungpradit W, Plianbangchang P. Formulation and characterization of curcuminoids loaded solid lipid nanoparticles. *Int J Pharm.* 2007; 337:299-306.
 39. Umney N, Rivers S. Conservation of Furniture. Elsevier, Oxford, UK, 2003; pp. 124-193.
 40. Mainardes RM, Evangelista RC. PLGA nanoparticles containing praziquantel: Effect of formulation variables on size distribution. *Int J Pharm.* 2005; 290:137-144.
 41. Zimmermann E, Müller RH. Electrolyte- and pH-stabilities of aqueous solid lipid nanoparticle (SLN™) dispersions in artificial gastrointestinal media. *Eur J Pharm Biopharm.* 2001; 52:203-210.
 42. Huang ZR, Hua SC, Yang YL, Fang JY. Development and evaluation of lipid nanoparticles for camptothecin delivery: A comparison of solid lipid nanoparticles, nanostructured lipid carriers, and lipid emulsion. *Acta Pharmacol Sin.* 2008; 29:1094-1102.
 43. Wang Y, Deng Y, Mao S, Jin S, Wang J, Bi D. Characterization and body distribution of β -elemene solid lipid nanoparticles (SLN). *Drug Dev Ind Pharm.* 2005; 31:769-778.
 44. Kumar VV, Chandrasekar D, Ramakrishna S, Kishan V, Rao YM, Diwan PV. Development and evaluation of nitrendipine loaded solid lipid nanoparticles: Influence of wax and glyceride lipids on plasma pharmacokinetics. *Int J Pharm.* 2007; 335:167-175.
 45. Silverman RB. The Organic Chemistry of Drug Design and Drug Action. Elsevier, New York, NY, USA, 2004; pp. 55-61.
 46. Yuan H, Miao J, Du YZ, You J, Hu FQ, Zeng S. Cellular uptake of solid lipid nanoparticles and cytotoxicity of encapsulated paclitaxel in A549 cancer cells. *Int J Pharm.* 2008; 348:137-145.

47. Biehn GF, Ernsberger ML. Polyvinyl alcohol as an emulsifying agent. *Ind Eng Chem.* 1948; 40:1449-1453.
48. Rebbin V, Jakubowski M, Pötz S, Fröba M. Synthesis and characterisation of spherical periodic mesoporous organosilicas (sph-PMOs) with variable pore diameters. *Microporous Mesoporous Mater.* 2004; 72:99-104.
49. Wissing SA, Kayser O, Müller RH. Solid lipid nanoparticles for parenteral drug delivery. *Adv Drug Deliv Rev.* 2004; 56:1257-1272.
50. Souto EB, Wissing SA, Barbosa CM, Müller RH. Development of a controlled release formulation based on SLN and NLC for topical clotrimazole delivery. *Int J Pharm.* 2004; 278:71-77.
51. Luo Y, Chen D, Ren L, Zhao X, Qin J. Solid lipid nanoparticles for enhancing vinpocetine's oral bioavailability. *J Control Rel.* 2006; 114:53-59.
52. Yuan H, Huang LF, Du YZ, Ying XY, You J, Hu FQ, Zeng S. Solid lipid nanoparticles prepared by solvent diffusion method in a nanoreactor system. *Colloids Surf B Biointerfaces.* 2008; 61:132-137.
53. Souto EB, Wissing SA, Barbosa CM, Müller RH. Evaluation of the physical stability of SLN and NLC before and after incorporation into hydrogel formulations. *Eur J Pharm Biopharm.* 2004; 58:83-90.
54. Doktorovova S, Souto EB. Nanostructured lipid carrier-based hydrogel formulations for drug delivery: A comprehensive review. *Expert Opin Drug Deliv.* 2009; 6:165-176.
55. Bhaskar K, Mohan CK, Lingam M, Mohan SJ, Venkateswarlu V, Rao YM. Development of Solid lipid nanoparticles and NLC enriched hydrogels for transdermal delivery of nitrendipine: *In vitro* and *in vivo* characteristics. *Drug Dev Ind Pharm.* 2009; 35:98-113.
56. Liu W, Hu M, Liu W, Xue C, Xu H, Yang X. Investigation of the carbopol gel of solid lipid nanoparticles for the transdermal iontophoretic delivery of triamcinolone acetonide acetate. *Int J Pharm.* 2008; 364:135-141.
57. Lippacher A, Müller RH, Mäder K. Liquid and semisolid SLN™ dispersions for topical application: Rheological characterization. *Eur J Pharm Biopharm.* 2004; 58:561-567.
58. Castro GA, Coelho AL, Oliveira CA, Mahecha GA, Oréfice RL, Ferreira LA. Formation of ion pairing as an alternative to improve encapsulation and stability and to reduce skin irritation of retinoic acid loaded in solid lipid nanoparticles. *Int J Pharm.* 2009; 381:77-83.
59. Küchler S, Wolf NB, Heilmann S, Weindl G, Helfmann J, Yahya MM, Stein C, Schäfer-Korting M. 3D-wound healing model: Influence of morphine and solid lipid nanoparticles. *J Biotechnol.* 2010; 148:24-30.
60. Wissing SA, Müller RH. Cosmetic applications for solid lipid nanoparticles (SLN). *Int J Pharm.* 2003; 254:65-68.
61. Song C, Liu S. A new healthy sunscreen system for human: Solid lipid nanoparticles as carrier for 3,4,5-trimethoxybenzoylchitin and the improvement by adding Vitamin E. *Int J Bio Macromol.* 2005; 36:116-119.
62. Gulbake A, Jain A, Khare P, Jain SK. Solid lipid nanoparticles bearing oxybenzone: *In-vitro* and *in-vivo* evaluation. *J Microencapsul.* 2010; 27:226-233.

(Received August 6, 2010; Revised September 17, 2010; Re-revised October 22, 2010; Accepted November 2, 2010)

Original Article**Comparative study on the different techniques for the preparation of sustained-release hydrophobic matrices of a highly water-soluble drug**Shady M. Abd El-Halim^{1,*}, Maha M. Amin², Omaima N. El-Gazayerly², Nabaweya A. Abd El-Gawad¹¹ Pharmaceutics Department, Faculty of Pharmacy, October 6 University, October 6 City, October 6 Governorate, Egypt;² Pharmaceutics Department, Faculty of Pharmacy, Cairo University, Cairo, Egypt.

ABSTRACT: The objective of the present study was to control the release of freely water-soluble salbutamol sulphate (SS) over a prolonged period of time by embedding the drug into slowly eroding waxy matrix materials such as Precirol[®] ATO 5, Compritol[®] 888 ATO, beeswax, paraffin wax, carnauba wax, and stearyl alcohol. The matrices were prepared by either direct compression or hot fusion techniques. The compatibility of the drug with the various excipients was examined using differential scanning calorimetry (DSC). A factorial design was employed to study the effect of polymer type, polymer concentration (15% and 35%), and filler type (Avicel[®] PH101 and dibasic calcium phosphate dehydrate (DCP) on the *in vitro* drug release at 6 h. Results of DSC confirmed drug-excipient compatibility. Increasing the polymer ratio resulted in a significant retardation of drug release. The use of DCP resulted in significant retardation and incomplete drug release while the use of Avicel did not. The hot fusion method was found to be more effective than the direct compression method in retarding SS release. A Precirol formulation, prepared using the hot fusion technique, had the slowest drug release, releasing about 31.3% of SS over 6 h. In contrast, Compritol, prepared using the direct compression technique, had the greatest retardation, providing sustained release of 59.3% within 6 h. A hydrophobic matrix system is thus a useful technique for prolonging the release of freely water-soluble drugs such as salbutamol sulphate.

Keywords: Salbutamol sulphate, controlled release, waxy materials, direct compression, hot fusion

*Address correspondence to:

Dr. Shady M. Abd El-Halim, Faculty of Pharmacy, October 6 University, Central axis, Part 1/1, October 6 City, October 6 Governorate, Egypt.
e-mail: Shady_kashasha@hotmail.com

1. Introduction

A hydrophobic matrix system is the earliest oral sustained-release platform for medicinal use (1). A wax matrix system is a well developed matrix system used for sustained drug delivery because of its effectiveness, low cost, ease of manufacture, and drug stability due to the chemical inertness of wax (2,3). Wax matrix dosage forms are used to embed a drug in an inert water insoluble matrix material in order to formulate sustained or slow release formulations, and especially those containing freely water-soluble drugs such as potassium chloride and tramadol hydrochloride (4-6).

Lipophilic matrix agents are frequently used in the preparation of sustained-release tablets (7). Materials such as Precirol[®] ATO5 (glyceryl palmitostearate), Compritol[®] 888 ATO (glyceryl behenate), beeswax (white wax), paraffin wax, carnauba wax, and stearyl alcohol provide several advantages ranging from good stability at varying pH values and moisture levels to chemical inertness, safe application, and lower cytotoxicity in humans due to the absence of solvents in the production process (8-10).

For highly water-soluble drugs, drug release for a prolonged period using a hydrophilic matrix system is limited because of rapid diffusion of the dissolved drug through the hydrophilic gel network or shearing of the hydrated polymer gel layer by the food present in the gastrointestinal tract, leading to dose dumping. Hydrophobic polymers (waxes) are suitable matrixing agents for such drugs, allowing the development of sustained-release dosage forms since they are water-insoluble and non-swelling materials (6,9,11,12).

When lipophilic matrix tablets are placed in dissolution media, several cracks, channels, and pores are reportedly formed on their surface (3). These channels are formed due to a rapid dissolution of the drug particles present on the surface of the matrix (13). The dissolution medium enters the channels, allowing more dissolution of the drug present at deeper sites of the matrix and leaching the dissolved drug through these channels (9,14).

Salbutamol sulphate is a direct acting sympathomimetic drug with predominantly β -adrenergic activity and selective action on β_2 receptors (15,16). Since SS is a freely water-soluble drug (17) and the half-life of orally administered salbutamol is approximately 5 h, the drug must be administered three to four times daily to maintain bronchodilatation (18). Therefore, this drug would be a suitable target for controlled-release formulations.

The purpose of the present study was to prolong SS release, thus increasing patient compliance by reducing the frequency of administration. This study also sought to investigate the effect of some formulation factors on the physical properties and on *in vitro* drug release at 6 h from different tablets prepared either by a direct compression or hot fusion technique.

2. Materials and Methods

2.1. Materials

Salbutamol (Albuterol) sulfate (SS) was donated by Sedico Company (6th October City, Egypt). Compritol[®] 888 ATO (glyceryl behenate) and Precirol[®] ATO5 (glyceryl palmitostearate) were donated by Gattefosse Co. (Saint-Priest, France). Beeswax, carnauba wax, paraffin wax, and stearyl alcohol were donated by Luna Cosmetics (Cairo, Egypt). Aerosil[®] was donated by Delta Pharm (10th of Ramadan City, Egypt). Avicel[®] PH 101 and dibasic calcium phosphate dihydrate (DCP) were purchased from Morgan Chemical Industrial Company (10th of Ramadan City, Egypt).

2.2. Drug-excipient interactions

Differential scanning calorimetric (DSC) analysis was used to investigate the physicochemical compatibility of the drug and the excipients used. Samples (2-4 mg) of drug alone, excipients, and a drug-excipient physical mixture (1:1, w/w) were sealed in a 30- μ L aluminum pans and heated in the DSC instrument (DSC-50, Shimadzu, Kyoto, Japan) in a dynamic nitrogen atmosphere with a flow rate of 50 mL/min. A temperature range of 30 to 300°C was used and the heating rate was 10°C/min.

2.3. Preparation of matrices by the direct compression (DC) method

A 2³ factorial design was used to study the effect of three different formulation variables, namely polymer type (Precirol[®] ATO5 or Compritol[®] 888 ATO), polymer concentration (15% or 35%), and filler type (DCP or Avicel[®] PH 101), on the *in vitro* release of SS at 6 h from matrices prepared using the DC technique. Each variable was set at two levels. Eight formulations were prepared according to the compositions shown in Table 1, with each containing 10.6 mg SS. The calculated amounts of the drug, hydrophobic polymer, and filler were mixed by geometric dilution in a glass mortar and then the calculated amount of lubricant (Aerosil[®] 0.5%) was added. Dry blend formulations were compressed into 200 mg tablets using a single punch (7 mm) machine (Model EKO-9920; Erweka, Heusenstamm, Germany). The compression force (6-8 kN) was kept constant throughout the experiment.

2.4. Preparation of matrices by the hot fusion method

A 6.2² multiple factorial design was used to study the effect of the same formulation variables on the *in vitro* release of SS at 6 h from matrices prepared using the hot fusion technique. The first variable, polymer type, was set at six levels (Precirol[®] ATO5, Compritol[®] 888 ATO, beeswax, carnauba wax, paraffin wax, or stearyl alcohol) while the second and third variables, polymer concentration and filler type, were set at two levels for polymer concentration (15% or 35%) and filler type (DCP or Avicel[®] PH 101), respectively. Twenty-four formulations were prepared according to the compositions shown in Table 2, with each containing 10.6 mg SS. The accurately weighed amount of the hydrophobic polymer or wax was melted. When a homogenous melt was obtained, the mixture of the drug and filler was continuously stirred until a homogenous dispersion was obtained. The molten mass was allowed to cool to room temperature and screened through a No. 20 sieve. Those granules retained on a No. 60 sieve were collected and mixed with the predetermined amount of lubricant (Aerosil[®] 0.5%) and compressed

Table 1. Composition of different formulations of directly compressed salbutamol sulphate hydrophobic matrix tablets

| Formulation No. | Precirol [®] ATO5 (mg) | Compritol [®] 888 ATO (mg) | DCP* (mg) | Avicel [®] (mg) |
|-----------------|---------------------------------|-------------------------------------|-----------|--------------------------|
| B1 | 30 | – | 158.4 | – |
| B2 | 70 | – | 118.4 | – |
| B3 | 30 | – | – | 158.4 |
| B4 | 70 | – | – | 118.4 |
| B5 | – | 30 | 158.4 | – |
| B6 | – | 70 | 118.4 | – |
| B7 | – | 30 | – | 158.4 |
| B8 | – | 70 | – | 118.4 |

All tablet formulations contain 10.6 mg salbutamol sulphate equivalent to 8.8 mg salbutamol base and 1 mg Aerosil[®] as lubricant.

* DCP indicates dibasic calcium phosphate dihydrate.

Table 2. Composition of different formulations of salbutamol sulphate hydrophobic matrix tablets prepared using a hot fusion technique

| Formulation No. | Precirol® ATO5 (mg) | Compritrol® 888 ATO (mg) | Beeswax (mg) | Carnauba wax (mg) | Paraffin wax (mg) | Stearyl alcohol (mg) | DCP* (mg) | Avicel® (mg) |
|-----------------|---------------------|--------------------------|--------------|-------------------|-------------------|----------------------|-----------|--------------|
| C1 | 30 | – | – | – | – | – | 158.4 | – |
| C2 | 70 | – | – | – | – | – | 118.4 | – |
| C3 | 30 | – | – | – | – | – | – | 158.4 |
| C4 | 70 | – | – | – | – | – | – | 118.4 |
| C5 | – | 30 | – | – | – | – | 158.4 | – |
| C6 | – | 70 | – | – | – | – | 118.4 | – |
| C7 | – | 30 | – | – | – | – | – | 158.4 |
| C8 | – | 70 | – | – | – | – | – | 118.4 |
| C9 | – | – | 30 | – | – | – | 158.4 | – |
| C10 | – | – | 70 | – | – | – | 118.4 | – |
| C11 | – | – | 30 | – | – | – | – | 158.4 |
| C12 | – | – | 70 | – | – | – | – | 118.4 |
| C13 | – | – | – | 30 | – | – | 158.4 | – |
| C14 | – | – | – | 70 | – | – | 118.4 | – |
| C15 | – | – | – | 30 | – | – | – | 158.4 |
| C16 | – | – | – | 70 | – | – | – | 118.4 |
| C17 | – | – | – | – | 30 | – | 158.4 | – |
| C18 | – | – | – | – | 70 | – | 118.4 | – |
| C19 | – | – | – | – | 30 | – | – | 158.4 |
| C20 | – | – | – | – | 70 | – | – | 118.4 |
| C21 | – | – | – | – | – | 30 | 158.4 | – |
| C22 | – | – | – | – | – | 70 | 118.4 | – |
| C23 | – | – | – | – | – | 30 | – | 158.4 |
| C24 | – | – | – | – | – | 70 | – | 118.4 |
| C24 | – | – | – | – | – | 70 | – | 118.4 |

All tablet formulations contain 10.6 mg salbutamol sulphate equivalent to 8.8 mg salbutamol base and 1 mg Aerosil® as a lubricant.

* DCP indicates dibasic calcium phosphate dihydrate.

into 200 mg tablets using a single punch (7 mm) machine. The compression force (6-8 kN) was kept constant throughout the experiment.

2.5. Quality control tests of the prepared tablet formulations

2.5.1. Weight variation

Twenty tablets of each formulation were individually weighed on an electronic balance (Type AGE-220, Shimadzu) and their average weight was calculated (19).

2.5.2. Uniformity of tablet thickness and diameter

Ten tablets of each formulation were measured for the uniformity of their thickness and diameter using Vernier Calipers (Steco, Wuppertal, Germany) at two different positions. The average value of the diameter and thickness was then calculated in millimeters.

2.5.3. Friability test

Ten tablets were weighed and placed in a friabilator (model PTF; Pharma Test, Hainburg, Germany). The drum was rotated 100 times, and then the tablets were removed, brushed, and reweighed. The percentage loss in weight was calculated as a measure of friability. The percentage loss was not to exceed 1% (20).

2.5.4. Content uniformity

Ten tablets of each formulation were selected and each was individually assayed for drug content. Each tablet was crushed and dissolved in 100 mL distilled water in a volumetric flask with the aid of a sonicator (type USR3; Julabo Labortechnik, Seelbach, Germany). The mixture was filtered using a Millipore filter (0.2 µm) and measured spectrophotometrically at a λ_{\max} of 276 nm using a UV/VIS Spectrophotometer (UV-1601 PC, Shimadzu) with distilled water as a blank (20).

2.5.5. In vitro release studies

In vitro release of SS from the prepared tablet formulations was performed using the USP Dissolution Tester, Apparatus II, Rotating paddle, (Type PTW, Pharma Test) at a rotation of 50 rpm (19,21). Studies were carried out at $37 \pm 0.5^\circ\text{C}$ in 250 mL of 0.1 N HCl (pH 1.2) for a period of two hours and then continued in phosphate buffer (pH 7.4) for 10 h after shifting the pH from pH 1.2 to pH 7.4 using a 2.5 M KH_2PO_4 solution containing 16.72% (w/v) NaOH (22). Samples were collected, filtered using a Millipore filter (0.2 µm), and analyzed for SS content by measuring the absorbance at a λ_{\max} of 276 nm. All release studies were done in triplicate.

2.5.6. Release kinetics

The release data were analyzed according to the

well-known Korsmeyer-Peppas diffusion model (23,24). Peppas *et al.* introduced an exponential model to analyze drug release from polymeric devices with various geometrical shapes (3,4) according to the following equation:

$$M_t/M_\infty = kt^n \quad \text{--- Eq. 1}$$

where M_t/M_∞ is the fraction of the drug released at time t and K is the kinetic constant; n is the release exponent indicative of the mechanism of release. This model is, however, valid only for the early stages ($\leq 60\%$) of drug release (25-27). The values of n have no definite relationship with polymer content (28). The value of $0.43 < n < 0.5$ for Fickian (Case I) release, $0.5 < n < 0.89$ for non-Fickian (Anomalous) release, $n = 0.89$ for Case II (Zero-order) release, and $n > 0.89$ for the super Case II type of release (first-order) (29-31). The release exponent, n , is the slope of the log fraction of drug release *versus* the log time curve.

A model independent parameter, the mean dissolution time (MDT), was employed for comparison of dissolution profiles of the different formulations of salbutamol sulphate tablets prepared and was calculated according to the following equation:

$$MDT_{in-vitro} = \frac{\sum_{i=1}^n t_{mid} \Delta M}{\sum_{i=1}^n \Delta M} \quad \text{--- Eq. 2}$$

where i is the sample number, n is the number of dissolution samples, t_{mid} is the time at the midpoint between i and $i - 1$, and ΔM is the additional amount of drug dissolved between i and $i - 1$ (32-34).

2.6. Statistics

Statistical analysis of the *in vitro* SS release from the different prepared formulations after 6 h was done by one-way analysis of variance (ANOVA) for multiple comparisons at $p < 0.05$. Statistical analysis was performed using StatView software version 4.53.

3. Results and Discussion

3.1. Drug-excipient interactions

Figure 1 shows the thermograms of SS and its physical mixtures (1:1 ratio, w/w) with the different excipients used. The DSC thermogram of the drug alone had two main prominent sharp endothermic peaks at 204.25°C and 280.32°C which were reported to be corresponding to the decomposition of the SS molecules (35). The thermograms of physical mixtures of the drug with the excipients used showed drug endothermic peaks together

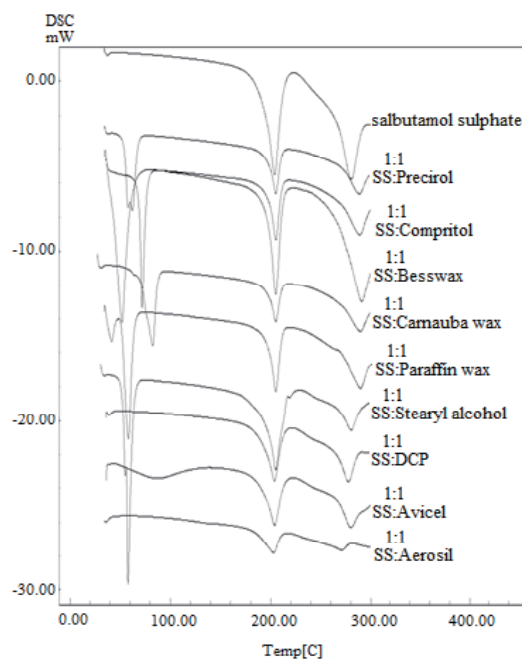


Figure 1. DSC thermograms of salbutamol sulphate and its physical mixtures (1:1, w/w) with the excipients used.

with characteristic peaks of the excipients used, indicating that there was no interaction between the drug and the excipients used.

3.2. Quality control tests of the prepared tablet formulations

The physical properties of the prepared tablets are presented in Table 3. Data revealed that the content uniformity of all formulations complied with the pharmacopeial limits (85-115%) (20).

3.3. *In vitro* release studies

Figures 2 and 3 show the *in vitro* release profiles of SS from the prepared tablet formulations. Statistical analysis was carried out to compare the different SS release profiles after 6 h (Q at 6 h) using one-way ANOVA. A high initial release of SS from the prepared tablet formulation was observed in the first hour and might be due to the fast dissolution of the drug particles present at the tablet surface, while the drug present in the deeper interstices of the tablet was released at a slower rate (9).

3.3.1. Influence of filler type

Clearly, as shown in Figure 4, more significant ($p < 0.05$) retardation of *in vitro* drug release at 6 h was observed upon use of DCP as a filler. This finding agrees with those of Liu *et al.* (36) and El-Shanawany (37), who reported that DCP was an insoluble and non-swelling filler. Thus, the tablets will remain intact throughout the dissolution process and the drug will be released by diffusion through small inter- and intra-particle spaces.

Table 3. Physical characterizations of the hydrophobic matrix tablets prepared

| Formulation No. | Weight (mg)* | Thickness (mm) | Diameter (mm) | Friability (%) | Content uniformity (%)* |
|-----------------|--------------|----------------|---------------|----------------|-------------------------|
| B1 | 199 ± 1.73 | 4.1 | 7 | 1.00 | 99.21 ± 1.53 |
| B2 | 200 ± 1.03 | 4.2 | 7 | 0.97 | 97.20 ± 2.60 |
| B3 | 203 ± 2.36 | 4.7 | 7 | 0.41 | 102.30 ± 1.92 |
| B4 | 201 ± 1.59 | 4.9 | 7 | 0.26 | 99.20 ± 1.71 |
| B5 | 200 ± 1.51 | 4.1 | 7 | 0.90 | 98.62 ± 2.04 |
| B6 | 199 ± 1.03 | 4.2 | 7 | 0.85 | 97.85 ± 3.20 |
| B7 | 202 ± 2.80 | 4.8 | 7 | 0.60 | 100.51 ± 2.72 |
| B8 | 201 ± 2.18 | 4.9 | 7 | 0.30 | 98.50 ± 2.42 |
| C1 | 197 ± 2.34 | 4.0 | 7 | 0.41 | 98.12 ± 1.73 |
| C2 | 200 ± 1.93 | 4.1 | 7 | 0.70 | 96.69 ± 3.01 |
| C3 | 201 ± 1.79 | 4.8 | 7 | 0.15 | 101.61 ± 2.62 |
| C4 | 202 ± 2.04 | 4.9 | 7 | 0.10 | 97.68 ± 2.97 |
| C5 | 201 ± 2.78 | 4.0 | 7 | 0.60 | 98.10 ± 1.94 |
| C6 | 199 ± 1.53 | 4.0 | 7 | 0.46 | 95.30 ± 2.60 |
| C7 | 203 ± 2.75 | 4.9 | 7 | 0.23 | 99.31 ± 2.02 |
| C8 | 202 ± 2.34 | 5.0 | 7 | 0.20 | 97.61 ± 3.32 |
| C9 | 199 ± 2.98 | 4.1 | 7 | 0.31 | 97.52 ± 2.82 |
| C10 | 198 ± 2.53 | 4.0 | 7 | 0.20 | 95.49 ± 2.90 |
| C11 | 201 ± 2.93 | 4.9 | 7 | 0.23 | 99.20 ± 1.81 |
| C12 | 201 ± 2.71 | 5.0 | 7 | 0.15 | 98.02 ± 2.91 |
| C13 | 200 ± 1.89 | 4.0 | 7 | 0.90 | 98.40 ± 2.37 |
| C14 | 200 ± 2.03 | 4.1 | 7 | 0.50 | 96.01 ± 2.59 |
| C15 | 202 ± 3.31 | 4.8 | 7 | 1.00 | 99.03 ± 2.93 |
| C16 | 203 ± 3.13 | 4.9 | 7 | 0.50 | 97.43 ± 2.41 |
| C17 | 200 ± 1.63 | 4.1 | 7 | 0.63 | 99.61 ± 1.96 |
| C18 | 199 ± 1.51 | 4.2 | 7 | 0.10 | 97.01 ± 2.80 |
| C19 | 201 ± 3.03 | 4.9 | 7 | 0.54 | 100.60 ± 2.91 |
| C20 | 202 ± 2.37 | 5.0 | 7 | 0.10 | 98.51 ± 3.43 |
| C21 | 200 ± 1.33 | 4.0 | 7 | 0.95 | 99.73 ± 2.08 |
| C22 | 197 ± 3.14 | 4.0 | 7 | 0.80 | 97.71 ± 2.45 |
| C23 | 201 ± 1.97 | 4.9 | 7 | 0.68 | 101.23 ± 2.04 |
| C24 | 201 ± 1.59 | 5.0 | 7 | 0.32 | 99.10 ± 1.72 |

* Data are presented as means ± S.D.

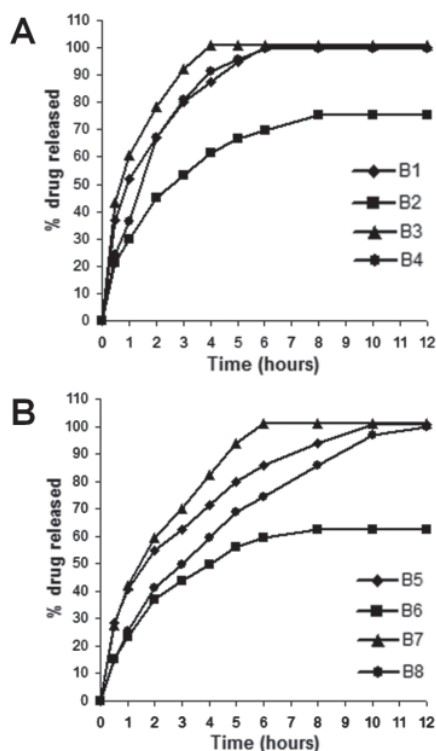


Figure 2. In vitro release profile of salbutamol sulphate from tablets prepared with a direct compression technique using Precirol® ATO5 (A) and Compritol® 888 ATO (B).

When Avicel® was used as a filler, water was absorbed into the tablet through capillaries, leading to swelling and formation of new cracks and channels from which a further amount of the drug was dissolved and released with no disintegration of the tablet. Unlike formulations prepared using Avicel®, tablet formulations prepared using DCP were found to have incomplete drug release, so no further investigations were carried out on those formulations prepared using DCP as a filler (36,37).

3.3.2. Influence of polymer type

One of the directly compressed formulations (Figure 2), Compritol® was significantly more successful ($p < 0.05$) at retarding drug release than Precirol®, as shown in Figure 4A. The least significant release (Q at 6 h = 74.5%) was obtained from formulation B8 prepared using 35% Compritol® and Avicel® as fillers. This might be due to the high melting range of Compritol® compared to Precirol®. These results are in accordance with previously published results (38,39) indicating that this phenomenon might be due to the greater loss of structure or weakening of bonds between particles at 37°C in the compressed matrices prepared from glyceride esters of fatty acids with a low melting point. Thus, the higher melting range of the used polymer, the less

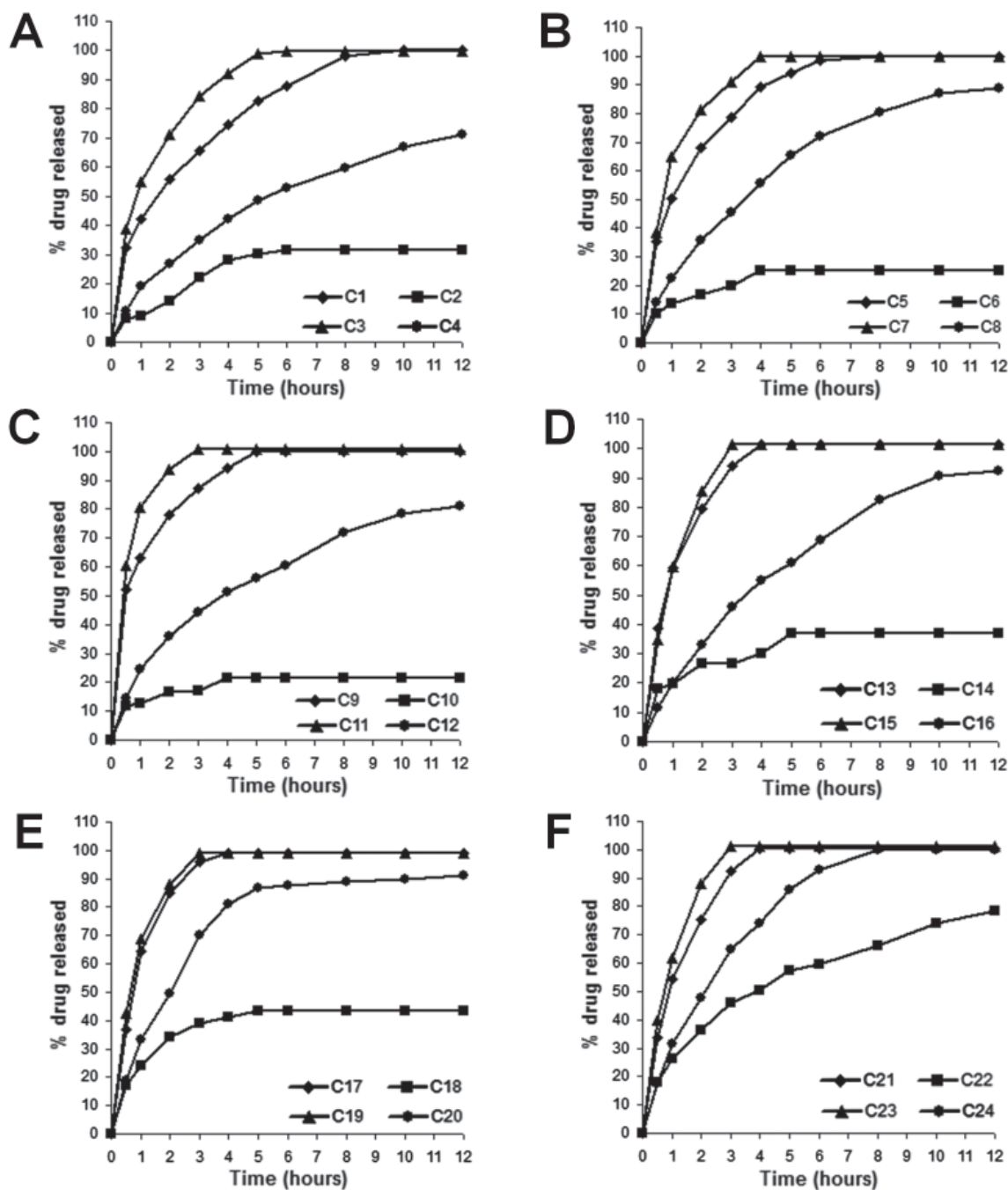


Figure 3. *In vitro* release profile of salbutamol sulphate from tablets prepared with a hot fusion technique using Precirol® ATO5 (A), Compritol® 888 ATO (B), beeswax (C), carnauba wax (D), paraffin wax (E), and stearyl alcohol (F).

drug released. Prepared using the hot fusion method (Figure 4B), 35% Precirol® (formulation C4) and 35% beeswax (formulation C12) retarded drug release more significantly ($p < 0.05$) than did other polymers, releasing about 52.8% and 60.5% after 6 h, respectively, when using Avicel® as a filler. In contrast, stearyl alcohol had the most significant release (Q at 6 h = 92.9%, $p < 0.05$) from formulation C24 prepared using a 35% stearyl alcohol concentration and Avicel® as a filler. The highest drug release from stearyl alcohol is in accordance with the findings of Karasulu *et al.* (40), who explained that, on the basis of polymeric structure, stearyl alcohol was

more convenient for drug diffusion. Stearyl alcohol also has a lower melting point and higher water absorption capacity than the other polymers, allowing more dissolution medium to penetrate the matrix system and resulting in faster drug release (40,41).

3.3.3. Influence of polymer concentration

As shown in Figure 4 reveal, increasing the polymer concentration from 15% to 35% resulted in greater retardation of drug release ($p < 0.05$). This might be due to an increased polymer concentration resulting in

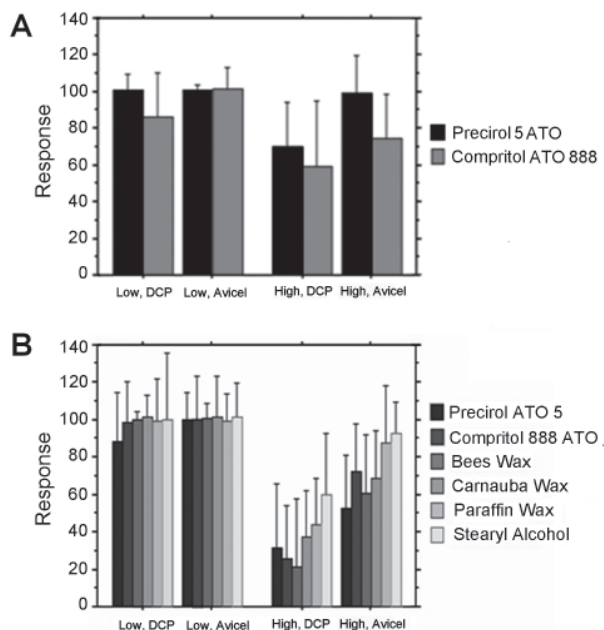


Figure 4. Interaction bar plot for the effect of polymer type, polymer concentration, and filler type on *in vitro* release at 6 h from hydrophobic tablet formulations prepared with a direct compression technique (A) and hot fusion technique (B).

a decrease in the total porosity of the matrices (initial porosity plus porosity due to dissolution of the drug), decreasing the penetration of the dissolution medium into the matrix system and thus reducing drug dissolution. In addition, increasing the polymer content led to an increase in the drug diffusion path length, which in turn retarded drug diffusion from the matrix (42).

3.3.4. Influence of the method of preparation

Drug release was greater from the matrices prepared by direct compression relative to that from matrices prepared by hot fusion. The slower release from the latter matrices could be due to the complete coating of the drug particles by the melted polymer. In such instances, there would presumably be less penetration of the dissolution medium into the matrix compared to that into matrices prepared by direct compression, and hence, dissolution and release of the drug would occur at a slower rate (36,43,44).

3.4. Release kinetics

The release exponent (n) and kinetic constant (k) were calculated from equation 1 and are shown in Table 4.

Table 4. MDT values of different formulations of salbutamol sulphate tablets and fitting of salbutamol sulphate release data to Korsmeyer-Peppas model

| Formulation No. | MDT (h)* | Correlation coefficient (r^2) | Release exponent (n) | Kinetic constant (K) | Mechanism |
|-----------------|----------|-----------------------------------|--------------------------|----------------------|--------------------------|
| B1 | 1.63 | – | – | – | – |
| B2 | 2.17 | 0.998 | 0.53 | 0.304 | Anomalous transport |
| B3 | 1.14 | – | – | – | – |
| B4 | 1.73 | – | – | – | – |
| B5 | 2.75 | 0.996 | 0.48 | 0.399 | Case I (Fickian release) |
| B6 | 2.19 | 0.997 | 0.60 | 0.235 | Anomalous transport |
| B7 | 2.03 | 0.996 | 0.55 | 0.409 | Anomalous transport |
| B8 | 3.77 | 0.994 | 0.68 | 0.246 | Anomalous transport |
| C1 | 2.46 | 0.999 | 0.40 | 0.425 | Case I (Fickian release) |
| C2 | 2.16 | 0.903 | 0.55 | 0.105 | Anomalous transport |
| C3 | 1.42 | – | – | – | – |
| C4 | 3.92 | 0.984 | 0.63 | 0.177 | Anomalous transport |
| C5 | 1.67 | – | – | – | – |
| C6 | 1.45 | 0.993 | 0.36 | 0.133 | Case I (Fickian release) |
| C7 | 1.09 | – | – | – | – |
| C8 | 3.45 | 0.999 | 0.66 | 0.222 | Anomalous transport |
| C9 | 1.17 | – | – | – | – |
| C10 | 1.19 | 0.948 | 0.24 | 0.134 | Case I (Fickian release) |
| C11 | 0.67 | – | – | – | – |
| C12 | 3.52 | 0.992 | 0.62 | 0.231 | Anomalous transport |
| C13 | 1.15 | – | – | – | – |
| C14 | 1.61 | 0.927 | 0.25 | 0.208 | Case I (Fickian release) |
| C15 | 1.04 | – | – | – | – |
| C16 | 3.80 | 0.999 | 0.76 | 0.198 | Anomalous transport |
| C17 | 0.99 | – | – | – | – |
| C18 | 1.27 | 0.996 | 0.47 | 0.339 | Case I (Fickian release) |
| C19 | 0.88 | – | – | – | – |
| C20 | 2.12 | 0.990 | 0.70 | 0.314 | Anomalous transport |
| C21 | 1.25 | – | – | – | – |
| C22 | 3.48 | 0.999 | 0.51 | 0.260 | Anomalous transport |
| C23 | 0.98 | – | – | – | – |
| C24 | 2.55 | 0.992 | 0.72 | 0.298 | Anomalous transport |

* MDT indicates mean dissolution time.

According to the Korsmeyer-Peppas diffusion model, formulations B5, C1, C6, C10, C14, and C18 fell under Case I (Fickian release) in which the rate of drug diffusion was much lower than that of polymer relaxation (*i.e.*, erosion) while formulations B2, B6, B7, B8, C2, C4, C8, C12, C16, C20, C22, and C24 exhibited anomalous transport in which the drug was delivered by the combined effect of drug diffusion and polymer relaxation (30,45). The release exponent for the remaining formulations is not shown because there were insufficient data points in the release profiles below 60% release to provide accurate values.

The MDT value was used to characterize the drug release rate from the dosage form and the retarding effect of the polymer. MDT values calculated from equation 2 are shown in Table 4. As is readily apparent, the higher the polymer level, the higher the value of MDT and the greater the retarding effect of the polymer. These findings are in accordance with those reported by Abdelkader *et al.* and Roni *et al.* (46,47).

4. Conclusion

A hydrophobic matrix system in which a drug is embedded into a slowly eroding waxy material was found to be a viable technique to produce sustained-release tablets, and especially those containing freely water-soluble drugs such as SS. The *in vitro* drug release profile can be modified by the selection of the filler excipient. Formulations prepared using DCP were found to hold little promise as DCP led to incomplete drug release. In contrast, those prepared using Avicel® proved more promising. Compared to the direct compression technique, the hot fusion method was found to be more efficient at retarding drug release. C4, the formulation of choice, succeeded in controlling drug release up to 52.8% within six hours.

Acknowledgements

The authors wish to thank personnel of CID Company, Cairo, Egypt for their assistance.

References

1. Qiu Y. Rational design of oral modified-release drug delivery systems. In: Developing Solid Oral Dosage Forms: Pharmaceutical Theory and Practice (Qiu Y, Chen Y, Zhang G, Liu L, Porter W, eds.). Academic Press, San Diego, CA, USA, 2009; pp. 469-499.
2. Qiu Y, Flood K, Marsh K, Carroll S, Trivedi J, Americ SP, Krill SL. Design of sustained-release matrix systems for a highly water-soluble compound, ABT-089. *Int J Pharm.* 1997; 157:43-52.
3. Sato H, Miyagawa Y, Okabe T, Miyajima M, Sunada H. Dissolution mechanism of diclofenac sodium from wax matrix granules. *J Pharm Sci.* 1997; 86:929-934.
4. Ozyazici M, Gökçe EH, Ertan G. Release and diffusional modeling of metronidazole lipid matrices. *Eur J Pharm*

5. Biopharm. 2006; 63:331-339.
6. Dredan J, Antal I, Racz I. Evaluation of mathematical models describing drug release from lipophilic matrices. *Int J Pharm.* 1996; 145:61-64.
7. Tiwari SB, Murthy TK, Pai MR, Mehta PR, Chowdary PB. Controlled release formulation of tramadol hydrochloride using hydrophilic and hydrophobic matrix system. *AAPS PharmSciTech.* 2003; 4:18-23.
8. Zhang Y, Schwartz JB. Melt granulation and heat treatment for wax matrix-controlled drug release. *Drug Dev Ind Pharm.* 2003; 29:131-138.
9. Uner M, Gönüllü U, Yener G, AltInkurt T. A new approach for preparing a controlled release ketoprofen tablets by using beeswax. *Farmaco.* 2005; 60:27-31.
10. Obaidat AA, Obaidat RM. Controlled release of tramadol hydrochloride from matrices prepared using glyceryl behenate. *Eur J Pharm Biopharm.* 2001; 52:231-235.
11. Obaidat AA. Evaluation of the mechanism of release of water soluble drug from a waxy inert matrix. *Acta Pharma Turc.* 1999; 61:199-202.
12. Reddy KR, Mutalik S, Reddy S. Once-daily sustained-release matrix tablets of nicorandil: Formulation and *in vitro* evaluation. *AAPS PharmSciTech.* 2003; 4:E61.
13. Huang HP, Mehta SC, Radebaugh GW, Fawzi MB. Mechanism of drug release from an acrylic polymer-wax matrix tablet. *J Pharm Sci.* 1994; 83:795-797.
14. Collett JH, Moreton RC. Modified-release peroral dosage forms. In: Aulton's Pharmaceutics: The Design and Manufacture of Medicines (Aulton ME, ed.). 3rd Ed., Churchill Livingstone, London, UK, 2007; pp. 483-499.
15. Cao QR, Kim TW, Lee BJ. Photoimages and the release characteristics of lipophilic matrix tablets containing highly water-soluble potassium citrate with high drug loadings. *Int J Pharm.* 2007; 339:19-24.
16. Pacifici GM, De Santi C, Mussi A, Ageletti CA. Interindividual variability in the rate of salbutamol sulphation in the human lung. *Eur J Clin Pharmacol.* 1996; 49:299-303.
17. Collomp K, Candau R, Lasne F, Labsy Z, Prefaut C, De Ceurriz J. Effects of short-term oral salbutamol administration on exercise endurance and metabolism. *J Appl Physiol.* 2000; 89:430-436.
18. Galichet LY, Moffat AC, Osselton MD, Widdop B. Monographs: Salbutamol Sulfate. In: Clarke's Analysis of Drugs and Poisons. 3rd ed., Pharmaceutical Press, London, UK, 2005; pp. 1546-1547.
19. San Vicente A, Hernández RM, Gascón AR, Calvo MB, Pedraz JL. Effect of aging on the release of salbutamol sulfate from lipid matrices. *Int J Pharm.* 2000; 208:13-21.
20. The USP NF. Asian ed. US Pharmacopoeial Convention, Twinbrook Parkway, Rockville, MD, USA, 2009; pp. 264-269, 386-387.
21. The British Pharmacopoeia. The Stationary Office, London, UK, 2008; pp. 1918-1920, A303-304, A423-424.
22. Sanghavi NM, Bijlani CP, Kamath PR, Sarwade VB. Matrix tablets of salbutamol sulphate. *Drug Dev Ind Pharm.* 1990; 16:1955-1961.
23. Kondo N, Iwao T, Hirai K, Fukuda M, Yamanouchi K, Yokoyama K, Miyaji M, Ishihara Y, Kon K, Ogawa Y, Mayumi T. Improved oral absorption of enteric coprecipitates of a poorly soluble drug. *J Pharm Sci.* 1994; 83:566-570.
24. Korsmeyer RW, Gurny R, Doelker E, Buri P, Peppas NA.

- Mechanism of solute release from porous hydrophilic polymers. *Int J Pharm.* 1983; 15:25-35.
24. Ritger PL, Peppas NA. A simple equation for description of solute release II. Fickian and anomalous release from swellable devices. *J Control Release.* 1987; 5:37-42.
 25. Costa P, Sousa Lobo JM. Modeling and comparison of dissolution profiles. *Eur J Pharm Sci.* 2001; 13:123-133.
 26. Siepman J, Peppas NA. Modeling of drug release from delivery systems based on hydroxypropyl methylcellulose (HPMC). *Adv Drug Deliv Rev.* 2001; 48:139-157.
 27. Gren T, Nyström C. Porous cellulose matrices containing lipophilic release modifiers – a potential oral extended-release system. *Int J Pharm.* 1999; 184:7-19.
 28. Reza MS, Quadir MA, Haider SS. Comparative evaluation of plastic, hydrophobic and hydrophilic polymers as matrices for controlled-release drug delivery. *J Pharm Pharmaceut Sci.* 2003; 6:282-291.
 29. Avachat A, Kotwal V. Design and evaluation of matrix-based controlled release tablets of diclofenac sodium and chondroitin sulphate. *AAPS PharmSciTech.* 2007; 8:E88.
 30. Sarfraz MK, Nisar-Ur-Rehman, Ahmed S, Ashraf M, Mohsin S. Ethyl cellulose-based solid matrix system for sustaining release of naproxen. *Pak J Biol Sci.* 2007; 10:668-672.
 31. Jagan MS, Kishan V, Madhusudan RY, Chalapathi RNV. Formulation of controlled release Levodopa and Carbidopa matrix tablets: Influence of some hydrophilic polymers on the release. *Curr Trends Biotech Pharm.* 2009; 3:204-209.
 32. Barakat NS, Elbagory IM, Almurshedi AS. Controlled-release carbamazepine matrix granules and tablets comprising lipophilic and hydrophilic components. *Drug Deliv.* 2009; 16:57-65.
 33. Varshosaz J, Tavakoli N, Kheirilahi F. Use of hydrophilic natural gums in formulation of sustained-release matrix tablets of tramadol hydrochloride. *AAPS PharmSciTech.* 2006; 7:E24.
 34. Varshosaz J, Tavakoli N, Eram SA. Use of natural gums and cellulose derivatives in production of sustained release metoprolol tablets. *Drug Deliv.* 2006; 13:113-119.
 35. Larhribh H, Martin GP, Marriott C, Prime D. The influence of carrier and drug morphology on drug delivery from dry powder formulations. *Int J Pharm.* 2003; 257:283-296.
 36. Liu J, Zhang F, McGinity JW. Properties of lipophilic matrix tablets containing phenylpropanolamine hydrochloride prepared by hot-melt extrusion. *Eur J Pharm Biopharm.* 2001; 52:181-190.
 37. El-Shanawany S. Sustained release of nitrofurantoin from inert wax matrices. *J Control Release.* 1993; 26:11-19.
 38. Shaikh NH, De Yanes SE, Shukla AJ, Block LH, Collins CC, Price JC. Effect of different binders on release characteristics of theophylline from compressed microspheres. *Drug Dev Ind Pharm.* 1991; 17:793-804.
 39. Almurshedi AS. Formulation and evaluation of extended-release carbamazepine granules prepared with inert fatty matrices (M. Sc. Thesis). College of Pharmacy, King Saud University, Saudi Arabia, 2007.
 40. Karasulu E, Yeşim Karasulu H, Ertan G, Kirilmaz L, Güneri T. Extended release lipophilic indomethacin microspheres: Formulation factors and mathematical equations fitted drug release rates. *Eur J Pharm Sci.* 2003; 19:99-104.
 41. Mahalingam R, Li X, Jasti BR. Semisolid dosages: Ointments, creams and gels. In: *Pharmaceutical Manufacturing Handbook: Production and Processes* (Gad SC, ed.). John Wiley & Sons, Inc., New Jersey, NJ, USA, 2008; pp. 267-288.
 42. Quadir MA, Rahman MS, Karim MZ, Akter S, Awkat MT, Reza MS. Evaluation of hydrophobic materials as matrices for controlled-release drug delivery. *Pak J Pharm Sci.* 2003; 16:17-28.
 43. Savolainen M, Khoo C, Glad H, Dahlqvist C, Juppo AM. Evaluation of controlled-release polar lipid microparticles. *Int J Pharm.* 2002; 244:151-161.
 44. Li FQ, Hu JH, Deng JX, Su H, Xu S, Liu JY. *In vitro* controlled release of sodium ferulate from Compritol 888 ATO-based matrix tablets. *Int J Pharm.* 2006; 324:152-157.
 45. Saha RN, Sajeev C, Sahoo J. A comparative study of controlled release matrix tablets of diclofenac sodium, ciprofloxacin hydrochloride, and theophylline. *Drug Deliv.* 2001; 8:149-154.
 46. Abdelkader H, Abdalla OY, Salem H. Formulation of controlled-release baclofen matrix tablets: Influence of some hydrophilic polymers on the release rate and *in vitro* evaluation. *AAPS PharmSciTech.* 2007; 8: E100-E108.
 47. Roni MA, Kibria G, Jalil R. Formulation and *in vitro* evaluation of alfuzosin extended release tablets using directly compressible eudragit. *Indian J Pharm Sci.* 2009; 71:252-258.

(Received September 8, 2010; Revised October 14, 2010; Accepted November 2, 2010)

Original Article

Effect of Ceolus KG-802 on the dissolution rate of fenofibrate liquisolid tablets: Preformulation and formulation development studies

Amrit B. Karmarkar*

Govt. College of Pharmacy, Karad, Dist. Satara, MS, India.

ABSTRACT: The purpose of the present research was to study the effects of Ceolus KG-802 on the dissolution behavior of fenofibrate liquisolid tablets. The fenofibrate liquisolid tablets were formulated using the mathematical model described by Spireas *et al.* In the present research, Ceolus KG-802, a different form of microcrystalline cellulose (PH 102 grade), was used as a carrier material. The developed formulations were subjected to preformulation studies such as differential scanning calorimetry, X-ray powder diffraction, and determination of flow properties. The liquisolid tablets prepared were studied for their *in vitro* dissolution and compared to liquisolid tablets prepared using Avicel PH 102. The *in vitro* dissolution profiles of liquisolid tablets prepared using Ceolus KG-802 indicated slower dissolution than those of liquisolid tablets prepared using Avicel PH 102, which was a subject of earlier studies. This might be due to the particle size, shape, and characteristic properties of Ceolus KG-802.

Keywords: Liquisolid tablets, fenofibrate, Avicel PH 102, Ceolus KG-802

1. Introduction

Dissolution remains a critical factor for absorption of drugs and especially so with water-insoluble drugs (1). Drugs whose absorption is dissolution rate-limited are classified as Biopharmaceutics Classification System (BCS) Class II. Innovative formulation approaches suited to these drugs should be designed to solve the bioavailability problem after oral administration. For water-insoluble drugs with poor solubility in both aqueous and organic media, formulation development

remains a challenging task (2,3). Fenofibrate is a BCS Class II drug used to decrease elevated plasma concentrations of low density lipoprotein and total cholesterol (4-6). Although low bioavailability of the drug is due to its poor solubility in water, the problem can overcome by enhancing its dissolution rate. Liquisolid tablet formulations have proven effective at improving the dissolution rate of fenofibrate (7-9).

Liquisolid tablets or compacts can be defined as immediate or sustained-release tablets or capsules that are prepared using the technique of "liquisolid systems". Included are adjuvants required for tableting or encapsulation, such as lubricants, and adjuvants required for rapid or sustained-release action, such as disintegrants or binders, respectively (10,11).

According to Spireas *et al.* (10,11), a carrier material is porous material with sufficient absorption properties. Microcrystalline cellulose is one such material. Earlier studies of fenofibrate with liquisolid tablets focused on use of Avicel PH 102 as a carrier material. Avicels (Trade mark of FMC Biopolymer) are purified, partially depolymerized α -celluloses. Their characteristic properties of compactibility, drug-carrying capacity, and rapid disintegration mean that they are a valuable tool for formulation development. Avicel PH 102 is a standard grade of Avicel with a large particle size and is used for direct compression, the dry phase of wet granulation, and dry granulation (12). Due to its properties, it has also been used to formulate liquisolid tablets of fenofibrate (7). Ceolus (a trademark of Asahi Kasei) is a type of microcrystalline cellulose prepared using Asahi Kasei's advanced processing technology. Ceolus grade KG-802 was initially introduced grade and is a super compactible grade of microcrystalline cellulose (13). Although both Avicel PH 102 and Ceolus KG-802 are types of microcrystalline cellulose, they have different physical properties that might result in different formulations.

The aim of the present study was to investigate the performance of liquisolid tablets prepared using Ceolus KG-802 as a carrier material for use in the formulation of liquisolid tablets.

*Address correspondence to:

Mr. Amrit B. Karmarkar, Govt. College of Pharmacy, Karad-415124, Dist. Satara, MS, India.
e-mail: abkarmarkar@gmail.com

2. Materials and Methods

2.1. Materials

Fenofibrate was kindly donated by Lupin Laboratories (Mumbai, India). Ceolus KG-802 was supplied by Signet (Mumbai, India). Aerosil 200 and sodium starch glycolate were kindly donated by Okasa Pharmaceuticals (Maharashtra, India) and Shital Chemicals (Gujarat, India), respectively. Propylene glycol and sodium lauryl sulfate were purchased from Loba Chemie (Mumbai, India). All other reagents and chemicals were of analytical grade.

2.2. Use of a mathematical model to design liquisolid tablets

Formulations of liquisolid systems were designed in accordance with new mathematical model described by Spireas *et al.* (10,11) (Table 1). In this study, propylene glycol was used as liquid vehicle; Ceolus KG-802 was used as the carrier and Aerosil 200 was used as the coating material. The formulation design of the liquisolid tablets remained the same as that in previous studies of Avicel PH 102 by Karmarkar *et al.* (7). Concentrations of 10, 20, and 30% (w/v) of the liquid vehicle propylene glycol were used along with carrier:coat ratios of 30, 40, and 50 to attain optimal fenofibrate solubility in the liquisolid formulations.

2.3. Preparation of liquisolid tablets

Liquisolid tablets were prepared as described before (1). Briefly, calculated quantities of fenofibrate and propylene glycol were accurately weighed in a 20-mL glass beaker and then heated to 80°C. The resulting hot medication was incorporated into calculated quantities of carrier (Ceolus KG-802) and coating materials (Aerosil 200 P). The mixing process was carried out in three steps as described by Spireas *et al.* (10,11). During the first stage, the system was blended at an approximate mixing rate of one rotation per second for approximately 1 min in order to evenly distribute liquid medication in the powder. In the second stage, the liquid/powder admixture

was evenly spread as a uniform layer on the surfaces of the mortar and left standing for approximately 5 min to allow the drug solution to be absorbed in the interior of powder particles. In the third stage, powder was scraped off the mortar surface by means of an aluminum spatula and then blended with 8% sodium starch glycolate for another 30 sec similar to the first stage. This yielded a final formulation of liquisolid tablets. The liquisolid formulations thus prepared were compressed with a tablet compression machine.

2.4. Precompression studies

2.4.1. Flow properties

Flow properties of liquisolid formulations were studied in terms of the angle of repose, Carr's index, and Hausner's ratio (14). Each analysis was carried out in triplicate. Bulk density measurements were carried out by placing a fixed weight of powder in a graduated cylinder and the volume occupied was measured and the initial bulk density was calculated. The cylinder was then tapped at a constant velocity until a constant volume was obtained. Then tapped density was calculated. The angle of repose was calculated using the fixed height cone method.

2.4.2. Differential scanning calorimetry (DSC)

A SDT2960 Differential Scanning Calorimeter (TA Instruments Inc., New Castle, DE, USA) was used to assess the thermotropic properties and thermal behavior of fenofibrate, Ceolus KG-802, and a liquisolid system. Samples (3-5 mg) were placed in aluminum pans and lids at constant heating of 15°C/min spanning a temperature range up to 250°C. Nitrogen was used as a purge gas through the DSC cell.

2.4.3. X-ray powder diffraction (XRD)

XRD patterns were studied using the Philips PW 3710 X-Ray Diffractometer. Samples were irradiated with Cu radiation at a wavelength of 1.540 Å and then analyzed between 10 and 40° (2θ). XRD patterns were determined for fenofibrate, Ceolus KG-802, and the liquisolid

Table 1. Formulation design of liquisolid tablets examined in this study

| Formulation batch code | Drug concentration in propylene glycol (% w/w) | Carrier:coating material ratio (R) | Ceolus KG-802 (mg) | Aerosil 200 (mg) |
|------------------------|--|------------------------------------|--------------------|------------------|
| CLS 1 | 10 | 30 | 197.5 | 6.58 |
| CLS 2 | 10 | 40 | 219.46 | 5.48 |
| CLS 3 | 10 | 50 | 235.97 | 4.71 |
| CLS 4 | 20 | 30 | 395.03 | 13.10 |
| CLS 5 | 20 | 40 | 438.93 | 10.97 |
| CLS 6 | 20 | 50 | 471.94 | 9.43 |
| CLS 7 | 30 | 30 | 592.59 | 19.75 |
| CLS 8 | 30 | 40 | 658.43 | 16.46 |
| CLS 9 | 30 | 50 | 707.96 | 14.15 |

system. An XRD study of Aerosil 200 was unnecessary as it was previously found to be a non-gritty amorphous powder (14).

2.4.4. Stereomicroscopic analysis

Stereomicroscopy was used to determine the morphological characteristics of the prepared liquisolid systems using a Nikon SMZ 800 microscope (Nikon, Inc., Melville, NY, USA). The sample was placed on a glass slide and observed; photographs were then taken.

2.5. Evaluation of liquisolid tablets

The hardness of liquisolid tablets was determined using a Pfizer Hardness Tester (Pfizer, New York, NY, USA). The mean hardness of each formulation was determined. The friability of prepared liquisolid tablets was determined using a Digital Tablet Friability Tester (Roche, Basel, Switzerland). Disintegration time was measured using a USP Disintegration Tester (Electrolab, Mumbai, India). All studies were done in triplicate.

2.6. In vitro dissolution studies of liquisolid tablets

Dissolution studies were performed using a USP Apparatus II Dissolution Tester (LabIndia, Thane, India). Liquisolid tablets were placed in a dissolution vessel containing 1,000 mL of 0.05 M sodium lauryl sulfate in water (16) maintained at $37 \pm 0.5^\circ\text{C}$ and stirred with a paddle at 50 rpm. Samples were collected periodically and replaced with dissolution medium. After filtration through Whatman filter paper 41, the concentration of fenofibrate was determined spectrophotometrically at 289.2 nm using a Shimadzu 1700 UV-Vis Spectrophotometer (Shimadzu, Kyoto, Japan). Dissolution profiles of liquisolid tablets were compared to those of three different marketed formulations. All studies were done in triplicate ($n = 3$).

3. Results and Discussion

Previous work by Karmarkar *et al.* (7) focused on evaluation of the usefulness of the liquisolid tablet technique as a tool for dissolution rate enhancement; the carrier used in that work was Avicel PH 102. In the present work, fenofibrate was selected as a model drug as it is poorly soluble in water and thus an ideal candidate for evaluating the rapid release potential of liquisolid tablets. In the current work, Ceolus KG-802 was used as a carrier in order to prepare liquisolid tablets. Earlier studies with fenofibrate have noted its solubility in propylene glycol (7). This is necessary in order to guarantee that the drug is readily soluble in such a solvent before being loaded into carrier and coating materials. According to the liquisolid hypothesis (15), the phenomena of absorption and adsorption occur when a drug candidate (dissolved in a non-volatile solvent) is incorporated into a carrier

and coating system. This is due to fact that the drug, in the form of a liquid medication, is initially absorbed into the carrier (here Ceolus KG-802); after saturation, the process of adsorption occurs. As Aerosil 200 has a high adsorptivity and large surface area, it yields liquisolid systems with desirable flow properties (15).

3.1. Precompression studies for liquisolid systems

3.1.1. Flow properties

The flowing nature of a blend/powder is an important part of the industrial production of a tablet dosage form. Flowability was therefore examined for various liquisolid formulations (CLS 1 to 9) prepared in the present study. Parameters such as the angle of repose, Carr's index, and Hausner's ratio are shown in Table 2. The angle of repose is characteristic of the flow rate of the powder. In general, an angle of repose $\geq 40^\circ$ indicates a powder with poor flowability (16). All formulations except CLS 1 and 7 had an angle of repose within the aforementioned range.

3.1.2. DSC behavior

DSC studies were carried out to determine interaction between the drug and excipients in prepared liquisolid formulations. These results will also indicate the success of stability studies (17). DSC thermograms of Ceolus KG-802, fenofibrate, and liquisolid formulations with Ceolus KG-802 are shown in Figure 1. Figure 1A shows

Table 2. Flowability parameters for various formulated batches of liquisolid powder systems

| Formulation batch code | Angle of repose (θ)* | Carr's index (%)* | Hausner's ratio* |
|------------------------|-------------------------------|-------------------|------------------|
| CLS 1 | 43.0 ± 0.2 | 19.3 ± 0.1 | 1.22 ± 0.02 |
| CLS 2 | 39.5 ± 0.3 | 20.2 ± 0.1 | 1.24 ± 0.02 |
| CLS 3 | 38.6 ± 0.2 | 22.3 ± 0.2 | 1.26 ± 0.02 |
| CLS 4 | 39.8 ± 0.2 | 20.1 ± 0.0 | 1.25 ± 0.01 |
| CLS 5 | 39.4 ± 0.2 | 22.0 ± 0.2 | 1.29 ± 0.01 |
| CLS 6 | 38.4 ± 0.3 | 23.3 ± 0.1 | 1.32 ± 0.01 |
| CLS 7 | 41.1 ± 0.3 | 24.1 ± 0.6 | 1.25 ± 0.01 |
| CLS 8 | 40.5 ± 0.3 | 23.8 ± 0.2 | 1.32 ± 0.01 |
| CLS 9 | 39.4 ± 0.2 | 25.3 ± 0.2 | 1.35 ± 0.01 |

* Data are shown as means \pm S.D.

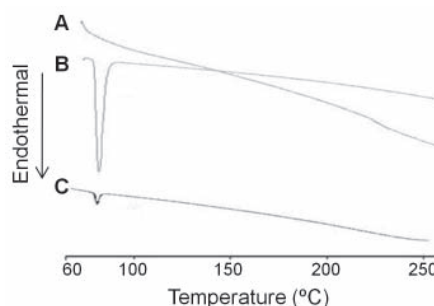


Figure 1. DSC thermograms of Ceolus KG-802 (A), fenofibrate (B), and a liquisolid system with Ceolus KG-802 (C).

a typical thermogram of Ceolus KG-802, indicating absence of an endothermic peak. In contrast, fenofibrate, as shown in Figure 1B, had a sharp characteristic peak in a temperature range of 79-82°C (with onset at 79.02°C and endset at 81.93°C) corresponding to its melting temperature (T_m). This suggests that the fenofibrate used was in pure form. A DSC thermogram of the liquisolid system with Ceolus KG-802 merely suggested the presence of the characteristic peak of fenofibrate (Figure 1C). This ensures formation of a drug solution in the liquisolid formulation and hence confirms that the drug was molecularly dispersed in the liquisolid system.

3.1.3. X-ray diffraction studies

Figure 2 shows typical XRD patterns of fenofibrate, Ceolus KG-802, and the liquisolid system with Ceolus KG-802. Clearly distinct characteristic peaks for fenofibrate at a diffraction angle of 2θ , *i.e.*, at 14.3°, 16.1°, and 22.2°, indicated that fenofibrate was in a crystalline state (Figure 2A). In contrast, the X-ray diffraction pattern for liquisolid powder lacked these distinct peaks (Figure 2C). The disappearance of certain fenofibrate peaks might be due to drug adsorption on the surface of the carrier after saturation of the absorption process. The lack of specific peaks (constructive reflections) for the liquisolid system revealed that fenofibrate was completely converted to a molecular form or solubilized form. This lack of crystallinity in the formulation might be due to solubilization of the drug, which was absorbed into the carrier material and adsorbed onto the carrier and coating materials, in the liquid vehicle. These results agree with DSC results, suggesting formation of a solid solution of fenofibrate within Ceolus KG-802 (the carrier material). This phenomenon might be responsible for enhanced

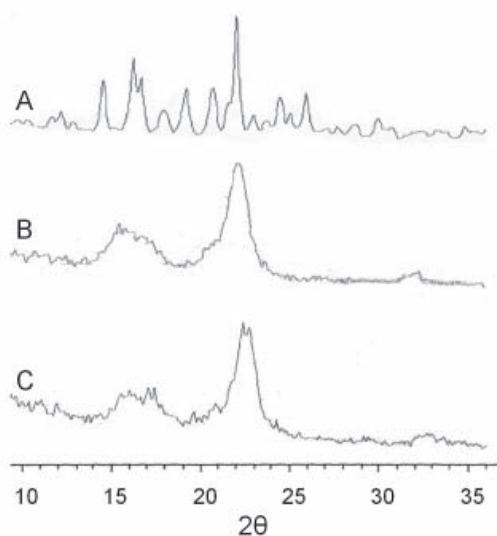


Figure 2. XRD patterns of fenofibrate (A), Ceolus KG-802 (B), and a liquisolid system with Ceolus KG-802 (C).

dissolution rates of fenofibrate liquisolid systems.

3.1.4. Stereomicroscopic analysis

Complete disappearance of the crystalline structure, as was indicated by DSC and XRD results, was also noted in stereomicroscopic images of the liquisolid system (Figure 3). This indicates that the drug is dispersed in molecular form inside the carrier matrix. However, the characteristic rod-shaped structure of Ceolus KG-802, which is responsible for the specific packing arrangement in the formulation, was retained in the formulation.

3.2. Evaluation of liquisolid tablets

Data on hardness, friability, and disintegration time for various formulated batches of liquisolid tablets are summarized in Table 3. A tablet should have a certain amount of strength or hardness and resistance to friability so that tablet will not break during handling. However, such aspects also affect tablet disintegration and drug dissolution. The average hardness of liquisolid tablets ranged from 30.4 ± 2.2 to 43.2 ± 1.0 N (Table 3). Tablet compactness may have been due to the highly compactable nature of Ceolus KG-802. As propylene glycol is an alcoholic compound, it might exhibit hydrogen bonding due to the presence of hydroxyl groups and may contribute to the compactness of tablets. Friability studies of liquisolid tablets resulted in values in the range of 0.002% to 0.205% (Table 3). This indicates that liquisolid tablets have sufficient durability to withstand handling. The low friability of the liquisolid tablets may also be due to Ceolus KG-802, as explained previously. The disintegration time was in the range of 6.46 ± 0.25 to 14.00 ± 0.26 min. This is a longer disintegration time than that obtained from liquisolid tablets with Avicel PH 102 (6). Hence, the longer disintegration time of formulations might be due to slower release rates. These findings are in accordance with dissolution rates.



Figure 3. A typical stereomicroscopic image of a liquisolid system prepared with Ceolus KG-802 as a carrier.

Table 3. Hardness, friability, and disintegration data for various batches of liquisolid tablet formulations

| Formulation batch code | Hardness (N)* | Percentage of grains obtained in a friability test (%) | Disintegration time (min)* |
|------------------------|---------------|--|----------------------------|
| CLS 1 | 33.3 ± 2.3 | 0.102 | 6.46 ± 0.25 |
| CLS 2 | 30.4 ± 2.2 | 0.005 | 7.06 ± 0.23 |
| CLS 3 | 35.1 ± 2.1 | 0.002 | 8.13 ± 0.30 |
| CLS 4 | 37.2 ± 1.4 | 0.167 | 10.40 ± 0.20 |
| CLS 5 | 36.4 ± 1.7 | 0.188 | 9.16 ± 0.15 |
| CLS 6 | 38.6 ± 1.5 | 0.123 | 8.36 ± 0.23 |
| CLS 7 | 43.2 ± 1.0 | 0.205 | 14.00 ± 0.26 |
| CLS 8 | 42.0 ± 2.1 | 0.112 | 12.20 ± 0.30 |
| CLS 9 | 40.4 ± 2.1 | 0.115 | 11.36 ± 0.15 |

* Data are shown as means ± S.D.

Table 4. Drug release by various liquisolid tablets and marketed formulations

| Formulation batch code* | Drug Release at 10 min (%)** | Drug Release at 45 min (%)** |
|-------------------------|------------------------------|------------------------------|
| CLS 1 | 79.0 ± 1.7 | 94.1 ± 1.8 |
| CLS 2 | 81.1 ± 1.0 | 95.8 ± 1.7 |
| CLS 3 | 82.9 ± 1.3 | 96.3 ± 1.8 |
| CLS 4 | 77.3 ± 1.3 | 91.8 ± 1.8 |
| CLS 5 | 81.8 ± 1.1 | 92.4 ± 1.8 |
| CLS 6 | 83.5 ± 0.7 | 93.1 ± 1.6 |
| CLS 7 | 70.8 ± 1.2 | 89.2 ± 1.4 |
| CLS 8 | 71.4 ± 1.1 | 90.5 ± 1.8 |
| CLS 9 | 76.4 ± 1.1 | 91.3 ± 1.3 |
| MKT | 68.3 ± 1.2 | 88.4 ± 2.0 |

* CLS, liquisolid tablets prepared using Ceolus KG-802; MKT, marketed formulation; ** Data are shown as means ± S.D.

3.3. In vitro dissolution studies

Dissolution rates of liquisolid formulations were compared to liquisolid tablets prepared using Avicel PH 102 in previous studies. As shown in Table 4, greater initial release or burst release ($Q_{10}\%$, *i.e.*, amount of drug released in 10 min) of liquisolid tablets (CLS 1 to 9) indicated that CLS 1 to 9 were effective. All liquisolid tablets had drug release greater than $88.4 \pm 2.0\%$ after 45 min (Table 4). According to the "diffusion layer model" of dissolution, the dissolution rate is in proportion to the concentration gradient in the stagnant diffusion layer (18). Drug dissolution is directly proportional to the surface area available for dissolution (19). In the current work, all dissolution tests were conducted at a constant speed (50 rpm) and in the same dissolution medium. Therefore, the thickness of the stagnant diffusion layer and diffusion coefficient for drug dissolution should be almost identical. Hence, surface area can be considered as a major factor responsible for enhancing the dissolution rate. As the liquid medication contains a drug in a molecularly dispersed form (dissolved in propylene glycol), an increase in the drug surface available for dissolution may be responsible for greater dissolution rates. A lower drug concentration in the liquid medication has also been found to result in more

rapid drug release. This is due to the fact that drugs at a high concentration tend to precipitate within silica pores (Aerosil 200). The dissolution profile of liquisolid tablets supports the aforementioned hypothesis. As noted by Spireas and Sadu (19), the solid/liquid interface between an individual liquisolid primary particle and the dissolving fluid involves minute quantities of aqueous medium clinging onto the particle surface. In such a micro-environment, the unlimited amounts of propylene glycol diffusing with the drug molecules out of a single liquisolid particle might be adequate to enhance the solubility of the drug by acting as a cosolvent with the aqueous dissolution medium. Moreover, the use of a superdisintegrant, sodium starch glycolate (used in each formulation at a concentration of 8% of the total weight), caused burst release by tablets. Such release has been found to enhance the dissolution rate of fenofibrate, as indicated by $Q_{10}\%$ values (Table 4).

Comparing the dissolution profiles of the liquisolid formulations (CLS 1 to 9) to those studied by Karmarkar *et al.* (7) indicated slower release from CLS 1 to 9. This might be due to use of Ceolus KG-802 instead of Avicel PH 102 in the present study. Ceolus KG-802 has a low bulk density and mainly exists as longer rod-shaped particles. It also has a larger length/diameter. Hence, during compression Ceolus KG-802 particles tend to arrange perpendicular to the applied force. This causes an increase in contact area and easy entanglement of particles (13). This nature might be due to the high hardness and low friability of CLS formulations 1 to 9. As a result, the drug might be released more slowly from the CLS formulations. The slower release by CLS formulations might be due to Ceolus KG-802's high polyethylene glycol retention capacity, which is also an indicator of liquid retention capacity (13). Thus, inhibition of liquid exudation may have led CLS formulations 1 to 9 to have slower release than formulations prepared using Avicel PH 102. However, release data indicating greater release than that from marketed formulations suggests that liquisolid formulations effectively enhanced dissolution rates.

4. Conclusion

The liquisolid tablet technique can effectively enhance dissolution rates of poorly water-soluble drugs such as fenofibrate. Propylene glycol was used as a liquid vehicle. Use of a highly compactable carrier such as Ceolus KG-802 resulted in slower dissolution rates compared to formulations prepared using Avicel PH 102. This might be due to the carrier's physical properties such as shape, size, bulk density, and liquid retention capacity.

References

1. Karmarkar AB, Gonjari ID, Hosmani AH. Liquisolid technology for dissolution rate enhancement or sustained release. *Expert Opin Drug Deliv.* 2010; 7:1227-1234.
2. Li X, Gu L, Xu Y, Wang Y. Preparation of fenofibrate nanosuspension and study of its pharmacokinetic behavior in rats. *Drug Dev Ind Pharm.* 2009; 35:827-833.
3. Amidon GL, Lennernäs H, Shah VP, Crison JR. A theoretical basis for a biopharmaceutical drug classification: The correlation of *in vitro* drug product dissolution and *in vivo* bioavailability. *Pharm Res.* 1995; 12:413-420.
4. Sweetman SC. *Martindale: The Complete Drug Reference.* 33rd ed. Pharmaceutical Press, London, UK, 2002.
5. Shi GQ, Dropinski JF, Zhang Y, *et al.* Novel 2,3-dihydrobenzofuran-2-carboxylic acids: Highly potent and subtype-selective PPAR α agonists with potent hypolipidemic activity. *J Med Chem.* 2005; 48:5589-5599.
6. Millionis HJ, Elisaf MS, Mikhailidis DP. Treatment of dyslipidaemias in patients with established vascular disease: A revival of the fibrates. *Curr Med Res Opin.* 2000; 16:21-32.
7. Karmarkar AB, Gonjari ID, Hosmani AH, Dhabale PN, Bhise SB. Dissolution rate enhancement of Fenofibrate using liquisolid tablet technique. *Lat Am J Pharm.* 2009; 28:219-225.
8. Karmarkar AB, Gonjari ID, Hosmani AH, Dhabale PN, Bhise SB. Dissolution rate enhancement of Fenofibrate using liquisolid tablet technique. Part II: Evaluation of *in vitro* dissolution profile comparison methods. *Lat Am J Pharm.* 2009; 28:538-543.
9. Karmarkar AB, Gonjari ID, Hosmani AH, Dhabale PN, Bhise SB. Liquisolid Tablets: A novel approach for drug delivery. *Int J Health Res.* 2009; 2:45-50.
10. Spireas S, Bolton M. Liquisolid Systems and Methods of Preparing Same. U.S. Patent 6,096,337. 2000.
11. Spireas S. Liquisolid Systems and Methods of Preparing Same. U.S. Patent 6,423,339 B1. 2002.
12. Signet – Selection Guide to Excipients, 2nd ed. Signet Chemical Corporation Pvt. Ltd., India, 2007.
13. Ceolus KG-802. Product information sheet. Asahi KASEI Chemicals Corporation. Functional Additives Division, Japan. (<http://www.ceolus.com>) (accessed May 26, 2010)
14. Staniforth J. Powder flow. In: *Pharmaceutics, the Science of Dosage Form Design*, 2nd ed. (Aulton M, ed.). Churchill Livingstone, Edinburgh, UK, 2000; pp. 197-210.
15. Spireas SS, Jarowski CI, Rihera BD. Powdered solution technology: Principles and mechanism. *Pharm Res.* 1992; 9:1351-1358.
16. Banker GS, Anderson NL. Tablets. In: *The Theory and Practice of Industrial Pharmacy*, 3rd ed. (Lachman L, Liberman HA, Kanig JL, eds.). Varghese Publishing House, Bombay, India, 1987; pp. 293-345.
17. Craig DQM. Pharmaceutical applications of DSC. In: *Thermal analysis of Pharmaceuticals* (Craig DQM, Reading M, eds.). CRC Press, Boca Raton, FL, USA, 2007; pp. 53-99.
18. Khaled KA. Formulation and evaluation of hydrochlorothiazide liquisolid tablets. *Saudi Pharm J.* 1988; 6:39-46.
19. Spireas S, Sadu S. Enhancement of prednisolone dissolution properties using liquisolid compacts. *Int J Pharm.* 1998; 166:177-188.

(Received November 10, 2010; Revised November 20, 2010; Accepted November 22, 2010)

Case Report

The treatment effect of the atopic dermatitis by electrolytic-reduction ion water lotion

Tetsuo Shu^{1,*}, Masahiro Okajima², Yuko Wada², Ken-ichi Shimokawa², Fumiyoshi Ishii^{2,**}

¹ Daikanyama Clinic of Cosmetic Surgery, Shibuya-ku, Tokyo, Japan;

² Department of Pharmaceutical Sciences, Meiji Pharmaceutical University, Tokyo, Japan.

ABSTRACT: A female in her late 20s was diagnosed with systemic atopic dermatitis in another hospital 5 years earlier and treated by steroid ointment application to the affected areas and oral steroid administration. She visited our hospital due to the aggravation of dermatitis symptoms over the entire face from 1 week earlier. Lesions were present on the face, chest, neck, and bilateral upper limbs, and, in particular, facial dermatitis was extensive. A diagnosis of systemic atopic dermatitis complicated by infection was made. As oral drugs, a herbal medicine and steroid/antihistamine combination tablet were used. As topical drugs, an steroid/antibiotic combination ointment and vitamin E/A ointment were applied. In addition, injections for the treatment of allergic disease were used, and acidic electrolyzed water and an electrolytic-reduction ion water (ERI) lotion were topically applied. While receiving the two types of oral drug, she received a subcutaneous injection once a week and the application of acidic electrolyzed water, ERI lotion, steroid/antibiotic combination ointment, and vitamin E/A ointment to the lesions twice a day. One week after the initiation of treatment, redness and swelling decreased. After 1 month, the swelling further decreased, but the redness remained. After 1.5 months, the redness further decreased, showing a favorable course. Three months after the initiation of treatment, slight redness remained, but the skin color was almost normal. This patient showed the improvement of skin redness and swelling and an almost normal skin state without pigmented scars. These results suggest the effectiveness of complex therapy consisting of a herbal medicine and steroid/antihistamine combination drug as oral drugs and

an steroid/antibiotic combination ointment and vitamin E/A ointment as topical drugs, injections for allergic disease, and acidic electrolyzed water and ERI lotion for disinfection and skin care.

Keywords: Electrolytic-reduction ion water, atopic dermatitis, acidic electrolyzed water, infectious disease

1. Introduction

Atopic dermatitis is caused by multiple factors including a genetic predisposition, and there is no drug therapy for the complete resolution of the disease itself. However, even when the condition becomes chronic, if symptoms are controlled by appropriate treatment, and the controlled state is maintained, spontaneous remission can be expected. Therefore, palliative therapy is performed in principle (1). Atopic dermatitis is accompanied by skin dryness and barrier function abnormality, and non-specific stimulatory responses and specific allergic responses are involved in its development. In many patients with an atopic predisposition, skin inflammation becomes chronic, and is accompanied by pruritus, and scratching behavior induces bacterial, fungal, or viral skin infection, aggravating symptoms, and the disease becomes chronic. The genetic factors predisposing to atopic dermatitis include diseases such as bronchial asthma, allergic rhinitis, conjunctivitis, or atopic dermatitis in the family or a past history and a predisposition for excessive IgE antibody production (2). Atopic dermatitis is mainly treated by the topical application of steroids or tacrolimus ointments of immunosuppressive agents to inflammatory skin areas, skin care with moisturizing and protective agents, and the oral administration of antihistamine and antiallergic agents for itching as adjunctive therapy to alleviate symptoms (3).

When an aqueous solution containing electrolytes such as NaCl or KCl-MgCl₂ is electrolyzed using an electrolysis cell with a diaphragm (septum or

*Dr. Tetsuo Shu passed away.

**Address correspondence to:

Dr. Fumiyoshi Ishii, Department of Pharmaceutical Sciences, Meiji Pharmaceutical University, 2-522-1 Noshio, Kiyose, Tokyo 204-8588, Japan.
e-mail: fishii@my-pharm.ac.jp

membrane) between the anode and cathode, acidic electrolyzed water is obtained on the anode side and alkaline electrolyzed water on the cathode side (4,5). Acidic electrolyzed water shows pH 2-3. Its oxidation-reduction potential (ORP) is more than 1,100 mV, and its active chlorine content (ACC) is 10-90 ppm. Acidic electrolyzed water with these characteristics is widely used as sterilizing/disinfecting agents or deodorants, and is particularly used in the food industry due to its high-level safety (5).

Alkaline electrolyzed water shows pH 10-13 and ORP -800 - -900 mV (5), and is used mainly for the cleaning of industrial products due to its cleansing and antioxidative effects (6).

In the dental field, recent studies have shown the disinfecting and antibacterial effects of acidic electrolyzed water on dental bacteria, particularly pathogenic bacteria causing periodontal disease (7,8). There have also been studies on the use of alkaline electrolyzed water in the medical field (9,10).

Electrolytic reduction ion water (ERI) S-100[®] as a new specific water is produced by the electrolysis of an aqueous solution containing electrolytes using a specific electrolysis cell. Physically, ERI S-100[®] contains an excessive amount of electrons, and has effects such as cleaning, disinfection, antioxidation, and emulsification due to its specific alkaline property and negative ions (6,11,12). In the medical field, healing effects on burns have also been reported (13,14).

In this patient with atopic dermatitis accompanied by infection, in addition to treatment with oral drugs, topical agents, and injections, adjunctive therapy with acidic electrolyzed water with sterilizing effects and ERI lotion with skin care effects was performed, and favorable results were obtained.

2. Materials and Methods

2.1. Materials

Acidic electrolyzed water and ERI lotion (S-100[®], 94.9%; glycerin, 3%; ascorbic acid, 2%; hyaluronic acid, 0.1%) manufactured by A.I. System Products Corp. was used. As the kampo preparation, we used Ourengedokutou[®] manufactured by Tsumura & Corp., Tokyo, Japan. For the steroid/antihistamine combination tablet, Emperacin[®] tablets (containing betamethasone *d*-chlorpheniramine maleate) manufactured by Sawai Pharmaceutical Co., Ltd., Osaka, Japan, was used. As the steroid/antibiotic combination ointment, Dexan-VG[®] 0.12% ointment (containing betamethasone valerate and gentamicin sulfate) manufactured by Fuji Pharma Co., Ltd., Tokyo, Japan, was employed. The vitamin A/E ointment was Juvela[®] (containing tocopherol and vitamin A oil) manufactured by Eisai Co., Ltd., Tokyo, Japan. For the

allergosis therapeutic drug, Histaglobin[®] subcutaneous injection manufactured by Nippon Zoki Pharmaceutical Co., Ltd., Osaka, Japan, was used.

2.2. Methods

Ourengedokutou[®] was administered at a daily dose of 7.5 g 3 times/day (before every meal or between meals), and Emperacin[®] (2 tablets at a time) was administered twice/day (after breakfast and supper). An appropriate amount of acidic electrolyzed water was applied to the affected areas twice daily, which was followed by the application of appropriate amounts of ERI lotion and a mixture of equal amounts of Dexan-VG[®] and Juvela[®] ointments. A subcutaneous Histaglobin[®] injection (1 vial/injection) was administered 1 week after the initiation of treatment and, subsequently, at 1-week intervals (total, 8 times).

3. Results

A female in her late 20s was diagnosed with systemic atopic dermatitis in another hospital 5 years earlier, and treated by steroid ointment application to affected areas and oral steroid administration. She visited our hospital due to the aggravation of dermatitis symptoms over the entire face from 1 week before the visit. Lesions were present over the face, chest, neck, and bilateral upper limbs, and, in particular, facial dermatitis was extensive. A diagnosis of systemic atopic dermatitis complicated by infection was made.

As oral drugs, a herbal medicine and steroid/antihistamine combination tablet were used. As topical drugs, an steroid/antibiotic combination ointment and vitamin E/A ointment were applied. In addition, subcutaneous Histaglobin[®] injections for the treatment of allergic disease were given, and acidic electrolyzed water and ERI lotion were topically applied for the sterilization of the skin surface and skin care. The treatment course is shown in Figure 1. Figures 1A-1D show photographs of the frontal face, right side of the face, left side of the face, and posterior neck, respectively, before treatment.

Compared with the pre-treatment state, redness and swelling decreased 1 week after the initiation of treatment (Figures 1E-1H). A subcutaneous Histaglobin[®] injection for the treatment of allergic disease was given at 1-week intervals. The course from 1 to 3 months after the initiation of treatment is shown in Figure 2. Swelling decreased 1 month after the initiation of treatment, but redness remained (Figures 2A-2C). Redness decreased after 1.5 months, showing a favorable course (Figures 2D-2F). Three months after the initiation of treatment, although slight redness was observed, the skin color was almost normal (Figures 2G-2I).

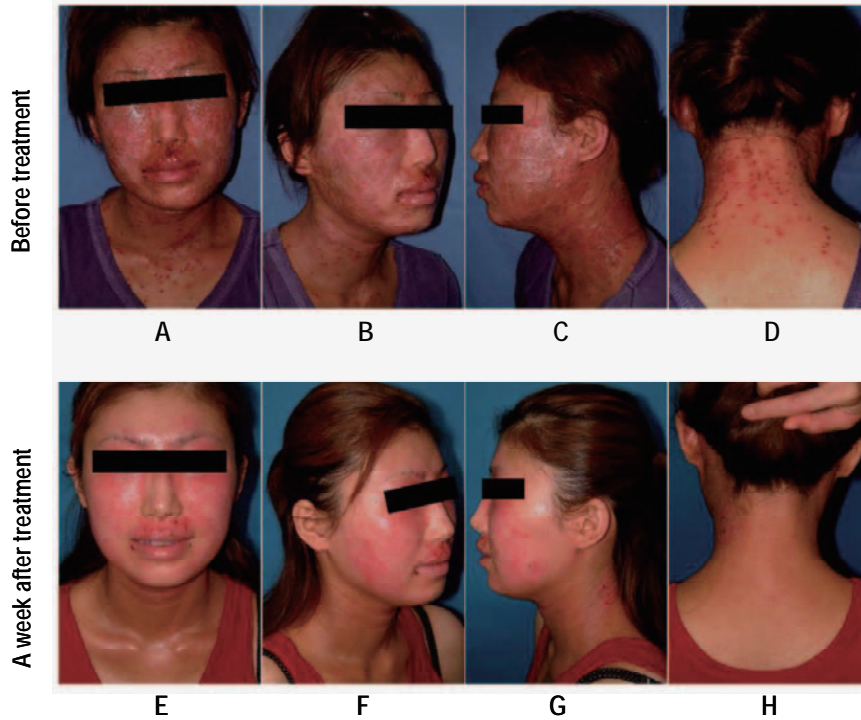


Figure 1. A case involving treatment of the facial surface and neck with ERI lotion, steroid/antibiotic combination ointment and vitamin E/A ointment. (A)-(D): Before treatment; (E)-(H): 1 week after treatment. (A), Front side; (B), Right side; (C), Left side; (D), Rear side; (E), Front side; (F), Right side; (G), Left side; (H), Rear side.

1 month
After treatment



1.5 months
After treatment



3 months
After treatment



Figure 2. A case involving treatment of the facial surface and neck with ERI lotion, steroid/antibiotic combination ointment and vitamin E/A ointment. (A)-(C): 1 month after treatment; (D)-(F): 1.5 months after treatment; (G)-(I): 3 months after treatment. (A), Front side; (B), Right side; (C), Left side; (D), Front side; (E), Left side; (F), Rear side; (G), Front side; (H), Right side; (I), Left side.

4. Discussion

Atopic differential tests of the patient's blood for single allergens revealed a class 6 IgE RAST score for *Dermatophagoides pteronyssinus*, cat skin debris, and dog skin debris, class 5 score for house dust 1, and a class 3 score for Japanese cedar. Therefore, she was informed of these allergens and given instructions for their elimination as adjunctive therapy.

She was initially treated by the application of an appropriate amount of acidic electrolyzed water to the affected areas for the sterilization and disinfection of skin surface bacteria, followed by the application of a steroid/antibiotic combination ointment. The Guidelines for Management of Atopic Dermatitis (1) recommend that a very strong or higher class topical steroid should be used first to improve eruptions, which is subsequently changed to a tacrolimus ointment with immunosuppressive effects. A study showed no increase in the incidence of skin infection using tacrolimus ointments (15), but others have reported an increase in the incidence of herpes simplex virus infection in the face and neck (16,17) using these ointments. In this patient, since severe infection was present in addition to atopic dermatitis, we did not use tacrolimus ointments with immunosuppressive effects but employed a strong class topical steroid containing an antibiotic.

In addition, to improve dryness, compensate for the decrease in barrier function, and prevent the relapse of inflammation due to scratching, skin care was performed with ERI lotion containing glycerin and hyaluronic acid with moisturizing effects, and vitamin E/A ointment with skin microcirculation-activating and skin protection effects.

Since dermatitis and infection symptoms improved 1 week after the initiation of treatment compared with the pre-treatment state, she was instructed to gradually reduce the dose of the topical steroid while paying attention to the possible relapse of inflammation, and similar treatment was continued (Figures 1A-1H).

Since the condition became stable after 1 month, the frequency of application of the topical steroid was gradually decreased while the application of the acidic electrolyzed water, ERI lotion, and vitamin E/A ointment was continued (Figures 2A-2C).

A marked improvement of symptoms was observed after 3 months compared with the pre-treatment state, suggesting that not only topical steroid application but also adjunctive skin care by the application of the acidic electrolyzed water, ERI lotion, and vitamin E/A ointment was also effective.

In this study, we used ERI lotion, expecting its effects on atopic dermatitis because its effects on burns have been suggested (13,14). Atopic dermatitis tends to induce bacterial/fungal/viral skin infection. Therefore, the application of ERI lotion as alkaline electrolyzed water, as well as acidic electrolyzed water,

is effective for the prevention of these infections. Povidone iodine and alcohol disinfectants have a skin-damaging action, whereas ERI lotion is less of a skin irritant, has emulsification effects, and does not contain surfactants used for the preparation of emulsions. Topical steroids are used twice/day in principle, and their long-term use runs the risk of severe adverse effects such as glaucoma due to increased ocular pressure or posterior capsule opacification. If dermatitis does not relapse, it is important to decrease the amount and frequency of topical steroid application according to the symptoms, and change topical steroid therapy to maintenance therapy with acidic electrolyzed water, ERI lotion, and vitamin E/A ointment.

5. Conclusion

In this patient, skin redness and swelling markedly improved, and healing to an almost normal state without pigmented scars was observed. These results suggest the effectiveness of complex therapy consisting of a herbal medicine and steroid/antihistamine combination tablet as oral drugs, a steroid/antibiotic combination ointment and vitamin E/A ointment as topical drugs, subcutaneous injections for the treatment of allergic disease, acidic electrolyzed water, and ERI lotion for treating atopic dermatitis complicated by infection.

References

1. Saeki H, Furue M, Furukawa F, Hide M, Ohtsuki M, Katayama I, Sasaki R, Suto H, Takehara K; COMMITTEE for GUIDELINES for the MANAGEMENT of ATOPIC DERMATITIS of JAPANESE DERMATOLOGICAL ASSOCIATION. Guidelines for management of atopic dermatitis. *J Dermatol.* 2009; 36:563-577.
2. Furue M, Saeki H, Furukawa F, Hide M, Ohtsuki M, Katayama I, Sasaki R, Suto H, Takehara K. Guidelines for management of atopic dermatitis. *Jpn J Dermatol.* 2009; 119:1515-1534.
3. Japanese FK506 Ointment Study Group. Clinical guidance for treatment of patients with atopic dermatitis by tacrolimus ointment 0.1% and 0.03%. *Jpn J Clinical Dermatol.* 2003; 57:1217-1234.
4. Guide for the electrolyzed reduced water. Functional Water Foundation. 2002; pp. 261-266.
5. Hricova D, Stephan R, Zweifel C. Electrolyzed water and its application in the food industry. *J Food Prot.* 2008; 71:1934-1947.
6. Okajima M. Proceedings of Japanese society for Applied Research in Negative Ion. 2002.
7. Ozawa H, Arai T. Guideline of the electrolyzed functional water in the dentistry. *J Tokyo Dental Association.* 2009; 57:4-10.
8. Kato T, Yamanaka A, Yamada K, Kimizuka R, Ishihara K, Okuda K. Evaluation of antimicrobial effect of electrolyzed oxidizing water (EO water) using oral microbial biofilm models. *Bacterial Adherence Biofilm.* 2006; 20:116-121.
9. Huang KC, Yang CC, Lee KT, Chien CT. Reduced

- hemodialysis-induced oxidative stress in end-stage renal disease patients by electrolyzed reduced water. *Kidney Int.* 2003; 64:704-714.
10. Huang KC, Yang CC, Hsu SP, Lee KT, Liu HW, Morisawa S, Otsubo K, Chien CT. Electrolyzed-reduced water reduced hemodialysis-induced erythrocyte impairment in end-stage renal disease patients. *Kidney Int.* 2006; 70:391-398.
 11. Konomatu A, Sugibayashi K, Okajima M, Ishii F. Preparation and stability of surfactant free emulsions using electrolyzed deoxidized and ionized water. *Material Tech.* 2003; 21:273-285.
 12. Kitagawa T, Okajima M, Shimokawa K, Ishii F. Physicochemical properties of magnesium aluminum silicates (smectites) gels prepared by electrolytic-reduction ion water. (1): Rheological properties. *Material Tech.* 2008; 26:50-54.
 13. Okajima M, Shimokawa K, Ishii F. The healing effect of electrolytic-reduction ion water on burn wounds. *BioSci Trends.* 2010; 4:31-36.
 14. Shu T, Okajima M, Shimokawa K, Ishii F. The treatment effect of the burn wound healing by electrolytic-reduction ion water lotion combination therapy. Part 2: Two degree burn of forearm to the dorsum of the hand. *BioSci Trends.* 2010; 4:213-217.
 15. Fleischer AB Jr, Ling M, Eichenfield L, Satoi Y, Jaracz E, Rico MJ, Maher RM; Tacrolimus Ointment Study Group. Tacrolimus ointment for the treatment of atopic dermatitis is not associated with an increase in cutaneous infections. *J Am Acad Dermatol.* 2002; 47:562-570.
 16. Furue M, Terao H, Rikihisa W, Urabe K, Kinukawa N, Nose Y, Koga T. Clinical dose and adverse effects of topical steroids in daily management of atopic dermatitis. *Br J Dermatol.* 2003; 148:128-133.
 17. Furue M, Terao H, Moroi Y, Koga T, Kubota Y, Nakayama J, Furukawa F, Tanaka Y, Katayama I, Kinukawa N, Nose Y, Urabe K. Dosage and adverse effects of topical tacrolimus and steroids in daily management of atopic dermatitis. *J Dermatol.* 2004; 31:277-283.

(Received October 25, 2010; Accepted December 17, 2010)

Author Index (2010)**A**

Abd El-Gawad AH, 4(2):85-92; 4(2):93-99
 Abd El-Gawad NA, 4(6):484-492
 Abd El-Halim SM, 4(6):484-492
 Abd-Allah FI, 4(4):257-266; 4(4):267-275
 Abdel Malak NS, 4(6):459-471; 4(6):472-483
 Abdel Rehim AA, 4(6):459-471
 Abdel Salam OME, 4(4):285-297
 Abdel-Aziz L, 4(6):418-422
 Abdel-Fattah L, 4(6):418-422
 Abdel-Rashid RS, 4(3):208-216
 Abu-Zaid NM, 4(4):276-284
 Ahmed AMS, 4(4):257-266; 4(4):267-275
 Ahmed MK, 4(2):77-84
 Akimitsu N, 4(4):235-239; 4(5):368-372
 Amer RI, 4(5):380-387
 Amin MM, 4(6):484-492
 Ammar AA, 4(2):77-84; 4(5):373-379
 Arakawa T, 4(5):326-333
 Attia AM, 4(2):100-108
 Ayoub N, 4(5):341-348
 Azuma I, 4(2):135-143

B

Badawi AA, 4(6):472-483
 Benincosa L, 4(1):44-53
 Bhise SB, 4(6):435-441
 Bhunia B, 4(6):453-458
 Bommareddy A, 4(3):184-189

C

Calhelha RC, 4(4):246-256
 Cao JC, 4(5):355-361
 Cao X, 4(6):405-411
 Chadha R, 4(3):190-201
 Chaothanaphat N, 4(1):19-25
 Chen RQ, 4(5):355-361
 Cheng F, 4(1):13-18
 Coutinho OP, 4(3):144-167; 4(4):246-256
 Cronenberger CL, 4(1):44-53

D

Das N, 4(5):298-313
 Dawaba HM, 4(4):257-266; 4(4):267-275
 Dhabale PN, 4(1):26-32
 Dhanawat M, 4(5):298-313

Dhumma-Upakorn P, 4(1):19-25

Diab YM, 4(3):202-207

Dixit Y, 4(5):314-325

Duan SF, 4(4):240-245

Dwivedi C, 4(3):184-189

E

Elbadry M, 4(6):399-404
 El-Bayoomy TS, 4(6):472-483
 El-Demerdash E, 4(4):276-284
 El-Gazayerly ON, 4(6):459-471; 4(6):484-492
 El-Ghobashy MR, 4(3):217-222
 El-Kosasy A, 4(6):418-422
 El-Leithy ES, 4(3):208-216
 El-Mesallamy HO, 4(4):276-284
 El-Naggar M, 4(5):341-348
 Elosaily GH, 4(5):373-379
 EL-Houssieny BM, 4(1):33-43
 Emam A, 4(6):399-404
 Emam AM, 4(3):202-207
 Eweis M, 4(6):399-404

F

Fang H, 4(1):5-12; 4(6):388-391
 Feng JH, 4(1):5-12
 Fujiyuki T, 4(5):349-354

G

Gad MZ, 4(4):276-284
 Gaied M, 4(6):418-422
 Gao JJ, 4(6):405-411
 Gao Y, 4(3):175-178; 4(3):179-183
 Gastonguay MR, 4(1):44-53
 Gedik G, 4(5):362-367
 Ghorab MK, 4(3):208-216
 Ghorab MM, 4(2):100-108
 Glue P, 4(1):44-53
 Gonjari ID, 4(1):26-32; 4(6):423-434
 Guan P, 4(6):388-391
 Guda TK, 4(2):85-92; 4(2):93-99
 Gupta S, 4(3):190-201

H

Halaçođlu MD, 4(2):123-128
 Hamamoto H, 4(5):349-354; 4(5):368-372

Hamouda HM, 4(1):33-43
Hasegawa S, 4(6):412-417
Hashimoto H, 4(1):1-4
Hellebrand EE, 4(2):54-61
Hirano A, 4(5):326-333
Hirotsu Y, 4(2):129-134
Hosmani AH, 4(1):26-32; 4(6):423-434

I

Ibrahim HK, 4(2):100-108
Ijiri K, 4(4):235-239; 4(5):368-372
Ikeda K, 4(2):129-134
Imamura K, 4(5):349-354
Ishii F, 4(6):499-503
Ito T, 4(5):368-372

J

Jain DS, 4(3):190-201
Jianmongkol S, 4(1):19-25

K

Kang KS, 4(4):223-234
Kar A, 4(5):314-325
Karekar PS, 4(2):70-76
Karmarkar AB, 4(1):26-32; 4(6):423-434;
4(6):493-498
Kashiwazaki Y, 4(2):135-143
Kassem AA, 4(5):373-379; 4(5):380-387
Kaushik RS, 4(3):184-189
Khade TS, 4(6):423-434
Khan ZK, 4(6):435-441
Kimura S, 4(6):412-417
Kita Y, 4(5):326-333
Kobayashi A, 4(6):412-417
Koga-Yamakawa E, 4(2):135-143
Koyama AH, 4(5):326-333
Kubota T, 4(6):412-417
Kuchekar BS, 4(3):168-174
Kumar PV, 4(6):392-398

L

Laird Forrest M, 4(4):240-245
Li X, 4(1):5-12
Li YG, 4(1):5-12
Li ZG, 4(1):13-18
Liang QD, 4(3):175-178; 4(3):179-183
Lindequist U, 4(5):341-348

Liu H, 4(5):355-361
Liu JF, 4(5):355-361
Liu M, 4(3):179-183
Liu ZP, 4(1):13-18
Lu BB, 4(3):175-178; 4(3):179-183

M

Ma BP, 4(3):175-178
Ma J, 4(3):179-183
Ma ZC, 4(3):175-178; 4(3):179-183
Machado VA, 4(4):246-256
Malhotra BK, 4(1):44-53
Manjanna KM, 4(2):109-122
Maruta H, 4(1):1-4
Marzouk MA, 4(2):77-84; 4(5):373-379;
4(5):380-387
Masuo Y, 4(5):368-372
Megally NY, 4(3):202-207
Miyauchi M, 4(2):135-143
Mohamed MA, 4(3):202-207
Mou JJ, 4(1):5-12
Murata M, 4(2):135-143
Myotoku M, 4(2):129-134

N

Nagarwal RC, 4(5):298-313
Nakamura Y, 4(4):235-239
Narade SB, 4(6):435-441
Nath LK, 4(6):453-458
Navale RB, 4(6):423-434
Nishimura R, 4(1):1-4
Noh JS, 4(4):223-234
Nouh AT, 4(2):85-92; 4(2):93-99

O

Okajima M, 4(6):499-503

P

Pandit JK, 4(5):298-313
Pani NR, 4(6):453-458
Park CH, 4(4):223-234
Parmar HS, 4(5):314-325
Patel M, 4(6):442-452
Patel R, 4(6):442-452
Patil SB, 4(6):435-441
Pore YV, 4(2):70-76; 4(3):168-174; 4(6):435-441
Pramod Kumar TM, 4(2):109-122

Q**Qin HD**, 4(1):13-18**Queiroz MRP**, 4(4):246-256**R****Rakwal R**, 4(5):368-372**S****Samy AM**, 4(2):77-84; 4(5):380-387**Sanad RA**, 4(6):472-483**Sancheti PP**, 4(2):70-76**Saxena B**, 4(5):334-340**Sekimizu K**, 4(5):349-354; 4(5):368-372**Selvam TP**, 4(6):392-398**Shafee N**, 4(4):285-297**Shah MR**, 4(2):70-76**Shaker DS**, 4(3):208-216**Shete DK**, 4(6):435-441**Shi YQ**, 4(1):13-18**Shibahara N**, 4(4):223-234**Shibato J**, 4(5):368-372**Shibuya K**, 4(2):135-143**Shimokawa K**, 4(6):499-503**Shiraki K**, 4(5):326-333**Shivakumar B**, 4(2):109-122**Shu T**, 4(6):499-503**Shukla G**, 4(3):190-201**Silva JP**, 4(3):144-167; 4(4):246-256**Singab AN**, 4(5):341-348**Singh S**, 4(3):190-201**Sleem AA**, 4(4):285-297**Soliman SM**, 4(6):459-471**Sudo T**, 4(1):1-4**Süha Yalçın A**, 4(5):362-367**Sumiya E**, 4(5):368-372**Surve SS**, 4(6):435-441**Sweeney KR**, 4(1):44-53**T****Tan HL**, 4(3):175-178; 4(3):179-183**Tan HN**, 4(5):355-361**Tanaka T**, 4(4):223-234**Tani H**, 4(4):235-239**Tano K**, 4(5):368-372**Türkođlu M**, 4(2):123-128; 4(5):362-367**U****Uđurlu T**, 4(2):123-128; 4(5):362-367**V****Varbiro G**, 4(2):54-61**Vyas VM**, 4(2):70-76**W****Wada Y**, 4(6):499-503**Wang FS**, 4(5):355-361**Wang HS**, 4(1):13-18**Wang L**, 4(2):62-69**Wang Q**, 4(1):5-12**Wang X**, 4(5):355-361**Wang YG**, 4(3):175-178; 4(3):179-183**Wang YG**, 4(5):355-361**X****Xiao CG**, 4(3):179-183**Xiao CR**, 4(3):175-178**Xie YM**, 4(4):240-245**Xu WF**, 4(1):5-12**Y****Yamabe N**, 4(4):223-234**Yamaguchi H**, 4(6):412-417**Yanagawa Y**, 4(2):135-143**Yang RL**, 4(6):405-411**Yılmaz AM**, 4(5):362-367**Yohda M**, 4(6):412-417**Yokozawa T**, 4(4):223-234**Yuan XW**, 4(6):405-411**Z****Zaazaa HE**, 4(3):217-222**Zhang BL**, 4(3):175-178; 4(3):179-183**Zhang J**, 4(1):5-12**Zhang XY**, 4(3):184-189**Zhou X**, 4(2):62-69**Zhu HW**, 4(1):5-12

Subject Index (2010)

Reviews

Development of mitochondrial permeability transition inhibitory agents: a novel drug target.

Hellebrand EE, Varbiro G

2010; 4(2):54-61.

Uses of single-particle tracking in living cells.

Zhou X, Wang L

2010; 4(2):62-69.

Free radicals in the regulation of damage and cell death – basic mechanisms and prevention.

Silva JP, Coutinho OP

2010; 4(3):144-167.

Bioactive constituents of Corni Fructus: The therapeutic use of morroniside, loganin, and 7-O-galloyl-D-sedoheptulose as renoprotective agents in type 2 diabetes.

Yokozawa T, Kang KS, Park CH, Noh JS, Yamabe N, Shibahara N, Tanaka T

2010; 4(4):223-234.

Development in malarial vaccine: A review.

Dhanawat M, Das N, Nagarwal RC, Pandit JK

2010; 4(5):298-313.

Fruit and vegetable peels: Paving the way towards the development of new generation therapeutics.

Parmar HS, Dixit Y, Kar A

2010; 4(5):314-325.

Potential application of arginine in interaction analysis.

Shiraki K, Hirano A, Kita Y, Koyama AH, Arakawa T

2010; 4(5):326-333.

Clinical development of histone deacetylase inhibitor romidepsin.

Guan P, Fang H

2010; 4(6): 388-391

Brief Reports

The direct PAK1 inhibitor, TAT-PAK18, blocks preferentially the growth of human ovarian cancer cell lines in which PAK1 is abnormally activated by autophosphorylation at Thr 423.

Hashimoto H, Sudo T, Maruta H, Nishimura R

2010; 4(1):1-4.

3D QSAR investigations on locomotor activity of 5-cyano-N1,6-disubstituted 2-thiouracil derivatives.

Kuchekar BS, Pore YV

2010; 4(3):168-174.

Serum fructose concentration in rats after single dose oral administration of Si-Wu-Tang.

Liang QD, Xiao CR, Ma ZC, Wang YG, Lu BB, Tan HL, Ma BP, Zhang BL, Gao Y

2010; 4(3):175-178.

Stability of MALAT-1, a nuclear long non-coding RNA in mammalian cells, varies in various cancer cells.

Tani H, Nakamura Y, Ijiri K, Akimitsu N
2010; 4(4):235-239.

Alkyne- and 1,6-elimination-succinimidyl carbonate-terminated heterobifunctional poly(ethylene glycol) for reversible "Click" PEGylation.

Xie YM, Duan SF, Laird Forrest M
2010; 4(4):240-245.

Synthesis, characterization, and anthelmintic activity of novel 6,7,8,9-tetrahydro-5H-5-phenyl-2-benzylidene-3-substituted hydrazino thiazolo (2,3-b) quinazoline derivatives and analogues.

Selvam TP, Kumar PV
2010; 4(6):392-398.

Original Articles

Design, synthesis, and primary activity evaluation of pyrrolidine derivatives as matrix metalloproteinase inhibitors.

Zhang J, Li X, Zhu HW, Wang Q, Feng JH, Mou JJ, Li YG, Fang H, Xu WF
2010; 4(1):5-12.

Hypotensive response in rats and toxicological mechanisms induced by shuanghuanglian, an herbal extract mixture.

Wang HS, Cheng F, Shi YQ, Li ZG, Qin HD, Liu ZP
2010; 4(1):13-18.

***In vitro* modulating effects of glutathione on vascular tension and involvement of extracellular calcium.**

Chaothanaphat N, Dhumma-Upakorn P, Jianmongkol S
2010; 4(1):19-25.

Evaluation of *in vitro* dissolution profile comparison methods of sustained release tramadol hydrochloride liquid compact formulations with marketed sustained release tablets.

Karmarkar AB, Gonjari ID, Hosmani AH, Dhabale PN
2010; 4(1):26-32.

Formulation and evaluation of clotrimazole from pluronic F₁₂₇ gels.

EL-Houssieny BM, Hamouda HM
2010; 4(1):33-43.

Exposure-response modeling and clinical trial simulation of the effect of tolterodine on QT intervals in healthy volunteers.

Sweeney KR, Gastonguay MR, Benincosa L, Cronenberger CL, Glue P, Malhotra BK
2010; 4(1):44-53.

Proton magnetic resonance (¹HNMR) spectroscopy and physicochemical studies of zaleplon-hydroxypropyl- β -cyclodextrin inclusion compounds.

Shah MR, Sancheti PP, Vyas VM, Karekar PS, Pore YV
2010; 4(2):70-76.

Enhancement of the dissolution profile of allopurinol by a solid dispersion technique.

Samy AM, Marzouk MA, Ammar AA, Ahmed MK
2010; 4(2):77-84.

Formulation and bioavailability of controlled release salbutamol sulphate tablets using natural additives.

Nouh AT, Abd El-Gawad AH, Guda TK
2010; 4(2):85-92.

Stability, bioavailability, and ulcerative activity of diclofenac sodium-mastic controlled release tablets.

Nouh AT, Abd El-Gawad AH, Guda TK
2010; 4(2):93-99.

Biopharmaceutical evaluation of formulated metformin/rosiglitazone tablets.

Ibrahim HK, Attia AM, Ghorab MM
2010; 4(2):100-108.

Calcium alginate cross-linked polymeric microbeads for oral sustained drug delivery in arthritis.

Manjanna KM, Pramod Kumar TM, Shivakumar B
2010; 4(2):109-122.

Effects of lubricants on binary direct compression mixtures.

Uđurlu T, Halaçođlu MD, Türkođlu M
2010; 4(2):123-128.

Effects of the herbal medicine Hachimi-jio-gan (Ba-Wei-Di-Huang-Wan) on insulin secretion and glucose tolerance in type 2 diabetic Goto-Kakizaki rats.

Hirotsani Y, Ikeda K, Myotoku M
2010; 4(2):129-134.

Phagocytosis plays a dual role in activating dendritic cells; digestive production of active Toll-like receptor ligands and cooperation with Toll-like receptor signaling.

Miyauchi M, Murata M, Shibuya K, Koga-Yamakawa E, Yanagawa Y, Azuma I, Kashiwazaki Y
2010; 4(2):135-143.

***Rehmanniae Radix* provides most of the free fructose and glucose in Si-Wu-Tang decoction.**

Ma J, Liang QD, Ma ZC, Wang YG, Liu M, Lu BB, Tan HL, Xiao CG, Zhang BL, Gao Y
2010; 4(3):179-183.

Effects of components present in flaxseed on human colon adenocarcinoma Caco-2 cells: Possible mechanisms of flaxseed on colon cancer development in animals.

Bommareddy A, Zhang XY, Kaushik RS, Dwivedi C
2010; 4(3):184-189.

Characterization, thermodynamic parameters and *in vivo* antimalarial activity of inclusion complexes of artemether.

Chadha R, Gupta S, Shukla G, Jain DS, Singh S
2010; 4(3):190-201.

Isolation and structure elucidation of antioxidant compounds from leaves of *Laurus nobilis* and *Emex spinosus*.

Emam AM, Mohamed MA, Diab YM, Megally NY
2010; 4(3):202-207.

Optimization and characterization of diclofenac sodium microspheres prepared by a modified coacervation method.

El-Leithy ES, Shaker DS, Ghorab MK, Abdel-Rashid RS
2010; 4(3):208-216.

Membrane electrodes for determination of two antihypertensive drugs in pharmaceutical formulations of either single or binary mixtures and in biological fluids.

El-Ghobashy MR, Zaazaa HE
2010; 4(3):217-222.

Di(hetero)arylamines in the benzo[b]thiophene series as novel potent antioxidants.

Silva JP, Machado VA, Calhelha RC, Queiroz MRP, Coutinho OP
2010; 4(4):246-256.

Development of a microemulsion-based formulation to improve the availability of poorly water-soluble drug.

Abd-Allah FI, Dawaba HM, Ahmed AMS
2010; 4(4):257-266.

Preparation, characterization, and stability studies of piroxicam-loaded microemulsions in topical formulations.

Abd-Allah FI, Dawaba HM, Ahmed AMS
2010; 4(4):267-275.

The potential therapeutic effect of nitric oxide modulators in experimentally-induced gastric ulcers.

El-Demerdash E, El-Mesallamy HO, Abu-Zaid NM, Gad MZ
2010; 4(4):276-284.

Effect of trazodone and nefazodone on hepatic injury induced by carbon tetrachloride.

Abdel Salam OME, Sleem AA, Shafee N
2010; 4(4):285-297.

Anti-hyperlipidemic activity of *Withania coagulans* in streptozotocin-induced diabetes: A potent anti-atherosclerotic agent.

Saxena B
2010; 4(5):334-340.

Investigation of phenolic leaf extract of *Heimia myrtifolia* (Lythraceae): Pharmacological properties (stimulation of mineralization of SaOS-2 osteosarcoma cells) and identification of polyphenols.

Ayoub N, Singab AN, El-Naggar M, Lindequist U
2010; 4(5):341-348.

Evaluation of therapeutic effects and pharmacokinetics of antibacterial chromogenic agents in a silkworm model of *Staphylococcus aureus* infection.

Fujiyuki T, Imamura K, Hamamoto H, Sekimizu K
2010; 4(5):349-354.

Effect of heparin-superoxide dismutase on γ -radiation induced DNA damage *in vitro* and *in vivo*.

Liu JF, Wang X, Tan HN, Liu H, Wang YG, Chen RQ, Cao JC, Wang FS
2010; 4(5):355-361.

***In vivo* evaluation of black and green tea dermal products against UV radiation.**

Türkođlu M, Uđurlu T, Gedik G, Yđlmaz AM, Süha Yalçın A
2010; 4(5):362-367.

Reduced expression of *Syt1* and *Ccdc21* and impaired induction of *Mt1* by oxidative stress in *SII-K1* knockout mice.

Tano K, Hamamoto H, Ito T, Sumiya E, Rakwal R, Shibato J, Masuo Y, Ijiri K, Sekimizu K, Akimitsu N
2010; 4(5):368-372.

Preparation and *in vitro* evaluation of self-nanoemulsifying drug delivery systems (SNEDDS) containing clotrimazole.

Kassem AA, Marzouk MA, Ammar AA, Elosaily GH
2010; 4(5):373-379.

Comparative evaluation of ketoconazole- β -cyclodextrin systems prepared by coprecipitation and kneading.

Marzouk MA, Kassem AA, Samy AM, Amer RI
2010; 4(5):380-387.

A new furoquinoline alkaloid with antifungal activity from the leaves of *Ruta chalepensis* L.

Emam A, Eweis M, Elbadry M
2010; 4(6):399-404

Taxonomic identification of a novel strain of *Streptomyces cavourensis* subsp. *washingtonensis*, ACMA006, exhibiting antitumor and antibacteria activity.

Yuan XW, Yang RL, Cao X, Gao JJ
2010; 4(6):405-411

Novel CYP2C19 629c>a mutant gene detection in Japanese subjects and estimation of its effect on conformation.

Kimura S, Hasegawa S, Kobayashi A, Yamaguchi H, Yohda M, Kubota T
2010; 4(6):412-417

Quantification of nebivolol hydrochloride in human plasma by liquid chromatography using fluorescence detection: Use in pharmacokinetic study.

Abdel-Fattah L, Abdel-Aziz L, El-Kosasy A, Gaied M
2010; 4(6):418-422

Use of factorial design in formulation and evaluation of ophthalmic gels of gatifloxacin: Comparison of different mucoadhesive polymers.

Gonjari ID, Karmarkar AB, Khade TS, Hosmani AH, Navale RB
2010; 4(6):423-434

Improvement in the dissolution profile of diacerein using a surfactant-based solid dispersion technique.

Patil SB, Shete DK, Narade SB, Surve SS, Khan ZK, Bhise SB, Pore YV
2010; 4(6):435-441

Solid-state characterization and *in vitro* dissolution behavior of lorazepam: Hydroxypropyl- β -cyclodextrin inclusion complex.

Patel R, Patel M
2010; 4(6):442-452

Formulation, development, and optimization of immediate release nateglinide tablets by factorial design.

Pani NR, Nath LK, Bhunia B
2010; 4(6):453-458

Formulation of microemulsion gel systems for transdermal delivery of celecoxib: *In vitro* permeation, anti-inflammatory activity and skin irritation tests.

Soliman SM, Abdel Malak NS, El-Gazayerly ON, Abdel Rehim AA
2010; 4(6):459-471

Preparation and characterization of oxybenzone-loaded solid lipid nanoparticles (SLNs) with enhanced safety and sunscreens efficacy: SPF and UVA-PF.

Sanad RA, Abdel Malak NS, El-Bayoomy TS, Badawi AA
2010; 4(6):472-483

Comparative study on the different techniques for the preparation of sustained-release hydrophobic matrices of a highly water-soluble drug.

Abd El-Halim SM, Amin MM, El-Gazayerly ON, Abd El-Gawad NA
2010; 4(6):484-492

Effect of Ceolus KG-802 on the dissolution rate of fenofibrate liquid tablets: Preformulation and formulation development studies.

Karmarkar AB
2010; 4(6):493-498

Case Report

The treatment effect of the atopic dermatitis by electrolytic-reduction ion water lotion.

Shu T, Okajima M, Wada Y, Shimokawa K, Ishii F
2010; 4(6):499-503

Acknowledgements

Drug Discoveries & Therapeutics is a peer-reviewed international journal published by *Shandong University China-Japan Cooperation Center for Drug Discovery & Screen (SDU-DDSC)* and *International Advancement Center for Medicine & Health Research (IACMHR)*. During the editing time, many scientists kindly provided lots of support to **Drug Discoveries & Therapeutics**. To ensure the quality of articles, they have contributed great expertise and time to the peer-review. Here, we greatly appreciated the efforts of the following scientists as reviewers:

| | |
|---|--|
| Kazumasa Aoyagi (<i>Ibaraki, Japan</i>) | Carla M. Lopes (<i>Porto, Portugal</i>) |
| Hidetoshi Arima (<i>Kumamoto, Japan</i>) | Azza A. Mahmoud (<i>Cairo, Egypt</i>) |
| Nagisa Arimitsu (<i>Tokyo, Japan</i>) | Amna Makky (<i>Cairo, Egypt</i>) |
| Yoshihiro Asano (<i>Ehime, Japan</i>) | Daniele Maggioni (<i>Monza, Italy</i>) |
| Ehab R. Bendas (<i>Cairo, Egypt</i>) | Yasuhiko Matsumoto (<i>Tokyo, Japan</i>) |
| Peter L. Bonate (<i>San Antonio, TX, USA</i>) | Manoj K. Mishra (<i>Bhubaneswar, India</i>) |
| Neal M. Davies (<i>Pullman, WA, USA</i>) | Vasee Moorthy (<i>Geneva, Switzerland</i>) |
| Gamal M. El-Maghraby (<i>Tanta, Egypt</i>) | Xianjun Qu (<i>Shandong, China</i>) |
| Dingzhi Fang (<i>Chengdu, China</i>) | Joshua D. Ramsey (<i>Stillwater, OK, USA</i>) |
| Radwan Farag (<i>Cairo, Egypt</i>) | Brundage Richard (<i>Minneapolis, MN, USA</i>) |
| Martin Friede (<i>Geneva, Switzerland</i>) | Masanobu Satake (<i>Sendai, Japan</i>) |
| Jianjun Gao (<i>Tokyo, Japan</i>) | Sanjot Savant (<i>Charleston, WV, USA</i>) |
| Rosa M. P. Gutierrez (<i>Mexico City, Mexico</i>) | Wulf Schultze (<i>Hamburg, Germany</i>) |
| Hironobu Ihn (<i>Kumamoto, Japan</i>) | Takashi Tokino (<i>Sapporo, Japan</i>) |
| Yoshinori Inagaki (<i>Tokyo, Japan</i>) | Viroj Wiwanitkit (<i>Bangkok, Thailand</i>) |
| Lobna A. A. Kassem (<i>Cairo, Egypt</i>) | Jianwei Xu (<i>Shanghai, China</i>) |
| Shun-ichiro Kawabata (<i>Fukuoka, Japan</i>) | Wenfang Xu (<i>Shandong, China</i>) |
| Marijana Z. Koncic (<i>Zagreb, Croatia</i>) | |
| Bok-Luel Lee (<i>Busan, Korea</i>) | |
| Xiaokang Li (<i>Tokyo, Japan</i>) | |

(December 25, 2010)

Drug Discoveries & Therapeutics

Guide for Authors

1. Scope of Articles

Drug Discoveries & Therapeutics mainly publishes articles related to basic and clinical pharmaceutical research such as pharmaceutical and therapeutical chemistry, pharmacology, pharmacy, pharmacokinetics, industrial pharmacy, pharmaceutical manufacturing, pharmaceutical technology, drug delivery, toxicology, and traditional herb medicine. Studies on drug-related fields such as biology, biochemistry, physiology, microbiology, and immunology are also within the scope of this journal.

2. Submission Types

Original Articles should be reports new, significant, innovative, and original findings. An Article should contain the following sections: Title page, Abstract, Introduction, Materials and Methods, Results, Discussion, Acknowledgments, References, Figure legends, and Tables. There are no specific length restrictions for the overall manuscript or individual sections. However, we expect authors to present and discuss their findings concisely.

Brief Reports should be short and clear reports on new original findings and not exceed 4,000 words with no more than two display items. *Drug Discoveries & Therapeutics* encourages younger researchers and doctors to report their research findings. Case reports are included in this category. A Brief Report contains the same sections as an Original Article, but Results and Discussion sections must be combined.

Reviews should include educational overviews for general researchers and doctors, and review articles for more specialized readers.

Policy Forum presents issues in science policy, including public health, the medical care system, and social science. Policy Forum essays should not exceed 2,000 words.

News articles should not exceed 500 words including one display item. These articles should function as an international news source with regard to topics in the life and social sciences and medicine. Submissions are not restricted to journal staff - anyone can submit news articles on subjects that would be of interest to *Drug Discoveries & Therapeutics'* readers.

Letters discuss material published in *Drug Discoveries & Therapeutics* in the last 6 months or issues of general interest. Letters should not exceed 800 words and 6 references.

3. Manuscript Preparation

Preparation of text. Manuscripts should be written in correct American English and submitted as a Microsoft Word (.doc) file in a single-column format. Manuscripts must be paginated and double-spaced throughout. Use Symbol font for all Greek characters. Do not import the figures into the text file but indicate their approximate locations directly on the manuscript. The manuscript file should be smaller than 5 MB in size.

Title page. The title page must include 1) the title of the paper, 2) name(s) and affiliation(s) of the author(s), 3) a statement indicating to whom correspondence and proofs should be sent along with a complete mailing address, telephone/fax numbers, and e-mail address, and 4) up to five key words or phrases.

Abstract. A one-paragraph abstract consisting of no more than 250 words must be included. It should state the purpose of the study, basic procedures used, main findings, and conclusions.

Abbreviations. All nonstandard abbreviations must be listed in alphabetical order, giving each abbreviation followed by its spelled-out version. Spell out the term upon first mention and follow it with the abbreviated form in parentheses. Thereafter, use the abbreviated form.

Introduction. The introduction should be a concise statement of the basis for the study and its scientific context.

Materials and Methods. Subsections under this heading should include sufficient instruction to replicate experiments, but well-established protocols may be simply referenced. *Drug Discoveries & Therapeutics* endorses the principles of the Declaration of Helsinki and expects that all research involving humans will have been conducted in accordance with these principles. All laboratory animal studies must be approved by the authors' Institutional Review Board(s).

Results. The results section should provide details of all of the experiments that are required to support the conclusions of the paper. If necessary, subheadings may be used for an orderly presentation. All figures, tables, and photographs must be referred in the text.

Discussion. The discussion should include conclusions derived from the study and supported by the data. Consideration should be given to the impact that these conclusions have on the body of knowledge in which context the experiments were conducted. In Brief Reports, Results and Discussion sections must be combined.

Acknowledgments. All funding sources should be credited in the Acknowledgments section. In addition, people who contributed to the work but who do not fit the criteria for authors should be listed along with their contributions.

References. References should be numbered in the order in which they appear in the text. Cite references in text using a number in parentheses. Citing of unpublished results and personal communications in the reference list is not recommended but these sources may be mentioned in the text. For all references, list all authors, but if there are more than fifteen authors, list the first three authors and add "*et al.*" Abbreviate journal names as they appear in PubMed. Web references can be included in the reference list.

Example 1:

Hamamoto H, Akimitsu N, Arimitsu N, Sekimizu K. Roles of the Duffy antigen and glycoprotein A in malaria infection and erythrocyte. *Drug Discov Ther.* 2008; 2:58-63.

Example 2:

Zhao X, Jing ZP, Xiong J, Jiang SJ. Suppression of experimental abdominal aortic aneurysm by tetracycline: a preliminary study. *Chin J Gen Surg.* 2002; 17:663-665. (in Chinese)

Example 3:

Mizuochi T. Microscale sequencing of N-linked oligosaccharides of glycoproteins using hydrazinolysis, Bio-Gel P-4, and sequential exoglycosidase digestion. In: *Methods in Molecular Biology: Vol. 14 Glycoprotein analysis in biomedicine* (Hounsell T, ed.). Humana Press, Totowa, NJ, USA, 1993; pp. 55-68.

Example 4:

Drug Discoveries & Therapeutics. Hot topics & news: China-Japan Medical Workshop on Drug Discoveries and Therapeutics 2007. <http://www.ddtjournal.com/hotnews.php> (accessed July 1, 2007).

Figure legends. Include a short title and a short explanation. Methods described in detail in the Materials and methods section should not be repeated in the legend. Symbols used in the figure must be explained. The number of data points represented in a graph must be indicated.

Tables. All tables should have a concise title and be typed double-spaced on pages separate from the text. Do not use vertical rules. Tables should be numbered with Arabic numerals consecutively in accordance with their appearance in the text. Place footnotes to tables below the table body and indicate them with lowercase superscript letters.

Language editing. Manuscripts submitted by authors whose primary language is not English should have their work proofread by a native English speaker before submission. The Editing Support Organization can provide English proofreading, Japanese-English translation, and Chinese-English translation services to authors who want to publish in *Drug Discoveries & Therapeutics* and need assistance before submitting an article. Authors can contact this organization directly at <http://www.iacmhr.com/iac-eso>.

IAC-ESO was established in order to facilitate manuscript preparation by researchers whose native language is not English and to help edit work intended for international academic journals. Quality revision, translation, and editing services are offered by our staff, who are native speakers of particular languages and who are familiar with academic writing and journal editing in English.

4. Figure Preparation

All figures should be clear and cited in numerical order in the text. Figures must fit a one- or two-column format on the journal page: 8.3 cm (3.3 in.) wide for a single column; 17.3 cm (6.8 in.) wide for a double column; maximum height: 24.0 cm (9.5 in.). Only use the following fonts in the figure: Arial and Helvetica. Provide all figures as separate files. Acceptable file formats are JPEG and TIFF. Please note that files saved in JPEG or TIFF format in PowerPoint lack sufficient resolution for publication. Each Figure file should be smaller than 10 MB in size. Do not compress files. A fee is charged for a color illustration or photograph.

5. Online Submission

Manuscripts should be submitted to *Drug Discoveries & Therapeutics* online at <http://www.ddtjournal.com>. The manuscript file should be smaller than 10 MB in size. If for any reason you are unable to submit a file online, please contact the Editorial Office by e-mail: office@ddtjournal.com

Editorial and Head Office

Wei TANG, MD PhD
Executive Editor
Drug Discoveries & Therapeutics
Pearl City Koishikawa 603,
2-4-5 Kasuga, Bunkyo-ku,
Tokyo 112-0003, Japan
Tel: 03-5840-9697
Fax: 03-5840-9698
E-mail: office@ddtjournal.com

Cover letter. A cover letter from the corresponding author including the following information must accompany the submission: name, address, phone and fax numbers, and e-mail address of the corresponding author. This should include a statement affirming that all authors concur with the

submission and that the material submitted for publication has not been previously published and is not under consideration for publication elsewhere and a statement regarding conflicting financial interests.

Authors may recommend up to three qualified reviewers other than members of Editorial board. Authors may also request that certain (but not more than three) reviewers not be chosen.

The cover letter should be submitted as a Microsoft Word (.doc) file (smaller than 1 MB) at the same time the work is submitted online.

6. Accepted Manuscripts

Proofs. Rough galley proofs in PDF format are supplied to the corresponding author *via* e-mail. Corrections must be returned within 4 working days of receipt of the proofs. Subsequent corrections will not be possible, so please ensure all desired corrections are indicated. Note that we may proceed with publication of the article if no response is received.

Transfer of copyrights. Upon acceptance of an article, authors will be asked to agree to a transfer of copyright. This transfer will ensure the widest possible dissemination of information. A letter will be sent to the corresponding author confirming receipt of the manuscript. A form facilitating transfer of copyright will be provided. If excerpts from other copyrighted works are included, the author(s) must obtain written permission from the copyright owners and credit the source(s) in the article.

Cover submissions. Authors whose manuscripts are accepted for publication in *Drug Discoveries & Therapeutics* may submit cover images. Color submission is welcome. A brief cover legend should be submitted with the image.

Revised June 20, 2009



Drug Discoveries & Therapeutics



Editorial Office

Pearl City Koishikawa 603,
2-4-5 Kasuga, Bunkyo-ku,
Tokyo 112-0003, Japan

Tel: 03-5840-9697
Fax: 03-5840-9698
E-mail: office@ddtjournal.com
URL: www.ddtjournal.com

JOURNAL PUBLISHING AGREEMENT

Ms No:

Article entitled:

Corresponding author:

To be published in Drug Discoveries & Therapeutics

Assignment of publishing rights:

I hereby assign to International Advancement Center for Medicine & Health Research Co., Ltd. (IACMHR Co., Ltd.) publishing Drug Discoveries & Therapeutics the copyright in the manuscript identified above and any supplemental tables and illustrations (the articles) in all forms and media, throughout the world, in all languages, for the full term of copyright, effective when and if the article is accepted for publication. This transfer includes the rights to provide the article in electronic and online forms and systems.

I understand that I retain or am hereby granted (without the need to obtain further permission) rights to use certain versions of the article for certain scholarly purpose and that no rights in patent, trademarks or other intellectual property rights are transferred to the journal. Rights to use the articles for personal use, internal institutional use and scholarly posting are retained.

Author warranties:

I affirm the author warranties noted below.

- 1) The article I have submitted to the journal is original and has not been published elsewhere.
- 2) The article is not currently being considered for publication by any other journal. If accepted, it will not be submitted elsewhere.
- 3) The article contains no libelous or other unlawful statements and does not contain any materials that invade individual privacy or proprietary rights or any statutory copyright.
- 4) I have obtained written permission from copyright owners for any excerpts from copyrighted works that are included and have credited the sources in my article.
- 5) I confirm that all commercial affiliations, stock or equity interests, or patent-licensing arrangements that could be considered to pose a financial conflict of interest regarding the article have been disclosed.
- 6) If the article was prepared jointly with other authors, I have informed the co-authors(s) of the terms of this publishing agreement and that I am signing on their behalf as their agents.

Your Status:

- I am the sole author of the manuscript.
 I am one author signing on behalf of all co-authors of the manuscript.

Please tick one of the above boxes (as appropriate) and then sign and date the document in black ink.

Signature:

Date:

Name printed:

Please return the completed and signed original of this form by express mail or fax, or by e-mailing a scanned copy of the signed original to:

Drug Discoveries & Therapeutics office

Pearl City Koishikawa 603, 2-4-5 Kasuga, Bunkyo-ku, Tokyo 112-0003, Japan

e-mail: proof-editing@ddtjournal.com

Fax: +81-3-5840-9698

